Fall 1-31-2004

The use of a water quality model to evaluate the impacts of combined sewer overflows on the lower Hudson River

Wen-Pin Shu
New Jersey Institute of Technology

ABSTRACT

THE USE OF A WATER QUALITY MODEL TO EVALUATE THE IMPACTS OF COMBINED SEWER OVERFLOWS ON THE LOWER HUDSON RIVER

by
Wen-Pin Shu

CSO discharges have long been recognized as a significant source of water pollution. While many sources of water pollution have been controlled over the past 20 years, CSOs continue to be a main environmental concern in several areas, especially in old cities. In the past, most CSO research focused on the CSO control processes, including floatables and suspended solids removal. Few studies have been conducted in the area of the impacts of CSO discharge on the receiving water quality. To achieve this purpose, a powerful water-modeling tool, WASP 6.1, is utilized in this study. The Lower Hudson River is selected as a case study. Data are collected from the US EPA, USGS, NYC DEP, and NJ DEP. After calibration, the receiving water quality model can be used to study the impacts of CSO with a series of scenarios, which include the major factors that would affect the water quality of the receiving water. DO, BOD, ammonia, fecal coliform, and mercury are the reference pollutants discussed in this study. The simulation results are able to predict the effect of various CSO abatement alternatives on water quality and to be used in the water quality management and planning processes.

THE USE OF A WATER QUALITY MODEL TO EVALUATE THE IMPACTS OF COMBINED SEWER OVERFLOWS ON THE LOWER HUDSON RIVER

by
Wen-Pin Shu

A Dissertation
Submitted to the Faculty of
New Jersey Institute of Technology
In Partial Fulfillment of the Requirements for the Degree of
Doctor of Philosophy in Environmental Engineering

Department of Civil and Environmental Engineering

January 2004

APPROVAL PAGE

THE USE OF A WATER QUALITY MODEL TO EVALUATE THE IMPACTS OF COMBINED SEWER OVERFLOWS ON THE LOWER HUDSON RIVER

Wen-Pin Shu

Dr. Hsin-Neng Hsieh, Dissertation Advisor — Date
Professor of Civil and Environmental Engineering, NJIT

Dr. Robert Dresnack, Committee Member — Date
Professor of Civil and Environmental Engineering, NJIT

Dr. Dorairaja Raghu, Committee Member — Date
Professor of Civil and Environmental Engineering, NJIT

Dr. Taha F. Marhaba, Committee Member — Date
Associate Professor of Civil and Environmental Engineering, NJIT

Dr. Daniel J. Watts, Committee Member — Date
Executive Director of the Otto H. York Center for
Environmental Engineering and Science

BIOGRAPHICAL SKETCH

Author: Wen-Pin Shu

Degree: Doctor of Philosophy

Date: January 2004

Undergraduate and Graduate Education:

- Doctor of Philosophy in Environmental Engineering,
  New Jersey Institute of Technology, Newark, NJ, 2004
- Master of Science in Environmental Engineering,
  New Jersey Institute of Technology, Newark, NJ, 1999
- Bachelor of Science in Chemical Engineering,
  Tung-Hai University, Taichung, Taiwan, R.O.C., 1994

Major: Environmental Engineering

To my beloved family

ACKNOWLEDGMENT

The author wishes to express his sincerest appreciation to his advisor, Professor Hsin-Neng Hsieh, for his support, guidance and friendship. Thanks also go to professors, Dr. Robert Dresnack, Dr. Daniel J. Watts, Dr. Dorairaja Raghu, and Dr. Taha F. Marhaba for participating as committee members and their valuable comments and suggestions.

Special thanks are giving to Dr. John R. Schuring who has dedicated himself to provide a better environment of this department for the advanced education and research.

The author also wishes to thank Jia-Chyi Hsu and all the friends in Taiwan for their patience and encouragement during the development of this dissertation.

TABLE OF CONTENTS

TABLE OF CONTENTS
(Continued)

TABLE OF CONTENTS
(Continued)

TABLE OF CONTENTS
(Continued)

LIST OF TABLES

LIST OF TABLES
(Continued)

LIST OF TABLES
(Continued)

LIST OF FIGURES

LIST OF FIGURES
(Continued)

LIST OF FIGURES
(Continued)

LIST OF FIGURES
(Continued)

LIST OF FIGURES
(Continued)

LIST OF FIGURES
(Continued)

LIST OF FIGURES
(Continued)

LIST OF ABBREVIATIONS

ADW	Antecedent Dry Weather Period
AGNPS	Agriculture Non-Point Source Pollution Model
AMSA	Association of Metropolitan Sewerage Authrorities
ANSWERS	Areal Non-Point Source Watershed Environmental Response Simulation
BOD	Biochemical Oxygen Demand
CEAM	EPA's Center for Exposure Assessment Modeling
CFR	Code of Federal Regulations
CBOD	Carbonaceous Biochemical Oxygen Demand
$CBOD_U$	Ultimate Carbonaceous Biochemical Oxygen Demand
CORMIX	Cornell Mixing Zone Expert System
CREAMS	Chemicals, Runoff and Erosion from Agriculture Management Systems Model
CSO	Combined Sewer Overflow
CSS	Combined Sewer System
CWA	Clean Water Act
DHI	Danish Hydraulic Institute
DMR	Discharge Monitoring Report
DO	Dissolved Oxygen
DOC	Dissolved Organic Carbon
DYNTOX	Dynamic Toxics Model
EMC	Event Mean Concentration

EXAM II	Exposure Analysis Modeling System II
FC	Fecal Coliform
Hg	Mercury
HSPF	Hydrological Simulation Program - FORTRAN
LTCP	Long-Term Control Plan
N	Nitrogen
NH_3	Ammonia
NJ DEP	New Jersey Department of Environmental Protection
NMC	Nine Minimum Control
NPDES	National Pollutant Discharge Elimination System
NRDC	Natural Resources Defense Council
NWISWeb	National Water Information System Web Site
NYC	New York City
NY-NJ HEP	New York-New Jersey Harbor Estuary Program
NYSDEC	New York State Department of Environmental Conservation
OP	Organic Phosphorus
P	Phosphorus
PAH	Polycyclic Aromatic Hydrocarbon
PCB	Polychlorinated Biphenyl
PO_4	Ortho-phosphate
POTW	Publicly Owned Treatment Works
QUAL2EU	Enhanced Stream Water Quality Model with Uncertainty Analysis
R^2	Correlation Coefficient Square

RMSE	Root Mean Square Error
SMPTOX3	Simplified Method Program-Variable Complexity Stream Toxic Model
SOD	Sediment Oxygen Demand
STORET	EPA's Storage and Retrieval of U.S. Waterways Parametric Data
STP	Sewage Treatment Plant
SWAT	Soil and Water Assessment Tool
SWEM	System-Wide Eutrophication Model
SWMM	Stormwater Management Model
TIGER	Topologically Integrated Geographic Encoding and Referencing
TMDL	Total Maximum Daily Load
TSS	Total Suspended Solids
USACE	United States Army Corps of Engineers
US EPA	United States Environmental Protection Agency
USGS	United States Geological Survey
VSS	Volatile Suspended Solids
WASP	Water Quality Analysis Simulation Program
WEF	Water Environment Federation
WLA	Waste Load Allocation Program
WTP	Water Treatment Plant
WWTP	Wastewater Treatment Plant

CHAPTER 1

INTRODUCTION

1.1 Background

A Combined Sewer System (CSS) is a wastewater collection system owned by a state or municipality (as defined by Section 502[4] of the Clean Water Act [CWA]) that conveys wastewaters (domestic, commercial, and industrial wastewaters) and storm water (surface drainage from rainfall or snowmelt) through a single-pipe system to a Publicly Owned Treatment Works (POTW) Treatment Plant (as defined in 40 Code of Federal Regulations [CFR] 403.3[p]) (US EPA, 1994a). During dry weather, combined sewers send all wastewater to the sewage treatment plants (STPs). Whereas during wet weather, runoff enters the sewer system and total flows can exceed the capacity of the CSSs or the treatment facilities. To prevent the STPs from flooding and backing up a mixture of urban runoff and raw sewage into streets and homes, the CSS is designed to overflow along with debris washed from the streets directly to surface water bodies, such as lakes, rivers, estuaries, or coastal waters. These overflows are called combined sewer overflows (CSOs).

Combined sewer systems were among the earliest sewers built in the United States and continued to be built until the middle of twentieth century. Currently, CSSs serve roughly 772 communities with about 43 million people. Eighty-five percent of CSSs are located in 11 of the 32 states, which have CSSs. Most communities with CSOs are located in the Northeast and Great Lake Regions, particularly in Pennsylvania,

Indiana, Ohio, Illinois, Michigan, New York, West Virginia, and Maine. Of the 772 CSO communities, approximately 30 percent have populations greater than 75,000, and approximately 30 percent are very small with total service populations of less than 10,000 (US EPA, 2001).

CSOs are point sources subjected to National Pollutant Discharge Elimination System (NPDES) permit requirements including both technology-based and water quality-based requirements of the CWA. National projections of annual CSO discharges are estimated at 1,260 billion gallons per year. CSOs are not subject to secondary treatment requirements applicable to POTWs. CSOs often contain high levels of suspended solids, pathogenic microorganisms, floatable debris, toxic pollutants, settleable solids, nutrients, oxygen-demanding organic compounds, oil and grease, and other pollutants (US EPA, 1994a). The presence of these pollutants in CSOs and the frequent large volume of the flows can degrade water quality and adversely impact aquatic animals, plants, and human health in certain situations. CSOs have been shown to be major contributors to impairment and aesthetic degradation of many receiving waters and have contributed to shellfish harvesting restrictions, beach closures, and even occasional fish kills (US EPA, 1999).

While much has been accomplished over the past 20 years in the area of wastewater treatment, CSOs continue to be a major environmental concern in many communities. According to the EPA's 1998 National Water Quality Inventory, CSOs are a source of impairment for 12 percent of assessed estuaries (in square miles) and two percent of assessed lakes (in shore miles) (US EPA, 2000). The Natural Resources Defense Council (NRDC) reported in its 2000 Testing the Waters report that sewage

spills (combined sewer overflows, sanitary sewer overflows, and breaks in sewer lines or septic systems) and overflows accounted for 2,230 beach closings and advisories in 2000 (NRDC, 2001). Localized impacts of uncontrolled CSO discharges have been well documented by some communities. For example, New York City reported that CSOs caused or contributed to shell fishing restrictions for more than 30,000 acres of shellfish beds (US EPA, 2001) and the State of New Jersey reported that CSOs caused or contributed to hundreds of days of ocean beach closings in 1987 (New York-New Jersey Harbor Estuary Program [NY-NJ HEP], 1996).

To ensure that all wet weather CSO discharge points are compliant with the requirements of the CWA, the US EPA initiated action to clarify requirements for CSOs through the publication of the National CSO Control Policy on April 19, 1994 (59 Federal Register 18688). To implement the National CSO Control Policy, there are two components - Nine Minimum Controls (NMC) and Long-Term Control Plans (LTCP). The Nine Minimum Controls are measures that can reduce the impacts of CSOs and that are not expected to require significant engineering studies or major construction. The primary achievement of this stage is the reduction and control of floatables and debris. It was reported that the goals of the NMCs had been achieved by 1997. Long-Term Control Plans will provide for full compliance with the CWA. In this stage, intensive CSO monitoring and modeling studies are required to characterize CSOs properties and their impacts on receiving water quality.

In recent years, the application of mathematical modeling techniques has become an important part of most water quality management and planning processes (Beck, 1985; Dillaha, 1998; Henderson-Sellers, 1991; Jamal, 1986; Orlob, 1992; Tim and Jolly, 1994).

The need to understand cause-effect relationships in water pollution, and the desire to develop a tool that can aid decision-makers in selecting appropriate technologies, are two important reasons for the construction of river simulation models (Heathcote, 1987; Thomann, 1982). Water quality models can be powerful tools to determine acceptable contaminant levels or to test alternative strategies for water quality management (Tim and Jolly, 1994).

1.2 Research Objectives

The primary purpose of this study is to develop a water quality model to investigate the impacts of CSO discharges on the Lower Hudson River. Once the model is calibrated and validated, it will be used:

1) To determine whether the river will meet the water quality criteria after receiving CSO discharges by comparing receiving water quality with applicable water quality criteria

2) To reveal the impact of the load on the receiving water quality by simulating calibrated models under various magnitudes of CSO loads

3) To investigate how the stream flowrate affects the receiving water quality after CSO discharges by simulating calibrated models under various scenarios of stream flowrate

4) To understand the CSO spatial distribution in receiving waters by comparing the simulation results at locations downstream and upstream from CSO discharge points.

5) To characterize the CSO temporal impacts by comparing simulation results before, during, and after a storm event.

6) To identify major water quality problems generated by CSO discharges on receiving waters.

With the same approach, the impacts of CSOs or other pollution sources on the receiving water quality can be studied in the future studies.

CHAPTER 2

LITERATURE SEARCH

2.1 Combined Sewer Overflows

2.1.1 Introduction

Overflows from combined sewers during storm events result in the discharge of untreated sanitary sewage to receiving waters. They also may contain pre-treated industrial wastewaters and untreated stormwater. CSOs contain pollutants that are present in domestic and industrial wastewaters, as well as those in the urban stormwater runoff that enters the combined sewer system. However, the quality characteristics of CSOs are not as easy to define within a referenced range as are those from other pollution sources. Combined sewer systems with their associated overflow points are relatively complex. Hydraulic conditions are highly variable due to the intermittent and variable characteristics of rainfall. The quality characteristics of CSO flows can also vary significantly from location to location and from storm to storm at a given location (US EPA, 1993). In other words, CSO water quality is site specific.

Higher pollutant concentrations may be associated with the initial peak flows, depending on factors such as the size and slope of the piping system, the time interval between storms, the drainage area characteristics and response, and the solids accumulation in the collection system (US EPA, 1993).

The initial peak flows, called the "first flush", occur in the early stages of a storm runoff or combined sewer overflow event, and represent a relative small percentage of the

total flow although containing a disproportionately large percentage of the total pollutant mass associated with the overall storm event (US EPA, 1993). Significant first flush effects are most likely to be present with small catchments, flat slopes, low impervious fractions, relatively simple conveyance system networks, and lines with low dry weather flow velocities that permit solids to accumulate in the line.

Rainfall, which produces large flows in the combined sewer system, is another site-specific property that affects the quantity and quality of CSO discharges. It is the factor that determines when and where overflows will occur, and the rates, volumes, and durations of the episodes. Rainfall amount varies from year to year, storm event to storm event, and hour to hour during individual events. Analysis and interpretation of rainfall records can provide useful information for identifying drainage area. The system characteristics impose site-specific influences on the flow rates and volumes that will occur during any storm event.

The length of any dry weather period can also affect the quality of CSOs. Moffa (1980) indicated that the extent of pollutant accumulation prior to a storm occurrence will depend on: (a) the residual of pollutants remaining from the previous storm; and (b) the amount accumulated during the intervening period, commonly referred to as the Antecedent Dry Weather Period (ADW). Mason and his co-workers (1977) also stated that the concentration of the first flush appears to be related to the number of dry days preceding the storm event. The accumulated pollutants will be scoured during the storm event and the duration over which an intense rainfall occurs will determine the quantity of available pollutants that are scoured from the system.

The fact that CSO quality characteristics are site specific limits the confidence with which data from other sites can be applied. If the study is based on default values incorporated in the models, the simulation result may generate significant errors (Mueller and Di Toro, 1981). An extensive sampling program is generally necessary in order to provide calibration and validation for a specific area. However, because of the technical difficulty and cost of developing comprehensive performance monitoring data, CSO modeling represents a situation where the theoretical prediction of flow and quality (based on models calibrated against limited data sets) may provide a more accurate basis for estimating CSO discharge characteristics. While many studies of the characteristics of CSOs have been published in the past, a comprehensive database for CSO simulation remains incomplete.

2.1.2 Characteristics of CSOs

Pollution issued from CSOs is extremely diverse in composition. Basically it includes typical wastewater pollution (organic carbon and nitrogen, phosphorus, heterotrophic bacteria, pathogenic micro-organisms, etc.) as well as typical urban runoff pollution (metals, polyaromatic hydrocarbons, etc.) (Seidl, Servais, and Mouchel, 1998). CSO impacts include adverse human health effects (e.g., gastrointestinal illness), beach closures, shellfish bed closures, toxicity for aquatic life, and aesthetic impairment. The pollutants of concern and the principal consequences of CSOs are presented in Table 2.1.

For a long time, sampling programs have been developed to characterize the quality of CSOs for the pre-design of abatement programs. The pollutant values of CSOs are a combination of runoff pollutant concentrations and sanitary sewage pollutant concentrations. A tabulation of typical pollutant concentrations in CSOs compared with

concentrations from other pollutant sources is displayed in Table 2.2. As shown, the typical values generally fall between the values of urban runoff and sanitary sewage. Site-specific concentrations that result from this mixture are dependent on the quality of the two base flows and the proportional mix (US EPA, 1977). A summary of CSO discharges from several studies is shown in Table 2.3. Highlights of the properties and their responses during storm events for each pollutant variable are given in the following paragraphs.

Stormwater runoff, combined sewer overflows, leaking sewer lines, as well as natural processes, all contribute significant amounts of organic matter to the receiving water. Organic matter, which refers to anything derived from living organisms, must then be broken down or decomposed by microorganisms within the river. Depending on the timing and size of the load, the decomposition of this material can require a substantial amount of oxygen. Martin (1995) indicated that the concentration of dissolved oxygen, during the storm runoff, decreased probably because oxygen was consumed by oxygen-demanding materials from CSOs, urban runoff, and resuspended sediments and because of the discharge of anoxic water from combined sewer overflows. In other words, concentrations of BOD in storm runoff generally were higher than those in base flow (dry weather flow condition).

Table 2.1 CSO Pollutants of Concern and Principal Consequences

Pollutant(s)	Principal Consequences
Bacteria (e.g., Fecal coliform, E. coli, enterococci) Viruses (e.g., hepatitis, cholera) Parasites (e.g., giardia, cryptosporidium)	Beach closure Odors Shellfish bed closures Drinking water contamination Adverse public health effects
Trash and floatables	Aesthetic impairment Odors Beach closures
Organic compounds, metals, oil, grease Toxic pollutants	Aquatic life impairment Adverse public health effects Fishing and Shellfishing restrictions
Biochemical oxygen demand (BOD)	Reduced oxygen level and fish kills
Solids deposition	Aquatic habitat impairment Shellfish bed closures
Nutrients (e.g., nitrogen, phosphorus)	Eutrophication, algae blooms Aesthetic impairment

Source: Association of Metropolitan Sewerage Authorities (AMSA). Modified from Approaches to Combined Sewer Overflow Program Development: A CSO Assessment Report. (AMSA, Washington, DC, 1994)

Table 2.2 Comparison of Typical Values for Pollutant Discharges

Contaminant Source	BOD_5 (mg/L)	TSS (mg/L)	COD (mg/L)	Total N (mg/L)	Total P (mg/L)	Fecal coliform (counts/100mL)
Rainfall	1--13	<1	9--16	--	0.02--0.15	--
Treated Wastewater	<5--30	<5--30	--	15--25	<1--5	<200
Urban Runoff	10--250	67--101	40--73	0.4--1.0	0.7--1.7	10^3--10^7
CSO	25--100	150--400	260--480	3.0--24	1.0--10	10^5--10^7
Sanitary Sewage	100--400	100--350	260--900	20--85	4.0--15	10^7--10^9

Source: Water Environment Federation (WEF). Prevention and Control of Sewer System Overflows. (WEF, 1999)

Table 2.3 Pollutant Concentrations in Combined Sewer Overflows

Location	Average pollutant concentration (mg/L)									Reference
	TSS	VSS	BOD	COD	Kjeldahl Nitrogen	Total Nitrogen	Total Phosphorus	Ortho-Phosphate	Fecal coliforms[b]	
Des Moines, Iowa	413	117	64	...	...	4.3	1.86	1.31	...	Davis and Borchard, 1974
Milwaukee, Wisconsin	321	109	59	264	4.9	6.3	1.23	0.86	...	Mason et al., 1977
Newtown Creek, NYC	306	182	222	481	...	...	...	...	...	US EPA, 1975
Spring Creek, NYC	347	...	111	358	...	16.6	4.5	...	...	Feuerstein and Maddaus, 1976
Poissy, France[a]	751	387	279	1005	...	43	17	...	...	Coyne & Bellier Inc., 1974
Racine, Wisconsin	551	154	158	...	...	...	2.78	0.92	201	Clark et al., 1975
Rochester, New York	273	...	65	...	2.6	...	...	0.88	1140	Lager et al., 1976
Average (not weighted)	370	140	115	367	3.8	9.1	1.95	1	670	
Range	273-551	109-182	59-222	264-481	2.6-4.9	4.3-16.6	1.23-2.78	0.86-1.31	201-1140	

a. Not included in average because of its high strength of municipal sewage when compared to these obtained in the United States.

b. 1000 organisms/100mL

Two nutrients, phosphorus and nitrogen, can significantly impact receiving waters. When present in sufficient concentrations they often trigger algal blooms, which eventually reduce the dissolved oxygen level of the water as decaying algal and other organic matter is broken down by microorganisms. Typical sources of phosphorus and nitrogen include fertilizers, animal wastes, automotive exhaust, organic material, soil, etc. From the investigation at Fall Creek, Indianapolis, Martin (1995) observed that concentrations of nutrients in storm runoff increased downstream and that they were higher than those in base flow except for nitrate plus nitrite.

In most cases, oxygen demand and nutrient parameters will be sufficient to characterize runoff problems and impacts. However, in recent years there has been an increasing awareness of a potential danger to receiving waters from low concentrations of toxicants and pathogens. Toxics refer to a variety of contaminants including trace metals such as mercury, arsenic, copper, cadmium and lead; and organic compounds such as PCBs (polychlorinated biphenyls), PAHs (polycyclic aromatic hydrocarbons) and pesticides and herbicides (e.g., DDT, Chlordane and atrazine) that reach receiving waters from stormwater runoff, atmospheric deposition and industrial and municipal discharges. Pathogens are disease-causing microorganisms, such as bacteria, protozoa, and viruses that are present in untreated or inadequately treated human sewage and domestic and wild animal wastes (New Jersey Department of Environmental Protection [NJ DEP], 1999). Typical values obtained for parameters in each category are given in Tables 2.4, 2.5, and 2.6. The values were obtained for a variety of reasons under different conditions and are presented as representative of ranges that may be expected.

Table 2.4 Metal Concentrations in Storm Water Runoff

Site	Pollutant concentration, mg/L						Reference
	Cadmium	Chromium	Copper	Nickel	Zinc	Lead	
New York City, NY	0.025	0.16	0.46	0.15	1.6	...	Klein et al., 1974
Durham, North Carolina	...	0.23	0.15	0.15	0.36	0.46	Colston, 1974
Rochester, NY	0.0021	0.0065	0.086	0.013	0.24	0.14	Clark et al., 1975
Drinking Water Standards	0.01	0.05	1	...	5	0.05	Manning et al., 1977

Table 2.5 Pesticide and Herbicide Concentrations in Storm Water Runoff (Parts Per Trillion)

Pesticide and herbicide	Racine, Wisconsin [b]			Hayward, California [c]		Drinking Water Standards [a]
	1971	1973	1974	1971~1972		
	Site 11	Site 11	Site 11	Average	Maximum	
Lindane	<1	130	<1	31	150	5000
Heptachlor	<1	<10	<1	0	0	100
Aldrin	14	<10	<1	4	70	1000
Heptachlor epoxide	16	<10	23	0	0	100
Methozchlor	58	<15	<1	..	..	10^6
Dieldrin	<1	<10	14	90	190	1000
Endrin	<1	100	<1	0	0	500
Methyl Parathion	..	..	..	0	0	..
Parathion	..	..	..	0	0	..
DDT	..	..	89	130	630	50000
DDD	..	..	34	6	80	..
DDE	..	..	<1	16	100	..
Chlordane	..	..	..	560	2400	3000
Diazinon	..	..	..	195	260	..
Malathion	..	..	..	128	540	..
Silvex	..	..	..	81	560	30000

a. Maximum permissible concentration
b. Clark et al., 1975
c. USGS, 1972

Table 2.6 Microorganisms in Storm Water Runoff

Site	Organisms/100mL					Reference
	Total coliform	Fecal coliform	Fecal streptococci	P. aeruginoea	Salmonella sp	
Baltimore, Maryland						Orivieri et al., 1977
Storm Water	120000	24000	170000	1100	0.13	
CSO	590000	230000	260000	5900	0.59	
Houston, Texas						Davis et al., 1976
upstream	258000	1300	650	85	<38	
downstream	403000	1800	2020	260	<62	
residential area	30100000	22000	13100	7560	<33	

Toxic contaminants typically cling to particles suspended in water and settle to the bottom, whereupon, they can ingested by bottom feeding organisms and potentially work their way up the food chain. Because of the high concentration of metals in urban runoff waters, increases of metal concentrations in organisms are another sub-lethal index of biological impact (Chebbo et al., 1995). Generally, concentrations of toxicants in storm runoff are higher then those in base flow. However, the water quality of CSOs is site-specific, especially for the toxicants and organic compounds. Concentrations of these contaminants are mainly related to the land use and the properties of the watershed.

Concentrations of fecal coliform bacteria in storm runoff were much greater than those in base flow (Martin, 1995). However, like concentrations of toxicants, the degrees of increase of the pathogen concentration are again site-specific. These values are dominated by the sanitary wastewater rather than the storm runoff.

2.2 Receiving Water Quality Modeling

2.2.1 River Water Quality Models

In the last 20 years, water quality modeling has been used as an important tool for water quality management and planning (Ambrose and Roesch, 1982; Beck, 1985; Thomann and Mueller, 1987). Simulation models can be used to assess the detailed and often complicated interactions among various water quality constituents, biological activities, and physical characteristics (Heng and Nikolaidis, 1998; Whitehead et al., 1981). However, the value of any simulation model depends upon the appropriateness of that model as a means of simulating the specific conditions and problems of the body of water in question, since there is no existing universal or all-purpose model (Ambrose and

Roesch, 1982; Beck, 1985; Stefan et al., 1990). In general, most water quality models are based on mass balance equations (Atkinson et al., 1998). The equation used in simulation of the one-dimensional advection of a pollutant is:

$$\frac{\partial C}{\partial t} + U\frac{\partial C}{\partial x} = \frac{\partial}{\partial x}\left[D\frac{\partial C}{\partial x}\right] \tag{2.1}$$

Where: C = concentration (M/L^3)
t = time (T)
U = mean longitudinal velocity (L/T)
x = distance (L)
D = dispersitivity (L^2/T)

Lateral mixing in a river is usually more rapid than in other waterbodies, thereby, resulting in approximately uniform conditions over the river cross section (US EPA, 1999) and one-dimensional (longitudinal) models are usually appropriate for simulating river systems (Lung, 1993; Stefan et al., 1990).

Simulating considerations depend upon the water quality parameters. Basic considerations and applied equations presented in the following paragraphs are commonly taken into account in water quality modeling.

In the DO simulation, the complexity of the model can be varied and it depends upon the purpose of the modeling. Simple spreadsheet models such as STREANDO IV (Zander and Love, 1990) have recently become available for DO analysis. In general, screening analysis using classical steady-state equations can examine DO impacts to rivers as a result of episodic loads. The classic steady-state equation, Streeter-Phelps equation, which can estimate the DO concentration downstream, can be shown as:

$$D = D_0 e^{-K_a t} + \frac{W}{Q}\left(\frac{K_d}{K_a - K_r}\right)\left[e^{-K_r t} - e^{-K_a t}\right] \quad (2.2)$$

Where: D = DO deficit downstream (M/V)

D_0 = initial DO deficit (M/V)

K_a = atmospheric reaeration rate (1/T)

t = time of passage from source to downstream location (T)

W = total pollutant loading rate (M/T)

Q = total river flow (V/T)

K_d = biochemical oxygen demand (BOD) deoxygenation rate (1/T)

K_r = BOD loss rate (1/T)

However, simple models cannot address multiple sources that change over time, nor can they address the effects of river morphology. When such issues are important, more sophisticated modeling techniques are necessary. More sophisticated modeling techniques can also assess the effects of sediment oxygen demand (SOD), plant respiration, and photosynthesis by aquatic plants (US EPA, 1999).

Nutrient discharges affect river eutrophication over time scales of several days to several weeks. Nutrient analysis considers the relationship between nutrients and algal growth. The current Waste Load Allocation Programs (WLA) guidance (US EPA, 1995d) considers only planktonic algae (rather than all aquatic plants) and discusses nutrient loadings and eutrophication in rivers primarily as a component in computing DO.

Pathogens and toxics contaminants are primarily a concern in the immediate vicinity of loading sources. They are controlled by lateral mixing, advection, and decay processes such as die-off (for pathogens), vaporization (for toxics), and settling and resuspension (for pathogens and toxics). When stream flow is small relative to loading

flow, lateral mixing may occur rapidly and a one-dimension model may be appropriate. The concentration of the pollutant can be presented by the following equation:

$$C_X = \frac{Q_u C_u + Q_e C_e}{Q_s} e^{\frac{-KX}{u}} \quad (2.3)$$

Where: C_x = max pollutant concentration at distance X from the outfall (M/L^3)

C_e = pollutant concentration in effluent (M/L^3)

C_u = pollutant concentration upstream from discharge (M/L^3)

Q_e = effluent flow (L^3/T)

Q_u = stream flow upstream from discharge (L^3/T)

Q_s = stream flow downstream from discharge, $Q_u + Q_e$ (L^3/T)

X = distance from outfall (L)

u = stream flow velocity (L/T)

K = net decay rate (1/T)

e = 2.71828...

In large rivers, lateral mixing may occur over a large distance. For this consideration, the estimation of a lateral dispersion coefficient is required, which can be measured by dye studies or by other methods (Fischer et al., 1979).

The model DYNTOX (LimnoTech, 1985) is specially designed for analysis of toxics in rivers.

2.2.2 Computer Models for Water Quality Simulation

Many computer models are supported by the EPA's Center for Exposure Assessment Modeling (CEAM). CEAM maintains a distribution center for water quality models and related databases. CEAM-supported models relevant to modeling impacts on receiving water include QUAL2EU, WASP6, HSPF, EXAMSII, CORMIX, MINTEQ, SMPTOX3,

and DYNTOX. The applicability and key characteristics of the CEAM-supported models are summarized in Table 2.7.

Enhanced Stream Water Quality Model with Uncertainty Analysis (QUAL2EU) is a one-dimensional model for rivers. It assumes steady-state flow and loading but allows simulation of diurnal variations in temperature or algae photosynthesis and respiration. QUAL2EU can simulate up to 15 water-quality variables, including temperature, bacteria, BOD, DO, ammonia, nitrate, nitrite, organic nitrogen, phosphate, organic phosphorus, algae, and additional conservative substances (Brown and Barnwell, 1987). Because it assumes steady flow and pollutant loading, its applicability to CSOs is limited. QUAL2EU can, however, use steady loading rates to generate worst-case projections for CSOs to the river. Additionally, in certain cases, experienced users may be able to use the model to simulate non-steady pollutant loadings under steady flow conditions by establishing certain initial conditions or by dynamically varying climatic conditions (Brown and Barnwell, 1987).

Water Quality Analysis Simulation Program 6.1 is an enhancement of the original WASP. The flexibility afforded by the WASP 6.1 is unique. WASP permits the modeler to structure one, two, and three-dimensional models (James, 1992; Lung, 1993; Orlob, 1992). It allows the specification of time-variable exchange coefficients, advective flows, waste loads and water quality boundary conditions; and permits tailored structuring of the kinetic processes, all within the larger modeling framework without having to write or rewrite large sections of computer code (Ambrose et al., 1988).

Table 2.3 Pollutant Concentrations in Combined Sewer Overflows

Location	Average pollutant concentration (mg/L)									Reference
	TSS	VSS	BOD	COD	Kjeldahl Nitrogen	Total Nitrogen	Total Phosphorus	Ortho-Phosphate	Fecal coliforms[b]	
Des Moines, Iowa	413	117	64	...	...	4.3	1.86	1.31	...	Davis and Borchard, 1974
Milwaukee, Wisconsin	321	109	59	264	4.9	6.3	1.23	0.86	...	Mason et al., 1977
Newtown Creek, NYC	306	182	222	481	...	...	...	...	...	US EPA, 1975
Spring Creek, NYC	347	...	111	358	...	16.6	4.5	...	...	Feuerstein and Maddaus, 1976
Poissy, France[a]	751	387	279	1005	...	43	17	...	...	Coyne & Bellier Inc., 1974
Racine, Wisconsin	551	154	158	...	...	...	2.78	0.92	201	Clark et al., 1975
Rochester, New York	273	...	65	...	2.6	...	...	0.88	1140	Lager et al., 1976
Average (not weighted)	370	140	115	367	3.8	9.1	1.95	1	670	
Range	273-551	109-182	59-222	264-481	2.6-4.9	4.3-16.6	1.23-2.78	0.86-1.31	201-1140	

a. Not included in average because of its high strength of municipal sewage when compared to these obtained in the United States.

b. 1000 organisms/100mL

Hydrological Simulation Program—Fortran (HSPF) is a one-dimensional, comprehensive hydrology and water quality simulation package, which can simulate both receiving water and runoff to CSSs for conventional and toxic organic pollutants. HSPF simulates the transport and fate of pollutants in rivers and reservoirs. It can study three sediment types: sand, silt, and clay (Johnson et al., 1984). HSPF has been applied to various watershed areas ranging from 52 to 7,200 km^2 in Central Iowa (Donigian, Bicknell, and Imhoff, 1995). The limitations of this model are due to its complicated characteristics and the comprehensive information required to derive it.

MIKE11 is an unsteady one-dimensional model that was developed by the Danish Hydraulic Institute (DHI). MIKE 11 permits simulation of various characteristics such as flows, water levels, water quality, transports of sediment and dissolved or suspended solids (DeVries and Hromadka, 1992). MIKE11 has been used around the world to simulate a number of rivers and estuary systems, including: the Nepal River in Nepal, the Paramatta and Georges Rivers in Australia, the Sarawak River in Malaysia, and the Chao Phraya Tidal River in Thailand (Marco, 1995).

Exposure Analysis Modeling Systems II (EXAMSII) can rapidly evaluate the fate, transport, and exposure concentrations of steady discharges of synthetic organic chemicals to aquatic systems. A recent upgrade of the model considers seasonal variations in transport and time-varying chemical loadings, making it quasi-dynamic. The user must specify transport fields to the model (Burns, 1982).

Cornell Mixing Zone Expert System (CORMIX) is an expert system for mixing zone analysis. It can simulate submerged or surface, buoyant or non-buoyant discharges into stratified or unstratified receiving waters, with emphasis on the geometry and

dilution characteristics of the initial mixing zone. The model uses a zone approach, in which a flow classification scheme determines which near-field mixing processes to calculate. The CORMIX model cannot be calibrated in the classic sense since rates are fixed based on the built-in logic of the expert system (Doneker and Jirka, 1990). CORMIX was originally developed assuming steady ambient conditions; Version 3 allows for application to some unsteady environments (e.g., tidal reversal conditions) where transient recirculation and pollutant build-up can occur (CEAM, 1998).

MINTEQ determines geochemical equilibrium for priority pollutant metals. Not a transport model, MINTEQ provides a means for modeling metal partitioning in discharges. It provides only steady-state predictions. The model usually must be run in connection with another fate and transport model, such as those described above. A number of assumptions (e.g., equilibrium conditions at the point of mixing between a CSO and the receiving water) must be made to link MINTEQ predictions to another fate and transport model, so it should be used cautiously in evaluating wet weather impacts (Brown and Allison, 1987).

Simplified Method Program-Variable Complexity Stream Toxics Model (SMPTOX3) is a one-dimensional steady-state model for simulating the transport of contaminants in the water column and bed sediments in the streams and non-tidal rivers. SMPTOX3 is an interactive computer program that uses an EPA technique for calculating concentrations of toxic substances in the water column and streambed as a result of point source discharges to streams and rivers. The model predicts pollutant concentrations in dissolved and particulate phases for the water column and bed sediments, as well as total suspended solids (LimnoTech, 1992).

Dynamic Toxics Model (DYNTOX) is a one-dimensional, probabilistic toxicity dilution model for transport in rivers. It provides Continuous, Monte Carlo, or Lognormal probability simulations that can be used to analyze the frequency and duration of ambient toxic concentrations resulting from a waste discharge. The model considers dilution and net first-order loss, but not sorption and benthic exchange (LimnoTech, 1985).

CE-QUAL-W2 is a reservoir and narrow estuary hydrodynamics and water quality model developed by the Waterways Experiment Station of the U.S. Army Corps of Engineers (USACE). The model provides dynamic two-dimensional (longitudinal and vertical) simulations. It accounts for density effects on flows as a function of the water temperature, salinity, and suspended solids concentration. CE-QUAL-W2 can simulate up to 21 water quality parameters in addition to temperature, including one passive tracer (e.g., dye), total dissolved solids, coliform bacteria, inorganic suspended solids, algal/nutrient/DO dynamics (11 parameters), alkalinity, pH, and carbonate species (4 parameters) (Brown and Barnwell, 1987; Devries and Hromadka, 1992).

A number of water quality models have been used in non-point source pollution simulation. In recent years, agriculture and urban runoff are two major types of non-point-source pollution, which can be simulated by these models. Some of these models will be reviewed in the following paragraphs.

The Agriculture Non-point Source Pollution Model (AGNPS), an event-based and continuous model, was developed by the Agriculture Research Service, US Department of Agriculture, and the University of Minnesota (Young et al., 1989). It can be used to simulate and predict runoff volume, peak rates, sediment load, erosion, and conventional pollutant concentrations for a single storm event.

The Areal Non-point Source Watershed Environmental Response Simulation (ANSWERS) is a continuous model and uses a grid-cell structure, which represents watershed information (Dillaha, 1998; Vieux and Needham, 1993). The model simulates hydrologic processes within each element including interception, infiltration, surface storage, surface flow, subsurface drainage, sediment drainage, and sediment attachment, transport, and deposit (City of Austin, 1992; Dillaha, 1998).

Chemicals, Runoff and Erosion from Agriculture Management Systems Model (CREAMS) is a daily rainfall hydrology model. The major purpose of this model is the analysis of agriculture pollution control, which is accomplished through an analysis of hydrology, erosion/sediment yield, and chemistry (nutrients and pesticides). This model is not applicable to a complicated watershed because it was developed for simulating field-scale areas homogeneous with a single land-use and soil and management practices (Crowder et al., 1984).

The Stormwater Management Model (SWMM) was developed by the US EPA. It is a comprehensive model for the simulation of urban runoff quantity and pollution in storm and combined sewer systems (James, 1992). The SWMM permits a wide range of simulation, including simulations of urban hydrology and water quality processes such as rainfall, snowmelt, surface runoff, subsurface contribution to runoff, routing, storage, and the treatment of flows (DeVries and Hromadka, 1992; Huber, 1995). However, SWMM does not include modules to simulate receiving water quality.

Most of these non-point source simulation models only address some water quality issues with spatial and temporal factor limitations. They have limited applications in this study.

Based upon the literature review, the opinions of modeling experts, and the characteristics of the pollutant source and the receiving water, WASP 6.1 was selected for this study.

2.3 Applications of WASP 6.1

The Water Quality Analysis Simulation Program – WASP 6.1, an enhancement of the original WASP (Di Toro et al., 1983; Connolly and Winfield, 1984; Ambrose, R.B. et al., 1988). This model helps users interpret and predict the water quality response to natural phenomena and man-made pollution for various pollution management decisions. WASP 6.1 is a dynamic compartment-modeling program for aquatic systems, including both the water column and the underlying benthos. The time-varying processes of advection, dispersion, point and diffuse mass loading, and boundary exchange are represented in the basic program.

The hydrodynamics model of WASP 6.1, DYNHYD5, is an update of DYNHYD4 (Ambrose, et al., 1988), which was an enhancement of the Potomac Estuary hydrodynamic model DYNHYD2 (Roesch et al., 1979) derived from the original Dynamic Estuary Model (Feigner and Harris, 1970). Water quality processes are represented in special kinetic subroutines that are either chosen from a library or written by the user. WASP is structured to permit easy substitution of kinetic subroutines into the overall package to form problem-specific models.

WASP 6.1 comes with four sub-models, EUTRO (eutrophication, conventional pollutant model), TOXI (organic chemical/simple metals model), Mercury, and Thermal/Fecal Coliform Models. Earlier versions of WASP, with EUTRO and TOXI

only, have been used to examine eutrophication of Tampa Bay (Martin, et al., 1996); phosphorus loading to Lake Okeechobee (James et al., 1998); eutrophication of the Neuse River and estuary (Lung and Paerl, 1988); eutrophication of the Black River (Pickett, 1997); eutrophication of the Upper Mississippi River and Lake Pepin (Lung and Larson, 1995); eutrophication and PCB pollution of the Great Lakes (Thomann, 1975; Thomann et al., 1976; Thomann et al., 1979; Di Toro and Connolly, 1980); eutrophication of the Potomac Estuary (Thomann and Fitzpatrick, 1982); kepone pollution of the James River Estuary (Ambrose, 1987); and heavy metal pollution of the Deep River, North Carolina (JRB, 1984). In addition to these, numerous other applications can be found in a review paper (Di Toro et al., 1983).

CHAPTER 3

APPROACH AND METHOD

3.1 Conceptual Modeling Approach

Wool (2002) indicated that a model is a "conceived image of reality"' or a theoretical construct, relating some stimulus to a response. In other words, "modeling" is a process to look for a relationship between loads and responses (water quality). The relationship can usually be achieved by adjusting transport and transform constants of the parameters found in the specific system. In this research, in order to investigate the impacts of the CSO discharge on receiving waters, a receiving water quality model is created. Initially, the model's load should include all the pollutant sources (e.g., CSO, municipal and industrial waste water, agriculture and urban runoff, etc.) because the modeler is looking for the totality of relationships in the receiving water system. After calibration and validation, CSO discharges can be altered in different scenarios to find out the impacts of change on receiving water quality by this model.

Generally, there are four primary steps in developing a model: data collection, model creation, model calibration and validation, and results interpretation. Each of these steps will be described in detail in the following sections.

3.1.1 Data Collection

Data collection is a very important and time-consuming step in model development. Accurate information on the characteristics of CSOs, and the biological and chemical characteristics of receiving water are critical in identifying CSO impacts on receiving waters (US EPA, 1999). Most of the time, data availability limits the applications of complicated models. However, most water quality models are complicated, particularly when they are linked to hydrodynamic models (Atkinson et al., 1998; Thomann, 1982). The lack of high quality data for the receiving water is therefore a significant constraint in model selection and development.

Data information comes from two main sources: existing data and monitoring programs. Existing data are historical records or local documents, which are available from the government or private companies. After reviewing the existing data, data gaps can be identified. A monitoring program is implemented to collect data, which can fill in these data gaps. Basically, monitoring data is much more reliable than other data sources. However, the technical difficulty and cost concerns in the field survey and lab analyses could be problems when implementing a monitoring program for a local project or research. Existing data may be the only source in some situations to support model development.

The input data needs for a specific receiving water model depend upon the hydraulic regime and model used. Three primary sets of data important in creating a receiving water quality model are: (a) water transport data, (b) water quality data, and (c) pollutant loads data.

(a) Water transport data

The water transport data provide information to define how water moves in the channel. These data include channel segment information, channel hydraulic characteristics, flow data, and mixing coefficients. Channel segment information provides geometric measures, such as length, width, depth, and volume of the stream channel. Hydraulic characteristics include depth and velocities of the stream. Mixing coefficients are properties of dispersion, such as dispersion coefficients. Among the transport data, flow records are the most important; they will affect the simulation results significantly.

The primary flow data source is the National Water Information System Web Site (NWISWeb), which is supported by the U.S. Geological Survey (USGS). Selected water-resources data for approximately 1.5 million sites across the United States from 1857 to present are available. Geometric information of the channel could be obtained from the U.S. Army Corps of Engineers or the mapping system of the U.S. Census Bureau. The USACE is responsible for reporting the conditions of federally maintained navigation channels. The Census Bureau developed a system called TIGER (topologically integrated geographic encoding and referencing), which produces digital maps in collaboration with the U.S. Geological Survey.

(b) Water quality data

Water quality input data are different types of variables used in different models. For eutrophication simulation, they include concentrations of ammonia, nitrate, organic nitrogen, orthophosphate, total phosphorus, CBOD (Ultimate, 5-day), dissolved oxygen, and chlorophyll-a. For toxicant simulation, chemical and sediment concentrations are needed.

Water quality data can be found in state monitoring data, local projects, or EPA's Storage and Retrieval of U.S. Waterways Parametric Data (STORET) system. STORET is the EPA's primary water quality database system. It has collected nation wide water quality data since 1960s. The New York City Department of Environmental Protection has conducted a water quality monitoring program, namely the Howard Survey, in the New York-New Jersey Harbor Estuary. It has 53 monitoring stations with water quality data (e.g., DO, BOD, nutrient, etc.) collected regularly. USGS also provides water quality data, however, the monitoring stations are few in some areas.

(c) Pollutant loads data

In receiving water quality modeling, pollutant loads come from three sources: (1) point-source loads, (2) CSO loads, and (3) other non-point-source loads.

The point sources are those inputs that are considered to have a well-defined point of discharge, which, under most circumstances, is usually continuous and independent of storm events. Properties and rates of load from these point sources in storm events are the same as in dry weather. The two principal point source groupings are municipal wastewater and industrial discharges. They are usually the major sources of the nutrients and BOD loading in the receiving waters. Most of the pollutant discharge information can be found from federal or local government documents. The National Pollutant Discharge Elimination System (NPDES) permit program controls water pollution by regulating point sources that discharge pollutants into waters of the United States. By connecting to its web site (http://cfpub.epa.gov/npdes/), technical and regulatory information about the NPDES permit program can be found.

CSO load data may be found in local government monitoring program or state Discharge Monitoring Report (DMR) data. Most local governments have contracted the CSO monitoring program to consulting firms, and some of the monitoring reports can be obtained from the state government. DMR are used to report self-monitoring results by NPDES Permittees.

Other non-point sources include agriculture, groundwater, and urban runoff. In each case, the distinguishing feature of the nonpoint sources is that the origin of the discharge is diffuse. In the other words, it is difficult to relate the discharge to a specific well-defined location. However, comparing these discharges with other sources, they usually have a relatively small amount of flowrate, and can be neglected unless some specific toxicants are contained in these sources that raise concerned.

Since there is a great deal of information involved in a model, data must be organized after it is collected. Usually, a spreadsheet software is used to document the data. If the database is too large, a software called Water Resources Data Sources can be downloaded from the internet for free (Georgia Environmental Protection Division, 1993) to manage the data. It is also easier to check and copy data by using this software.

3.1.2 Model Creation

The choice of the appropriate modeling level or complexity depends upon the problem under investigation. Generally, the model complexity could be controlled by spatial variability, time variability, transport patterns, loading patterns, and chemical interactions. However, increasing model complexity does not usually result in an increase in model credibility because the ratios of model credibility and complexity would decrease as model complexity increases (Thomann, 1992). In other words, there may be

no significant advantage to the use of a dynamic model when a steady state model will suffice.

Receiving water modeling can involve single events or long-term simulations. Single event simulations are usually favored when using complex models, which require more input data and take significantly longer to run (although advances in computer technology keep pushing the limits of what can practically be achieved). Long-term simulations can predict water quality impacts on an annual basis.

CSO loads commonly are simulated separately from other loads in order to assess the relative impacts of CSOs. This is appropriate because the equations that best approximate receiving water quality are usually linear and so effects are additive (one exception, however, is the non-linear algal growth response to nutrient loadings).

The basic principle of both the hydrodynamics and water-quality programs is the conservation of mass. This principle requires that the mass of each water quality constituent being investigated must be accounted for in one way or another. To perform these mass balance computations, models must be supplied with the following input data to define seven important characteristics:

1) simulation and output control,
2) model segmentation,
3) advective and dispersive transport,
4) boundary concentrations,
5) point and diffuse source waste loads,
6) kinetic parameters, constants, and time functions, and
7) initial concentrations.

More detail about WASP 6.1 model creating will be described in Section 3.2.

3.1.3 Model Calibration and Validation

The model should be run initially to estimate events for which receiving water hydraulic and quality monitoring were actually conducted, and the model results should be compared to the measurements. The objective of model calibration is to adjust the input parameters so that there will be closer agreement between the simulated values and observed data (Ambrose, 1992; Bierman and Dolan, 1986). Both water quality and water quantity variables should be calibrated (Dames & Moore Inc. and AScI, 1994). Dilks et al. (1990) pointed out that hydrodynamic models should be calibrated before they are used to supply flow and volume data to water quality model. However, as Martin et al. (1990) stated, calibration processes for the models are still not well developed.

Achieving a high degree of accuracy in calibration can be difficult because:

1) Three-dimensional receiving water models are still not commonly used for CSO projects, so models involve spatial averaging (over the depth, width or cross-section). Thus, model results are not directly comparable with measurements, unless the measurements also have sufficient spatial resolution to allow comparable averaging.

2) Receiving water hydrodynamics are affected by numerous factors that are difficult to account for. Those include fluctuating winds, large-scale eddies, and density effects.

3) Pollutant loading inputs typically are estimates rather than precisely known values.

4) Loadings from non-CSO sources, such as storm water, upstream boundaries, point sources, and atmospheric deposition, often are not accurately known.

Validation is a process that estimates the magnitudes of predictive errors without coefficient adjustments (Heathcote, 1998; Lung, 1986; Ambrose, 1992). Validation allows researchers to compare a calibrated model prediction with predictions generated

from a second independent input data set that includes data about both flow and water quality under different external conditions (Canale et al., 1995; McCutcheon, 1989; Thomann, 1982). Cheng and Lockerbie (1994) have shown that model validation usually involves testing of calibrated models using different field data sets.

Inadequate model calibration and verification can result in spurious model results, particularly when the models are used for absolute predictions. Data limitations may require that the model results be used only for relative comparisons. Therefore, most models are more accurate when applied in a relative rather than an absolute manner.

3.1.4 Results Interpretation

Once a model is calibrated and verified, it can be used for following purposes:

1) When used for continuous rather than event simulation, as suggested by the CSO Control Policy, simulation models can predict the frequency of exceedances of water quality criteria.

2) The key result of receiving water modeling is the prediction of future conditions due to implementation of CSO control alternatives. In most cases, CSO control decisions will have to be supported by model predictions of the pollutant load reductions necessary to achieve water quality standards. In the receiving waters, criteria or design water quality conditions might be periods of low flow and high temperature that are established based on a review of available data. Flow, temperature, and other variables for these periods then form the basis for analysis of future conditions.

3) It is useful to assess the sensitivity of model results to variations in parameters, rate constants, and coefficients. A sensitivity analysis can determine which parameters, rate constants, and coefficients merit particular attention in evaluating CSO control alternatives.

It is important to note three factors that may influence the model output and produce unreasonable data. First, suspect data may result from calibration or verification data that are insufficient or inappropriately applied. Second, any given model, including detailed models, may not represent enough detail to adequately describe existing

conditions and generate reliable output. Finally, all models have limitations and the selected model may not be capable of simulating desired conditions. Model results must therefore be interpreted within the limitations of their testing and their range of application.

3.2 WASP 6.1 Model

3.2.1 Model Selection

The choice of model depends on the nature of data available for the system being investigated and the detail required in the assessment. Generally, the selection of a water quality model depends on six criteria (US EPA, 1987):

1) availability of pertinent documentation,
2) ease of application,
3) available time and resources.
4) applicability of model processes and variables,
5) hydrodynamic model capabilities, and
6) evidence of demonstrated applicability to size and type of project

After evaluation, WASP 6.1 was selected for this study. Some of the advantages of the WASP 6.1 model that render it favorable for this study are as follows:

1) WASP 6.1 has high flexibility in both spatial and temporal options. It can be used for both steady state and dynamic conditions and simulated under one, two, or three-dimensional systems.
2) WASP 6.1 can simulate most water quality constituents in almost any type of waterbodies.
3) The water quality, flow, and loading data required by WASP 6.1 are readily available for the study river.
4) WASP 6.1 is a free model and is available to the public.

5) WASP 6.1 is widely used around the world, especially in North America.

On the other hand, WASP 6.1 also has some limitations; it cannot handle floatable and sinkable materials as well as mixing zone situations. Thus, CSO discharges are assumed to be instantaneously, completely mixed with the receiving water in this study.

3.2.2 Overview of the WASP 6.1 Modeling System

As introduced earlier, WASP is a dynamic compartment model that can be used to analyze a variety of water quality problems in diverse water bodies such as ponds, streams, lakes, reservoirs, rivers, estuaries, and coastal waters. Version 6.1 of WASP, which was developed in 2002, is an enhancement of WASP 6.0. Basically, it consists of two stand-alone computer programs, DYNHYD5 and WASP 6, which can be run in conjunction or separately. The hydrodynamics program, DYNHYD5, simulates the movement of water while the water quality program, WASP 6, simulates the movement and interaction of pollutants within the water.

WASP 6.1 is supplied with four kinetic sub-models to simulate several major classes of water quality problems: conventional pollution (involving dissolved oxygen, biochemical oxygen demand, nutrients and eutrophication), toxic pollution (involving organic chemicals, metals, and sediments), mercury (including elemental Hg, divalent Hg, and methyl-Hg), thermal, and fecal coliform. The linkage of either sub-model with the WASP 6.1 program gives the models EUTRO, TOXI, Mercury, and Heat, respectively.

To create a water quality model in WASP 6.1, twelve entry data groups must be defined. They are model identification and simulation control, systems, segments, segment parameter scale factors, exchange, flows, boundaries, loads, time step, print

interval, time function, and constants. These input data, together with the general WASP 6.1 mass balance equations and the specific chemical kinetics equations, uniquely define a special set of water quality equations. These are numerically integrated by WASP 6.1 as the simulation proceeds in time. At user-specified print intervals, WASP 6.1 saves the values of all display variables for subsequent retrieval by a post-processor program. These programs allow the user to interactively produce graphs and tables of variables of all display variables.

3.2.3 The Model Network

To define model network is the very first step in the model creating process. It provides the model with the information about how the water moves. In other words, the hydrodynamic system must be defined before investigating water quality problems. The model network is a set of expanded control volumes, or "segments" that together represent the physical configuration of the water. Concentrations of water quality constituents are calculated within each segment. Transport rates of water quality constituents are calculated across the interface of adjoining segments. Segments in WASP may be one of four types: epilimnion layer (surface water), hypolimnion layers (subsurface), upper benthic layer, and lower benthic layers. The segment type plays an important role in bed sedimentation and in certain transformation processes.

Segment volumes and the simulation time step are directly related. As one increases or decreases, the other must do the same to insure stability and numerical accuracy. Segment size can vary dramatically. Characteristic sizes are dictated more by the spatial and temporal scale of the problem being analyzed than by the characteristics of the water body or the pollutant.

Time step consideration is used to determine the water quality frequency distribution that must be predicted. Basically, reducing the model time step allows better simulation of the frequency distribution. This increase in predictive ability, however, also entails an increase in the resolution of the input data.

Once the temporal variability has been determined, then the spatial variability of the water body must be considered. Generally, the most important spatial characteristics must be homogeneous within a segment. In some cases, this restriction can be relaxed by judicious averaging over width, depth, and/or length. Other important spatial characteristics to consider (depending upon the problem being analyzed) include temperature, light penetration, velocity, pH, benthic characteristics or fluxes, and sediment concentrations. A final, general guideline may be helpful in obtaining accurate simulations: water column volumes should be roughly the same. If flows vary significantly downstream, then segment volumes should increase or decrease proportionately.

3.2.4 The Model Mass Balance Algorithm

A mass balance equation for dissolved constituents in a body of water must account for all the material entering and leaving through direct and diffuse loading; advective and dispersive transport; and physical, chemical, and biological transformation (US EPA, 2000). Generally, mass balance for a one-dimensional model can be calculated by the following equation (Ambrose et al., 1993a):

$$\frac{\partial}{\partial t}(AC) = \frac{\partial}{\partial x}\left(-U_x AC + E_x A\frac{\partial C}{\partial x}\right) + A(S_L + S_B) + AS_K \qquad (3.1)$$

Where:

C = Concentration of the water quality constituent, mg/L or g/m^3

t = Time, days

U_X = Longitudinal advective velocities, m/day

E_X = Longitudinal diffusion coefficients, m^2/day

S_L = Direct and diffuse loading rate, g/m^3-day

S_B = Boundary loading rate (including upstream, downstream, benthic and atmospheric), g/m^3-day

S_K = Total kinetic transformation rate; positive is source, negative is sink, g/m^3-day

A = Cross-section area, m^2

The transformation processes are variable from model to model. It could be as simple as describing by an equation; it also could be as complex as solving a series of equations. The transformation process is defined depending on the purpose of the project.

In the EUTRO module, the reaction for each variable (BOD, DO, Ammonia, Nitrate, Organic Nitrogen, Orthophosphate, Organic phosphate), and its relationships to the other variables can be written as the following equations.

For BOD:

$$\frac{\partial C_5}{\partial t} = a_{OC}K_{1D}C_4 - k_d\theta_d^{T-20}\left(\frac{C_6}{K_{BOD}+C_6}\right)C_5 - \frac{v_{s3}(1-f_{D5})}{D}C_5 - \frac{5}{4}\frac{32}{14}k_{2D}\theta_{2D}^{T-20}\left(\frac{K_{NO3}}{K_{NO3}+C_6}\right)C_2$$

Death Oxidation Settling Denitrification

(3.2)

For DO:

$$\frac{\partial C_6}{\partial t} = k_2(C_8 - C_6) - k_d\theta_d^{T-20}\left(\frac{C_6}{K_{BOD}+C_6}\right)C_5 - \frac{64}{14}k_{12}\theta_{12}^{T-20}\left(\frac{C_6}{K_{NIT}+C_6}\right)C_1 \qquad (3.3)$$

Reaeration Oxidation Nitrification

$$-\frac{SOD}{D}\theta_s^{T-20} + G_{p1}\left(\frac{32}{12} + \frac{48}{14}\frac{14}{12}(1-P_{NH3})\right)C_4 - \frac{32}{12}k_{1R}\theta_{1R}^{T-20}C_4$$

Sediment demand Phytoplankton growth Respiration

Where:

a_{OC}: Oxygen to carbon ratio

a_{NC}: Phytoplankton nitrogen-carbon ratio

k_d: Deoxygenation rate @20°C

Θ_d: Temperature coefficient of deoxygenation rate

k_{BOD}: Half saturation constant for oxygen limitation

k_{12}: Nitrification rate @20°C

Θ_{12}: Temperature coefficient of nitrification rate

k_{NIT}: Half saturation constant for oxygen limitation in nitrification

k_{1R}: Phytoplankton respiration rate @20°C

Θ_{1R}: Temperature coefficient of phytoplankton respiration rate

SOD: Sediment Oxygen demand @20°C

Θ_S: Temperature coefficient of sediment Oxygen demand

For Ammonia:

$$\frac{\partial C_1}{\partial t} = D_{P1}a_{NC}(1-f_{ON})C_4 + k_{71}\theta_{71}^{T-20}\left(\frac{C_4}{K_{mPC}+C_4}\right)C_7 - G_{P1}a_{NC}P_{NH3}C_4 - k_{12}\theta_{12}^{T-20}\left(\frac{C_6}{K_{NIT}+C_6}\right)C_1 \qquad (3.4)$$

Death Mineralization Growth Settling

For Nitrate:

$$\frac{\partial C_2}{\partial t} = k_{12}\theta_{12}^{T-20}\left(\frac{C_6}{K_{NIT}+C_6}\right)C_1 - G_{P1}a_{NC}(1-P_{NH3})C_4 - k_{2D}\theta_{2D}^{T-20}\left(\frac{K_{NO3}}{K_{NO3}+C_4}\right)C_2 \qquad (3.5)$$

Nitrification Growth Denitrification

Where: $P_{NH3} = C_1\left(\frac{C_2}{(K_{mN}+C_1)(K_{mN}+C_2)}\right) + C_1\left(\frac{K_{mN}}{(C_1+C_2)(K_{mN}+C_2)}\right)$

For Organic Nitrogen:

$$\frac{\partial C_7}{\partial t} = D_{P1}a_{NC}f_{ON}C_4 - k_{71}\theta_{71}^{T-20}\left(\frac{C_4}{K_{mPC}+C_4}\right)C_7 - \frac{v_{s4}(1-f_{D7})}{D}C_7 \qquad (3.6)$$

Death Mineralization Settling

Where:

a_{NC}: Nitrogen to carbon ratio

K_{71}: Organic nitrogen mineralization rate@20°C

Θ_{71}: Temperature coefficient of Organic nitrogen mineralization rate

K_{12}: Nitrification rate@20°C

Θ_{12}: Temperature coefficient of Nitrification rate

K_{NIT}: Half saturation constant for oxygen limitation of nitrification

K_{2D}: Denitrification rate@20°C

Θ_{2D}: Temperature coefficient of Denitrification rate

K_{NO3}: Michaelis constant for denitrification

f_{ON}: Fraction of dead and respired phytoplankton recycled to the organic nitrogen pool

$(1-f_{ON})$: Fraction of dead and respired phytoplankton recycled to the ammonia nitrogen pool

P_{NH3}: Preference for ammonia uptake term

f_{D7}: Fraction of dissolved organic nitrogen

For Ortho-Phosphate:

$$\frac{\partial C_3}{\partial t} = D_{P1} a_{PC} (1 - f_{OP}) C_4 + k_{83} \theta_{83}^{T-20} \left(\frac{C_4}{K_{mPC} + C_4} \right) C_8 - G_{P1} a_{PC} C_4 \qquad (3.7)$$

Death Mineralization Growth

For Organic Phosphorus:

$$\frac{\partial C_8}{\partial t} = D_{P1} a_{PC} f_{OP} C_4 - k_{83} \theta_{83}^{T-20} \left(\frac{C_4}{K_{mPC} + C_4} \right) C_8 - \frac{v_{83} (1 - f_{D8})}{D} C_8 \qquad (3.8)$$

Death Mineralization Settling

Where:

a_{PC}: Phosphorus to carbon ratio

G_{P1}: Specific phytoplankton growth rate

D_{P1}: Specific phytoplankton loss rate

K_{83}: Dissolved organic phosphorus mineralization @20°C

Θ_{83}: Temperature coefficient of Dissolved organic phosphorus mineralization

K_{mPc}: Half saturation constant for phytoplankton limitation of phosphorus cycle

f_{OP}: Fraction of dead and respired phytoplankton recycled to the organic phosphorus pool

f_{D8}: Fraction of dissolved organic phosphorus in the water column

v_{83}: Organic matter settling velocity

In the TOXI module, several physical-chemical processes can affect the transport and fate of toxic chemicals in the aquatic environment. Some chemicals undergo a complex set of reactions, while others behave in a more simplified manner. WASP 6.1 allows the simulation of a variety of processes that may affect toxic chemicals.

In an aquatic environment, an organic chemical may be transferred between phases and may be degraded by any of a number of physical, chemical and biological processes. These include physical processes such as hydrophobic sorption, volatilization,

and sedimentation; chemical processes such as ionization, precipitation, dissolution, hydrolysis, photolysis, oxidation and reduction; and biological processes such as biodegradation and bioconcentration. WASP 6.1 explicitly handles most of these processes, excluding only reduction and precipitation-dissolution. All processes are described by rate equations. Rate equations may be quantified by first-order constants or by second-order chemical specific constants and environment-specific parameters that may vary in space and time.

In the Mercury model, three forms of mercury can be simulated: elemental Hg, divalent Hg, and methyl-Hg. These forms can be inter-changed in the environment. Divalent Hg released from sources such as power plants can be transformed to methyl Hg (bioaccumulated) or reduced to elemental Hg, which is non-reactive. Element Hg can oxidize to divalent Hg or vaporize to air. Usually, loss of Hg is due to volatilization and burial. The model allows for the interaction with three different solids types (sand, silt, and clay) and allows for the parameterization of the major components of mercury cycling in an aquatic environment.

The Heat model allows the user to simulate the change of temperature in receiving water using one of two approaches (full heat balance and equilibrium heat balance) as well as to model the fate and transport of fecal coliform.

The WASP is designed to provide a broad framework applicable to many environmental problems and to allow the user to match the model complexity with the requirements of the problem. After a series of evaluation, the WASP 6.1 was selected for creating a water quality model in this study.

CHAPTER 4

CASE STUDY: THE LOWER HUDSON RIVER BACKGROUND AND MODEL CREATION

To understand the impacts of CSOs on receiving waters and to establish an appropriate water quality model for the CSOs system, the Lower Hudson River, which has 40 CSO outfalls from New Jersey side, was selected as a case study. Background and historical water quality issues of the study area are introduced first in this chapter. The steps described in the previous chapters are followed to create receiving water models by using WASP 6.1. Three sub-modules were created in this study: EUTRO for DO, BOD and nitrogen simulation, Heat for pathogen simulation, and Mercury for mercury analysis.

4.1 Study Area

With a length of 306 miles and drainage area of 13,370 square miles in northeastern New York (93 percent), and parts of Vermont (3 percent), Massachusetts (2 percent), New Jersey (2 percent), and Connecticut (less than 1 percent), the Hudson River ranks 71st among 135 U.S. rivers that are more than 100 miles in length (Limburg et al., 1986). On the basis of mean annual discharge (1941 – 1970), the Hudson ranks 26th (19,500 cfs) of large rivers in the United States (Iseri and Langbein, 1974). Freshwater tributaries contribute approximately 81 percent of the total freshwater inflow to the New York Harbor (Table 4.1). The remainder of the freshwater input is contributed by wastewater (15 percent); urban runoff (4 percent); CSOs (1 percent); and industrial discharges, landfill leachate, and precipitation (less than 0.5 percent) (Brosnan and O'Shea, 1996).

Table 4.1 1989 Sources of "Freshwater" Flow into the NY/NJ Harbor

Water Source	Total flow (in percent) [a]
Tributaries	81%
Municipal point sources	15%
Urban runoff	4%
Combined sewer overflows (CSOs)	1%
Others	< 0.5%

Source: T. M. Brosnan and M. L. O'Shea. "Long-Term improvements in water quality due to sewage abatement in the Lower Hudson River." Estuaries. 19(4): 890-900.
a. Values across may not equal 100% due to rounding.

Mean monthly precipitation in the Hudson drainage basin has very little variation (about 80 mm/month), but monthly surface water discharge to the Hudson can vary by about an order of magnitude, due to the large seasonal difference in evapotranspiration, which ranges from about 0.5 mm/day during January to about 5 mm/day during July (Simpson and Anderson, 2001). Seasonal and interannual variation of streamflow of the Hudson River recorded at Green Island, New York, near Troy (USGS gage station: 01358000) is characterized by high flow during March through May, with the monthly mean peak flow of 927 m^3/s (32,719 cfs) observed in April. High spring flows are the result of spring snowmelt and runoff over the mountainous drainage basin. Low-flow conditions occur during July through September, with the mean monthly minimum of 164 m^3/s (5,797 cfs) observed during August.

Based on the data availability, the river section selected for this study is that from the New York City Limit (boundary between Westchester and Bronx counties) to the Battery (Figure 4.1). The length of the Lower Hudson River for this study is approximately 25 km. The width of the channel is approximately 1.5 km. This section is maintained as a shipping channel, and dredged to maintain a minimum depth of 9 to 11 meters, although portions of the river are much deeper. In this area, there are 40 CSO outfalls that are located in New Jersey. Most of 40 outfalls are from Jersey City,

Hoboken, Weehawken, and Edgewater; some of them are from West New York, North Bergen, Guttenberg, and Fort Lee (Table 4.2). Although New York City is one of the few large cities with combined sewer systems, there is no CSO discharge point in this section. All the CSOs in NYC are discharged to the East River and Jamaica Bay.

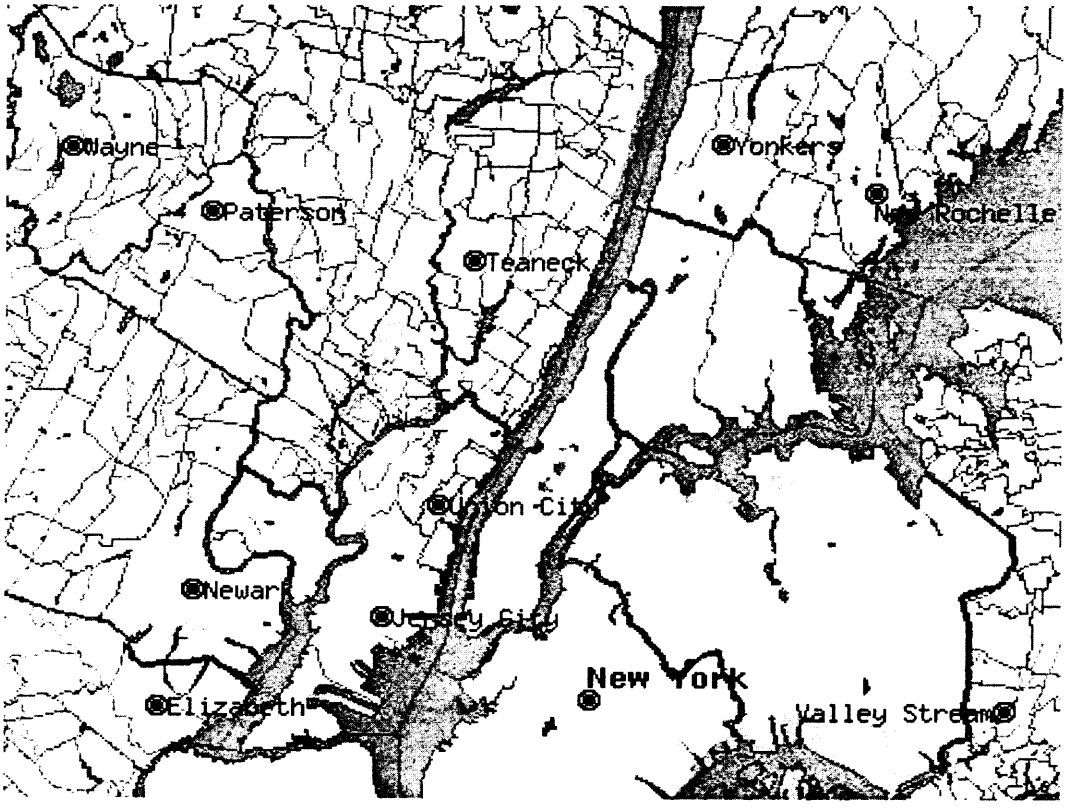

Figure 4.1 Map of the Study Area.

Table 4.2 Combined Sewer Overflow Discharge Points in the Study Area

Local Government Unit	Number of CSO Points	Receiving Waterbody
Fort Lee Borough	2	Hudson River
Edgewater MUA	7	Hudson River
North Bergen Township	2	Hudson River
Guttenberg	1	Hudson River
West New York MSU	2	Hudson River
Hoboken-Union City-Weehawken SA	11	Hudson River
Jersey City Sewerage Authority	15	Hudson River
Total	40	Hudson River

Source: U.S. Environmental Protection Agency (EPA). Report to Congress: Implementation and Enforcement of the Combined Sewer Overflow Control Policy. EPA 833-R-01-003. Office of Water, US EPA, Washington, DC.

Water uses of the Hudson River and New York Harbor include public water supply, municipal and industrial wastewater disposal, commercial shipping and navigation, recreational boating, swimming, and commercial and recreational fishing. Although commercial fishing was once a significant component of the New York – New Jersey regional economy, the abundance of commercially important fish and shellfish has declined considerably during the past century. The loss of once abundant fishery resources has been attributed to disease, over fishing, loss of habitat, and most important, poor water quality conditions (US EPA, 2000a).

4.2 Historical Water Quality Issues

Historically, water quality problems in the Hudson have included severe oxygen depletion and closure of shellfish beds and recreational beaches due to bacterial contamination. More recently, nutrient enrichment, algal blooms, heavy metals, sediment contamination, and bioaccumulation of toxics such as PCBs in striped bass (Faber, 1992; Thomann et al., 1991) and bald eagles (Revkin, 1997) have also become areas of concern. Due to the limited field data available and the model complexity, only four primary water quality concerns, DO, nitrogen, fecal coliform, and mercury, were simulated in this study.

DO is the most meaningful and direct signal relating municipal and industrial discharges to downstream water quality response over a wide range of temporal and spatial scales. In addition to DO's significance as a measure of aquatic ecosystem health, there are two very practical reasons for choosing DO as the signal for assessing changes in water quality. These are: (1) Historical records for DO go back as far as the early 20th century for many major waterbodies; (2) Basic testing procedures for measuring DO have

introduced few biases over the past century, thereby providing the analytical consistency needed for comparing historical and modern data (Wolman, 1971).

Long-term summer DO saturation records, collected almost continuously since 1909 at a station in the Hudson River near 42nd street on the west side of Manhattan (Figure 4.2), clearly document the trend of DO variation in the past century (Brosnan and O'Shea, 1996). Over a 40-year period from the 1920s through 1960s, summer oxygen saturation levels were only about 35 percent to 50 percent at the surface and 25 percent to 40 percent in bottom waters. Due to the impact of upgrading water pollution control facilities to full secondary treatment, which resulted in significant reductions in biochemical oxygen demand loading, DO saturation levels increased to about 90 percent at the surface and greater than 60 percent in the bottom waters by 1996 (Brosnan and O'Shea, 1996). DO concentrations have increased significantly since 1980s harbor wide (Brosnan and O'Shea, 1996; Parker and O'Reilly, 1991). In many waterways, the greatest oxygen and BOD_5 improvements were recorded between 1968 and 1984, coinciding with the greatest WPCP (Water Pollution Control Plant) construction and upgrading activity (O'Shea and Brosnan, 1997).

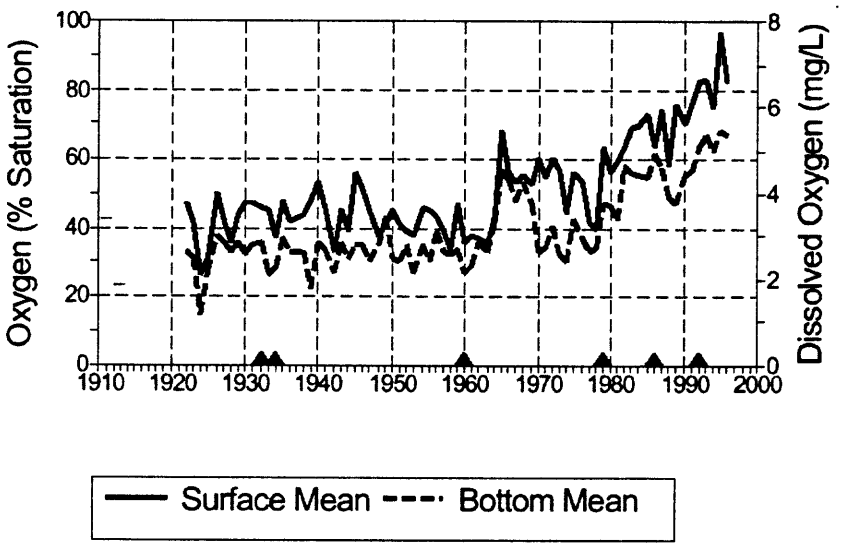

Figure 4.2 Long-Term Trends of DO (Summer Average) at 42nd Street in the Hudson River. Source: M. L. O'Shea and T. M. Brosnan. New York Harbor Water Quality Survey. Main Report and Appendices 1995. New York Department of Environmental Protection, Bureau of wastewater Pollution Control, Division of Scientific Service, Marine Sciences Section, Wards Island, NY.

According to the 2001 New York Harbor Water Quality Report, more detailed DO concentrations records were obtained for the Inner Harbor area, which includes the Hudson River from NYC-Westchester line, through the Battery to the Verrazano Narrows; the Lower East River to the Battery; and the Kill Van Kull-Arthur Kill system over the past 30 years. Figure 4.3 presents average summer DO values in the Inner Harbor, which have risen to levels above NYSDEC (New York State Department of Environmental Conservation) standards for primary contact recreation and commercial fisheries. Bottom water values have risen from 3 mg/L in 1970 to 5 mg/L at present. The mitigation of impacts from the WPCPs and CSOs has shown that swings in DO may be due to natural phenomenon such as weather (NYCDEP, 2001).

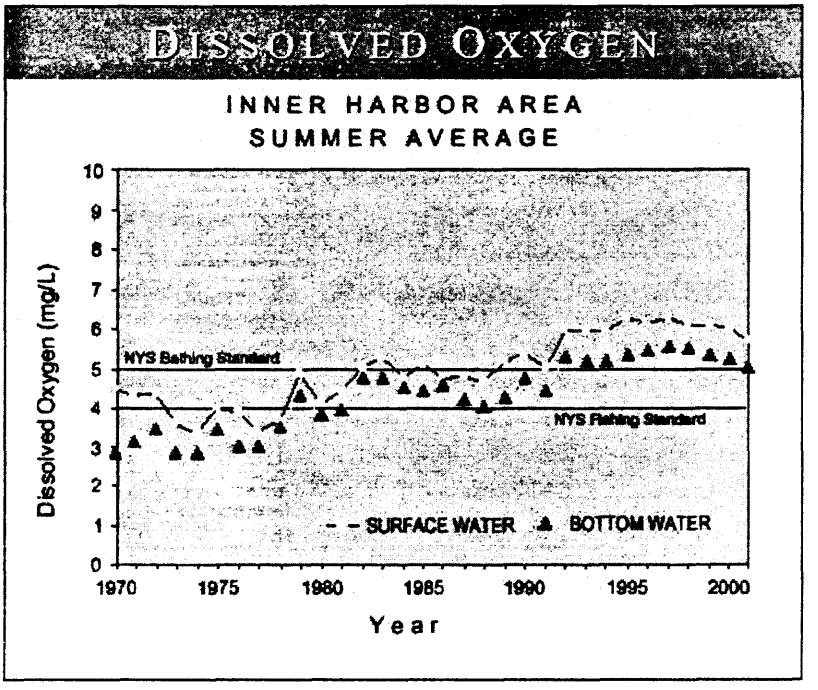

Figure 4.3 DO (Summer Average) Concentrations in the Inner Harbor. Source: New York City Department of Environmental Protection (NYCDEP). 2001 New York Harbor Water Quality Report. NYCDEP.

Eutrophication is the excessive growth of aquatic plants, both attached and planktonic to levels that are considered to be an interference with desirable water uses. The growth of aquatic plants result from many causes. One of the principal stimulants is an excess level of nutrients such as nitrogen and phosphorus (Thomann and Mueller, 1987). This problem has become increasingly acute in the mid 20th century due to the discharge of such nutrients by municipal and industrial sources, as well as from agricultural and urban runoff. However, the great improvement in nitrogen concentrations in the harbor seen in Figure 4.4 are attributed to new construction and upgrades of municipal wastewater plants in the Hudson-Raritan metropolitan region during the 1970s.

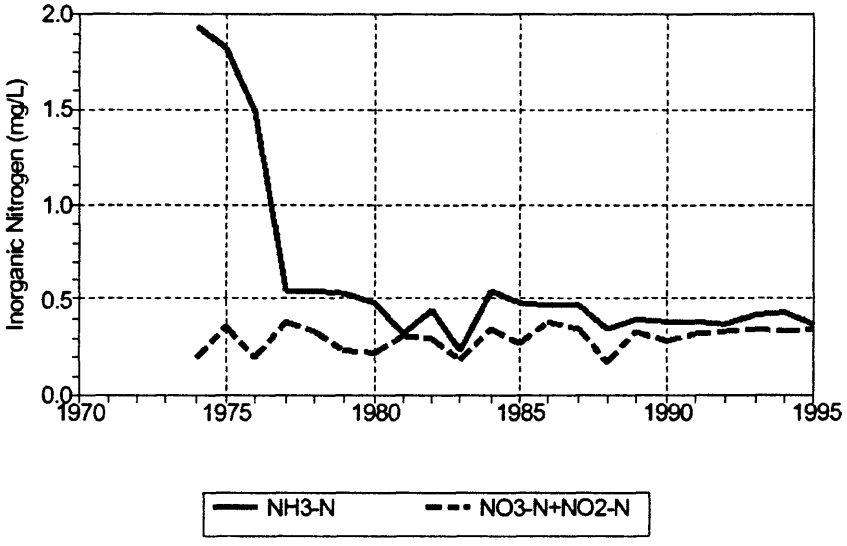

Figure 4.4 Long-Term Trend in Summer Mean Inorganic Nitrogen. Data Represent Harbor Wide Composite of 40 Stations Monitored Since at Least 1970. Source: M. L. O'Shea and T. M. Brosnan. New York Harbor Water Quality Survey. Main Report and Appendices 1995. New York Department of Environmental Protection, Bureau of Wastewater Pollution Control, Division of Scientific Service, Marine Sciences Section, Wards Island, NY.

By using historical data collected at 40 stations in the Inner Harbor area from 1973 to 2001, an analysis of harbor wide long-term trends clearly documented more than an order-of-magnitude improvement in total coliform and fecal coliform (FC) concentrations (Figure 4.5). The FC levels averaged over 2000 cells/100ml in the early 70's and have declined to below 100cells/100ml currently. The dramatic decline in bacterial levels is attributed to water pollution control infrastructure improvements that eliminated raw sewage discharges and upgraded all water pollution control plants to include disinfection by chlorination (O'Shea and Brosnan, 1997). Year to year variations have become more apparent with the reduction of FC to levels below standards.

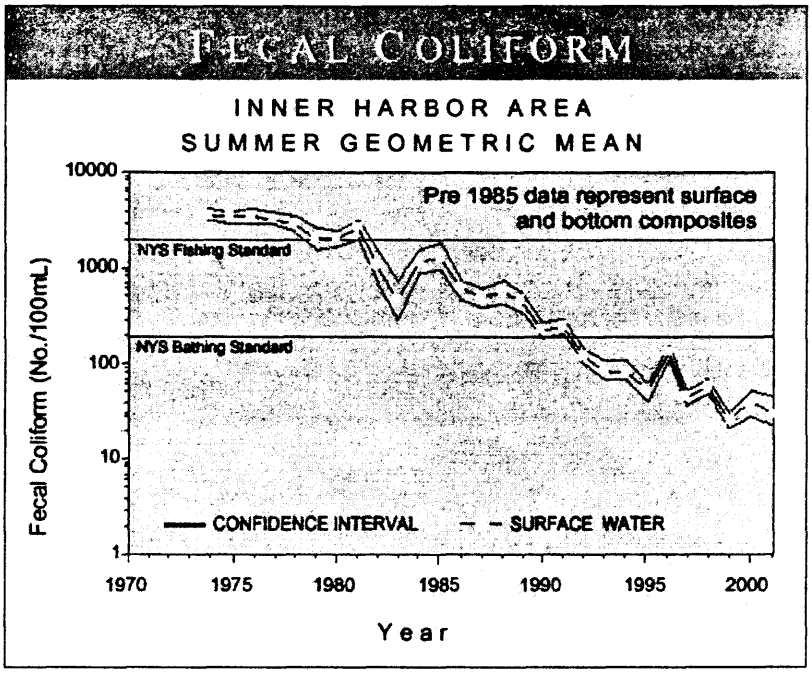

Figure 4-5 Fecal Coliform (Summer Average) Concentrations in the Inner Harbor. Source: New York City Department of Environmental Protection (NYCDEP). 2001 New York Harbor Water Quality Report. NYCDEP.

Past data have indicated that the Inner Harbor is prone to short duration episodic degradation following rain events due to additional FC loadings from storm drains and combined sewer overflows (CSOs). It has also been proven that the bacterial levels for most areas of the harbor could be reduced by approximately 50 percent by increased surveillance and maintenance of the entire sewer distribution system, including the capture of combined sewage during rain events (Brosnan and O'Shea, 1996a). While this continues to be true, the overall impact of such capture has been lessened. The fecal coliform simulation model could demonstrate this phenomenon mathematically.

According to the project report prepared by the Industrial Ecology for Pollution Prevention of the Harbor Consortium of the New York Academy of Sciences, whose objectives were to quantify the sources of past and present emissions of mercury in the

Hudson-Raritan basin (HRB), mercury inputs to NY/NJ Harbor since the mid-eighties have decreased by a factor of ten. Prior to 1985, the mercury concentration in Hudson River was estimated at 0.1 to 0.6 parts per billion (ppb). In contrast, multiple samples of the Hudson waters in the Harbor, in 1991, showed an average concentration of 0.021 ppb (Themelis and Gregory, 2001).

A similar improvement has been noted in sediments, a principal conveyor of mercury into the harbor. Core samples of sediments that were deposited in the past have revealed average mercury concentrations of 5-10 parts per million. In contrast, a 1993 survey of 84 samples of surficial sediments showed an average concentration of only 0.79 ppm. A similar survey in 1994 indicated an average surficial concentration of 0.70 ppm (Themelis and Gregory, 2001).

The rapid decrease of mercury into the Harbor by the end of the 20th century is partly due to the drastic curtailment of mercury use in the U.S., from a peak of 2,800 tons/year in the sixties to less than 350 tons by 2000. It is also due to switching from coal to gas fired boilers in the Hudson-Raritan basin area and the change from the polluting incinerators of the past to modern Waste-to-Energy plants (Themelis and Gregory, 2001). More recent investigations conducted under the auspices of the NY/NJ Harbor Estuary Program (HEP) indicated significantly lower metal concentrations, with harbor wide exceedances found only for mercury. Current monitoring and modeling efforts have greatly reduced the extent of waters suspected to be in violation of standards for nickel, lead, and copper (US EPA, 2000a).

Over the past several years, state-of-the-art coupled hydrodynamic and water quality models have been developed for water quality management studies of the harbor,

including New York City's Harbor-Wide Eutrophication Model and, most recently, the System-Wide Eutrophication Model (SWEM) (HydroQual, 1995, 1996, 1999). Earlier models, developed for US EPA's 208 Study of the harbor (Hazen and Sawyer, 1978; Higgins et al., 1978; Leo et al., 1978; O'Connor and Muller, 1984), have been used to assess the impact of secondary treatment requirements on DO in the Harbor. The more recent New York City models, employing improved loading estimates and state-of-the-art hydrodynamics (Blumberg et al., 1997), are being used to determine the feasibility and effectiveness of management alternatives for New York City point source of nitrogen. For example, SWEM will enable New York City to evaluate options as part of the facility planning for the Newton Creek WPCP. This model is further assisting the New York-New Jersey Harbor Estuary Program in understanding the complex relationships between physical transport processes, nitrogen loading, algal biomass, and DO in New York Harbor (HEP, 1996). Using a steady-state toxics model, the New York-New Jersey Harbor Estuary Program has also developed mass balance analyses for copper, nickel, and lead and a preliminary mass balance for mercury (HydroQual, 1995a).

4.3 Data Collection

As mentioned in the previous chapter, three sets of data were needed to create a receiving water quality model: water transport, water quality, and pollutant loads data.

a) Water transport data

Water transport data include geometric information of the study area and the stream flow.

To provide the geometric information for the Lower Hudson River, the width and length of the channel were measured from the TIGER digital map. The depth of the channel was estimated from the surface water monitoring data presented in STORET.

The stream flow data of the Hudson River were collected from U.S. Geological Survey. Since there is no gauge station located in the study area, the data in the nearest stations were used to estimate the flow rate at the lower section of the Hudson River. Five stations from Hadley to Green Island, NY were selected (Hadley, Fort Edward, Stillwater, Waterford, and Green Island). For each station, flow data for the period from July to October 1995 were used. Table 4.3 summarizes the flow data from these 5 selected stations. Based on the assumption that the flow rate is related to the drainage area, the flow rate at the up-boundary (NYC Limit) of the study area could be estimated by the derived relationship of flow rate and drainage area from the 5 monitoring stations. The relationship was derived by using regression analysis and can be expressed by the following equation:

$$\text{Flowrate} = 0.3364*(\text{Drainage Area}) + 1591 \qquad R^2 = 0.9705$$

Where: Flowrate = ft^3/s

Drainage area = mi^2

R = Correlation Coefficient

Table 4.3 Estimation of Flow Rate

Monitoring Station	Drainage Area	Flow rate (7/28)	
	mi^2	cfs	m^3/sec
Hadley	1664	2000	54
Fort Edward	2810	2500	67.5
Stillwater	3773	3000	81
Waterford	4604	3300	89
Green Island	8090	4200	113
Estimate			
U-Boundary	12900	5930	160

All the point source discharge information is based upon a reference report --- An Evaluation of the National Investment in Municipal Wastewater Treatment (US EPA, 2000). It provides pollution discharge records (both municipal and industrial discharge) and discharge criteria after various levels of treatment. Table 4.4 summarizes the water quantity and quality for the primary point sources in the study area. All the water quality values, shown in Table 4.4, were estimated from the reference paper based upon the degree of treatment (US EPA, 2000a).

Table 4.4 Characteristics of the Primary Point Sources in the Lower Hudson River

WTP	Location	Discharge (m^3/s)	$CBOD_U$	DO	NH_3-N	O-N	NO_3-N	O-P	Ortho-P
North River WTP	Seg.8	7.46	91.5	6.5	4.4	5.5	1	1.2	1.3
Edgewater STP	Seg.9	0.13	91.5	6.5	4.4	5.5	1	1.2	1.3
Woodclift STP	Seg12	0.10	172	2.1	9.6	12.0	2.2	2.6	2.7
West New York STP	Seg.13	0.30	172	2.1	9.6	12.0	2.2	2.6	2.7
Central STP	Seg.14	0.23	172	2.1	9.6	12.0	2.2	2.6	2.7
Hoboken STP	Seg.16	0.58	91.5	6.5	4.4	5.5	1	1.2	1.3

The CSO loads data came from the data monitored in three cities: Hoboken, Weehawken Township, and the City of Union City, New Jersey (CH2M HILL, 1996). The CSO load monitoring data of Jersey City were not available in this study, although Jersey City produced a large amount of CSO loads in this study area. The monitoring data were collected between July 28 and October 28, 1995. There were 9 storm events during this period. The pollutant loads for each storm event could be calculated by the measured flows and event mean concentrations (EMCs) for the tri-city area. Since the concentration data and the pollutographs (a plot to show the concentration vs. time) expose typically large variation in the concentration of pollutants within a storm event and from storm to storm, EMC was used to represent the water quality of CSOs in this study. EMC is the flow-weighted average concentration of a constituent during a period of storm runoff for

By using the same method, the flow rate for any location in the study area during the simulation period can also be estimated. This calculation will be confirmed in the salinity calibration.

b) Water quality data

Water quality data for the receiving water could be used as an initial condition in modeling, as well as observed data for calibration. For DO and pathogen simulations, since the data provided by STORET could not match the data provided by the Tri-City CSOs monitoring data, additional water quality data were obtained from the Howard Survey. There are 7 sampling stations in the Howard Survey for the study area. By using interpolation, water quality data at any location between two stations could be derived.

However, for mercury simulation, due to the absence of any long-term continuous mercury monitoring record in this area, observed data are not available for the mercury model. All the initial concentrations and boundary conditions in the mercury model were taken from similar mercury analyses of other aquatic systems. Absolute mercury concentration predictions could not be performed in this study due to the lack of information for calibration and validation. However, the mercury model can still be used for comparison study in various CSO control scenarios.

c) Pollutant loads data

Pollutant loads came from three sources: point sources, CSOs, and other non-point sources. As mentioned earlier, since the flow rate of the non-point sources was relatively smaller than other sources in this area, the loads resulting from non-point sources were neglected.

a specific area, which includes the variability of concentration exhibited during a storm event (Fisher and Katz, 1988). Table 4.5 shows the comparison of maximum and minimum EMCs in the Tri-City CSO system with the EPA reference data (US EPA, 1977), which is non-weighted average data collected from the northeastern area of the United States. The table indicates that all the EMCs derived from the Tri-City monitoring program for each pollutant variable are within the range of values presented by the Tri-City monitoring data and close to the EPA values. The weighted-average EMCs of the Tri-City area were used to calculate pollutant loads in this study.

Table 4.5 Comparison of EMCs

	EMCs (mg/L)			Loading factor		
	Tri-City Sites (Max)	Tri-City Sites (Min)	EPA	Tri-City Sites (Max)	Tri-City Sites (Min)	EPA
CBOD	528	64	367	1.44	0.17	1
BOD5	302	26	115	2.63	0.23	1
DO	8.38	5.91	7.44	1.13	0.79	1
NH3-N	4.21	0.64	2.08	2.02	0.31	1
Total Organic N	4.76	1.07	2.64	1.80	0.41	1
Total Organic P	3.27	1.08	0.95	3.44	1.14	1
Total Inorganic P	1.39	0.3	1	1.39	0.30	1
Fecal Coliform [a]	1915.9	197.3	670	2.86	0.26	1
Mercury [b]	6.39	1.30	---	---	---	---

a. Unit: 1000cells/100ml.
b. Unit: ppb

The estimates of pollutant load can be expressed by the following equation:

$$L = 10^{-3} \times V \times EMC$$

Where: L is load for the storm and discharge point (kg).

V is volume of overflow (m^3).

EMC is the volume-weighted average EMC (mg/L).

10^{-3} is the conversion factor.

Table 4.6 shows the calculated results of pollutant load for two monitored cities (Hoboken and Weehawken) and for one of nine monitored storm events (7/28/1995). Loads for other storm events were estimated by the same method.

Based on the assumption that all the outfalls have the same load properties in the study area, the pollutant loads for each segment can be calculated by the Tri-City CSO load data. After calculating the average load for one outfall in the Tri-City area, CSO load for each segment could be expressed by the following equation:

CSO load in Segment j = (Avg. load)*(# of outfalls in Segment j)

Table 4.6 Calculated CSO Loads at Hoboken and Weehawken

Date	Parameters	Load Units	Hoboken (6 outfalls)			Weehawken (5 outfalls)		
			Overflows (m^3)	EMCs (mg/L)	Total Load	Overflows (m^3)	EMCs (mg/L)	Total Load
7/28/95	BOD5	Kg	14838.8	101	1488.66	8971.4	65	580
	DO	kg	14838.8	7.95	117.18	8971.4	7.72	69.25
	COD	kg	14838.8	168.26	2480.02	8971.4	163.25	1473.4
	TKN	kg	14838.8	8.64	127.35	8971.4	9.59	86.02
	NH3-N	kg	14838.8	1.34	19.75	8971.4	1.8	16.14
	NO3-N	kg	14838.8	0.38	5.60	8971.4	0.73	6.55
	NO2-N	kg	14838.8	0.04	0.59	8971.4	0.06	0.54
	Total Phosphorus	kg	14838.8	2.47	36.41	8971.4	2.06	18.47
	Ortho-Phosphate	kg	14838.8	0.67	9.88	8971.4	0.51	4.57
	Total Hardness	kg	14838.8	39.74	585.74	8971.4	34.51	0.31
	Fecal Coliform.	10^9cells	14838.8	759,782[a]	112,447	8971.4	743,423[a]	6,668
	Mercury	kg	14838.8	193[b]	2.86	8971.4	3,834[b]	34.40

a. Unit: No. Cell/100ml
b. Unit: ppb

4.4 Model Implementation

4.4.1 Basic Assumptions

It is not possible to cover all possible factors, such as atmospheric input, biochemical reaction, etc., due to the data availability and model limitations. To create an appropriate and reasonable model, the following assumptions were made for this study.

For river modeling:

1) To simplify the model, rapid lateral mixing was assumed. In other words, lateral dispersion was neglected.

2) All the loads or any other inflows were assumed to be instantaneously, completely mixed with the receiving water. Both the water quality and quantity properties of the stream would be the same at any position in each designated segment.

3) Based on the assumption that the volume of the estuary, on average, remains constant, a tidally averaged model was used to describe the tide effect. Since the inflow tide equals outflow tide in this study, the impact of a tidal flow can be described by using dispersion or a tidal mixing coefficient.

4) Numerous factors, which may affect receiving water hydrodynamics, were difficult to account for in this study. These factors, which include large scale eddies, density effects, and leaching from undefined sources, were not considered.

For Input data:

1) It was assumed that the flowrate was related to the drainage area. A derived equation based on existing data is used for flowrate estimation.

2) It was assumed that the water quality data at any location could be derived between two conjunctive sampling stations by using interpolation.

3) The properties of all the point source pollutants remained constant during the simulation period in this study based on the assumptions that all the point-source loads were independent for each storm event. The impacts of pollutants from all the other non-point sources were neglected due to their relativity small flow rate.

4) In the pollutant loads estimation, CSO loads properties were assumed to be the same in all outfalls in the study area.

4.4.2 River Segmentation

The first thing in model implementation is to design an appropriate segment network. The river segmentation was based on proximity to water sampling stations, loading locations, hydraulic geometry, and water quality classification. The study area was divided into 19 segments (Figure 4.6). The water column layer was the only layer considered in each segment for the EUTRO model and FC simulation in this study. The vertical and lateral resolutions were not included because the river was assumed to be well mixed vertically and laterally. All the geometric data are measured from TIGER digital maps. Table 4.7 summarizes the information about the segments. It includes the scale of each segment and derived values of volume and cross-section area. The volumes of the segments in this study vary from 15.1 to 32.0 x 10^6 m^3, and the lengths of the segments are from 1090 to 1750 m. By using the continuity equation, the velocity in each segment was derived from cross-section area and estimated flow rate.

For the mercury simulations, since the interaction between the water column and the surficial sediment has major impact in constituent distribution in the aquatic system, 10 cm deep surficial sediment layers were added beneath the water column layers for each segment.

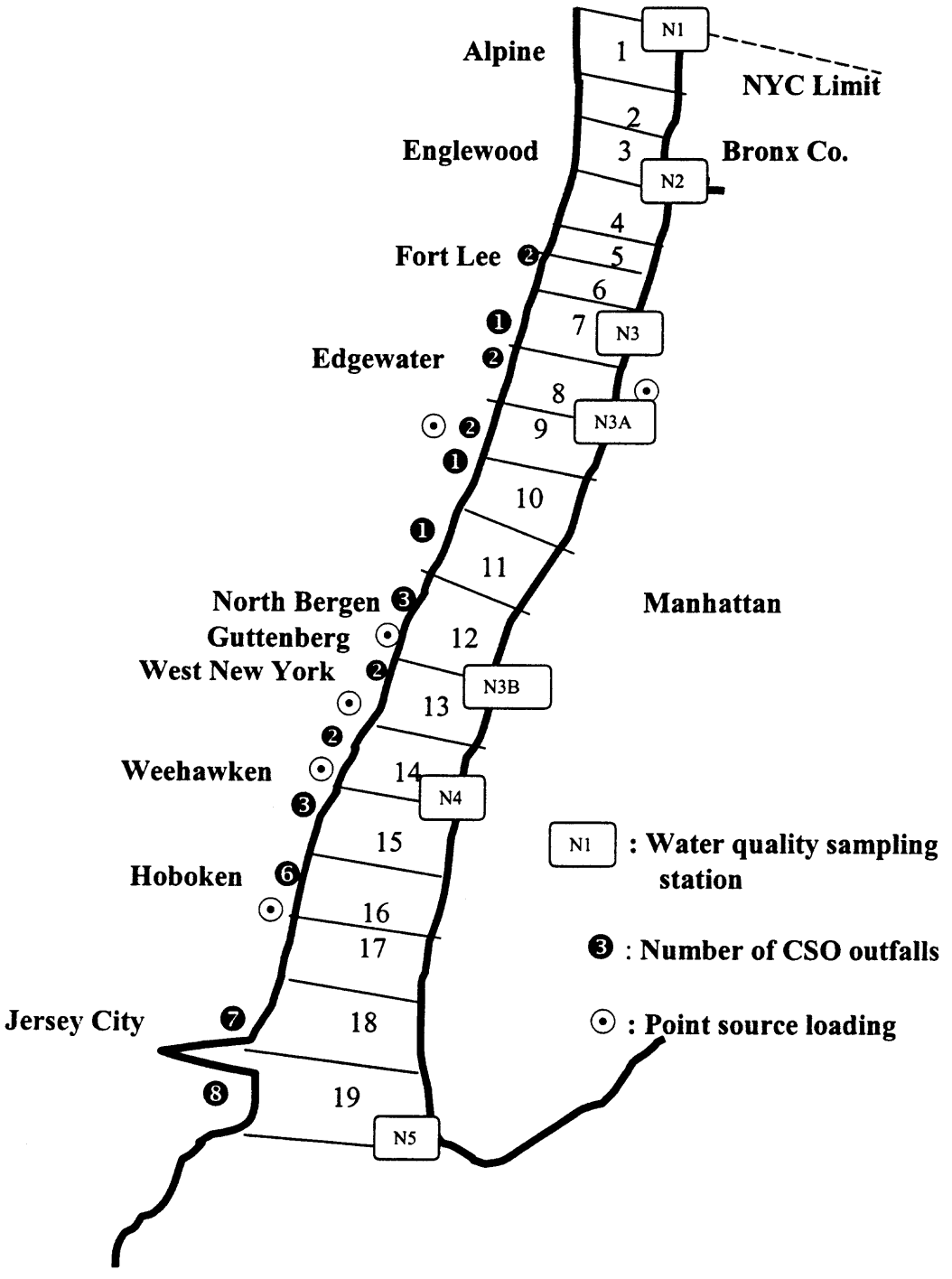

Figure 4.6 EUTRO Model Segmentation Schematic Diagram.

Table 4.7 Geometric Information of the 19 Segments

Segment Volume					Cross section Area	
Segment	Length(m)	Width(m)	Depth(m)	Volume(m^3)	Boundary	Area(m^2)
1	1410	1480	9.2	19198560	0~1	13340
2	1410	1540	9.2	19976880	1~2	13892
3	1410	1610	9.2	20884920	2~3	14444
4	1750	1490	11.4	29725500	3~4	18696
5	1750	1180	11.4	23541000	4~5	15276
6	1090	1050	13.2	15107400	5~6	13596
7	1090	1090	13.2	15682920	6~7	14124
8	1090	1130	13.2	16258440	7~8	14652
9	1090	1170	13.2	16833960	8~9	15180
10	1090	1210	13.2	17409480	9~10	15708
11	1090	1260	13.2	18128880	10~11	16236
12	1440	1270	11.6	21214080	11~12	14848
13	1440	1250	11.6	20880000	12~13	14616
14	1440	1240	11.6	20712960	13~14	14384
15	1360	1290	15.3	26842320	14~15	18819
16	1360	1420	15.3	29547360	15~16	20655
17	1360	1540	15.3	32044320	16~17	22644
18	1130	1530	15.6	26970840	17~18	24960
19	1130	1390	15.6	24502920	18~19	22776
					19~0	20592

4.4.3 Input Data for the Model

Input data for the WASP 6.1 simulation model are divided into 12 groups. This section presents an overview for each group. Subsequent sections detail the input data for various water quality simulations.

1) Model Identification and Simulation control: This data group is used for model identification and simulation control options.

2) Time step: the model time step can be set by the user or calculated by the WASP. Time step should be less than residence time in any segment. Inappropriate time step setting may generate instability and numerical faults in simulation and the model would be terminated during simulation.

3) Print interval: The print interval is the user specified time function in which simulation results will be written to the simulation result file.

4) Segments: This data entry allows the user to define the number of segments that will be considered in the simulation. Segment volume and constituent concentrations are also placed in this part.

5) Flows: This data group allows the user to define how the water moves. There are two options for flow simulation: one uses external hydrodynamic flows and another is defined by the user. The latter option is selected for this study. Input parameters in this group include transport field, advective flows, and segment routing (upstream and downstream). The flow input data in this study are estimated using the USGS daily flow records.

6) Systems: The system data entry allows the user to define the system in which variables (such as BOD, NH_3, etc.) will be simulated in modeling. It also defines the scale factor and conversion factor.

7) Parameter Scale Factors: This part defines which environmental parameters, such as temperature, light extension coefficient, salinity, and SOD, will be considered in the simulation as well as specifies a parameter scale factor. The environmental parameters used in this study were derived by using the data from the Howard Survey.

8) Constants: The data entry group includes constants and kinetics for the water quality constituents being simulated by the particular WASP model. The kinetic coefficient values used were based upon the results of some experimental studies (Canale et al., 1995; Heathcote, 1987; Lung and Paerl, 1988).

9) Time functions: The time function data entry forms allow the user to enter time variable environmental information.

10) Exchange: This data group defines the dispersive flows. Tidal effects can be described by adjusting the dispersion coefficient in this group.

11) Boundaries: Boundary concentrations must be specified for any segment receiving flow inputs, outputs, or exchanges from outside the model network. The boundary segments are automatically determined by WASP 6.1 when the user defines the transport patterns. Therefore, the user cannot enter boundary information until the transport information has been defined. In this study, the upstream boundary for inflow and the downstream boundary for outflow, and all the point sources inputs were defined during the simulation.

12) Loads: Basically, waste load data can be entered into WASP6.1 for each water quality variable for a given segment in two different ways. The first method calculates the waste loads by multiplying the concentration with the corresponding flow, and the resulting loads are defined in the group of "Boundaries" along with their related flow functions. Usually, this method is applied for the load sources with large discharges. In this study, point sources, such as discharges from WTPs, are entered by this method because their discharges are larger than those from the other sources, and their impact on hydrodynamic behaviors is therefore large. The other method, which inputs the waste discharges directly in the group called "Load" in the WASP model,

is usually used for the loads of less concern about water quantity because of their relatively small discharges. In this study, only the CSO loads were placed in this group and their hydrodynamic impacts were neglected. Usually, the load is treated as a point source in this method and it has a continuous time function. However, the combined sewer overflows are non-point sources and do not have a continuous loading time function. Technically, the input data can be processed as a point source load by setting the load rate as zero for the previous day and for the following day of a specific storm event. The Load input data was derived from the Tri-City CSO monitoring data as discussed previously.

4.4.4 DO/BOD/Nitrogen Simulation

To simulate dissolved oxygen with WASP 6.1, use the preprocessor to create a EUTRO input dataset. This section summarizes the input parameters in each group, described in the previous chapter, which must be specified in order to solve the WASP 6.1 mass balance equation.

1) Model Identification and Simulation control:

   a) Simulation type: EUTRO.

   b) Simulation title: DO simulation in the Lower Hudson River.

   c) Time Range: 7/12/1995, 12:00AM to 9/19/1995, 12:00 PM.

   d) Hydrodynamics: Net flow.

   e) Restart option: No restart.

   f) Bed Volume: Static.

   g) Time step: WASP calculated.

2) Time step:

   To maintain stability and minimize numerical dispersion, the WASP calculated time step was used.

3) Print interval:

The print interval was kept the same value at 0.5 day for whole simulation period.

4) Segments:

a) Segments: The study area was divided into 19 segments. All the geometric data are shown in Table 4.7.

b) Initial concentrations: Water quality data, summarized in Table 4.8, were obtained from the Howard Survey.

Table 4.8 Initial Concentration of EUTRO Model (Date: 7/12/95)

Sampling Station	Segment	DO mg/L	BOD mg/L	Chlorophyl-a ug/L	Salinity psu	NH3-N mg/L	NO3-N mg/L	Organic-P mg/L	Ortho-PO4 mg/L
N1	Boundary	5.37	4.8	13.54	16.66	0.25	0.63	0.11	0.05
	1	5.37	4.75	11.78	16.62	0.27	0.63	0.11	0.06
	2	5.37	4.7	10.02	16.59	0.29	0.62	0.11	0.07
	3	5.36	4.65	5.26	16.55	0.3	0.61	0.11	0.08
N2	4	5.36	4.6	6.5	16.52	0.32	0.61	0.11	0.09
	5	5.19	4.57	5.9	17.8	0.36	0.59	0.12	0.07
	6	5.03	4.54	5.3	19.08	0.4	0.57	0.12	0.05
N3	7	4.87	4.5	4.8	20.46	0.45	0.55	0.13	0.04
	8	4.92	4.4	5.5	21.1	0.42	0.54	0.13	0.04
N3B	9	4.96	4.3	6.2	21.71	0.39	0.53	0.12	0.03
	10	4.92	4.3	6.07	22.15	0.39	0.52	0.12	0.03
	11	4.88	4.3	5.95	22.59	0.4	0.51	0.12	0.03
	12	4.84	4.3	5.83	23.03	0.41	0.5	0.12	0.03
N3A	13	4.8	4.3	5.7	23.47	0.41	0.49	0.12	0.03
	14	4.85	4.4	5.75	23.13	0.41	0.5	0.12	0.03
N4	15	4.9	4.5	5.8	22.8	0.4	0.5	0.12	0.03
	16	5.02	4.68	8	23.33	0.4	0.48	0.12	0.03
	17	5.14	4.86	10.2	23.86	0.41	0.46	0.12	0.03
	18	5.26	5.04	12.4	24.39	0.41	0.44	0.12	0.04
	19	5.37	5.22	14.7	24.91	0.42	0.42	0.12	0.04
N5	Boundary	5.48	5.4	17	25.43	0.42	0.4	0.12	0.04

5) Flows:

Seven flow functions, one mainstream flow and six point source discharges, are defined in EUTRO model. The mainstream flow input data were estimated from the USGS daily flow records. The discharges of six point sources, which

include North River WTP, Edgewater STP, Woodclift STP, West New York STP, Central STP, and Hoboken STP, were estimated from the average daily discharge record reported in 1996 Clean Water Needs Survey (US EPA, 1996a).

6) Systems:

Select "simulate" for all the system, except for selecting "constant" for Chlorophyl-a system and "bypass" for PO_4 and OP. For this implementation, the BOD system was used to represent ultimate CBOD ($CBOD_U$).

7) Parameter Scale Factors:

Specify the environmental condition by a time function or a spatial constant for each segment. In this module, temperature was set as time function 1, which was obtained from the Howard Survey. The SOD concentration, estimated from the reference (Thomann, 1972), was set as 1.5 $g\text{-}O_2/m^2day$ for all segments.

8) Constants:

Appendix B summarized kinetic constants used in previous similar water quality modeling studies. The constants, used initially in this study, were selected from Appendix B and are shown in Table 4.9. Specified values for constants apply over the entire network for the whole simulation. Some of these constants were adjusted to fit observed data during the calibration process.

Table 4.9 Kinetic Constants Used in the Initial Simulation

Constant	Unit	Value
Nitrification Rate @20°C	1/day	0.11
Nitrification Temperature Coefficient	---	1.08
Half-Saturation: Nitrification Oxygen Limit	mg O2/L	2
Denitrification Rate @20°C	1/day	0.09
Denitrification Temperature Coefficient	---	1.045
Half Saturation: Denitrification Oxygen Limit	mg O2/L	0.1
Dissolved Organic Nitrogen Mineralization Rate @20°C	1/day	0.075
Dissolved Organic Nitrogen Mineralization Temperature Coefficient	---	1.08
Organic Nitrogen Decay in Sediments	1/day	0.0004
Organic Nitrogen Decay in Sediment Temperature Coefficient	---	1.08
Fraction of Phytoplankton Death Recycled to Organic Nitrogen,	---	0.5
Mineralization Rate of Dissolved Organic Phosphorus @20°C	---	0.22
Dissolved Organic Phosphorus Mineralization Temperature Coefficient	---	1.08
Organic Phosphorus Decay Rate in Sediments	1/day	0.0004
Organic Phosphorus Decay in Sediments Temperature Coefficient	---	1.08
Fraction of Phytoplankton Death Recycled to Organic Phosphorus	---	0.5
Oxygen::Carbon Stoichiometeric Ratio	---	2.67
Reaeration Rate Constant @20°C	1/day	4.4
CBOD Decay Rate @20°C	1/day	0.18
CBOD Decay Rate Temperature Correction	---	1.047
CBOD Decay Rate in Sediments	1/day	0.0004
CBOD Decay Rate in Sediments Temperature Correction	---	1.08
CBOD Half Saturation Oxygen Limit	mg O2/L	0.5
Phytoplankton Maximum Growth Rate @20°C	1/day	2
Phytoplankton Growth Temperature Coefficient	---	1.068
Phytoplankton Maximum Quantum Yield Constant	Mg C/mole photons	720
Phytoplankton Self Shading Extinction	---	0.017
Phytoplankton Carbon::Chlorophyll Ratio	---	35
Phytoplankton Optimal Light Saturation	Ly/day	350
Phytoplankton Half-Saturation Constant for Nitrogen	mg-N/L	25
Phytoplankton Half-Saturation Constant for Phosphorus	mg-P/L	1
Phytoplankton Endogenous Respiration Rate @20°C	1/day	0.125
Phytoplankton Respiration Temperature Coefficient	---	1.045
Phytoplankton Death Rate Non-Zooplankton Predation	1/day	0.02
Phytoplankton Zooplankton Grazing Rate	L/cell-day	0
Phytoplankton Phosphorus : Carbon Ratio	---	0.025
Phytoplankton Nitrogen : Carbon Ratio	---	0.25
Nutrient Limitation Option	---	0

9) Time functions:

Only one water temperature time function was specified in the EUTRO model. The data came from the Howard Survey.

10) Exchange:

The dispersion coefficient was initially set as 600 m^2/s based upon the reference data in the Hudson estuary (O'Connor and Mueller, 1984). The value was adjusted in the salinity calibration.

11) Boundaries:

In this study, seven flow functions were defined earlier. The boundary concentrations for each constituent must be specified for each defined flow function. The boundary concentrations of the mainstream were obtained from the Howard Survey. All the water quality data for the point source discharges are shown in Table 4.4.

12) Loads:

The load input data were derived from the Tri-City monitoring data as discussed previously. Appendix A summarizes the load input data for each pollutant in each segment.

4.4.5 Pathogen Simulation

Fecal coliform, a human-health related indicator, was selected in the pathogen simulation. The HEAT module was used to simulate bacteria in WASP 6.1. For a portion of the dataset including time step, print interval, segmentations, flow functions, and exchange coefficients, the FC simulation inputs are the same as those used for the EUTRO model. Because these parameters have been described in the previous sections, they are not repeated here. This section highlights the parameters that were added or modified in the FC balance simulation.

The Heat model can simulate not only the coliform distribution but also the water temperature variation. However, to simplify the model complexity, select "simulate" for coliform, and "bypass" for all the other pollutants in the system.

Temperature, concentrations of salinity and fecal coliform were specified for the initial condition. It should be noted that the unit of fecal coliform concentration in the input data is cell/ml, and not the commonly used 100 cells/ml, which is used in the FC mass balance equation in WASP model.

Fecal coliform was the only pollutant input for the boundary conditions. In seven defined flow functions, only the concentrations in the mainstream were specified in the boundary condition. Because of the relatively low fecal coliform concentrations in point source discharges, the bacteria loads form the point sources were neglected.

Coliform bacteria death rate (day^{-1}) was the primary constant specified for the FC simulation. The reference values of the coliform bacteria death rate were between 0 to 6.1 for New York Harbor (Thomann and Mueller, 1987). It was initially set as 2.0 day^{-1} and later adjusted in the calibration process.

The FC load data, summarized in Appendix A, were derived from the Tri-City monitoring data. The load unit of fecal coliform is billion cells/day in the HEAT model.

4.4.6 Mercury Simulation

It is more complicated to create a mercury simulation model than to create DO or FC simulation models. The difficulties come from: (1) The observed data for mercury was not available for the study area; and (2) The mechanisms of transport or transformation processes of mercury are complicated and uncertain, and the reference constant values are limited. Although most of the reaction constants and environmental parameters,

which include initial and boundary concentrations, were taken from similar mercury simulation models (Ambrose and Wool, 2002), the model predicted value could only be used as a reference because of the lack of calibration. However, it can still be useful in investigating the impacts of CSO loading. For example, the use of the sensitivity analysis for various parameters in mercury distribution processes can be instructive.

Before creating a mercury model, the following assumptions were made to simplify the model.

1) The Mercury model can simulate three mercury components --- elemental mercury [Hg^0], inorganic divalent mercury [Hg(II)], and monomethyl mercury [MeHg]. Because the concentrations of Hg^0 and MeHg are much less than that of Hg(II), inorganic divalent mercury was treated as a single total mercury component in this study.

2) The loading property of the mercury introduced by atmospheric deposition and all the other point and non-point sources were kept the same during the simulation period. The difference between simulated results was only introduced by the various CSO loading scenarios.

3) Processes simulated in the Mercury model include advection, sediment exchange, reduction, volatilization, methylation, and demethylation in the water column; and methylation and demethylation in the sediment. Except for the sorption, which is represented as equilibrium reactions governed by specified partition coefficients, all the other transformation processes are represented as first-order reactions governed by specified rate constants.

4) Two types of solids were simulated --- silt and sand. Silt is suspended both in the water column and in the sediment. It was assumed that 10 mg/L of silt entered at the upstream boundary. It was also assumed that sand makes up half of the benthic sediment compartments. The concentration was set as 50,000 mg/L in sediment for both silt and sand.

Part of the dataset in the mercury simulation, which includes time step, print interval, and exchange coefficients is the same as those used in DO and FC simulation, so only those added or modified in mercury simulation are highlighted here.

The segmentation of the Mercury model has been briefly introduced in the previous sections. In addition to the 19 water column segments, 19 surficial sediment

layers were added beneath the water layers and the depth of the sediment layer was 10 cm. The volume and cross-section areas, which were used to define the flow function of pore water, were derived. The cross-section used here is the interface area between the water column and the sediment layer.

The initial concentrations of mercury were specified in the Mercury model. The initial Hg(II) concentration was set as 0.3 μg/L (0.3 ppb) in the water column, which was estimated from the Hg concentration in the Hudson River in 1970, and 6.0 ng/g (6.0 ppb) in sediment, which was quoted from a similar mercury simulation model (Ambrose and Wool, 2002). The other two mercury component concentrations were set at zero. Again, for the mass balance calculation in the WASP model, the units, μg/L and ng/g, were converted to mg/L and mg/kg, respectively.

In addition to the existing surface water flow functions, two new flow functions, which describe the silt transport process between the water column and the sediment, were defined. The settling and resuspension velocities of silt were set as 0.3 m/day and 0.006 m/day, respectively. For pore water exchange, 10^{-5} cm^2/sec was used for the sediment-water column diffusion coefficient. To keep all the units the same as those defined for surface water, conversion factors were also specified.

Several environmental parameters were also specified in the Mercury model. Changes of temperature and wind speed were set as time functions. The concentration of dissolved organic carbon (DOC), which has an impact on equilibrium sorption between mercury components, was set as 5 mg/L based upon the reference values (Thomann and Mueller, 1987). Some transformation processes, including reduction and demethylation,

are driven by sunlight. The light extinction coefficient was assumed to be 0.5 m^{-1} for the water column layers.

Because of the lack of observed data, calibration processes could not be performed by adjusting the reaction constants. To represent the worst condition, the maximum reference values were selected for all the kinetic constants in the mercury simulation.

The mercury load data, summarized in Appendix A, were derived from the Tri-City monitoring data. The load unit of mercury used is 10^{-3} kg/day in the Mercury model. A conversion factor 10^{-3} was set in input data for converting load unit to kg/day to match requisition of WASP model in mass balance.

4.4.7 Result Generation

Once the model was successfully executed, the Graphical Post-Processor of WASP 6.1 was used to rapidly evaluate the results of the model simulations and its support programs. Several options for data output can be applied. ArcView shape file can be used in the spatial analysis mode to aid the user in displaying the model network with respect to its geography and surrounding characteristics. The binary model geometry file can be used to provide the spatial grid geometry information. The x/y plot can be used to display the distribution of the variables with respect to time, segment, or distance. In this study, the x/y plot was used to compare simulation results of various scenarios.

CHAPTER 5

MODEL CALIBRATION AND VALIDATION

Model results must be tested against field observed data during calibration and validation. Generally, receiving water models are calibrated by varying the kinetic constants. Usually the variation starts with hydraulics parameters and then continues with water quality parameters. For the EUTRO model, the first two-months collected data, from July 12, 1995 to September 19, 1995 were used to calibrate the model. The remaining data from September 19, 1995 to October 31, 1995 were used as the second independent field data to verify the calibrated model. In this study, due to the limited observed data, validation was not performed for the FC simulation. The same limitation restricts the calibration and validation in the Mercury model due to the lack of initial and boundary conditions.

5.1 Calibration Approach

After determination of the water quality and flow data and environmental parameters, values for model coefficients and process rate constants were selected through calibration and the results of this process were plotted against the available field data. The calibration approach used here was to fix the values of as many model coefficients as possible, based on direct measurement. Subsequently, values for the remaining coefficients were adjusted within ranges reported in the literature to produce the best fit between model output and field observations. Model coefficients were not allowed to assume arbitrary values in order to obtain the best possible curve fit in a strictly

mathematical sense. The principal literature sources used to guide the calibration effort are summarized in Appendix B.

For convenience in calibration, WASP6.1 has a function to display observed data versus the predicted model result. However, observed data must be stored in a particular form, such as in a Paradox 4.5 or other higher database format (*.DB) to be available for plotting. In this study, Database Desktop 7.0 (Borland International, Inc., 1992), the software that can create, view, sort, modify, and query data tables in a variety of Paradox, dBASE, and SQL formats, was used to create observed data files.

Two perspectives of calibration were applied in this study: temporal variation and spatial distribution. In temporal variation, the model displays the variation of variables with respect to time in a specific segment. It was used to calibrate the model to match the field data for the whole simulation period. In spatial distribution, the model displays the distribution of variables with respect to segments in a specific date. It was used to calibrate the model to match the observed measurements overall in the study area.

The goal for the calibration was to produce maximum correspondence between field data and modeling output, which can be evaluated by Correlation Coefficient Square (R^2), and a minimum in difference between predicted and observed values, which can be examined by Root Mean Square Error (RMSE). The post-processor of WASP provides both calculation functions for curves defined within the x/y plot window. The RMSE is calculated by the following equation:

$$RMSE = \{[\Sigma (Co - C_p)^2] / N\}^{0.5}$$

Where: Co: Observed value
Cp: Predicted value
N: Number of measurements

A high Correlation Coefficient Square indicates that the model is predicted in a similar variation pattern as the data observed in the field. On the other hand, a low RMSE presents the condition that the average absolute values between predicted and observed data for monitoring points during the simulated period are close. During the calibration process, both criteria must be considered. Good agreement in only the predicted pattern or only the predicted values alone might not indicate the best fit for calibration.

5.2 Model Calibration

In the EUTRO model, calibration starts with physical parameters such as hydraulics or salinity, then proceeds with DO/BOD, NH_3, phosphorus, and Chlorophyll, preferably in this sequence. However, for DO/BOD/nitrogen simulation, phosphorus, and Chlorophyll were not simulated and were not counted in the calibration process. Several parameters are commonly used to calibrate in the DO/BOD simulation. The primary parameters used in the calibration process are DO reaeration rate, nitrification rate, BOD decay rate, and oxygen demand in sediments (SOD). In the FC simulation, the bacteria death rate is the primary consideration during the calibration process.

5.2.1 Physical Parameters Calibration

Hydraulic parameters should be adjusted before water quality calibration. Stream flows and longitudinal dispersion are two primary parameters considered in hydraulic calibration.

Since all the flow data were estimated from USGS and relative reports, no field data were available for comparison during calibration. The alternative method used in this study was to use a conservative substance. A conservative substance, such as

salinity, is one that does not undergo any chemical or biological transformation or degradation in a given ecosystem. By comparing the concentration of the salinity between the predicted and observed data, it can determine if the dispersion or flowrate was overestimated or underestimated.

Longitudinal dispersion is one of the important processes that govern transport of water quality constituents in an estuary system. The mechanisms controlling the longitudinal dispersion of dissolved and suspended matter in estuaries are numerous and complicated (Chatwin and Allen, 1985). The accurate determination of dispersion coefficients is an essential requirement for the simulation of dispersive transport. According to the reference report (Hydroscience, 1971), a high value of 600 m^2/s was used initially for the dispersivity because it was assumed that mixing in the estuary is very intensive owing to tidal effects. In general, the coefficients should vary from segment to segment as a result of local geometry and friction, and a slight trend of landward decrease should be employed. However, in this study, a simplifying assumption, based upon the fact that the study area was constricted and close to the river mouth, that the coefficient be kept constant for all the segments was made. In order to verify the dispersion coefficients, simulation of salinity was performed.

Table 5.1 presents the trial sequence of salinity calibration. Both parameters, dispersion coefficient and flowrate, were calibrated during the process. The initial input of flow function and dispersion coefficient, 600 m^2/s, were verified after calibration. Table 5.2 summarized the final result. In the simulation period, July 12 to September 19, 1995, all the sampling points (Segments 4, 7, 9, 13, 15 and 19) generally show good agreement, especially for the downstream segments. Correlation Coefficient Squares

were above 0.90, except in segment 7 (0.8), and RMSE were within 5%, except in segment 13 (10.1%) and segment 15 (7.5%). Figure 5.1 illustrates the plots of calibration result for each segment.

Comparing the predicted value with the observed data, salinity calibration results also show a good match in spatial distribution (Table 5.3). Figure 5.2 indicates that most observed data points fall close to the predicted trend line, except for the data on 9/19. This could be due to sampling or sample analysis error or that the sampling date was too close to the storm events (9/17 and 9/22) to have a stable reading of salinity.

Table 5.1 Trial Sequence of Salinity Calibration (Simulation Period: 7/12/95 ~9/19/95)

Trial	Correlation Coefficient Square			RMSE			Dispersion	
	Seg9	Seg15	Seg19	Seg9	Seg15	Seg19	Coefficient	Flowrate
1	0.89	0.93	1.00	0.78(4.4%)	1.50(7.2%)	0.17(0.7%)	300	x1
2	0.90	0.92	1.00	0.87(4.8%)	1.56(7.4%)	0.15(0.7%)	450	x1
3	0.91	0.91	1.00	0.92(5.0%)	1.59(7.5%)	0.15(0.7%)	600	x1
4	0.92	0.91	1.00	0.95(5.2%)	1.61(7.6%)	0.14(0.6%)	750	x1
5	0.92	0.90	1.00	0.96(5.3%)	1.62(7.6%)	0.14(0.6%)	900	x1
6	0.92	0.90	1.00	0.99(5.4%)	1.64(7.7%)	0.14(0.6%)	1200	x1
7	0.88	0.93	0.99	0.78(4.4%)	1.51(7.2%)	0.16(0.7%)	600---300	x1
8	0.91	0.90	1.00	0.96(5.3%)	1.62(7.6%)	0.14(0.6%)	600---900	x1
9	0.84	0.93	0.99	0.66(3.7%)	1.41(6.8%)	0.19(0.8%)	600---200	x1
10	0.91	0.91	1.00	0.87(4.8%)	1.56(7.4%)	0.15(0.7%)	600	x1.2
11	0.91	0.91	1.00	0.90(4.9%)	1.58(7.5%)	0.15(0.7%)	600	x1.1
12	0.91	0.91	1.00	0.94(5.1%)	1.61(7.6%)	0.14(0.6%)	600	x0.9
13	0.91	0.91	1.00	0.96(5.3%)	1.62(7.7%)	0.14(0.6%)	600	x0.8

Table 5.2 Statistical Result of Salinity Calibration (Temporal Variation)

Segment	Seg4	Seg7	Seg9	Seg13	Seg15	Seg19
R^2	0.96	0.80	0.91	0.91	0.96	0.99
RMSE	0.43	0.35	0.92	2.03	1.59	0.15
%	2.8%	2.0%	5.0%	10.1%	7.5%	0.7%

Table 5.3 Statistical Result of Salinity Calibration (Spatial Distribution)

Date	8/8	8/23	8/30	9/19
R^2	0.81	0.74	0.94	0.64
RMSE	1.02	1.54	0.77	2.42
%	5.9%	8.5%	4.0%	14.8%

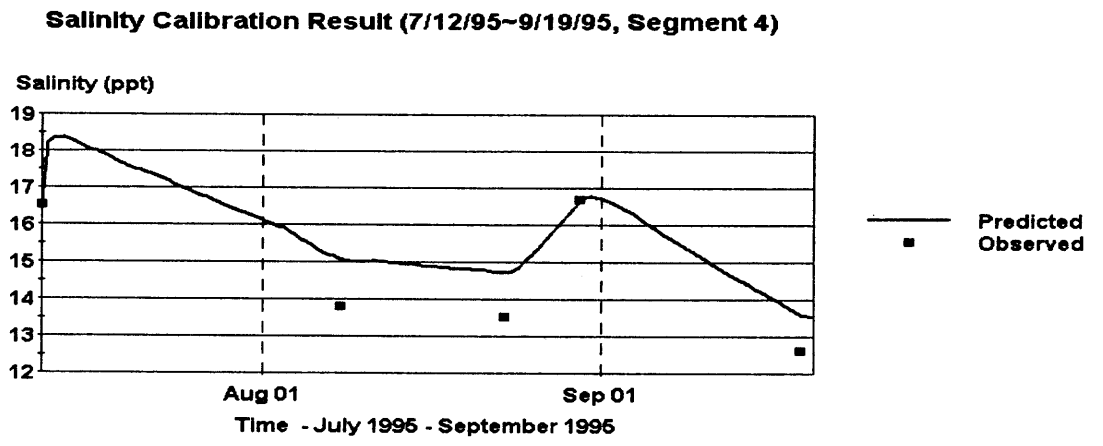

Figure 5.1(a) Salinity Calibration – Segment 4 (Temporal Variation).

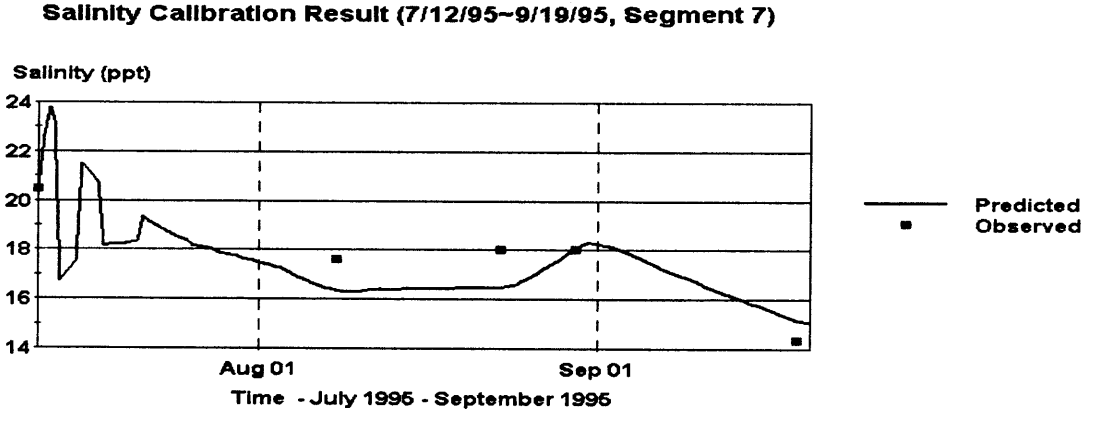

Figure 5.1(b) Salinity Calibration – Segment 7 (Temporal Variation).

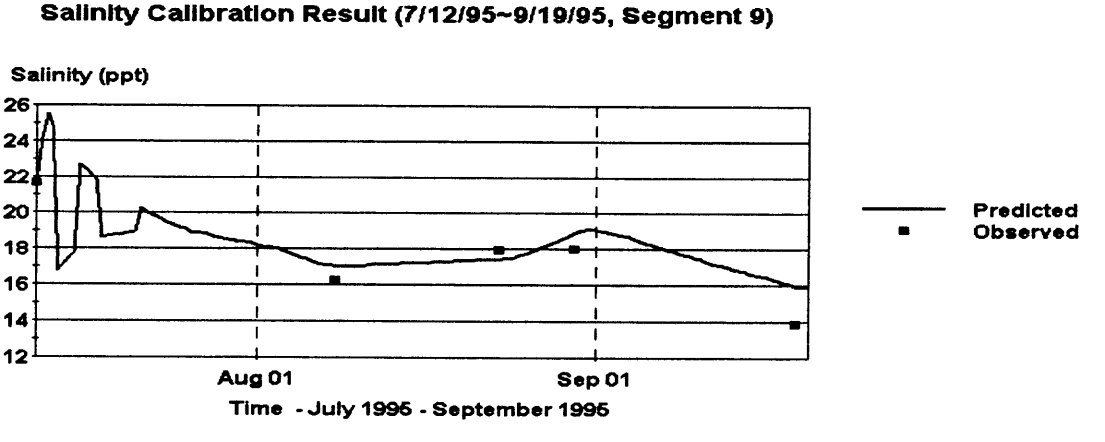

Figure 5.1(c) Salinity Calibration – Segment 9 (Temporal Variation).

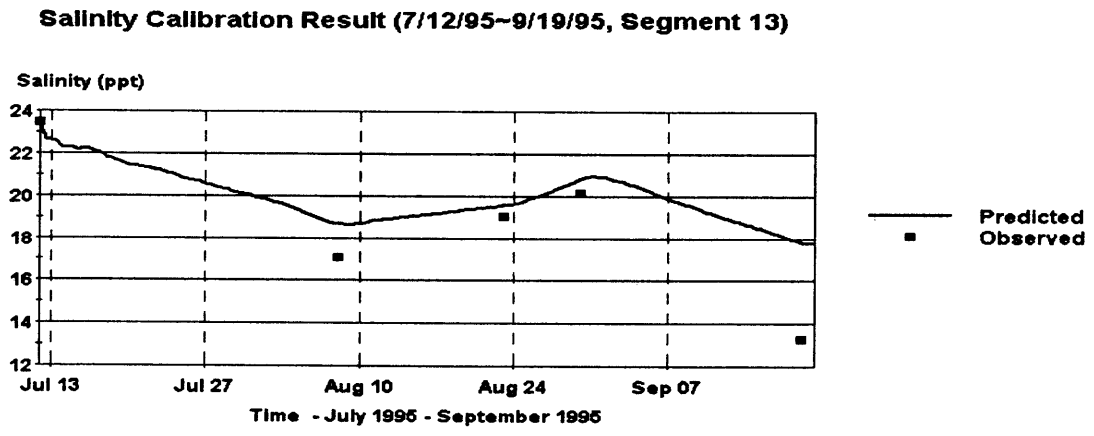

Figure 5.1(d) Salinity Calibration – Segment 13 (Temporal Variation).

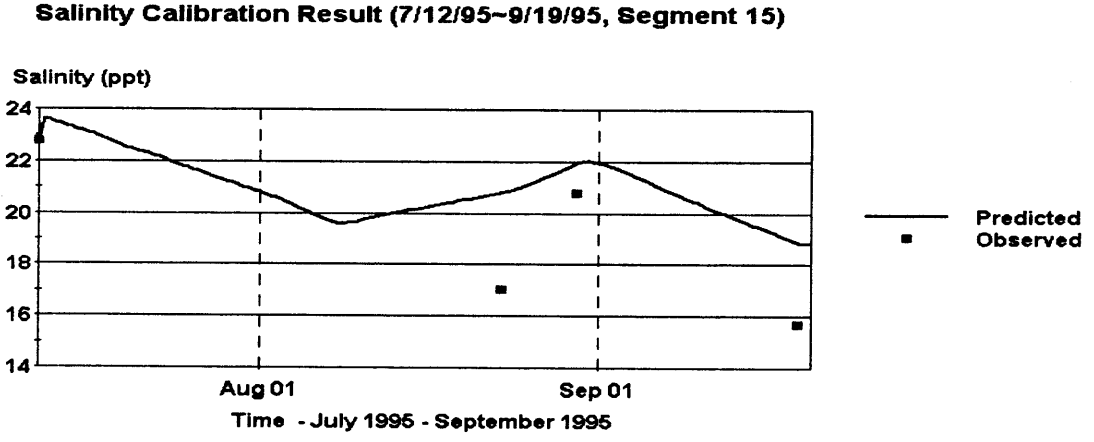

Figure 5.1(e) Salinity Calibration – Segment 15 (Temporal Variation).

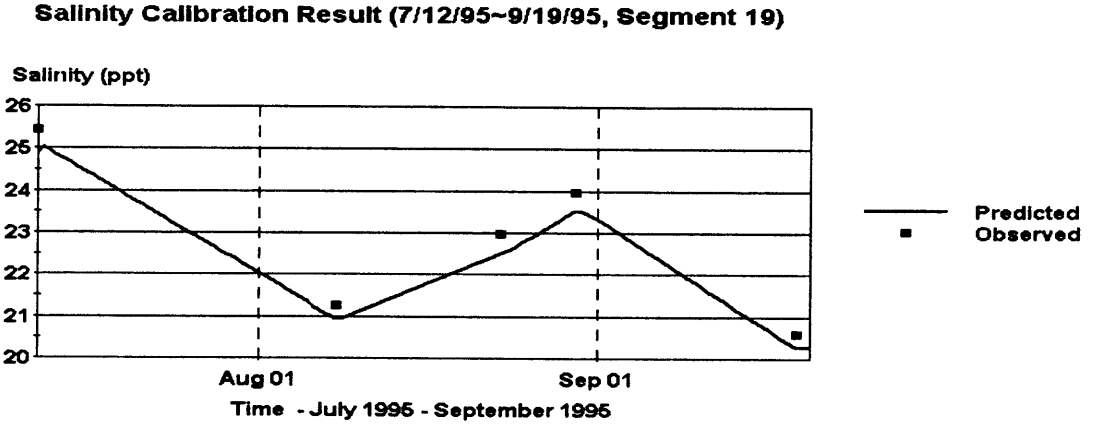

Figure 5.1(f) Salinity Calibration – Segment 19 (Temporal Variation).

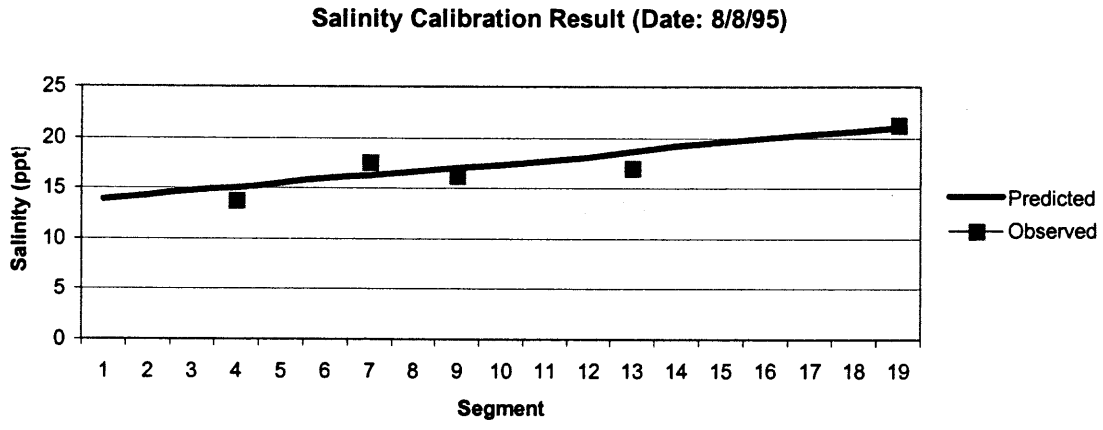

Figure 5.2(a) Salinity Calibration – 8/8/95 (Spatial Distribution).

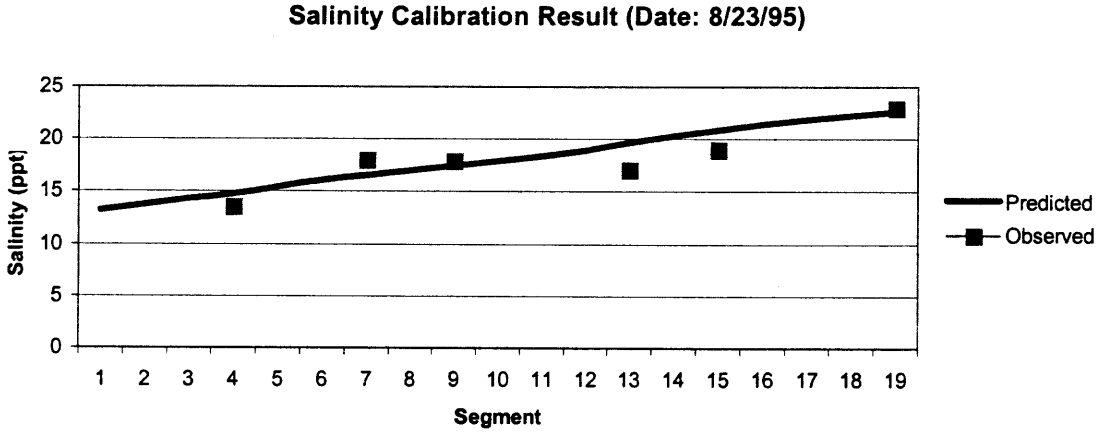

Figure 5.2(b) Salinity Calibration – 8/23/95 (Spatial Distribution).

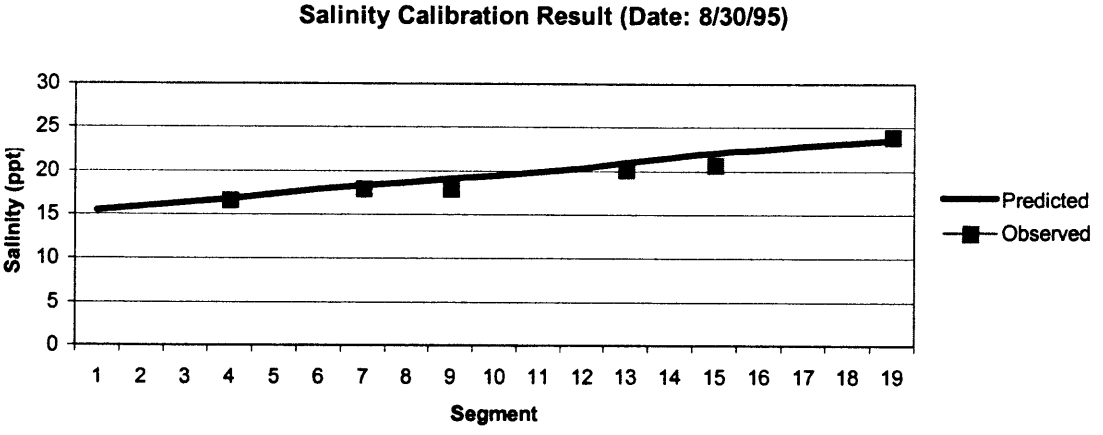

Figure 5.2(c) Salinity Calibration – 8/30/95 (Spatial Distribution).

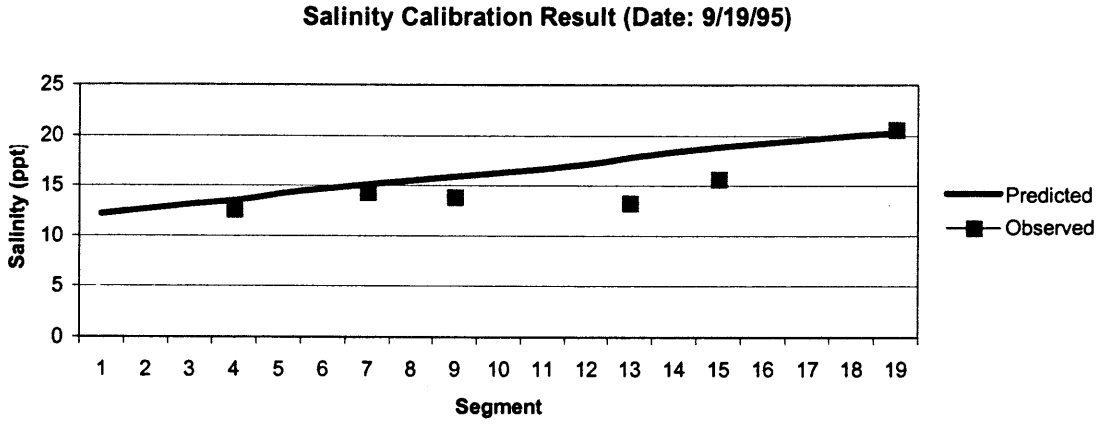

Figure 5.2(d) Salinity Calibration – 9/19/95 (Spatial Distribution).

5.2.2 DO/BOD/Nitrogen Calibration

According to the mechanisms of DO transport and transform processes, the primary reaction coefficients controlling the DO level in an aquatic system include: DO reaeration rate constant, nitrification rate constant, BOD decay rate constant, and sediment oxygen demand. These initial input coefficient values were based upon the reference values of previous studies. However, they must be adjusted to fit a specific water system through model calibration.

Table 5.4 presents the trial sequence of DO calibration. During the calibration, each reaction constant was selected and adjusted individually first, until the best-fit condition was obtained. The final result was the combination of all the optimum states of each of the adjusted constants. During calibration, the reaeration rate constant (K_1) was changed from 4.4 day^{-1} to 0.35 day^{-1}, the nitrification rate (K_2) was increased from 0.11 day^{-1} to 0.20 day^{-1}, and the BOD decay rate (K_3) was adjusted from 0.18 day^{-1} to 0.25 day^{-1}. The concentration of SOD, which was kept at 1.5 $g\text{-}O_2/m^2$, had relatively low

Table 5.4 Trial Sequence of DO Calibration

	R^2			RMSE			(0.22~2)	(0.02~0.20)	(0.02~1.08)	(0~2)
Trial	Seg9	Seg15	Seg19	Seg9	Seg15	Seg19	K_1 [b]	K_2 [b]	K_3 [b]	SOD
1[a]	0.23	0.53	0.95	0.12(1.3%)	2.71(40.3%)	0.18(2.8%)	4.4	0.11	0.18	1.5
2	0.20	0.42	0.91	4.84(67.6%)	2.71(39.3%)	0.21(3.2%)	10			
3	0.54	0.49	0.94	0.02(0.3%)	2.71(39.8%)	0.19(2.9%)	6			
4	0.20	0.69	0.98	5.80(88.5%)	2.74(42.2%)	0.17(2.6%)	2			
5	0.49	0.85	0.99	0.68(10%)	2.75(43.9%)	0.16(2.6%)	1			
6	0.45	0.93	0.99	0.78(11.9%)	2.76(45.7%)	0.16(2.6%)	0.5			
7	0.19	0.94	1.00	6.02(165%)	2.77(46.5%)	0.16(2.6%)	0.4			
8	0.84	0.95	1.00	0.81(19.4%)	2.76(46.6%)	0.16(2.6%)	0.35			
9	0.48	0.95	1.00	0.65(7.2%)	2.76(46.9%)	0.16(2.6%)	0.3			
10	0.64	0.96	1.00	2.0(31.4%)	2.78(47.6%)	0.16(2.6%)	0.25			
11	0.38	0.59	0.98	2.63(38.4%)	2.82(43.3%)	0.27(4.4%)		10		
12	0.50	0.59	0.98	2.50(36.3%)	2.81(43.1%)	0.25(4.0%)		6		
13	0.26	0.56	0.96	0.07(0.7%)	2.75(41.4%)	0.20(3.1%)		1		
14	0.26	0.55	0.96	0.07(0.6%)	2.73(40.9%)	0.19(2.9%)		0.5		
15	0.24	0.54	0.96	0.10(0.8%)	2.72(40.5%)	0.18(2.9%)		0.25		
16	0.24	0.54	0.95	0.10(0.9%)	2.72(40.4%)	0.18(2.8%)		0.2		
17	0.23	0.53	0.95	0.12(1.3%)	2.71(40.3%)	0.18(2.8%)		0.1		
18	0.23	0.53	0.95	0.13(1.4%)	2.71(40.2%)	0.18(2.8%)		0.05		
19	0.23	0.53	0.95	0.14(1.5%)	2.71(40.1%)	0.18(2.7%)		0.02		
20	0.71	0.61	0.95	2.36(35%)	2.87(45.3%)	0.30(4.9%)			5.6	
21	0.83	0.59	0.96	0.45(9.4%)	2.85(44.5%)	0.25(4.0%)			2.5	
22	0.10	0.56	0.96	5.40(120%)	2.83(43.5%)	0.22(3.6%)			1.1	
23	0.10	0.56	0.96	5.40(120%)	2.83(43.3%)	0.22(3.4%)			1	
24	0.08	0.55	0.96	5.40(124%)	2.82(43%)	0.21(3.3%)			0.85	
25	0.08	0.55	0.96	5.40(124%)	2.80(42.6%)	0.21(3.3%)			0.7	
26	0.29	0.55	0.96	0.14(1.5%)	2.77(41.8%)	0.20(3.1%)			0.5	
27	0.29	0.54	0.96	0.07(0.8%)	2.76(41.4%)	0.20(3.0%)			0.4	
28	0.23	0.53	0.95	0.05(0.4%)	2.73(40.7%)	0.19(2.9%)			0.25	
29	0.24	0.53	0.95	0.15(1.6%)	2.71(40%)	0.18(2.8%)			0.15	
30	0.30	0.53	0.95	0.42(4.5%)	2.67(39.3%)	0.17(2.6%)	4.4	0.11	0.05	1.5
31	0.27	0.93	0.99	5.43(104%)	3.09(57.3%)	0.24(4.0%)	0.35	0.5	0.4	
32	0.33	0.93	0.99	6.01(117%)	3.04(55.2%)	0.23(3.7%)	0.35	0.25	0.4	
33	0.17	0.94	0.99	6.01(188%)	3.03(54.8%)	0.22(3.7%)	0.35	0.2	0.4	
34	0.44	0.95	1.00	1.64(25.5%)	2.94(52.4%)	0.21(3.4%)	0.35	0.5	0.25	
35	0.17	0.95	1.00	6.03(180%)	2.89(50.5%)	0.19(3.1%)	0.35	0.25	0.25	
36[c]	0.80	0.95	1.00	0.43(7.0%)	2.87(49.9%)	0.19(3.1%)	0.35	0.2	0.25	1.5
37	0.83	0.95	1.00	0.54(13.2%)	2.83(48.7%)	0.18(2.9%)				0
38	0.83	0.95	1.00	0.50(12.4%)	2.85(49.1%)	0.18(2.9%)				0.5
39	0.82	0.95	1.00	0.47(11.5%)	2.86(49.5%)	0.19(3.0%)				1
40	0.49	0.95	1.00	0.39(6.5%)	2.88(50.3%)	0.19(3.1%)				2

a. Initial input of DO model.

b. K_1: reaeration rate constant; K_2: nitrification rate constant; K_3: BOD decay rate constant.

c. Final calibration result of DO model.

sensitivity (DO concentration was not changed with SOD variation) in this study. Tables 5.5 and 5.6 summarize the final statistical results of DO calibration.

Table 5.5 Statistical Result of DO Calibration (Temporal Variation)

Segment	Seg4	Seg7	Seg9	Seg13	Seg15	Seg19
R^2	0.98	0.47	0.80	0.91	0.95	1.00
RMSE	2.33	0.13	0.43	2.19	2.87	0.19
%	34.5%	2.2%	7.0%	38.4%	49.9%	3.1%
Ave. Conc.(mg/l)	6.8	6.2	6.1	5.7	5.7	6.2

Table 5.6 Statistical Result of DO Calibration (Spatial Distribution)

Date	8/8	8/23	8/30	9/19
R^2	0.11	0.08	0.00	0.08
RMSE	2.90	3.59	2.82	3.91
%	54.9%	52.7%	49.7%	47.2%

From the perspective of statistics in temporal variation, the predicted values do not match the field data well. Some of the segments (Segments 4, 13 and 15) have high correlation coefficients but the predicted values are away from the observed data. The predicted values of some segments (Segments 7 and 9) are close to the observed values but they do not have a similar variation pattern. The worst statistical values are shown in spatial distribution (Table 5-5). Small R^2 (0.00~0.11) and large RMSE (47.2%~54.9%) are found for all segments. However, according to the plots of calibration, shown in Figures 5.3 and 5.4, the predicted values are still in good agreement with the field data because most of the observed data lie close to the predicted trend line. A statistical agreement, that could not be reached, could be due to the following two reasons:

1. Figure 5.3 shows that the predicted curve is shaped like a series of blocks between Segment 5 and Segment 13. This severely affects the statistical results of the calibration. The unstable predicted values are the result of the large-scale segmentation. Because of the large size of the segment, the concentration calculated by the model varies considerably and it produces unstable values during the simulated time step. The situation could be improved by dividing the segments into smaller grids. However, due to the

limited data available, it was not practical to further dissect the segments into many smaller pieces in this study.

2. The predicted DO values obtained on September 19, 1995 are far away from the field measurement. It could be that the sampling date was too close to the two consecutive storm events. Furthermore, DO concentration with values above 10 mg/L in the summer is unreasonable. The statistical result would be improved if the observed data was neglected or adjusted.

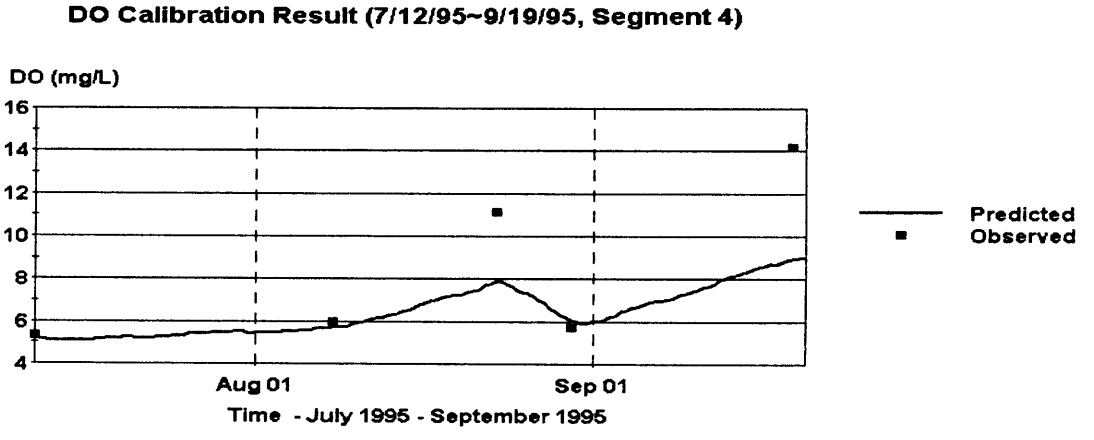

Figure 5.3(a) DO Calibration – Segment 4 (Temporal Variation).

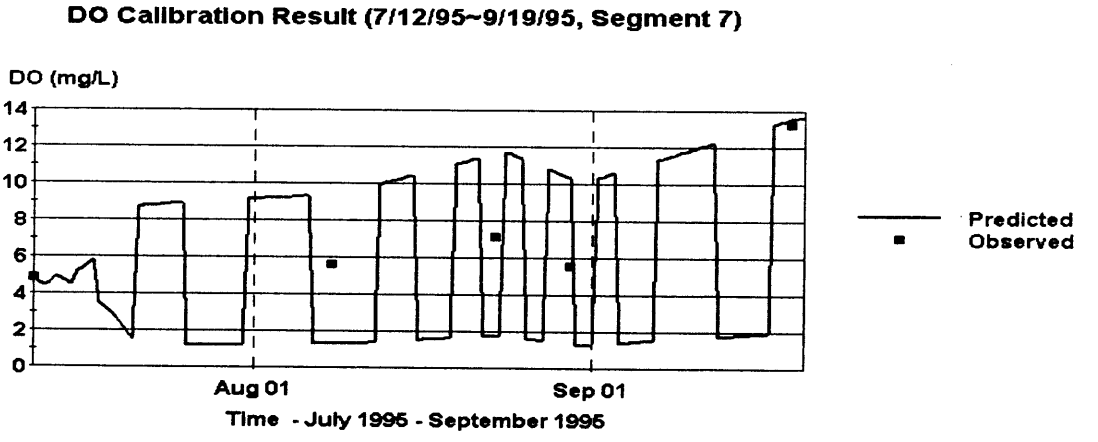

Figure 5.3(b) DO Calibration – Segment 7 (Temporal Variation).

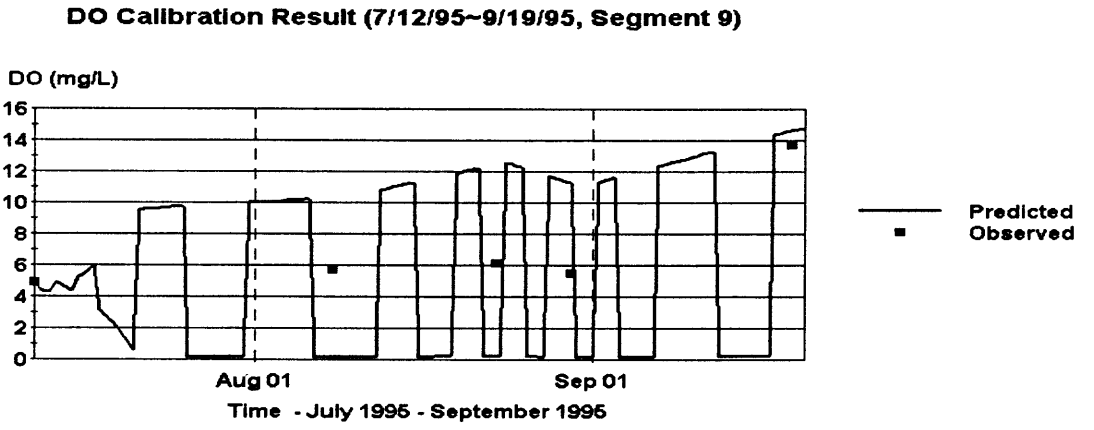

Figure 5.3(c) DO Calibration – Segment 9 (Temporal Variation).

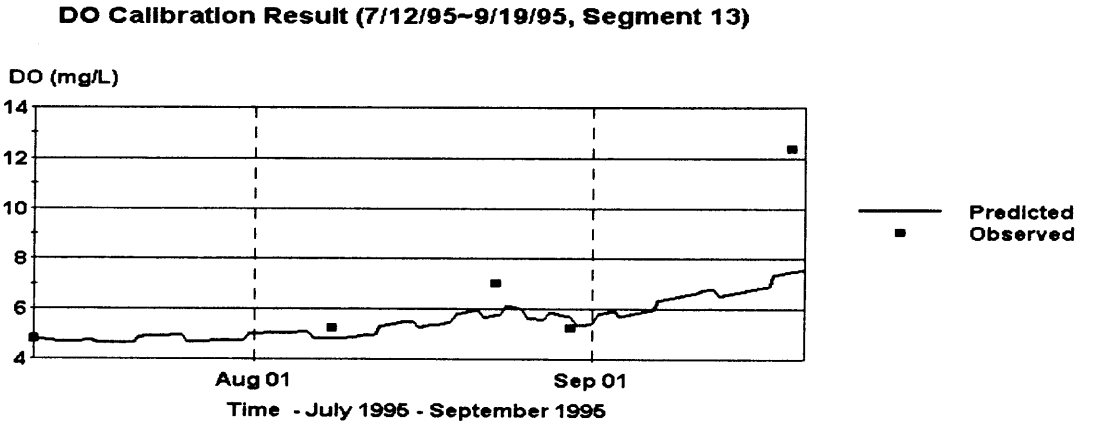

Figure 5.3(d) DO Calibration – Segment 13 (Temporal Variation).

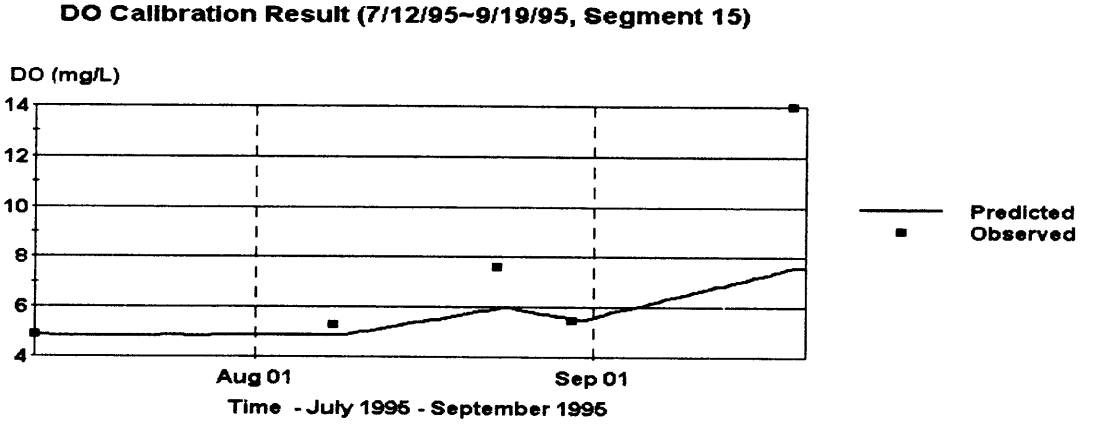

Figure 5.3(e) DO Calibration – Segment 15 (Temporal Variation).

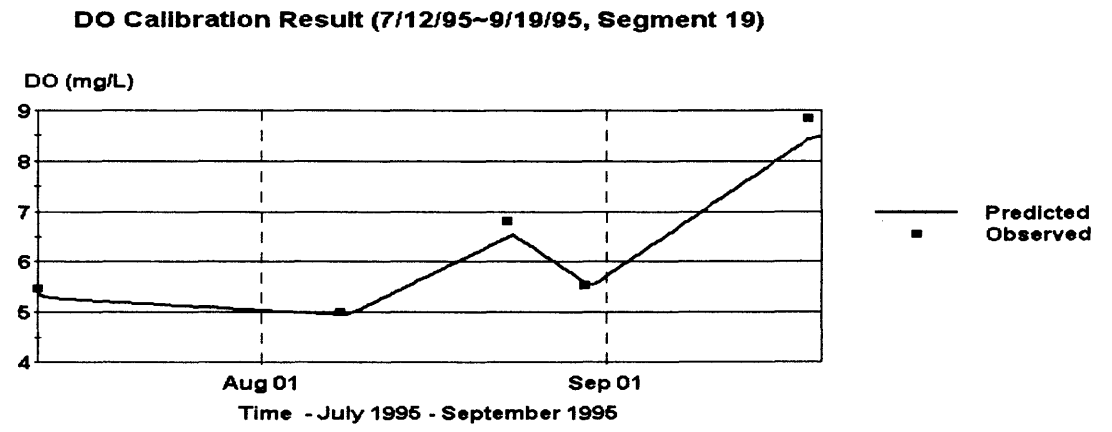

Figure 5.3(f) DO Calibration – Segment 19 (Temporal Variation).

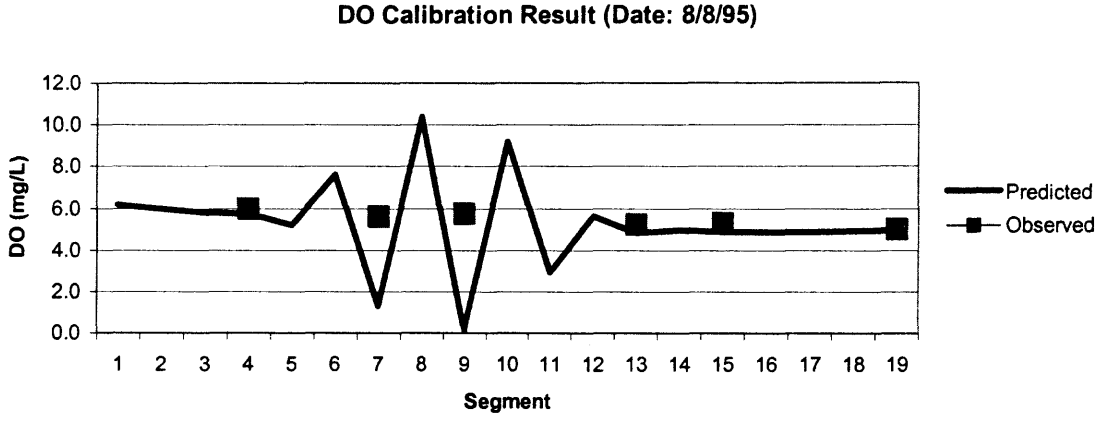

Figure 5.4(a) DO Calibration – 8/8/95 (Spatial Distribution).

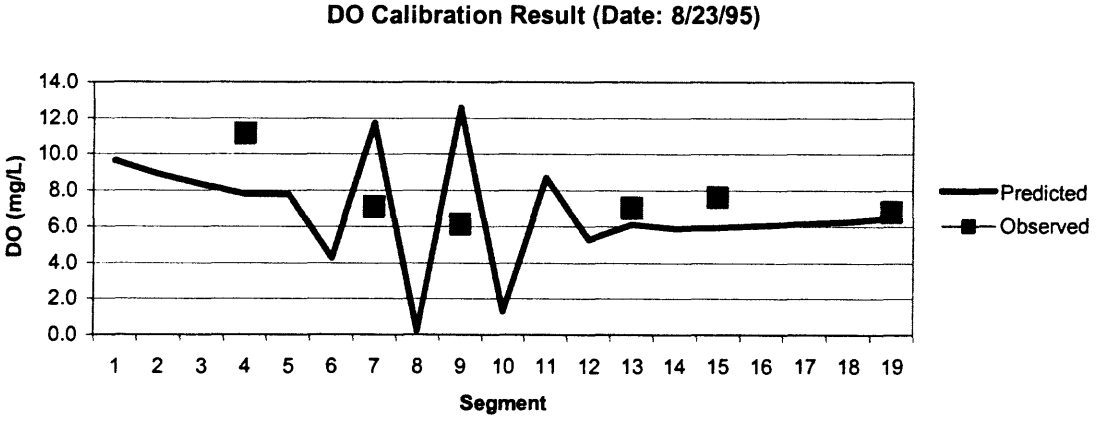

Figure 5.4(b) DO Calibration – 8/23/95 (Spatial Distribution).

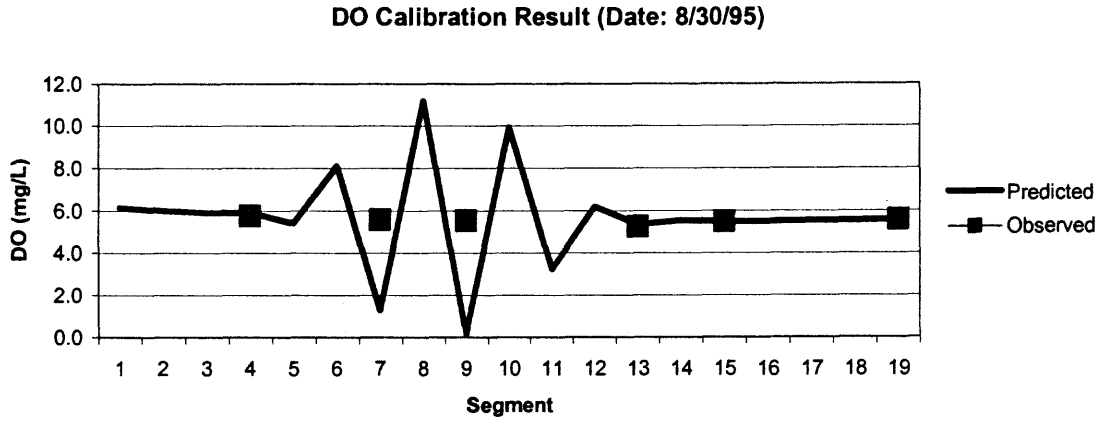

Figure 5.4(c) DO Calibration – 8/30/95 (Spatial Distribution).

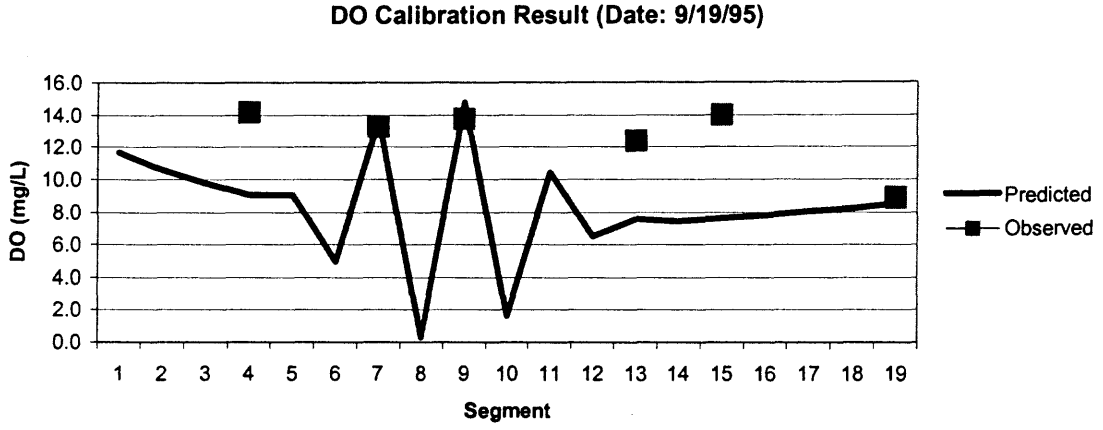

Figure 5.4(d) DO Calibration – 9/19/95 (Spatial Distribution).

Along with the DO calibration, BOD was calibrated simultaneously. Different types of BOD parameters used (for example, BOD_5 and NBOD) would produce different calibration results. Again, the BOD presented here is $CBOD_U$. Table 5.7 to Table 5.9 present the trial sequence, statistical results of temporal variation and spatial distribution of BOD calibration, respectively. Table 5.8 indicates that R^2 values are above 0.75 for all the segments in the study area except in Segment 15 (0.08) and most of the RMSE values

Table 5.7 Trial Sequence of BOD Calibration

	R^2			RMSE			(0.22~2)	(0.02~0.20)	(0.02~1.08)	(0~2)
Trial	Seg9	Seg15	Seg19	Seg9	Seg15	Seg19	K_1[b]	K_2[b]	K_3[b]	SOD
1[a]	0.84	0.11	1.00	1.12(28.0%)	4.77(136%)	0.13(3.6%)	4.4	0.11	0.18	1.5
2	0.84	0.11	1.00	1.12(27.8%)	4.77(136%)	0.13(3.6%)	10			
3	0.84	0.11	1.00	1.12(27.8%)	4.77(136%)	0.13(3.6%)	6			
4	0.84	0.11	1.00	1.14(28.4%)	4.77(136%)	0.13(3.6%)	2			
5	0.82	0.11	1.00	0.98(23.9%)	4.76(135%)	0.13(3.6%)	1			
6	0.82	0.11	1.00	0.81(19.7%)	4.76(135%)	0.13(3.6%)	0.5			
7	0.77	0.11	1.00	1.46(38.2%)	4.76(135%)	0.13(3.6%)	0.4			
8	0.88	0.11	1.00	0.65(16.5%)	4.76(135%)	0.13(3.6%)	0.35			
9	0.78	0.12	1.00	0.59(13.4%)	4.76(135%)	0.13(3.6%)	0.3			
10	0.82	0.11	1.00	1.07(26.5%)	4.77(136%)	0.13(3.6%)	0.25			
11	0.84	0.11	1.00	1.12(28.0%)	4.77(136%)	0.13(3.6%)		10		
12	0.84	0.11	1.00	1.10(27.1%)	4.77(136%)	0.13(3.6%)		6		
13	0.84	0.11	1.00	1.10(27.1%)	4.77(136%)	0.13(3.6%)		1		
14	0.84	0.11	1.00	1.10(27.1%)	4.77(136%)	0.13(3.6%)		0.5		
15	0.84	0.11	1.00	1.10(27.1%)	4.77(136%)	0.13(3.6%)		0.25		
16	0.84	0.11	1.00	1.10(27.1%)	4.77(136%)	0.13(3.6%)		0.2		
17	0.84	0.11	1.00	1.10(27.1%)	4.77(136%)	0.13(3.6%)		0.1		
18	0.84	0.11	1.00	1.10(27.1%)	4.77(136%)	0.13(3.6%)		0.05		
19	0.84	0.11	1.00	1.10(27.1%)	4.77(136%)	0.13(3.6%)		0.02		
20	0.02	0.02	0.86	3.95(406%)	6.24(530%)	0.30(11.2%)			5.6	
21	0.09	0.01	0.93	3.55(259%)	6.04(378%)	0.20(6.8%)			2.5	
22	0.31	0.00	0.97	2.89(137%)	5.67(257%)	0.09(2.9%)			1.1	
23	0.35	0.00	0.97	2.79(125%)	5.62(246%)	0.08(2.4%)			1	
24	0.44	0.00	0.98	2.60(108%)	5.53(229%)	0.06(1.7%)			0.85	
25	0.54	0.00	0.98	2.38(90.3%)	5.42(211%)	0.03(0.9%)			0.7	
26	0.69	0.01	0.99	1.96(63.9%)	5.23(184%)	0.02(0.5%)			0.5	
27	0.75	0.03	0.99	1.74(52.5%)	5.11(170%)	0.05(1.3%)			0.4	
28	0.82	0.08	1.00	1.33(35.1%)	4.89(147%)	0.10(2.8%)			0.25	
29	0.85	0.13	1.00	0.99(23.7%)	4.71(131%)	0.14(4.0%)			0.15	
30	0.83	0.21	1.00	0.58(124%)	4.47(114%)	0.20(5.3%)	4.4	0.11	0.05	
31	0.66	0.03	0.99	2.19(66.9%)	5.12(169%)	0.05(1.3%)	0.35	0.5	0.4	
32	0.20	0.03	0.99	2.64(85.3%)	5.11(169%)	0.05(1.4%)	0.35	0.25	0.4	
33	0.50	0.03	0.99	2.65(101%)	5.11(169%)	0.05(1.4%)	0.35	0.2	0.4	
34	0.80	0.07	1.00	1.28(33.9%)	4.90(147%)	0.10(2.8%)	0.35	0.5	0.25	
35	0.56	0.08	1.00	1.90(56.4%)	4.89(146%)	0.10(2.9%)	0.35	0.25	0.25	
36[c]	0.86	0.08	1.00	0.73(18.8%)	4.88(146%)	0.10(2.9%)	0.35	0.2	0.25	1.5
37	0.86	0.08	1.00	0.73(20.2%)	4.89(146%)	0.10(2.9%)				0
38	0.86	0.08	1.00	0.73(20.2%)	4.89(146%)	0.10(2.9%)				0.5
39	0.86	0.08	1.00	0.73(20.2%)	4.89(146%)	0.10(2.9%)				1
40	0.75	0.08	1.00	0.73(18.8%)	4.89(146%)	0.10(2.9%)				2

a. Initial input of DO model.

b. K_1: reaeration rate constant; K_2: nitrification rate constant; K_3: BOD decay rate constant.

c. Final calibration result of DO model

are below 25%, though the values vary widely from a small value of 2.9% (Segment 19) to the largest 146% (Segment 15). The largest value seen in Segment 15 primarily comes from the unreasonably high-observed measurement on September 19 shown in Figure 5.5. Spatial distribution, revealed in Table 5.9, shows low R^2 (0.00~0.59) and high RMSE (25.1%~58.8%). Because of the large size of the segment, several flexuous peaks are observed between Segment 5 to Segment 12 in the calibration plot (Figure 5.6). Similar findings occurred as those observed in the DO calibration, the result of BOD calibration shows low agreement in statistically, but the observed data stay close to the acceptable predicted trend in plots.

Table 5.8 Statistical Result of BOD Calibration (Temporal Variation)

Segment	Seg4	Seg7	Seg9	Seg13	Seg15	Seg19
R^2	0.74	0.87	0.75	0.97	0.08	1.00
RMSE	1.15	2.52	0.73	0.29	4.88	0.1
%	24.7%	61.7%	18.8%	8.5%	146.0%	2.9%
Ave. Conc.	4.5	4.1	3.9	3.4	3.3	3.5

Table 5.9 Statistical Result of BOD Calibration (Spatial Distribution)

Date	8/8	8/23	8/30	9/19
R^2	0.11	0.00	0.33	0.59
RMSE	1.44	0.99	0.83	2.70
%	52.4%	25.1%	58.8%	40.9%

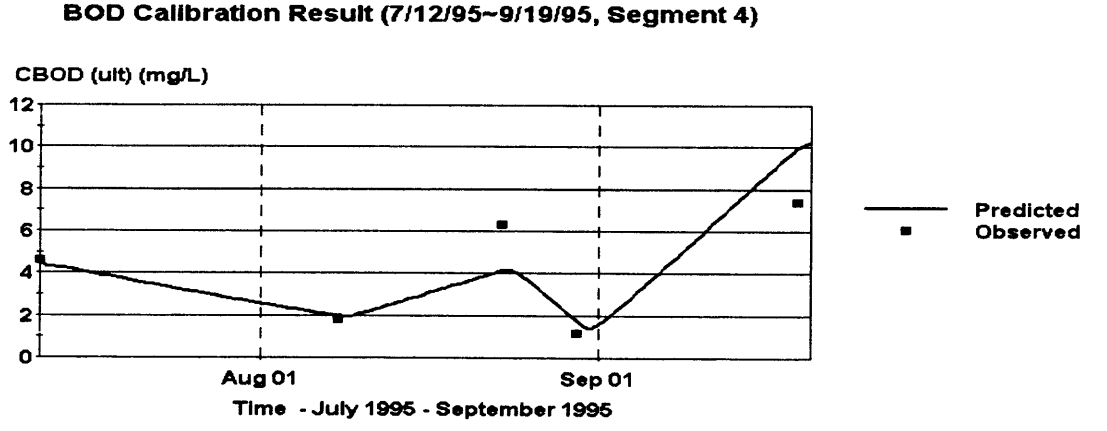

Figure 5.5(a) BOD Calibration – Segment 4 (Temporal Variation).

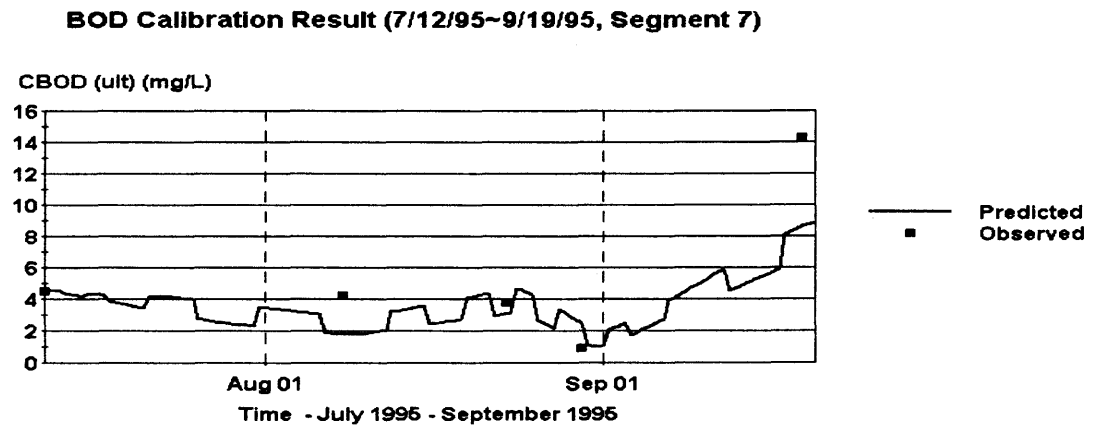

Figure 5.5(b) BOD Calibration – Segment 7 (Temporal Variation).

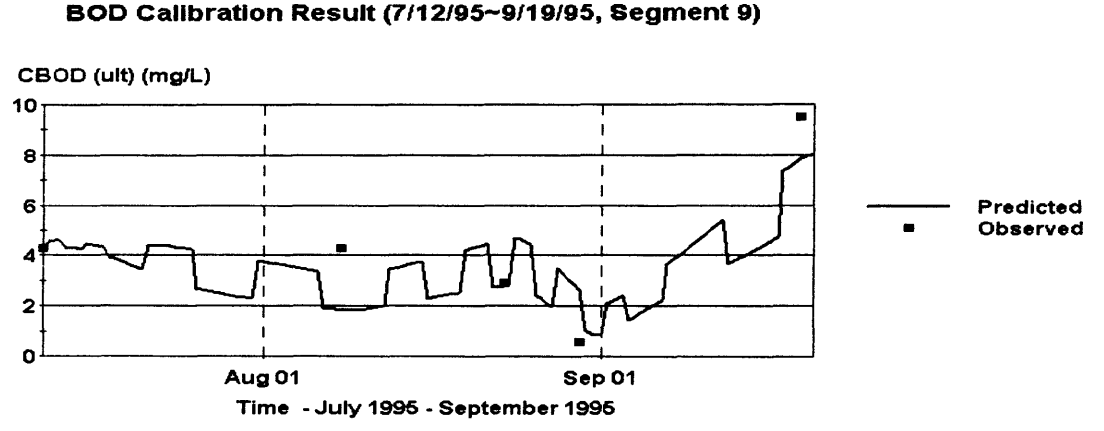

Figure 5.5(c) BOD Calibration – Segment 9 (Temporal Variation).

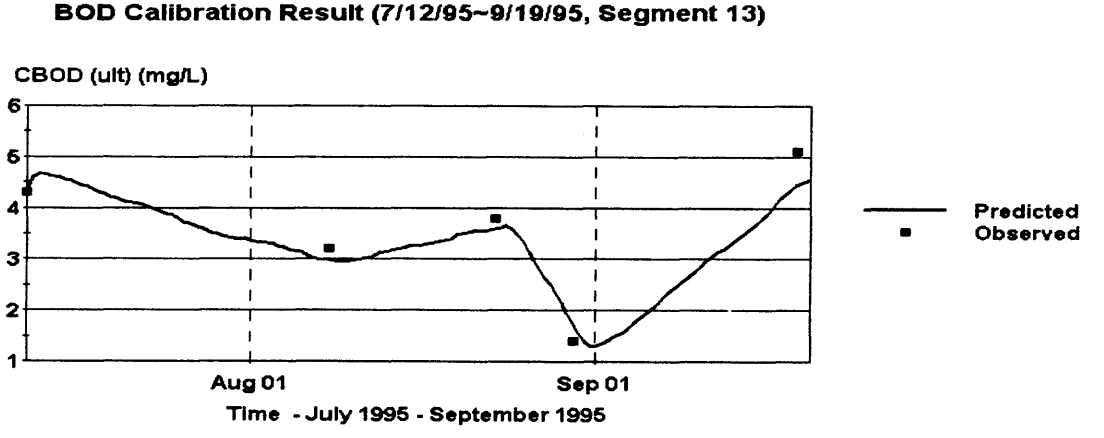

Figure 5.5(d) BOD Calibration – Segment 13 (Temporal Variation).

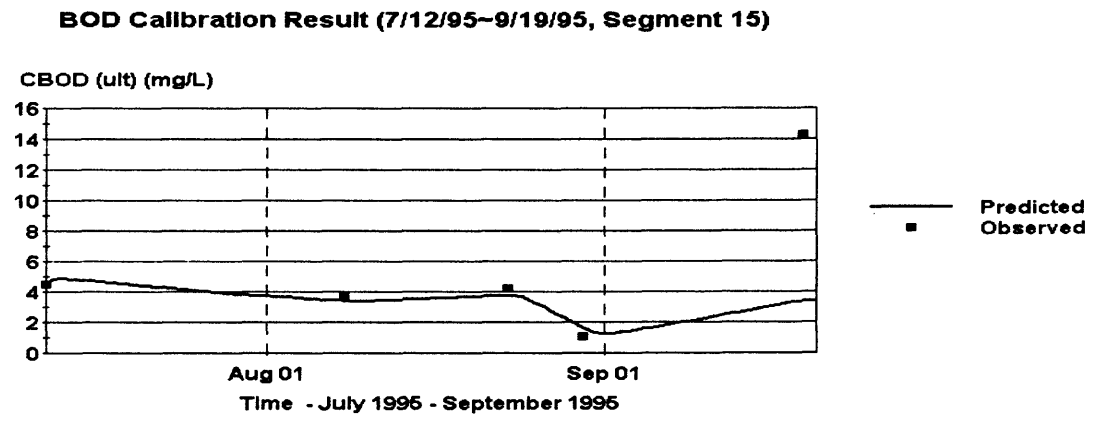

Figure 5.5(e) BOD Calibration – Segment 15 (Temporal Variation).

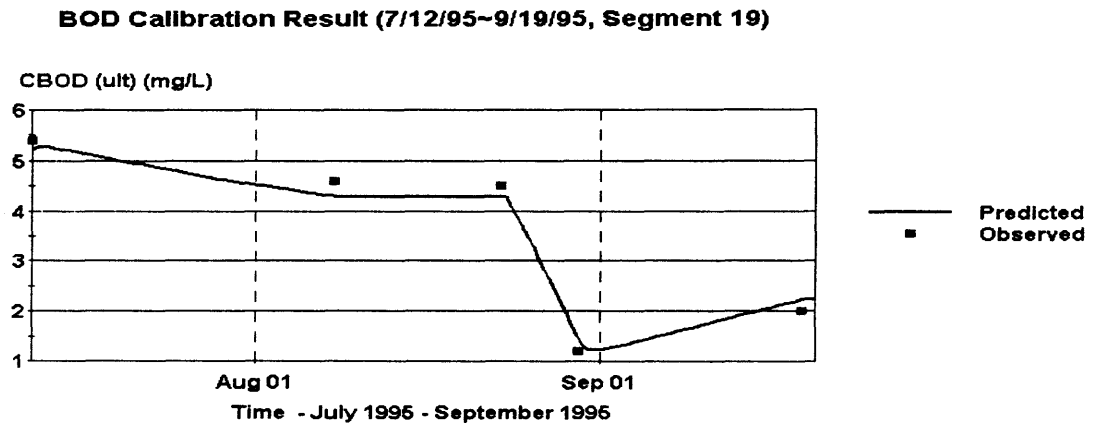

Figure 5.5(f) BOD Calibration – Segment 19 (Temporal Variation).

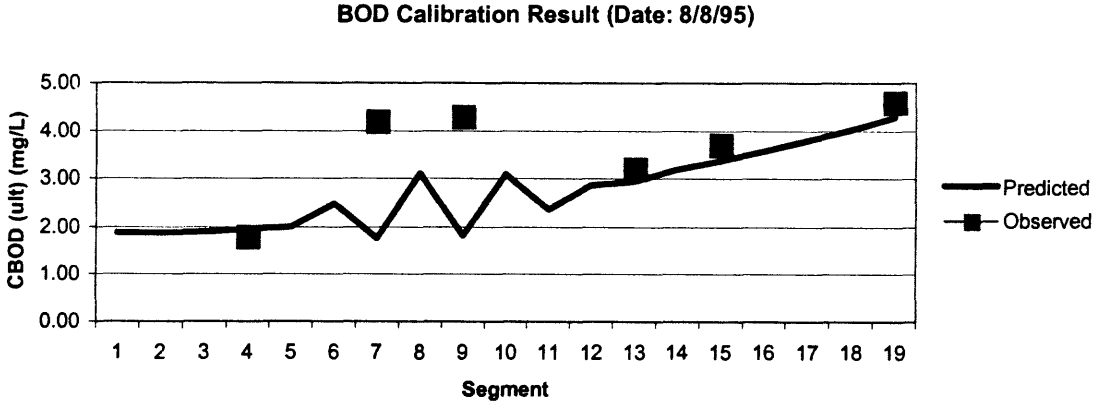

Figure 5.6(a) BOD Calibration – 8/8/95 (Spatial Distribution).

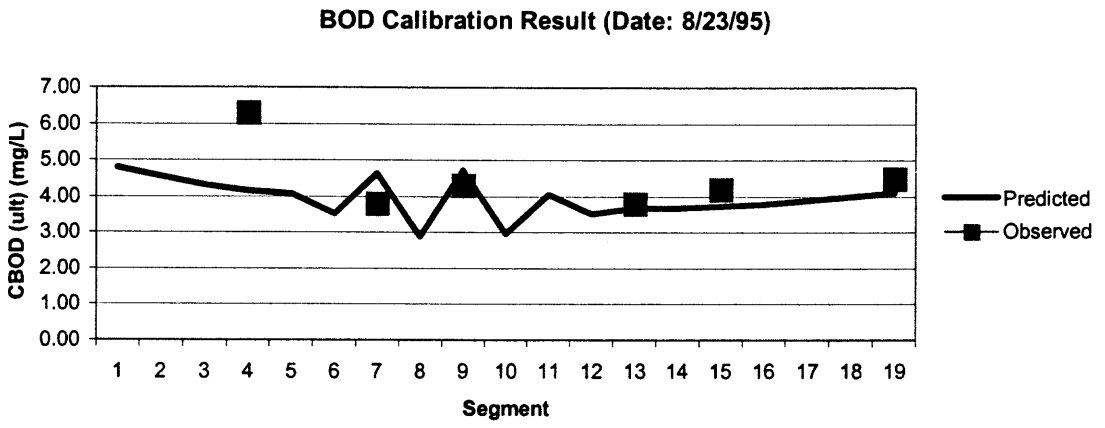

Figure 5.6(b) BOD Calibration – 8/23/95 (Spatial Distribution).

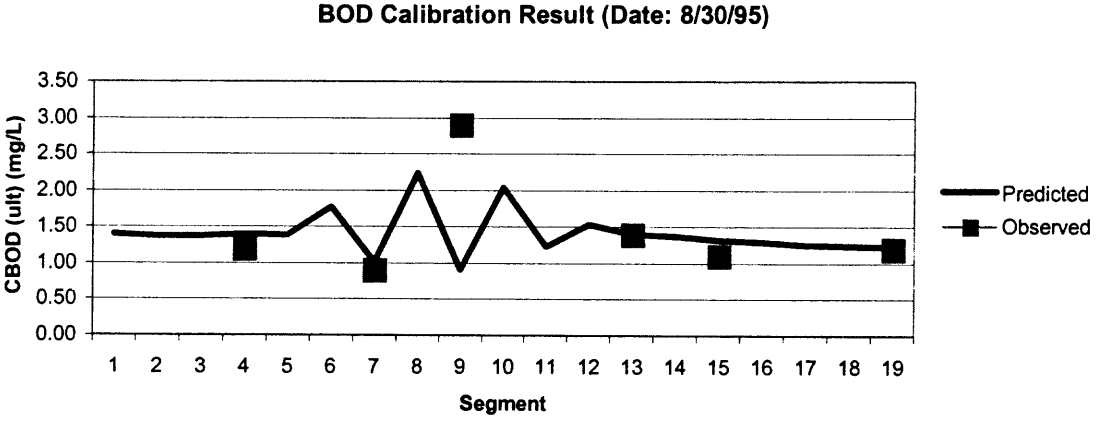

Figure 5.6(c) BOD Calibration – 8/30/95 (Spatial Distribution).

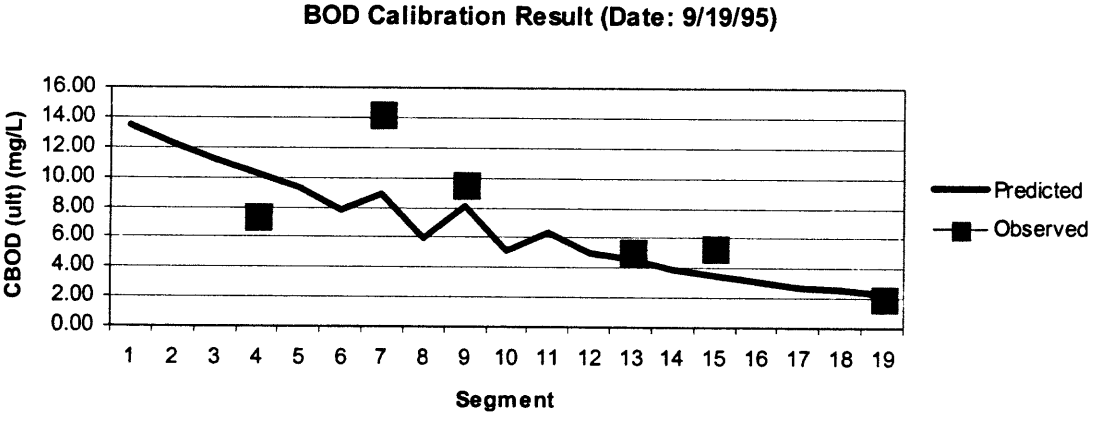

Figure 5.6(d) BOD Calibration – 9/19/95 (Spatial Distribution).

The mechanisms of nitrogen transport and transformation processes will also affect the DO concentration in receiving waters. Tables 5.10 to 5.12 summarize the trial sequence and statistical results of temporal variation and spatial distribution of ammonia (represented by NH_3-N) calibration, respectively. Temporal variation, revealed in Table 5.11, indicates that the wide variation of R^2 range from a small value of 0.08 (Segment 9) to the largest 1.0 (Segment 19). Meanwhile, RMSE values are steadily between 30 to 40 percent, except in Segment 4 (19.9%) and Segment 19 (0.1%). The poor statistical results are found in spatial distribution, where the R^2 values are below 0.35 (0.13 ~0.35) and RMSE values are higher than 30% (31.9% ~ 94.9%). However, as mentioned earlier in the DO and BOD calibration section, the low agreement between predicted and observed data shown in statistical results primarily comes from the large scale segmentation and the questionable field sampling data on September 19. This perspective is verified again in Figures 5.7 and 5.8, which show that the observed data stay close to the acceptable predicted trend in the plots, except the spatial distribution on September 19, where the observed data are much lower than the predicted values.

Table 5.10 Trial Sequence of NH_3-N Calibration

	R^2			RMSE			(0.22~2)	(0.02~0.20)	(0.02~1.08)	(0~2)
Trial	Seg9	Seg15	Seg19	Seg9	Seg15	Seg19	K1	K2	K3	SOD
31	0.83	0.21	1	0.58(124%)	4.47(114%)	0.20(5.3%)	4.4	0.11	0.05	
32	0.66	0.03	0.99	2.19(66.9%)	5.12(169%)	0.05(1.3%)	0.35	0.5	0.4	
33	0.2	0.03	0.99	2.64(85.3%)	5.11(169%)	0.05(1.4%)	0.35	0.25	0.4	
34	0.5	0.03	0.99	2.65(101%)	5.11(169%)	0.05(1.4%)	0.35	0.2	0.4	
35	0.8	0.07	1	1.28(33.9%)	4.90(147%)	0.10(2.8%)	0.35	0.5	0.25	
36	0.56	0.08	1	1.90(56.4%)	4.89(146%)	0.10(2.9%)	0.35	0.25	0.25	
37	0.86	0.08	1	0.73(18.8%)	4.88(146%)	0.10(2.9%)	0.35	0.2	0.25	1.5
38	0.86	0.08	1	0.73(20.2%)	4.89(146%)	0.10(2.9%)				0
39	0.86	0.08	1	0.73(20.2%)	4.89(146%)	0.10(2.9%)				0.5
40	0.86	0.08	1	0.73(20.2%)	4.89(146%)	0.10(2.9%)				1
41	0.75	0.08	1	0.73(18.8%)	4.89(146%)	0.10(2.9%)				2

Table 5.11 Statistical Result of NH_3-N Calibration (Temporal Variation)

Segment	Seg4	Seg7	Seg9	Seg13	Seg15	Seg19
R2	0.88	0.57	0.08	0.65	0.72	1.00
RMSE	0.04	0.08	0.09	0.09	0.1	0
%	19.9%	31.5%	36.7%	31.0%	32.3%	0.1%
Ave. Conc.	0.20	0.25	0.26	0.28	0.30	0.32

Table 5.12 Statistical Result of NH_3-N Calibration (Spatial Distribution)

Date	8/8	8/23	8/30	9/19
R2	0.26	0.35	0.19	0.13
RMSE	0.09	0.19	0.09	0.16
%	31.9%	94.3%	33.1%	94.9%

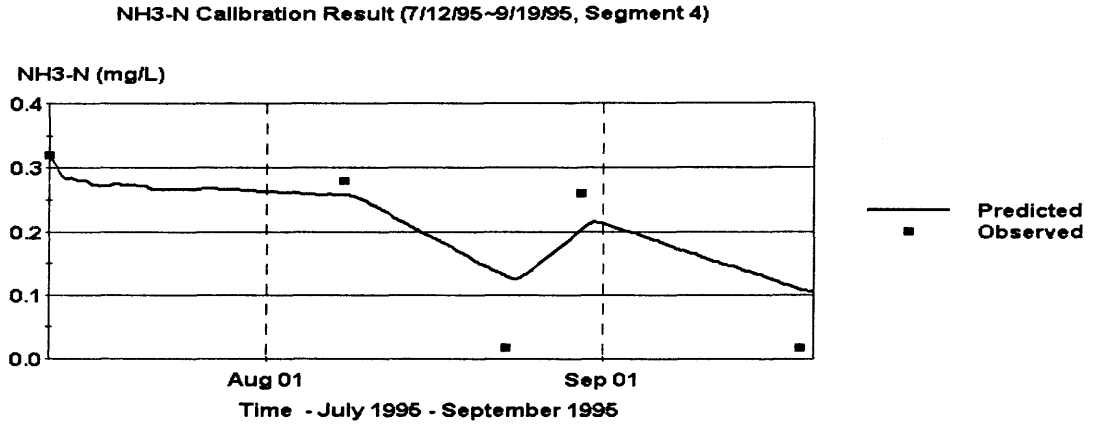

Figure 5.7(a) NH_3-N Calibration – Segment 4 (Temporal Variation).

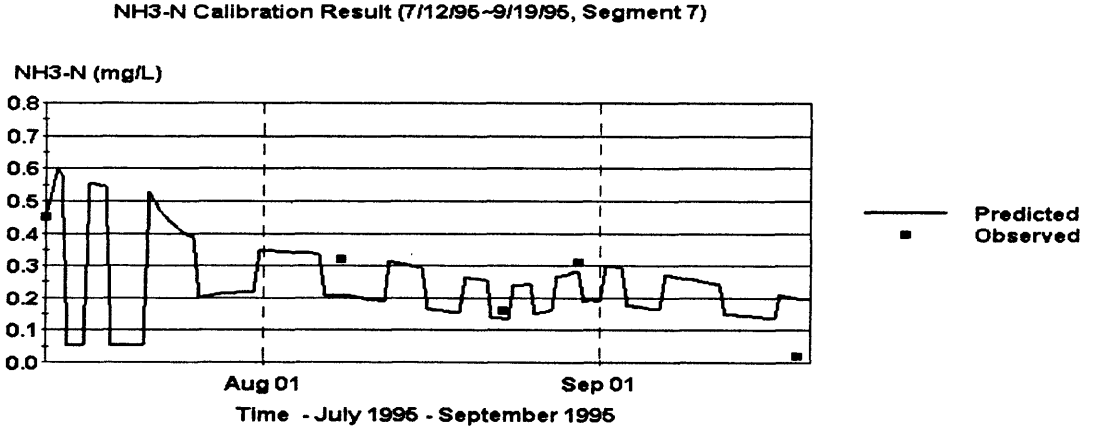

Figure 5.7(b) NH_3-N Calibration – Segment 7 (Temporal Variation).

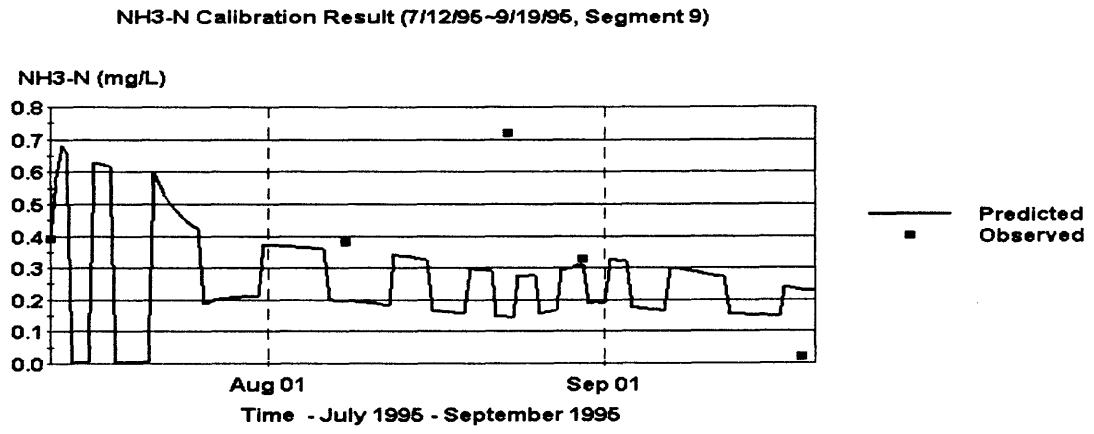

Figure 5.7(c) NH_3-N Calibration – Segment 9 (Temporal Variation).

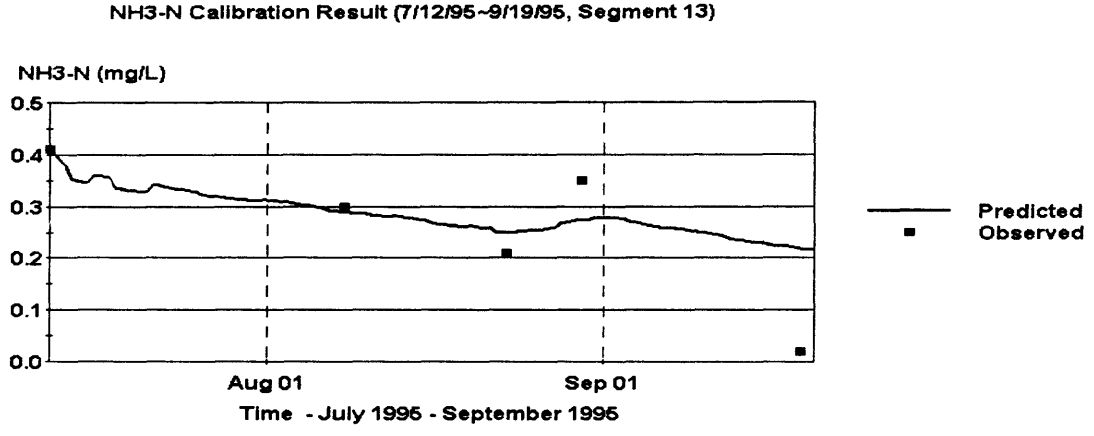

Figure 5.7(d) NH_3-N Calibration – Segment 13 (Temporal Variation).

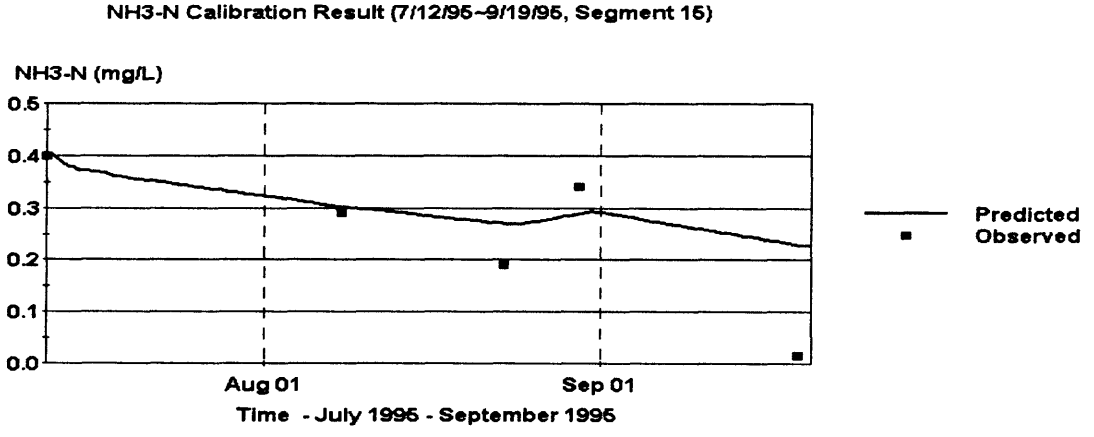

Figure 5.7(e) NH_3-N Calibration – Segment 15 (Temporal Variation).

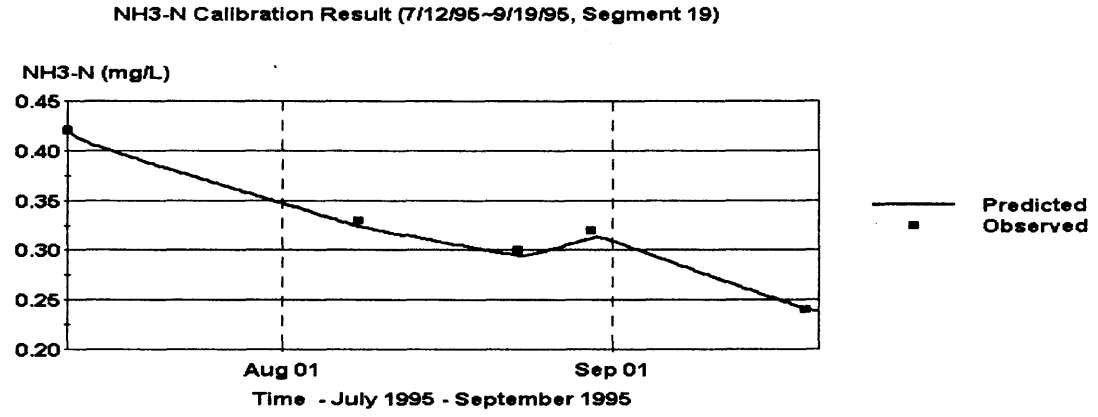

Figure 5.7(f) NH_3-N Calibration – Segment 19 (Temporal Variation).

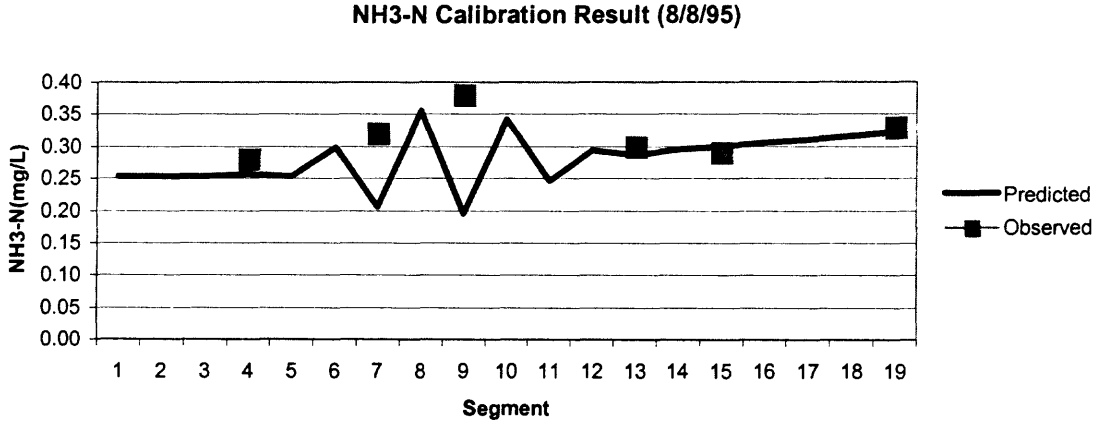

Figure 5.8(a) NH_3-N Calibration – 8/8/95 (Spatial Distribution).

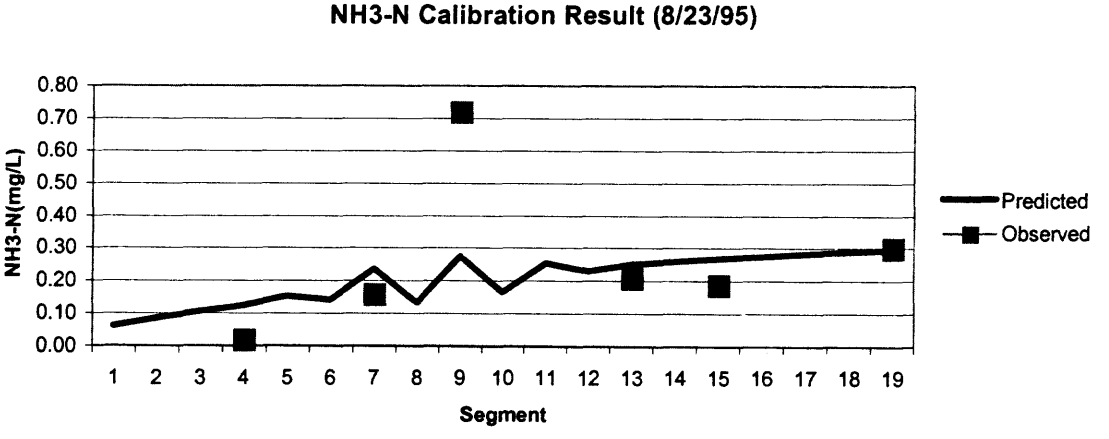

Figure 5.8(b) NH_3-N Calibration – 8/23/95 (Spatial Distribution).

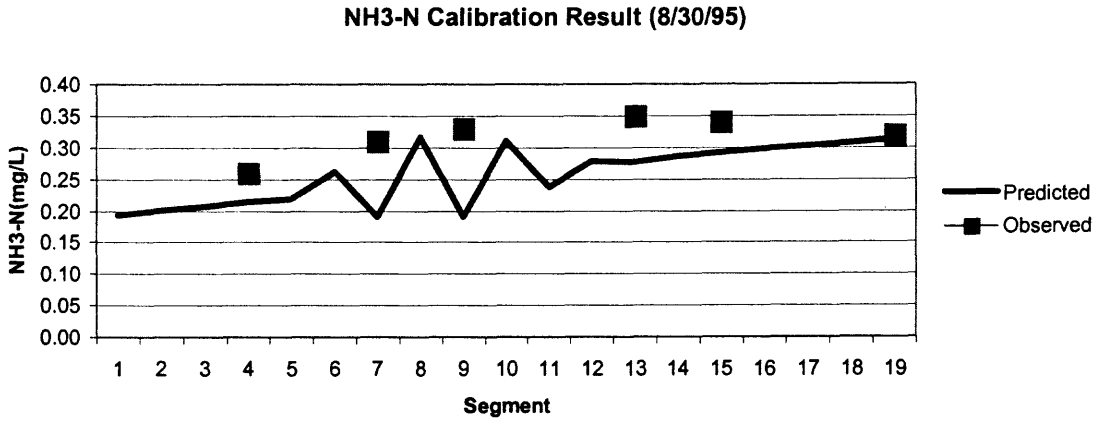

Figure 5.8(c) NH_3-N Calibration – 8/30/95 (Spatial Distribution).

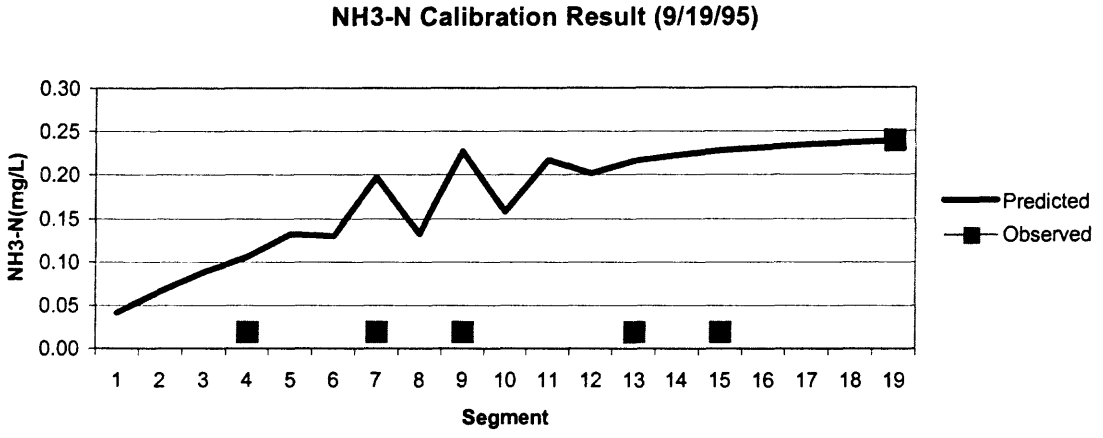

Figure 5.8(d) NH_3-N Calibration – 9/19/95 (Spatial Distribution).

5.2.3 Fecal Coliform Calibration

The primary environmental constant that controls fecal coliform transport and transformation in the aquatic system is the coliform bacteria death rate (day^{-1}). The bacteria death rate encompasses the reduction of bacterial numbers as a result of protozoan predation, sunlight disinfection, and natural death. Re-growth of fecal coliform in the study was assumed negligible. The rate of bacteria death has been considered by many to be linearly dependent on temperature, with the organisms being more persistent

at lower temperatures. However, the bacteria death rate was assumed to be a constant in this study due to the relatively small variation in temperature during the summer. Table 5.13 presents the trial sequence of FC calibration. According to the Hydroscience study (1977), the range of the bacteria death rate in New York Harbor was between 0 to 6.1 day^{-1}. The constant was initially set as 3.0 day^{-1} and adjusted to 0.25 day^{-1} during the model calibration.

Table 5.13 Trial Sequence of FC Calibration

	R^2			RMSE			(0~6.1)
Trial	Seg9	Seg15	Seg19	Seg9	Seg15	Seg19	Bacteria Death Rate
1	0.01	0.95	0.98	0.01(17.2%)	1.63(130%)	0.15(13.2%)	0.00
2[a]	0.14	0.91	0.99	0.04(62.8%)	1.11(125%%)	0.01(1.3%)	0.25
3	0.11	0.86	0.99	0.06(24.2%)	0.79(117%)	0.12(12.6%)	0.50
4	0.23	0.73	0.99	0.07(47.2%)	0.44(100.4%)	0.25(29.6%)	1.00
5	0.18	0.12	0.97	0(2.4%)	0.06(41.0%)	0.46(67.5%)	3.00
6	0.23	0.04	0.96	0(24.2%)	0.02(19%)	0.51(79.9%)	4.00
7	0.11	0.01	0.95	0.01(117%)	0(1.8%)	0.55(91%)	5.00
8	0.08	0.00	0.94	0.01(222%)	0.01(23.2%)	0.58(102%)	6.10

Tables 5.14 and 5.15 summarize the statistical results of FC calibration in temporal variation and spatial distribution, respectively. In temporal analysis, Correlation Coefficient Squares vary dramatically from 0.01 (Segment 4) to 0.99 (Segment 19) and RMSE values also show a wide range from over 100% (Segment 13) to 1.3% (Segment 19). The low agreement in statistical results primarily comes from the poor agreement between predicted and observed data on 8/23 and 9/19. The measurements or analyses performed on these two days could be erroneous, because the observed values are much higher than the predicted values on 8/23 and lower on 9/19. Due to the limited number of samples, these few errors in sampling data may exaggerate the difference in data agreement in the statistics. This phenomenon is also observed in the calibration result for

spatial analysis. The low R^2 (0.00) for the data on 9/19 and the high RMSE (996.9%) for the data on 8/23 are shown in Table 5.15 and Figure 5.10.

Table 5.14 Statistical Result of FC Calibration (Temporal Variation)

Segment	Seg4	Seg7	Seg9	Seg13	Seg15	Seg19
R^2	0.01	0.20	0.14	0.24	0.91	0.99
RMSE	0.30	0.01	0.04	1.04	1.11	0.01
%	113.7%	19.8%	62.8%	135.6%	125.0%	1.3%

Table 5.15 Statistical Result of FC Calibration (Spatial Distribution)

Date	8/8	8/23	8/30	9/19
R^2	0.09	0.29	0.65	0.00
RMSE	0.34	0.55	0.33	1.37
%	57.5%	996.6%	166.2%	126.5%

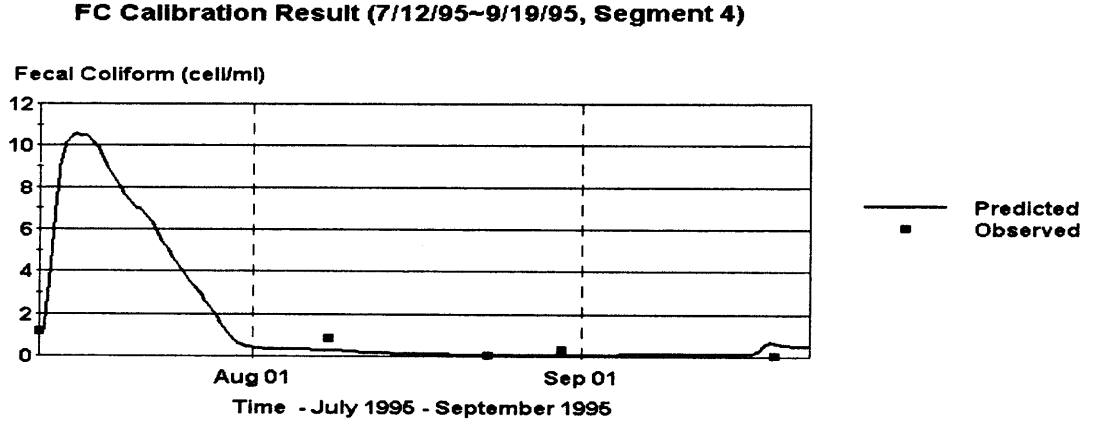

Figure 5.9(a) FC Calibration –Segment 4 (Temporal Variation).

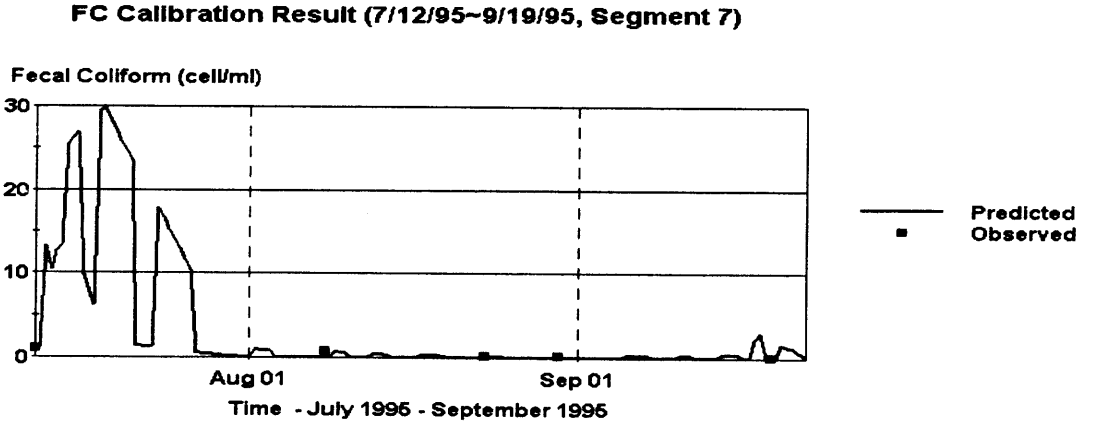

Figure 5.9(b) FC Calibration –Segment 7 (Temporal Variation).

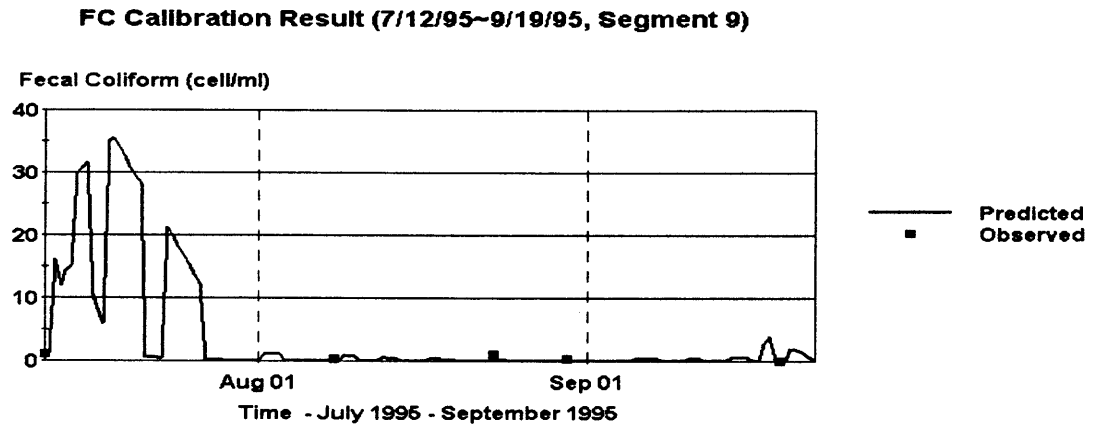

Figure 5.9(c) FC Calibration –Segment 9 (Temporal Variation).

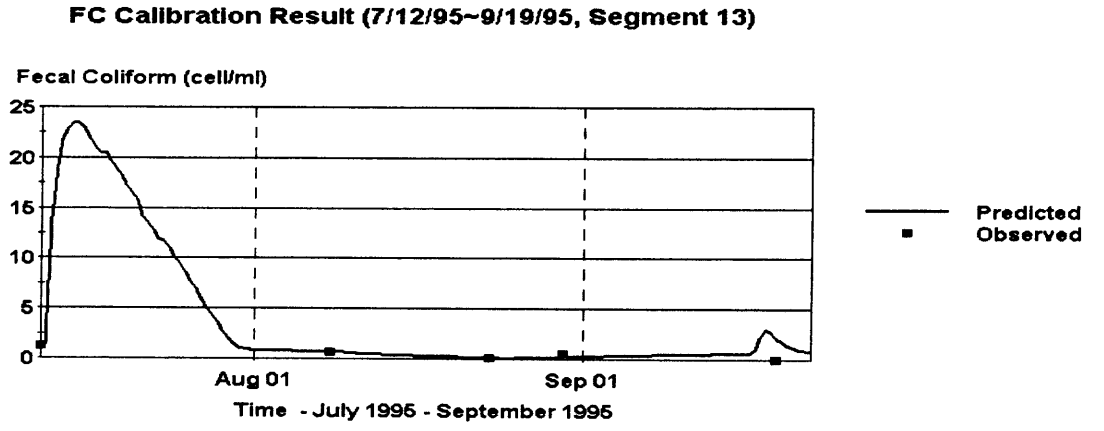

Figure 5.9(d) FC Calibration –Segment 13 (Temporal Variation).

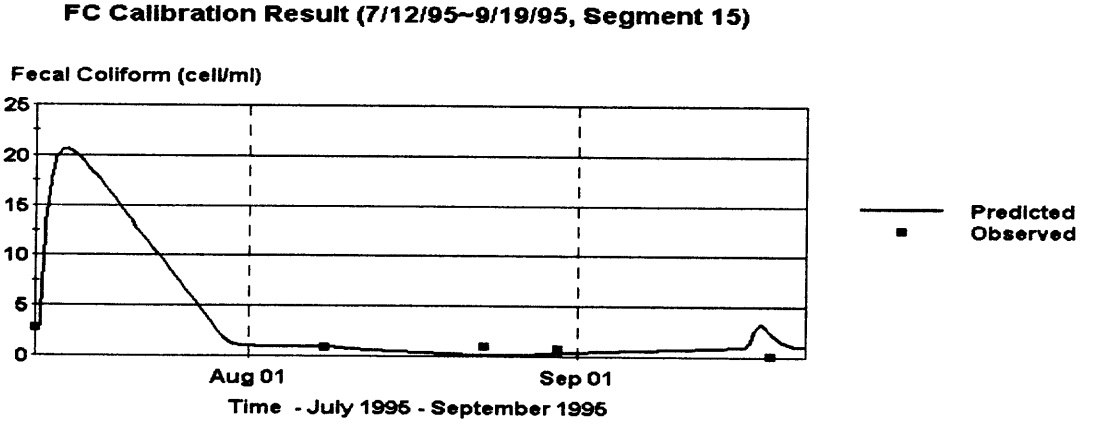

Figure 5.9(e) FC Calibration –Segment 15 (Temporal Variation).

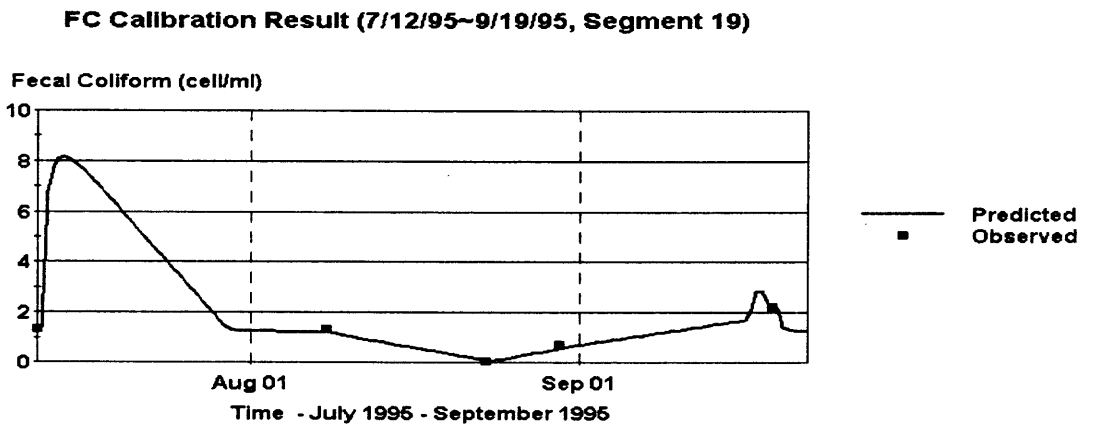

Figure 5.9(f) FC Calibration –Segment 19 (Temporal Variation).

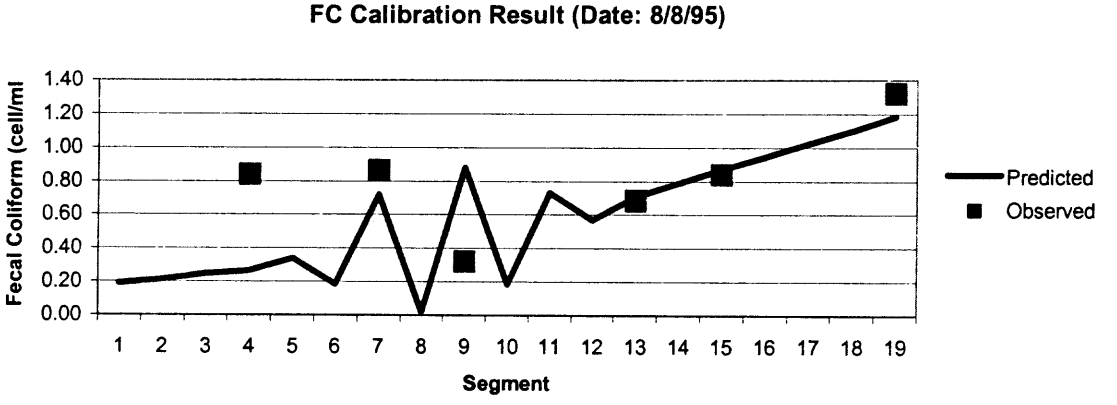

Figure 5.10(a) FC Calibration – 8/8/95 (Spatial Distribution).

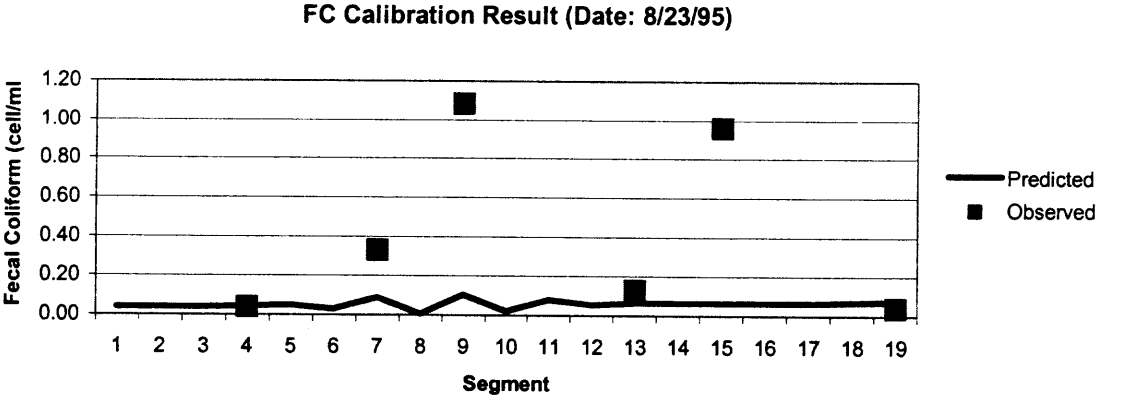

Figure 5.10(b) FC Calibration – 8/23/95 (Spatial Distribution).

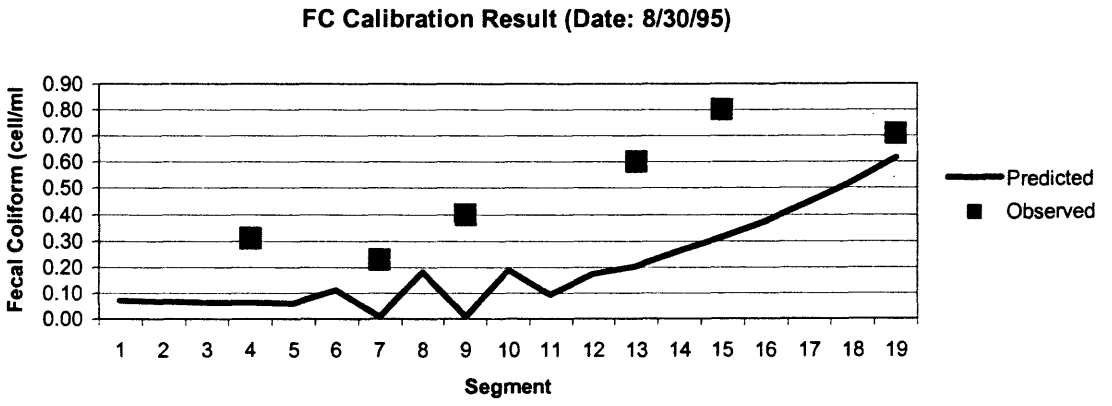

Figure 5.10(c) FC Calibration – 8/30/95 (Spatial Distribution).

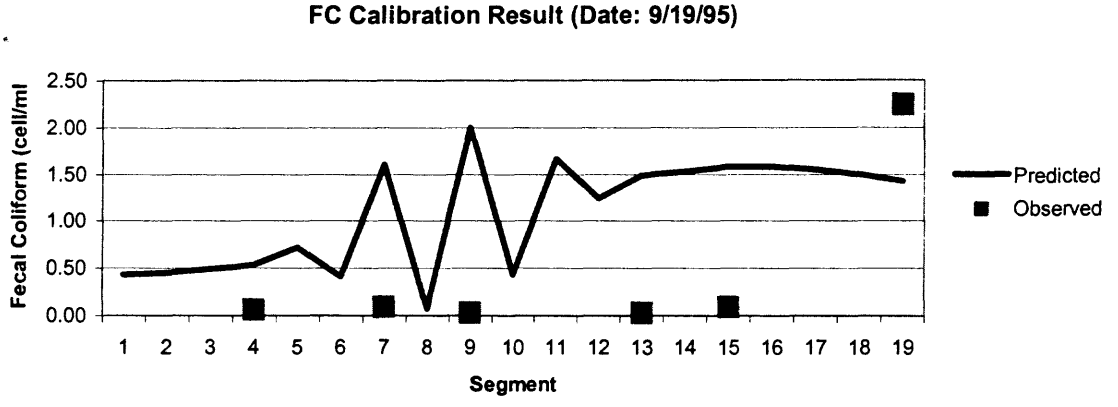

Figure 5.10(d) FC Calibration – 9/19/95 (Spatial Distribution).

In summary, the concentration of bacteria is affected by the local geometric and environmental condition. According to the plots of the calibration result, the model predicts FC concentrations that are in good agreement with observed data for most of the simulation period and segments, except for a few particular periods and segments. More detailed observed data are needed to create a more sensitive model.

5.3 Model Validation

To determine if the model assumptions and calibration parameters are applicable for the study area beyond the calibration period, a 43-days simulation was conducted for the period from September 19 to October 31, 1995 for the EUTRO model. External forcing functions for this simulation are specified using a second individual field data set for stream flow rate, initial concentration, boundary condition, water temperature, and external pollutant loadings. Segmentation, sediment properties, and all model coefficients and process rate constants remain the same as those defined in the model calibration process.

5.3.1 Physical Parameters Validation

Tables 5.16 and 5.17 present the validation result of salinity. High Correlation Coefficient Square values, especially in temporal variation (0.83 ~1.00), indicate that the calibrated reaction constants and process rate constants are reliable and the calibrated model can be used to simulate the study water system. Most of the RMSE values were found to be higher than 15% except in Segment 19 (0.5%). The inaccuracy of the boundary concentrations could produce the high RMSE values and the limited number of sample measurements again magnifies the statistical results. Figure 5.11 reveals that the model predicted values are higher than the field measurements, especially for the data on October 31, 1995. Figure 5.12, which presents the spatial distribution of salinity, shows the same trend on that day. It also indicates that the worst condition occurs in segments downstream rather than upstream.

Table 5.16 Statistical Result of Salinity Validation (Temporal Variation)

Segment	Seg4	Seg7	Seg9	Seg13	Seg15	Seg19
R^2	0.99	0.98	0.94	0.83	0.83	1.00
RMSE	1.86	2.11	2.4	3.08	3.67	0.09
%	16.5%	16.0%	17.5%	20.3%	21.8%	0.5%

Table 5.17 Statistical Result of Salinity Validation (Spatial Distribution)

Date	9/19	10/11	10/31
R^2	0.71	0.81	0.74
RMSE	1.48	1.90	4.04
%	5.9%	10.0%	46.0%

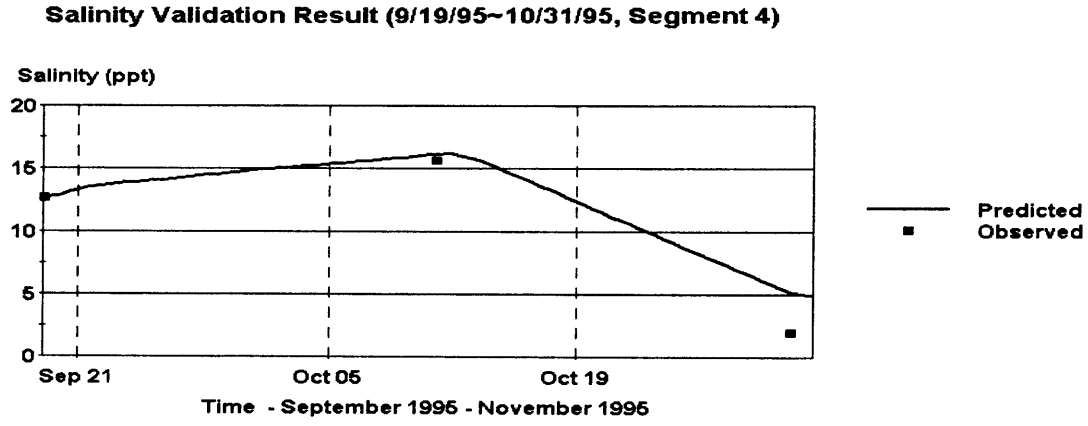

Figure 5.11(a) Salinity Validation – Segment 4 (Temporal Variation).

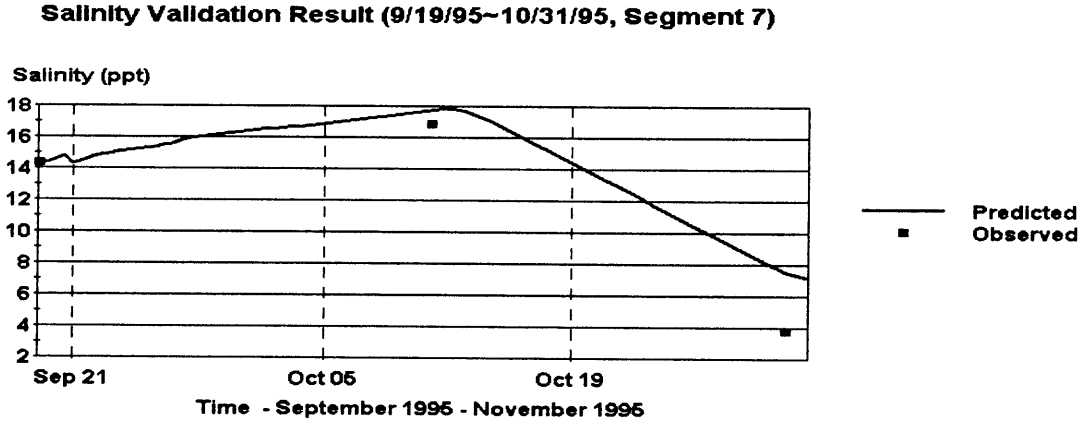

Figure 5.11(b) Salinity Validation – Segment 7 (Temporal Variation).

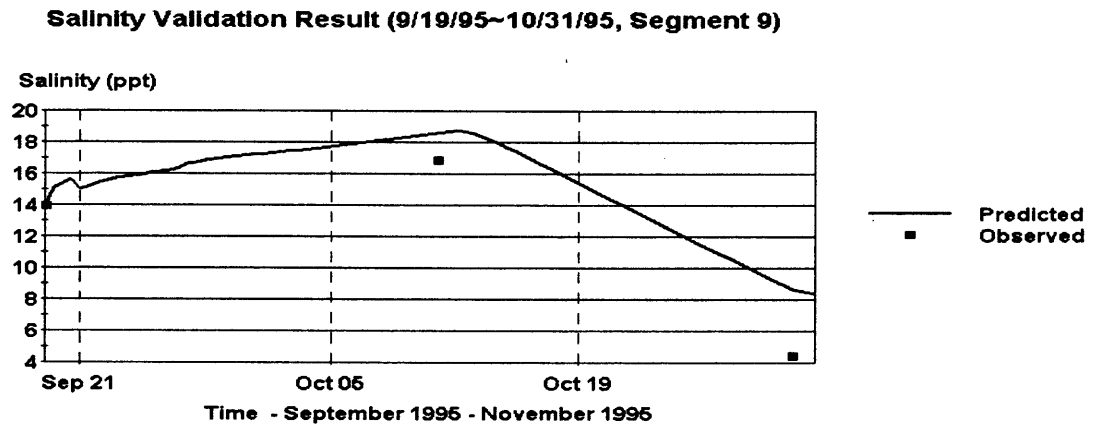

Figure 5.11(c) Salinity Validation – Segment 9 (Temporal Variation).

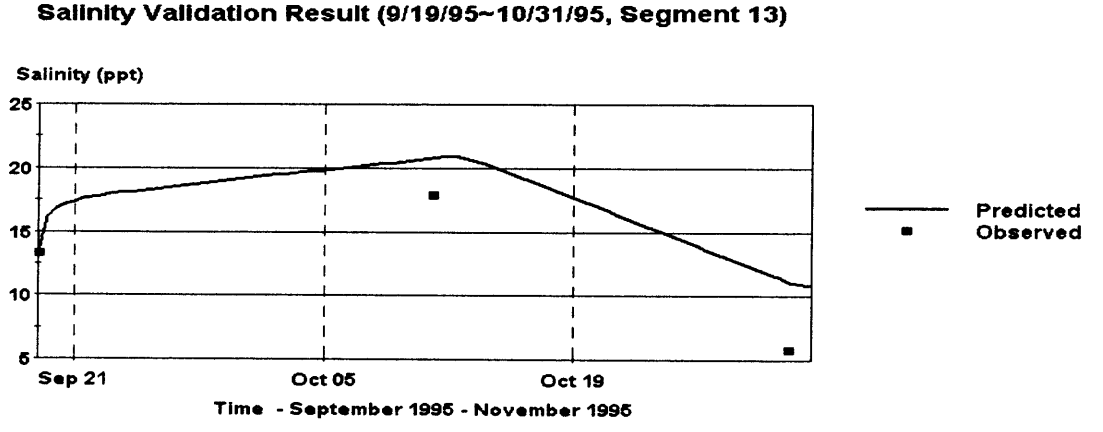

Figure 5.11(d) Salinity Validation – Segment 13 (Temporal Variation).

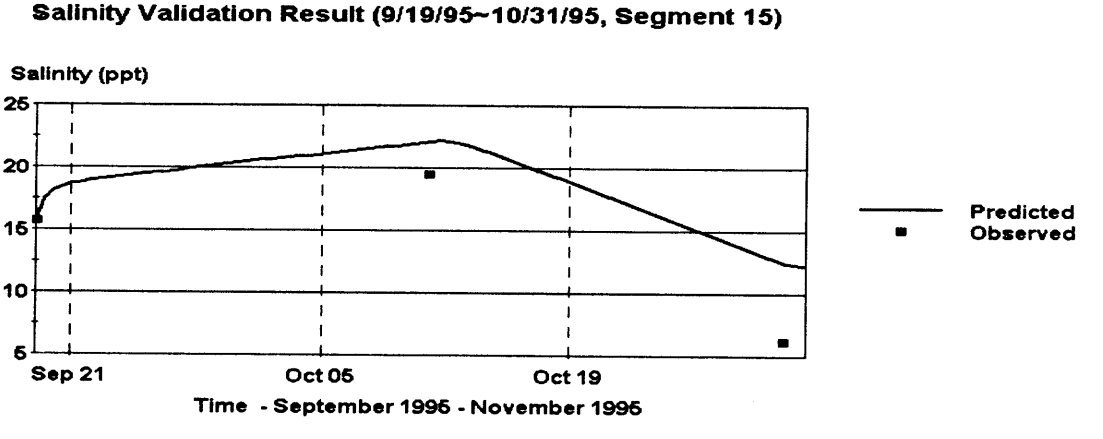

Figure 5.11(e) Salinity Validation – Segment 15 (Temporal Variation).

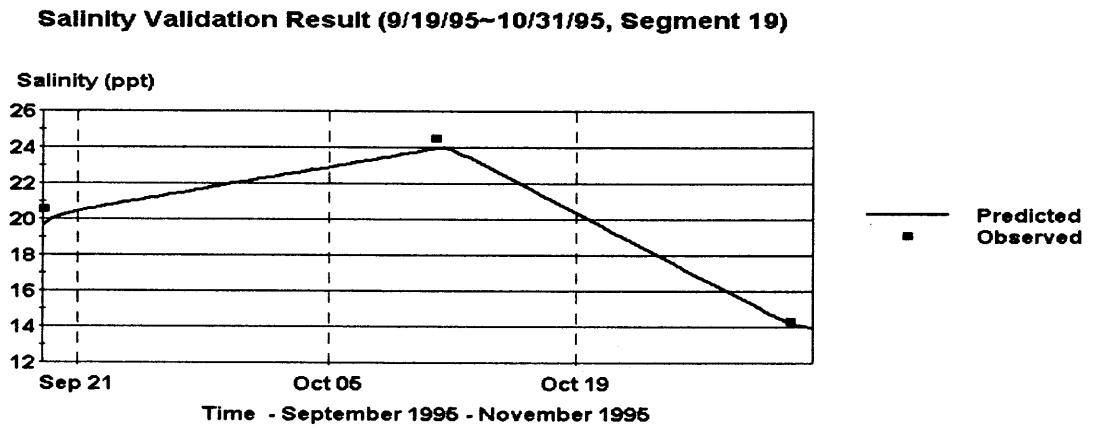

Figure 5.11(f) Salinity Validation – Segment 19 (Temporal Variation).

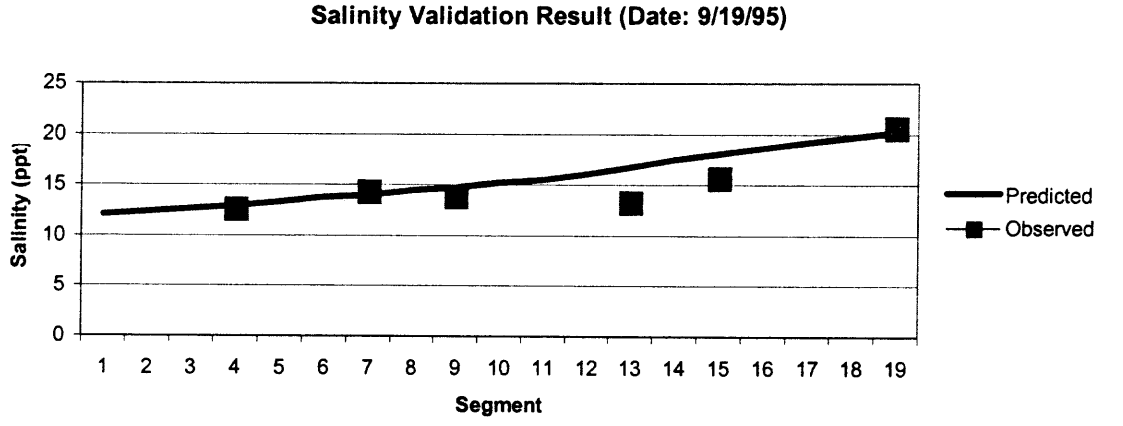

Figure 5.12(a) Salinity Validation – 9/19/95 (Spatial Distribution).

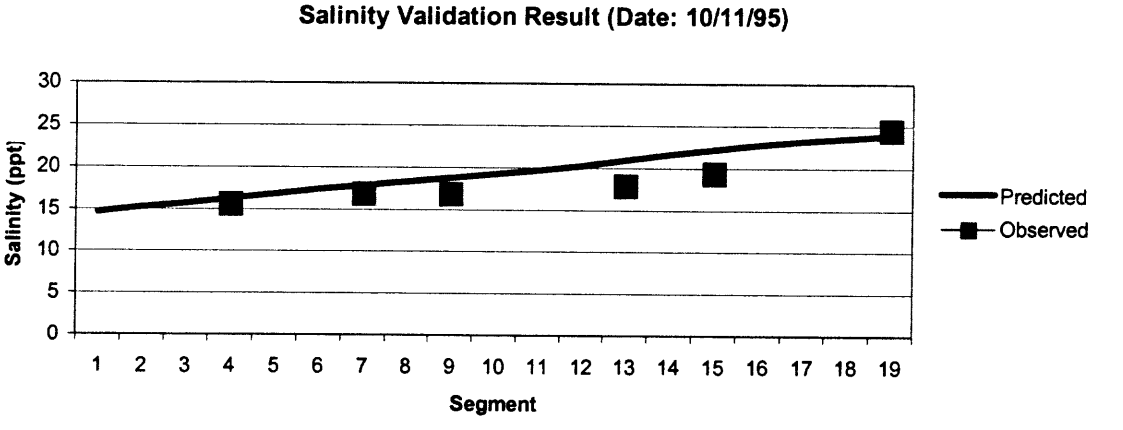

Figure 5.12(b) Salinity Validation – 10/11/95 (Spatial Distribution).

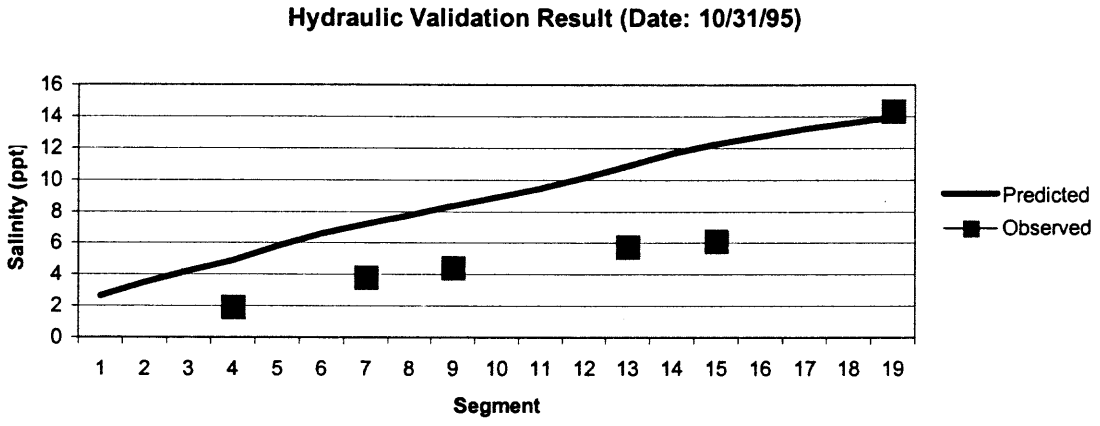

Figure 5.12(c) Salinity Validation – 10/31/95 (Spatial Distribution).

5.3.2 DO/BOD/Nitrogen Validation

Table 5.18 summarizes the statistical result of the DO validation in temporal variation. It indicates that the predicted data are in good agreement with the observed data for Segments 4, 13, 15 and 19. In these segments, the values of Correlation Coefficient Square are higher than 0.98 and the RMSE values are within 8.0%. Due to the presence of a wave-like curve in the predicted value plot between Segment 5 and Segment 13, the statistical results shown in Segments 7 and 9 are poor. The RMSE of Segment 9 is even higher than 100%. The same situation occurred in the spatial distribution analysis, which is shown in Table 5.19. The low Correlation Coefficient Square values show poor correlation between the predicted and the observed values. However, as mentioned earlier in the DO calibration process, these poor statistical numbers do not present the reality of the validation result. Figures 5.13 and 5.14 prove that most of the observed data fall close to the predicted trend lines, especially the data on October 11 and October 31.

Table 5.18 Statistical Result of DO Validation (Temporal Variation)

Segment	Seg4	Seg7	Seg9	Seg13	Seg15	Seg19
R^2	1.00	0.86	0.87	0.98	0.98	0.98
RMSE	0.33	3.8	4.76	0.62	0.61	0.03
%	3.6%	71.8%	108.0%	7.7%	7.1%	0.4%

Table 5.19 Statistical Result of DO Validation (Spatial Distribution)

Date	9/19	10/11	10/31
R^2	0.02	0.02	0.08
RMSE	4.45	2.58	4.35
%	48.3%	50.5%	57.7%

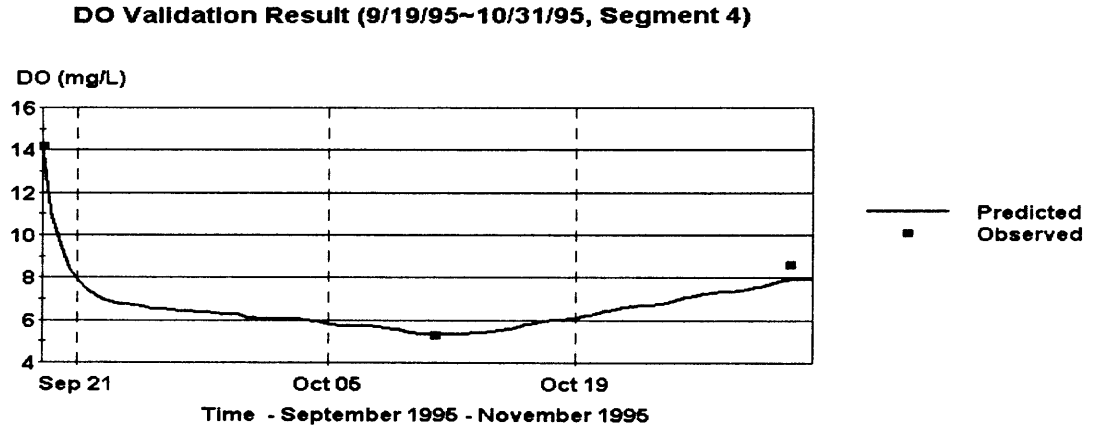

Figure 5.13(a) DO Validation – Segment 4 (Temporal Variation).

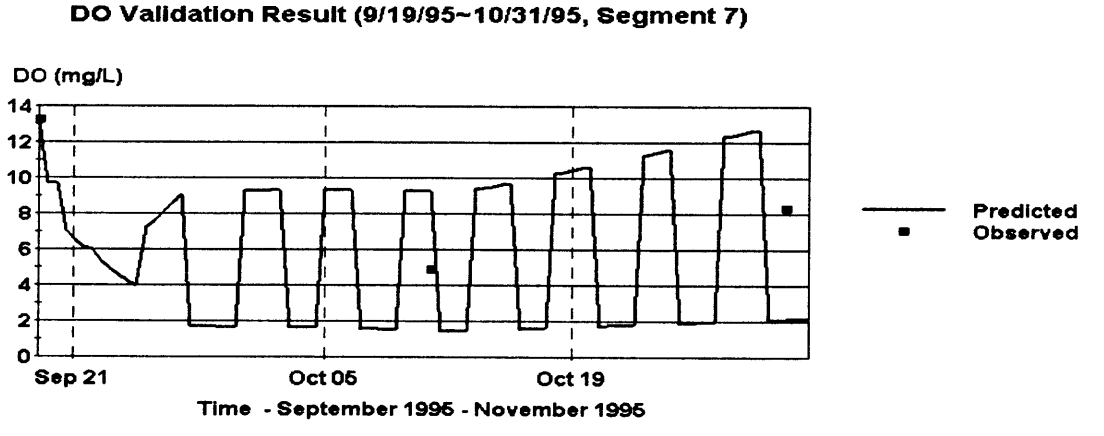

Figure 5.13(b) DO Validation – Segment 7 (Temporal Variation).

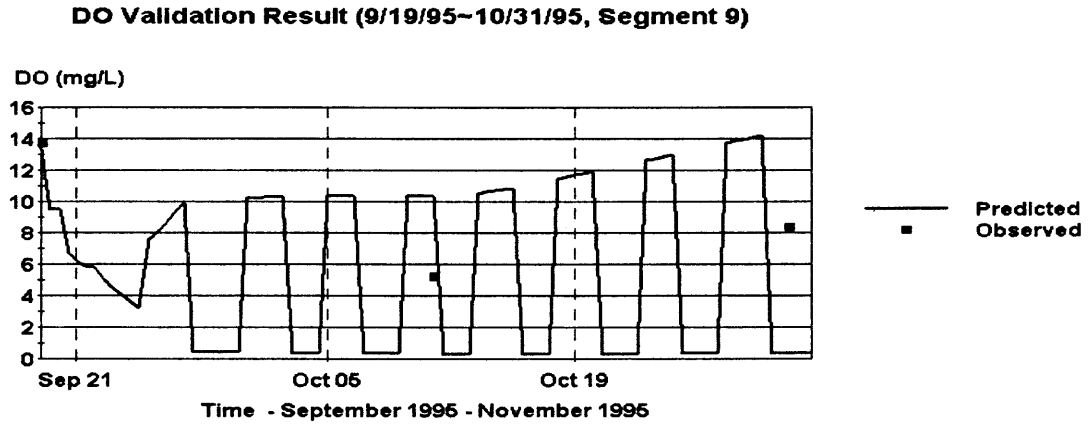

Figure 5.13(c) DO Validation – Segment 9 (Temporal Variation).

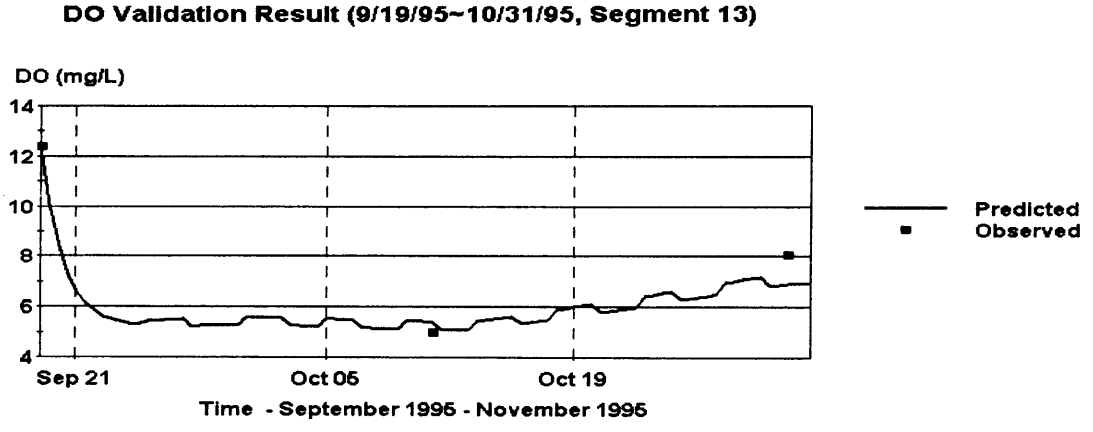

Figure 5.13(d) DO Validation – Segment 13 (Temporal Variation).

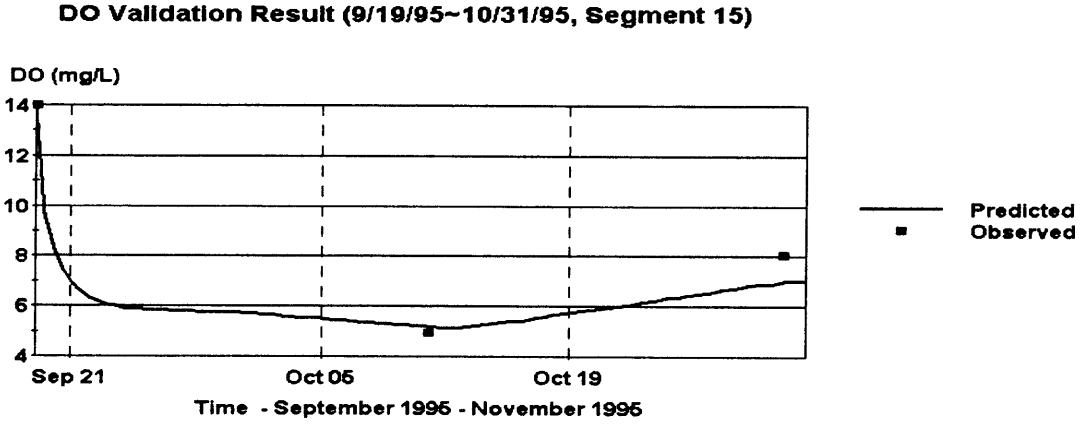

Figure 5.13(e) DO Validation – Segment 15 (Temporal Variation).

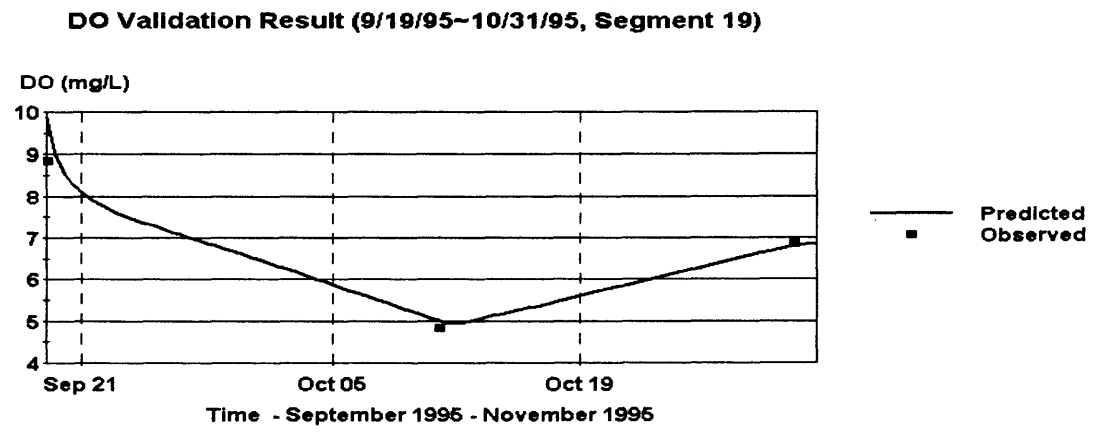

Figure 5.13(f) DO Validation – Segment 19 (Temporal Variation).

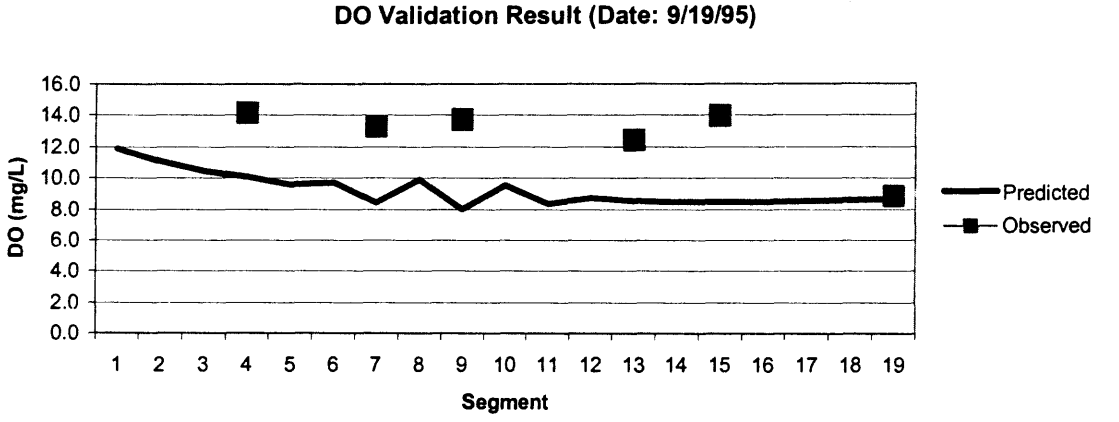

Figure 5.14(a) DO Validation – 9/19/95 (Spatial Distribution).

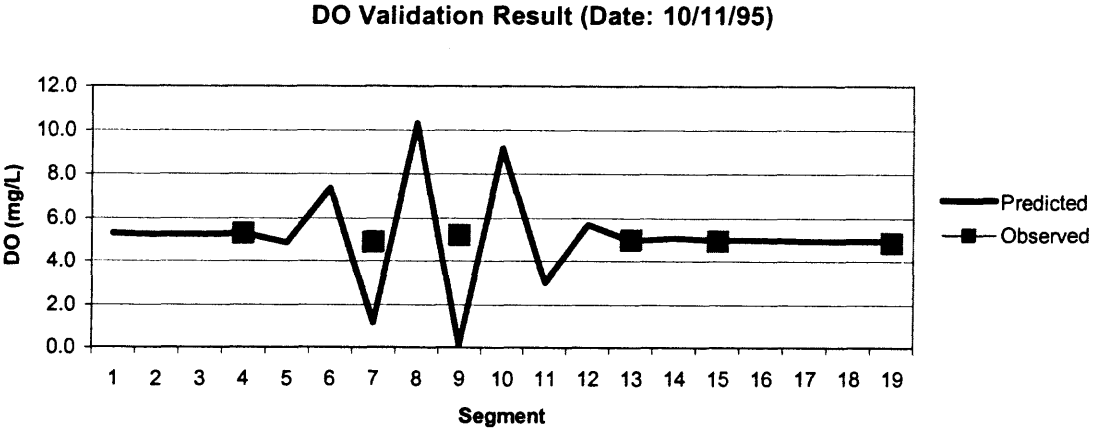

Figure 5.14(b) DO Validation – 10/11/95 (Spatial Distribution).

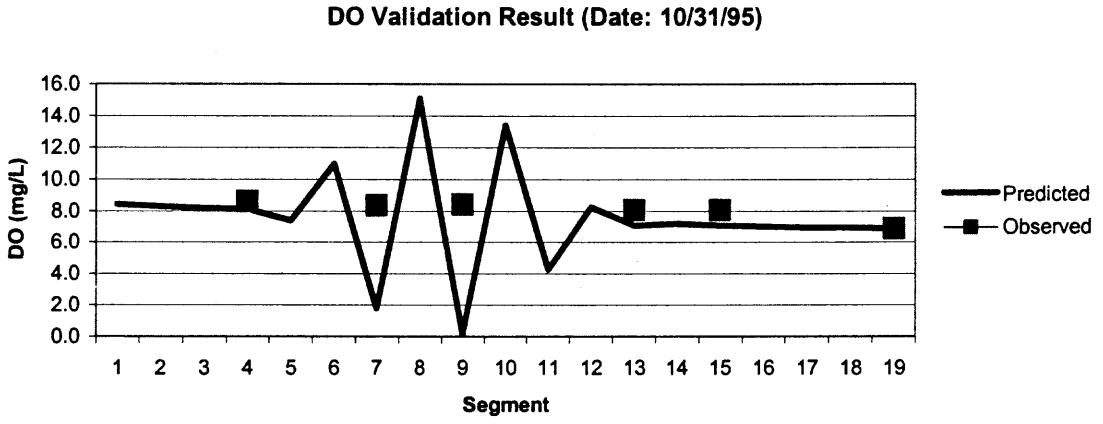

Figure 5.14(c) DO Validation – 10/31/95 (Spatial Distribution).

Statistically, the BOD validation results are much better than the DO's; though the plots show similar wave-like curves during the simulation. Both the Correlation Coefficient Square and the RMSE values show that the model predicted data are in good agreement with the observed data. For each segment, the value of Correlation Coefficient Square is close to 1.0 and the RMSE value is within 10%. In the spatial distribution analysis, again, the statistical result is affected by the unstable wave-like curve. The plots show that the predicted and observed data are closely placed and most of the field measurements are close to the predicted trend line. Tables 5.20 and 5.21 and Figures 5.15 and 5.16 present the statistical results and plots of BOD validation in temporal variations and spatial distributions, respectively.

Table 5.20 Statistical Result of BOD Validation (Temporal Variation)

Segment	Seg4	Seg7	Seg9	Seg13	Seg15	Seg19
R^2	0.99	1.00	1.00	1.00	1.00	1.00
RMSE	0.17	0.39	0.45	0.14	0.20	0.04
%	4.0%	6.3%	9.9%	4.1%	3.3%	1.4%

Table 5.21 Statistical Result of BOD Validation (Spatial Distribution)

Date	9/19	10/11	10/31
R^2	0.77	0.07	0.22
RMSE	2.02	0.50	0.49
%	27.2%	16.9%	24.7%

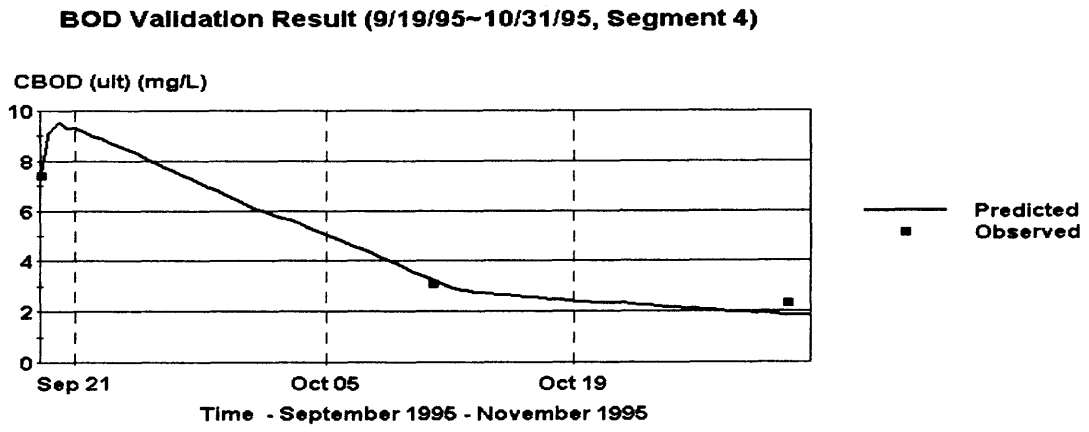

Figure 5.15(a) BOD Validation – Segment 4 (Temporal Variation).

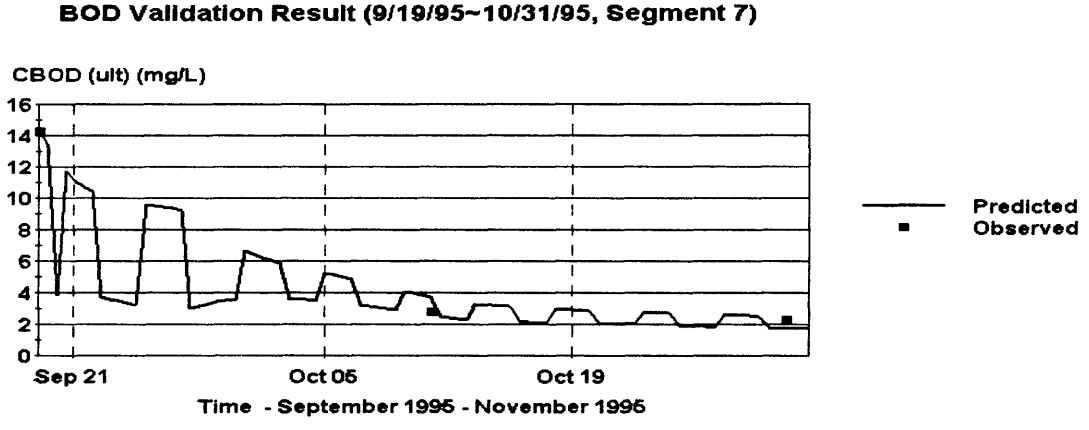

Figure 5.15(b) BOD Validation – Segment 7 (Temporal Variation).

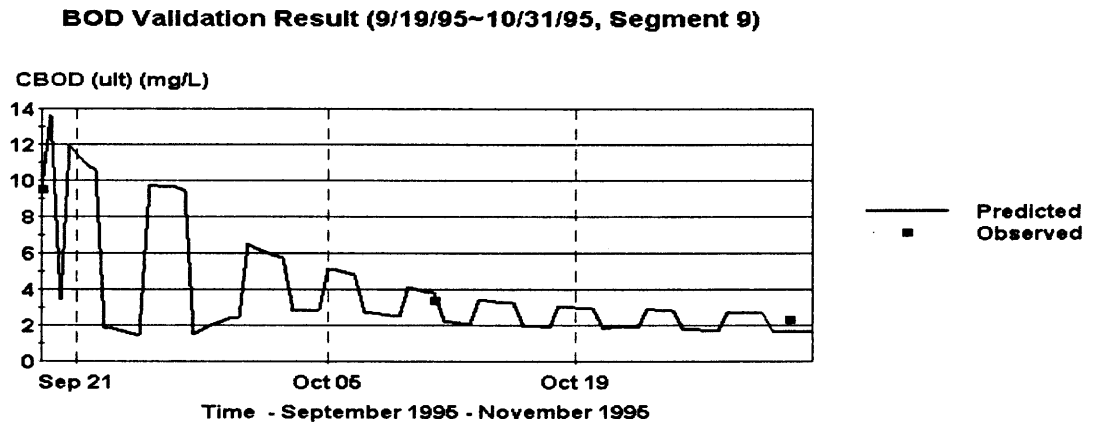

Figure 5.15(c) BOD Validation – Segment 9 (Temporal Variation).

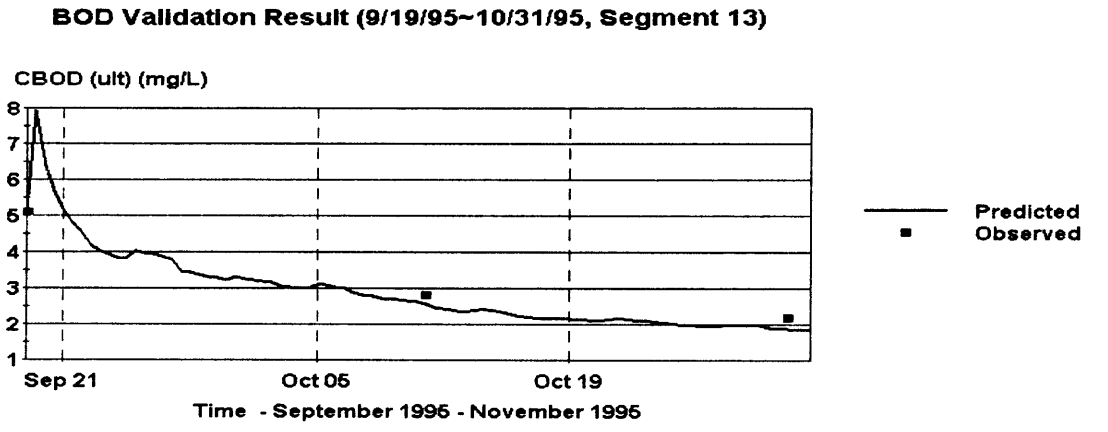

Figure 5.15(d) BOD Validation – Segment 13 (Temporal Variation).

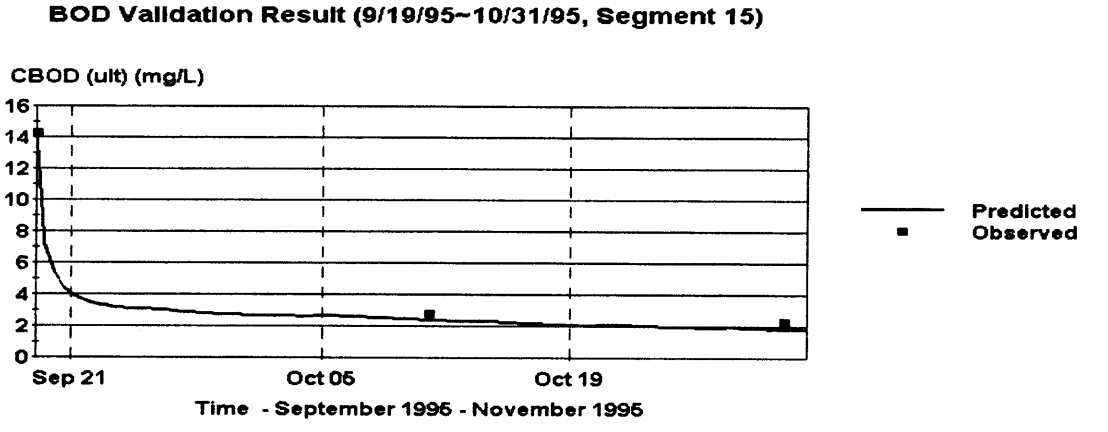

Figure 5.15(e) BOD Validation – Segment 15 (Temporal Variation).

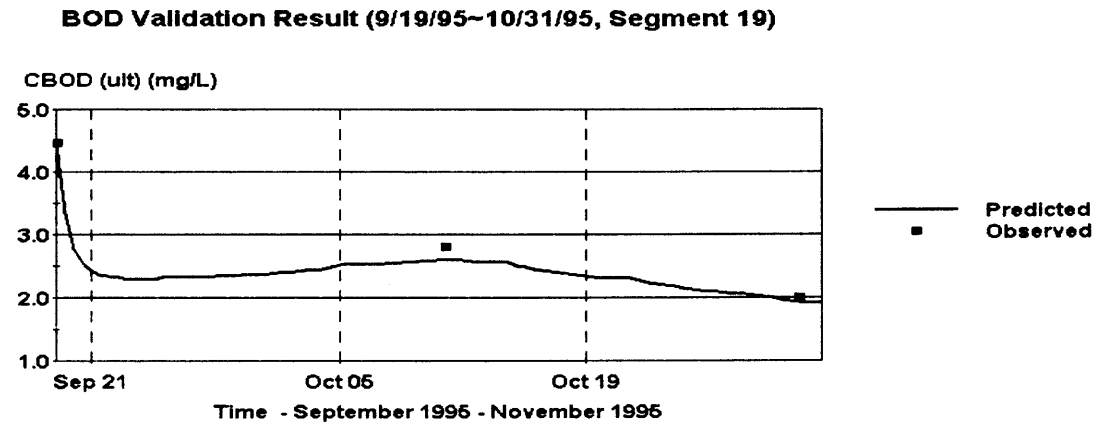

Figure 5.15(f) BOD Validation – Segment 19 (Temporal Variation).

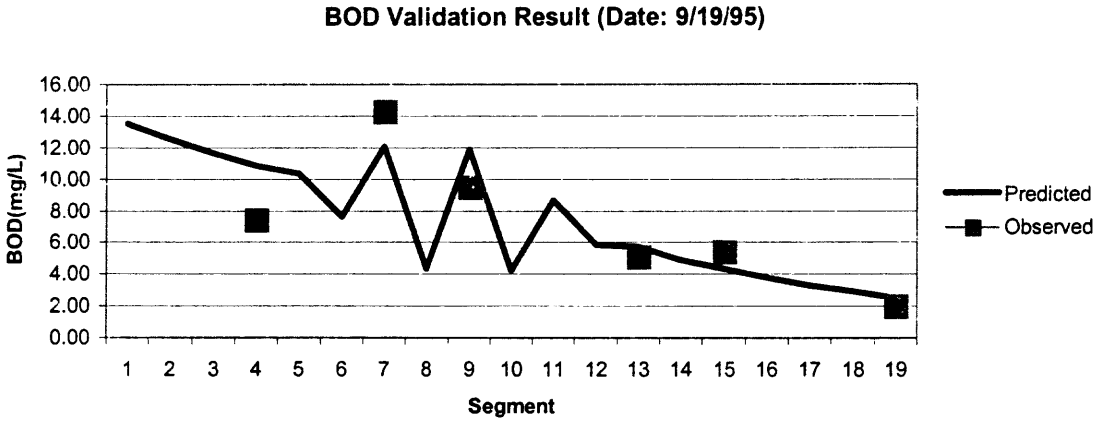

Figure 5.16(a) BOD Validation – 9/19/95 (Spatial Distribution).

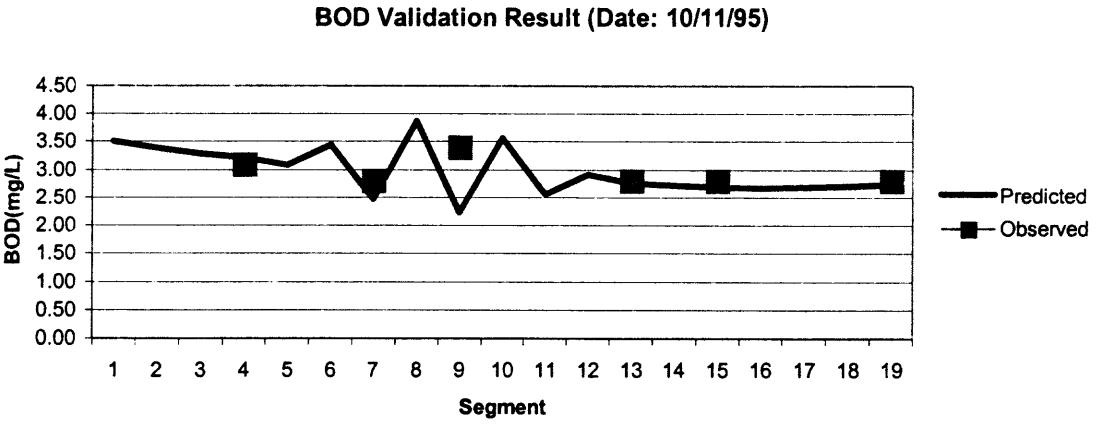

Figure 5.16(b) BOD Validation – 10/11/95 (Spatial Distribution).

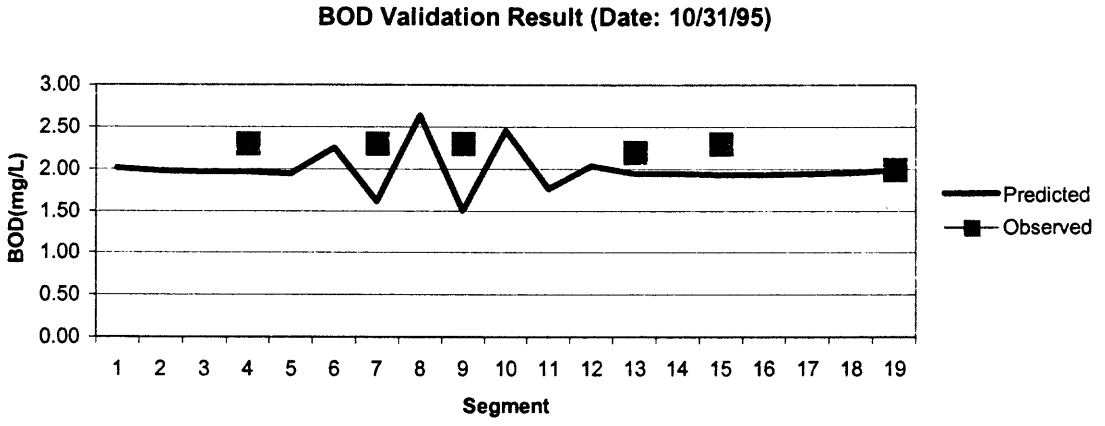

Figure 5.16(c) BOD Validation – 10/31/95 (Spatial Distribution).

The statistical validation result of NH_3-N in the perspective of temporal variation, which is summarized in Table 5.22, shows that the model predicted values are in good agreement with the field data for Segments 7 and 19. The Correlation Coefficient Square value is close to 1.0 and the RMSE value is within 7% in these segments. Other segments have strong correlation between the predicted and the observed data (higher than 0.94) but the RMSE values for these segments are higher than 20%. The high RMSE values may be introduced by the limited sampling numbers and the wave-like curve. The similar poor statistical results also can be observed in the spatial distribution analysis (Table 5.23). The RMSE value on September 19 is even higher than 90% (90.9%). However, as with other validation results shown in the plots, most of the observed data for NH_3-N validation fall close to the predicted trend lines, except in the plot of September 19. This indicates that these poor statistical numbers do not present the reality of the validation result. Figures 5.17 and 5.18 present the validation results in plots for the temporal variation and the spatial distribution analyses, respectively.

Table 5.22 Statistical Result of NH_3-N Validation (Temporal Variation)

Segment	Seg4	Seg7	Seg9	Seg13	Seg15	Seg19
R2	0.95	0.99	0.94	0.94	0.95	0.99
RMSE	0.05	0.01	0.05	0.07	0.07	0.01
%	27.5%	6.9%	25.2%	25.4%	23.8%	2.2%

Table 5.23 Statistical Result of NH3-N Validation (Spatial Distribution)

Date	9/19	10/11	10/31
R2	0.41	0.85	0.69
RMSE	0.13	0.06	0.08
%	90.9%	11.2%	40.0%

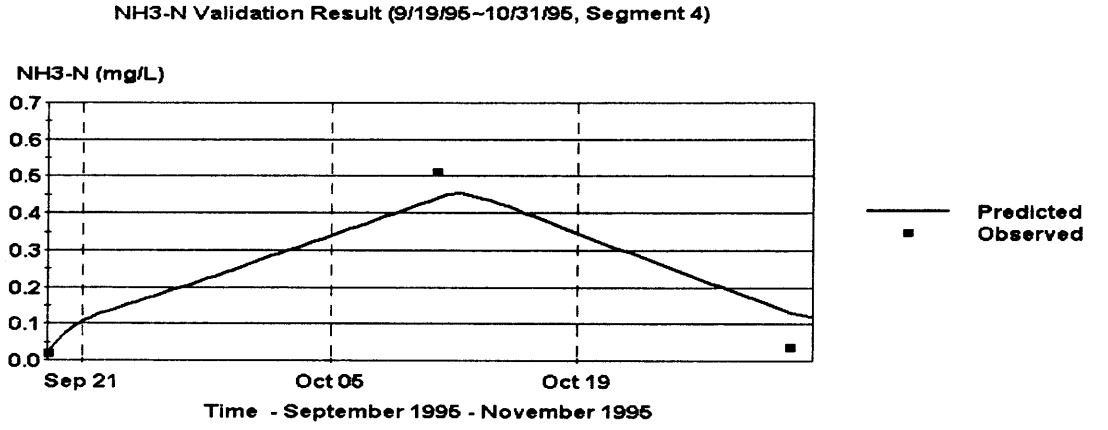

Figure 5.17(a) NH_3-N Validation – Segment 4 (Temporal Variation).

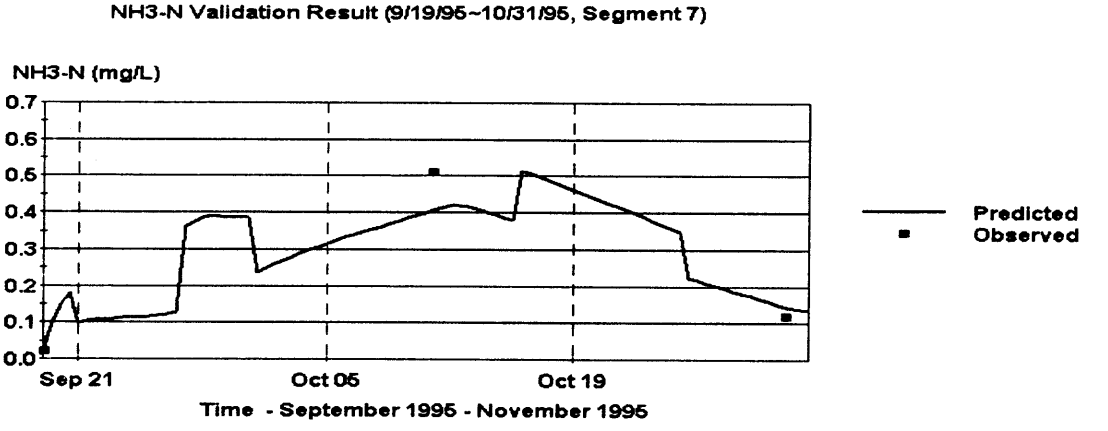

Figure 5.17(b) NH_3-N Validation – Segment 7 (Temporal Variation).

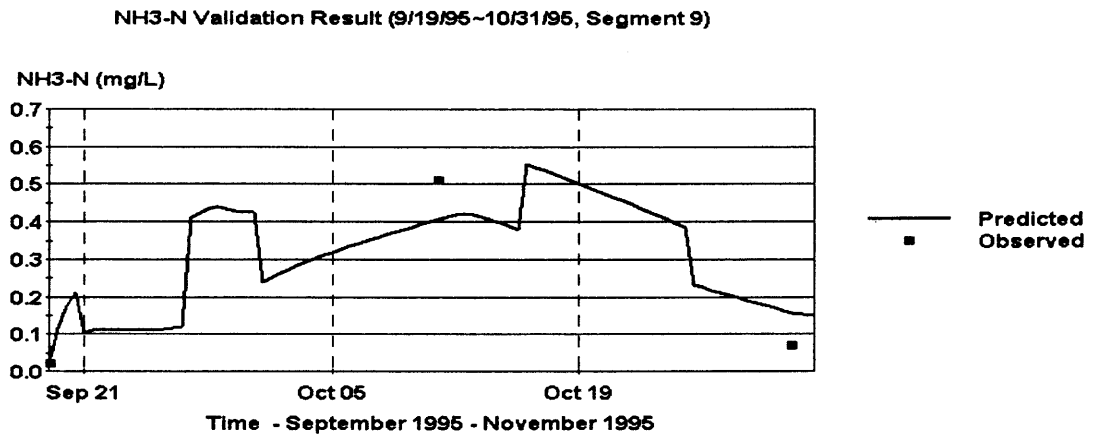

Figure 5.17(c) NH_3-N Validation – Segment 9 (Temporal Variation).

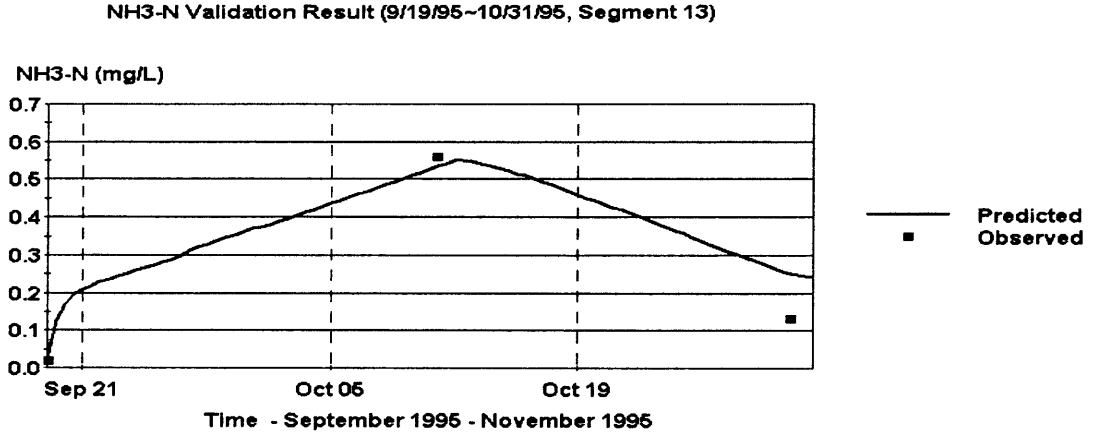

Figure 5.17(d) NH_3-N Validation – Segment 13 (Temporal Variation).

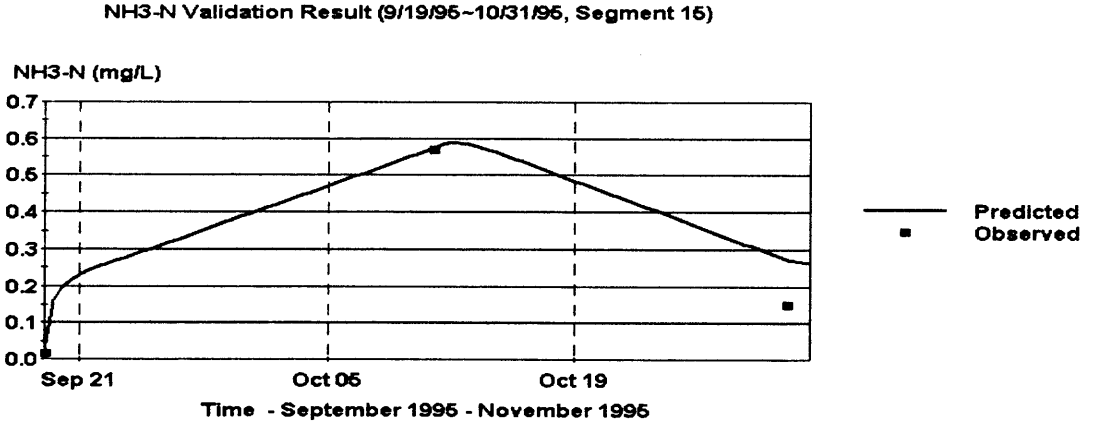

Figure 5.17(e) NH_3-N Validation – Segment 15 (Temporal Variation).

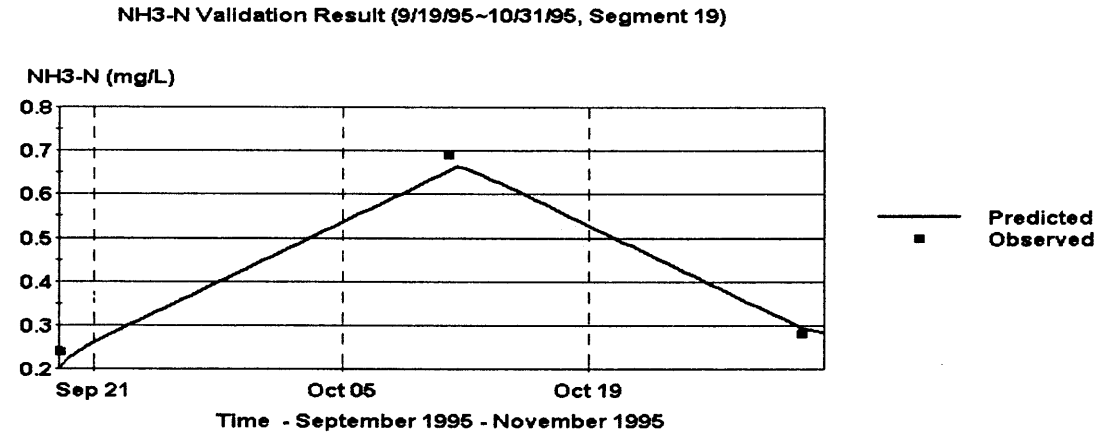

Figure 5.17(f) NH_3-N Validation – Segment 19 (Temporal Variation).

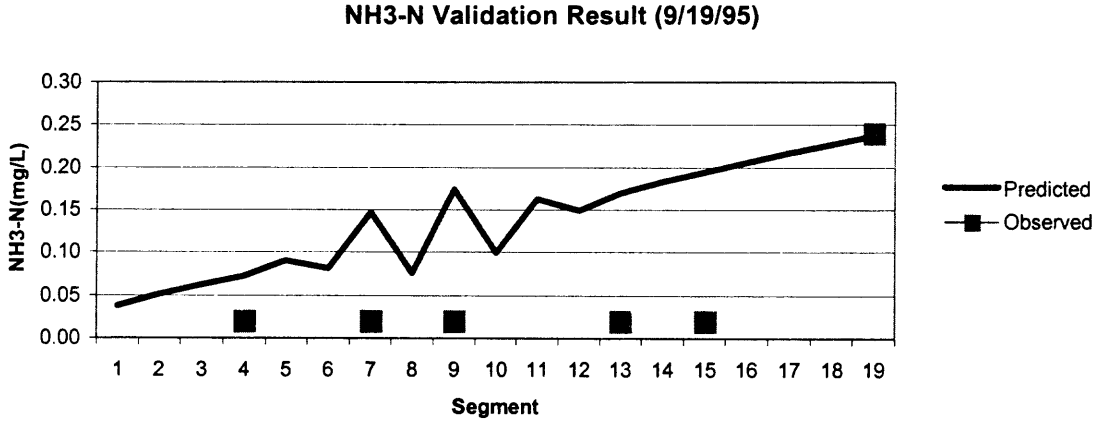

Figure 5.18(a) NH_3-N Validation – 9/19/95 (Spatial Distribution).

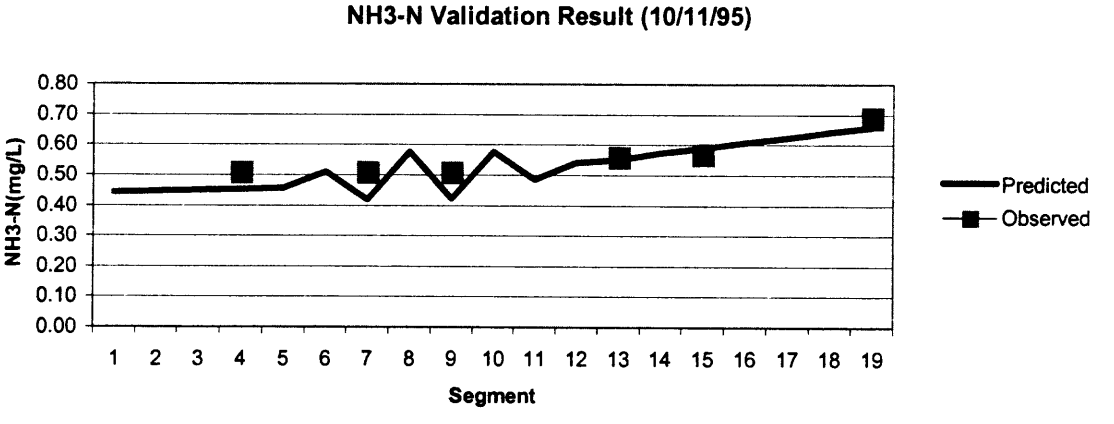

Figure 5.18(b) NH_3-N Validation – 10/11/95 (Spatial Distribution).

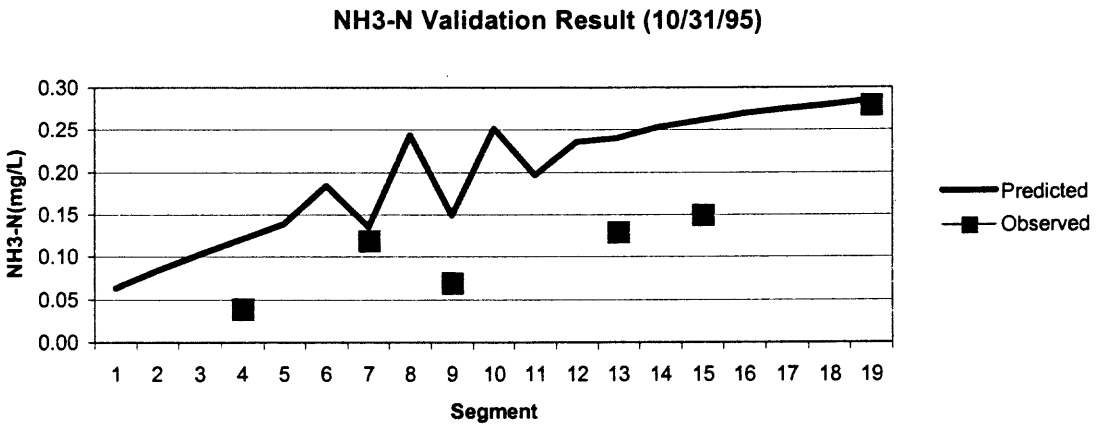

Figure 5.18(c) NH_3-N Validation – 10/31/95 (Spatial Distribution).

5.4 Sensitivity Analysis

In order to determine the relative effects of the various parameters on water quality, sensitivity analyses were performed on several variables. These analyses were performed by varying critical parameters, which include both water quality transport and transformation constants, one at a time while the change in the model output was observed. The transport parameters are variables such as flowrate and dispersion coefficient. The transformation constants, in this study, are reaeration rate, BOD decay rate, nitrification rate, and SOD for the DO simulation; bacteria death rate for the FC simulation; and partition coefficient and DOC (dissolved organic carbon) for the Mercury model. All the parameters were analyzed individually by the following method.

Hann and Zhang (1996) indicated that the sensitivity of parameters to a specific constituent in a system could be presented by the relative sensitivity. The parameters with high relative sensitivity produce larger variation in the specific variable concentration

than those with low relative sensitivity if the parameters have the same degree of increase or decrease. The relative sensitivity is calculated by the following equation:

$$S_r = (\delta_m / \delta_p) * (P / M)$$

$$\text{Where } \delta_m = M_{p+\Delta p} - M_{p-\Delta p}$$

$$\delta_p = 2*\Delta p$$

In this equation, δ_m is the change of the averaged modeled value; δ_p is the change in the input parameter value. P is the parameter estimate in the calibration run, and M is the mean simulated value in the calibration. Δp is defined as (10% * P). $M_{p+\Delta p}$ and $M_{p-\Delta p}$ are the mean simulated values with P increased by Δp and decreased by Δp, respectively.

Table 5.24 Result of the Sensitivity Analysis

Parameter	Relativity Sensitivity				
	Salinity	DO	CBODU	Fecal Coliform	Mercury
Dispersion Coefficient	0.01	0.08	0.11	-0.02	-0.11
Flowrate	-0.01	-0.04	0.05	-0.22	-0.06
Solids Flow	---	---	---	---	0.003
DO Reaeration Rate	---	0.16	~0	---	---
Nitrification Rate	---	-0.02	~0	---	---
BOD Decay Rate	---	-0.07	-0.18	---	---
SOD	---	0.01	~0	---	---
Bacteria Death Rate	---	---	---	-0.3	---
Partition Coefficient	---	---	---	---	~0
DOC	---	---	---	---	~0

Table 5.24 summarizes the sensitivity analysis result. In general, the calculated relative sensitivities are low, especially for the transformation coefficients in the Mercury model. In other words, the concentrations of pollutants were not sensitive to the environmental parameters presented in this study. The low relative sensitivity may be the result of the high dilution effect caused by the high flowrate in the study area. However, by comparing the relative sensitivity of parameters, the most important parameter for

each of the pollutants can still be located. In the EUTRO model, DO level is much more sensitive to the reaeration constant than the other parameters, and BOD is only sensitive to the BOD decay rate. For FC simulation, the concentration of fecal coliform is influenced both by the bacteria death rate and the stream flowrate. In the Mercury model, the pollutant concentration is controlled by the transport parameters rather than the transformation coefficients.

5.5 Summary

The successful development, calibration, and validation of a water quality model require the synthesis of a large amount of information. Rarely is all of the information available, which could explain why the development of a model with perfect calibration and validation for all parameters is rarely reached. Based on the available field data, those unknown or least known parameters were adjusted to more adequately simulate the measured conditions within the study area. These parameters included the water quality transport constants and transform coefficients.

Because of the assumptions made to simplify the model that the system is homogeneous and that values for most of the environmental conditions are constant; the model could not be expected to predict accurately the absolute values exactly as determined by field measurements. However, for a reliable model, one should track the variation and predict values within the range of the field data. Generally, simulation results agree with observations for DO simulation and FC model after calibration. The resulting few of poor statistical values of calibration could come from the large-scale segmentation and inaccuracy of the sampling program. This model could be improved

later by dividing segments into finer cells and by employing an intensive sampling program.

The calibrated environmental parameters were validated for the EUTRO model. However, the limited field data available constrained the validation process for the FC model. Increased information on the field data can result in less uncertainty of model predictions and greater understanding of the aquatic system. Sensitivity analysis can be used to study the relative effects of the various parameters on water quality, such as the study of mercury concentration in the river and sediment by using the Mercury model in this study.

CHAPTER 6

THE IMPACTS OF THE CSO LOADING ON RECEIVING WATER QUALITY

The calibrated WASP6.1 water quality model, which includes three sub-models: EUTRO, Heat, and Mercury, was used to investigate the impact of CSO discharge on receiving water mathematically. The water quality criteria and critical conditions are used as the reference to evaluate the water quality. The impacts of CSO were studied with a series of scenarios, which include the major factors that would affect the water quality of the receiving water. The impacts from the quantity of CSO load were evaluated first by varying the load input. The flowrate of the receiving water, which exerts a dilution effect on the water quality, was then examined. The temporal variation and spatial distribution of the pollutants in the receiving water were tested last.

6.1 Result Interpretation

Since the purpose of this study is to develop a mathematical model to study the effect of discharge of CSO on receiving water quality, so the result of this study can be used by water resource managers and scientists to (1) calculate pollutant loads from combined sewer overflows for monitored storm events; (2) describe temporal variations for pollutant concentrations in the receiving water from storm to storm; (3) describe spatial distribution of selected pollutants discharging from combined sewers to the receiving water; and (4) provide data and information to define appropriate management methods to reduce or eliminate untreated CSO discharges. A comprehensive control plan addressing the characteristics of the combined sewer system and overflows, which

identifies the impact of CSOs on receiving water uses and establishes performance goals for the CSO control program, will provide the basis for selecting and locating appropriate technologies (or technology combinations) in the system (US EPA, 1993). To simulate the impacts of CSOs, the following scenarios were studied.

1) The impact of the load on the receiving water quality: By altering CSO load scale in the calibrated model, results can simulate the impact of CSO loads on the receiving water quality.

2) The impact of the receiving water flowrate on the water quality: High-flowrate in receiving waters may dilute the CSO load.

3) Spatial effect of CSO loading: By setting only one CSO discharge point in the calibrated model, a check can be made of the spatial distribution of the pollutants in the receiving water.

4) Temporal effect of CSO loading: By setting only one CSO discharge event in the calibrated model, an observation of the temporal variation of the constituents during the simulation period can be made.

Table 6.1 summarizes the scenarios, which were studied in this research.

6.2 Water Quality Criteria and Critical Conditions

Prior to investigation of the impact of combined sewer discharges on receiving water, the water quality criteria and critical condition for the river studied must be determined for use in the water quality model. Water quality criteria are the references that can be used to evaluate the effects on receiving waters and the worst water quality situation can be produced under the critical condition.

Table 6.1 Summery of Simulation Scenarios and Related Methods

Objective	Sub-objective	Method	Scenario	**Applied pollutants**
The impact of load on receiving water quality	The impact of CSO loads on receiving water quality	Alter scale factor of load input in the calibrated model	S1-1: load unit * 0	DO, BOD, NH_3-N, FC, Hg
			S1-2: load unit * 1	
			S1-3: load unit * 5	
			S1-4: load unit * 10	
	Effects of the sources of pollution on water quality	Alter loading source (CSO and WWTP) in the calibrated model	S2-1: No load	DO, BOD
			S2-2: W/O CSO	
			S2-3: Original	
			S2-4: No treatment	
	Effects of initial concentration on predicted concentration	Alter initial concentration in the calibrated model	S3-1: Original	Hg
			S3-2: Initial conc. * 2	
			S3-3: Initial conc. * 0.5	
The impact of receiving water flowrate on receiving water quality	The impact of stream flowrate on water quality	Alter scale factor of flowrate input in the calibrated model	S4-1: Original	DO, BOD, NH_3-N, FC, Hg
			S4-2: Flow function * 0.1	
			S4-3: Flow function * 0.5	
			S4-4: Flow function * 2	
			S4-5: Flow function * 10	
	The impact of geometric data on predicted concentration	Simulate flowrate scenarios without modifying geometric data	S5-1: Original	BOD
			S5-2: Flow function * 0.1	
			S5-3: Flow function * 0.5	
			S5-4: Flow function * 2	
			S5-5: Flow function * 10	
Spatial distribution analysis	The spatial distribution of pollutants after CSO discharges	Simulate pollutant distribution w/ and w/o load discharged in a sole location	S6-1: W/O CSO load	FC, Hg
			S6-2: W/ CSO load	
	The impact of tidal dispersion on pollutant spatial distribution	Simulate pollutant distribution w/ and w/o load under no dispersion condition	S7-1: W/O CSO load	FC
			S7-2: W/ CSO load	
Temporal variation analysis	The temporal variation of pollutants after CSO discharges	Simulate pollutant variation with various magnitude of loads discharged in a sole location and storm event	S8-1: load unit * 0	Hg
			S8-2: load unit * 1	
			S8-3: load unit * 5	
			S8-4: load unit * 10	
	The temporal variation of pollutants after CSO discharges under low flowrate	Simulate temporal variation scenarios under low flowrate	S9-1: load unit * 0	Hg
			S9-2: load unit * 1	
			S9-3: load unit * 5	
			S9-4: load unit * 10	

6.2.1 Water Quality Criteria

A water quality criterion is the concentration of a water quality measure that will meet a specific water use (US EPA, 1979). Unlike a water quality standard, which is the translation of a water quality criterion into a legally enforceable mass discharge or effluent limitation, a water quality criterion is based upon the purpose of water use. Different purposes of water uses have different levels of water quality criteria. For instance, the water quality criterion for drinking water must have higher water quality demand than the water for irrigation.

According to the Surface Water Quality Standards of New Jersey (NJDEP, 1985), surface water is divided into different classifications based upon their applied area, which includes fresh water, pinelands waters, saline waters of estuaries, and coastal saline waters. Each classification also defines various designed uses of the waters. For example, fresh waters are used for maintenance, migration and propagation of the natural aquatic biota; pineland waters are the source for cranberry bog water supply and other agricultural uses. Water quality criteria are then established based upon the applied area and designated uses of the surface water. Table 6.2 summarizes the water quality criteria, which includes DO, FC, and mercury for various classifications.

This approach for water quality criteria classification is not generally feasible because of the apparent difficulty in identifying natural background conditions. Therefore, in DO evaluation, the US EPA suggested a single minimum concentration of 5 mg/L at any time, instead of the use of a complicated classification, which would be enough to protect the diversity of aquatic life. In this study, 5 mg/L was used as a primary criterion to evaluate the DO condition in the surface water.

Table 6.2 Surface Water Quality Criteria of New Jersey

Substance	Criteria	Classification [a]
1.Dissolved Oxygen (mg/L)	i. Not less than 7.0 at any time	FW2-TP
	ii. 24 hour average not less than 6.0. Not less than 5.0 at any time.	FW2-TM
	iii. 24 hours average not less than 5.0. Not less than 4.0 at any time.	FW2-NT
	iv. Not less than 4.0 at any time.	Tidal portions of FW2-NT
	v. Not less than 5.0 at any time.	SC
	vi. Not less than 4.0 at any time.	SE2
	Vii. Not less than 3.0 at any time.	SE3
2.Ammonia (mg/L)	i. 0.5	FW2-TP
2.Fecal Coliform (cell/100ml)	i. Fecal coliform levels shall not exceed a geometric average of 50/100ml.	Within 1500 feet of shore-line in SC Waters
	ii. Fecal coliform levels shall not exceed a geometric average of 200/100ml nor should more than 10 percent of the total samples taken during any 30-day period exceed 400/100ml.	FW2, SE1, and SC 1500 feet to 3 miles from the shoreline.
	iii. Fecal coliform levels shall not exceed a geometric average of 770/100ml.	Tidal portions of FW2-NT, SE2
	iv. Fecal coliform levels shall not exceed a geometric average of 1500/100ml.	SE3
3. Mercury, Total (ug/L)	i. 2	FW2

Source: New Jersey Department of Environmental Protection (NJDEP). Surface Water Quality Standards, N.J.A.C. 7:9-4.1 et seq. Division of Water Quality, NJDEP.

a. FW: fresh waters. SC: coastal saline waters. SE: saline waters of estuaries. TP: trout production. TM: trout maintenance. NT: nontrout waters.

6.2.2 Critical Conditions

The critical environmental conditions must be determined first before their use in the model interpretation. These conditions include background water quality, flowrate, wind speed, incident light, and temperature. Depending on the parameter of concern, the environmental conditions that are critical vary considerably. Table 6.3 outlines the critical input conditions required for each model. Even though the same input factors may be critical for two or more water quality parameters, they can act on those parameters in a different manner. For example, dissolved oxygen parameter is most adversely affected by high temperatures when biochemical rates are maximal and reaeration is minimal at low wind speed. The impact of fecal coliform on water quality, on the other hand, is most severe under the conditions of low temperature, which would cause minimal die-off, and high wind speed, which could result in rapid transport to a sensitive area in the water system (Moffa et al., 1980).

Table 6.3 Critical Environmental Conditions for Water Quality Models

Critical Input Condition	Type of Water Quality Model		
	DO	FC	Mercury
Temperature	Yes	Yes	Yes
Flowrate	Yes	Yes	Yes
Wind Speed	Yes	Yes	Yes
Light Intensity	No	Yes	No
Initial Concentration	Yes	Yes	Yes

Critical water temperature depends on the locale as well as the parameter of concern. Information regarding critical water temperature in this study was obtained from USGS. It should be noted that for some parameters, low temperature is critical, but for others, higher temperatures will have a greater water quality impact. 20°C and 26°C were

used as low and high critical temperatures during the summer period (July to October) in this study.

The volume of streamflow (the dilution factor) is another critical variable in determining the concentration of pollutants in receiving water. Basically, the worst-case conditions are observed at the period of low flow in the stream channel. For the lower Hudson River section, according to the USGS surface water data, 24.3 m^3/s was the critical low flowrate during the summer period.

6.3 The Impacts of CSO Load

The first goal of the study is to determine the impact of CSO loads on receiving water. At the same time, the predicted result can predict whether this load violates water quality criteria. Based on the previous studies, CSO loads vary from storm to storm and site to site. In other words, they are site specific and highly variable. CSO load could also be affected by the technologies employed in CSO control. Lack of a sufficient CSO control system would discharge the CSO into the receiving water and impair the water quality. Other conditions that may cause unexpected CSO loads discharge include insufficient treatment capacity or non-treatment conditions. Since the presence of CSOs occurs at the time that the flowrate exceeds the capacity of the combined sewer systems or wastewater treatment facilities, how much a CSO will discharge is related to the capacity and operation of the corresponding control facilities. This could happen during heavy storms, power failures, or when the wastewater water treatment facility is out of order. If these should happen, the receiving water quality will deteriorate accordingly. Meanwhile, the

critical capacity of wastewater treatment in treating CSO could be simulated in different CSO load scenarios.

Based on the calibrated water quality model, the CSO loads were changed through four levels: no CSO load, original CSO load, and 5 times and 10 times the original CSO load. All the other parameters and variables were kept the same as the calibrated model. Other than the FC model, which was simulated for only two months (7/12/95 ~ 9/19/95) due to limited field data, both the EUTRO and Mercury models were simulated three and half months (7/12/95 ~ 9/19/95). The simulation of the mercury model is used for sensitivity analysis only.

Figure 6.1 presents the load impacts on DO concentrations. In general, the change of CSO load has little effect on the DO level. Figure 6.1 shows that roughly the same predicted DO concentrations were observed for all the load scenarios. From mid August to mid September, the DO concentration rises gradually from 5.1 mg/L to 6.5 mg/L. After that, the DO level drops back to 5.1 mg/L in the following month, from mid September to mid October. At the late simulation period, DO dramatically increases 2.4 mg/L in concentration to 7.5 mg/L in half a month.

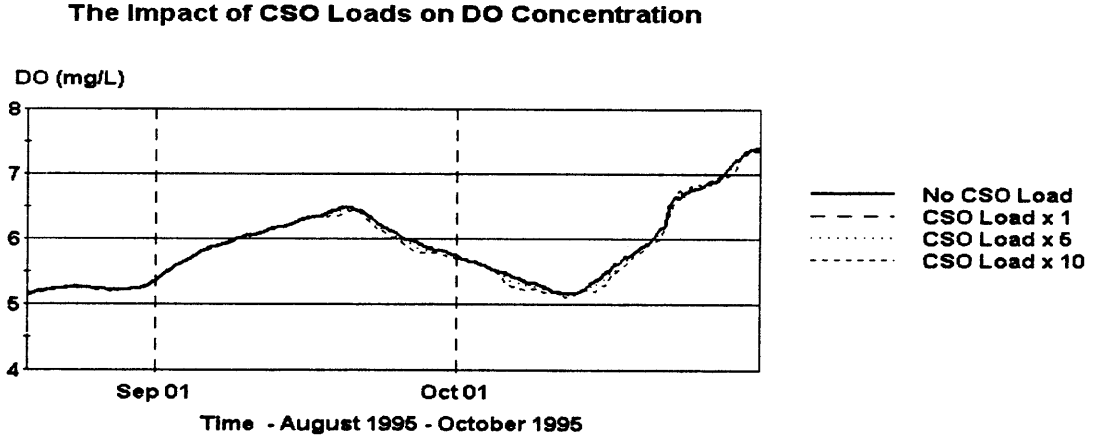

Figure 6.1 The Impact of CSO Loads on DO Concentration.

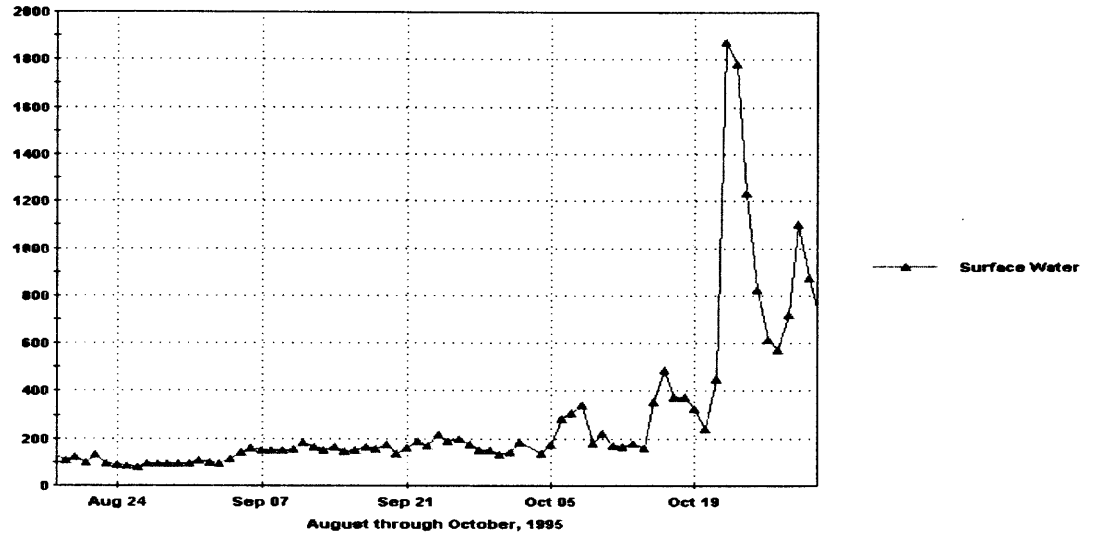

Figure 6.2 The Flowrate of the Mainstream.

The variation of the DO concentration during the simulation period is affected by several factors, which include reaeration of the river, dispersion caused by tides and the stream flowrate. Among these, flowrate is the probably most significant factor in this study. Figure 6.2 shows the variation of the mainstream flowrate. The flowrate increased slightly from 150 m^3/s to 200 m^3/s during mid August to late September. After fluctuating for a short period of time, the flowrate rose significantly to a value over 1800 m^3/s in the next 15 days. It is observed in Figure 6.2 that the stream flowrate has a similar pattern as the DO and the DO changes are roughly proportional to the stream flowrate.

Comparing the predicted curves with and without CSO loads, the concentration of dissolved oxygen drops slightly when the combined sewer overflows discharge into the river, which started in mid September. The same phenomenon is seen when the discharges are 10 times that of the original. In addition, the modeling result shows that the DO levels vary between 5 mg/L to a value close to 8 mg/L. Based on the water

quality criteria for DO for the surface water, 5 mg/L, the DO level is not a water quality concern for the study area. This means either that the load is too small to have any effect, or the reaeration of the Hudson River is large enough to replete the DO depletion.

Unlike the DO curves, the concentration of $CBOD_U$ (represented as BOD in the following paragraphs) varies much more in response to CSO discharges. Figure 6.3 shows the simulations for the river with and without the introduction of CSO. The appearance of peaks under CSO load conditions in Figure 6.3 reveals that these peaks are the result of CSO discharges by comparing the curves with no CSO load and with CSO load. In addition, by inspecting these curves with input load data, the peaks occur at exactly the same time when the CSO loads were introduced. These peaks also indicate that the variations of BOD level are proportional to the magnitude of the CSO load. BOD concentration would increase with a value of 1.0 and 0.5 mg/L if 10 and 5 times the original CSO load were discharged into the river, respectively. However, this occurrence is temporary. These peaks would show only in a short period of time. The BOD concentration will go back to the original level once the CSO load stops. This phenomenon will be discussed more later in following section.

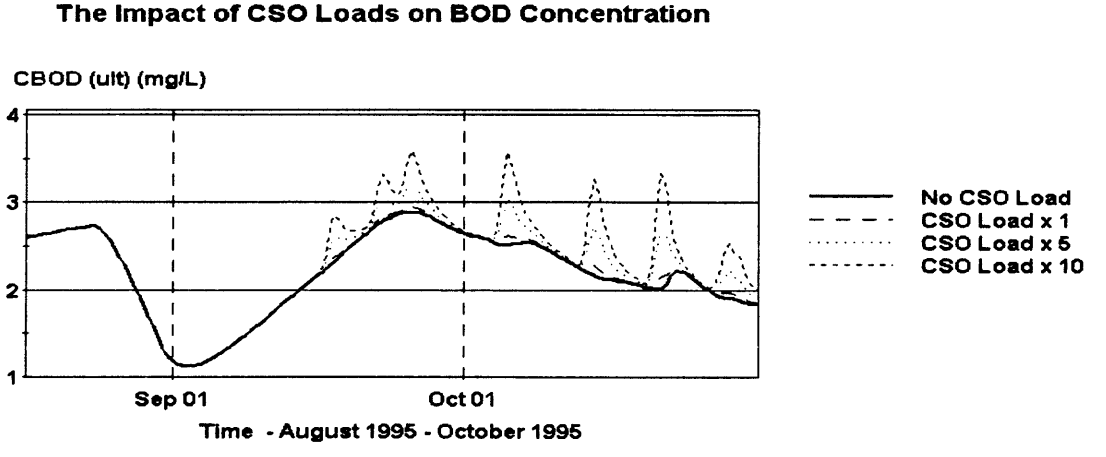

Figure 6.3 The Impact of CSO Loads on BOD Concentration.

Figure 6.4 shows the impacts of CSO load on NH_3-N concentration. Similar to the DO curve, the change of CSO load has little effect on the ammonia curve. It can be observed from the figure that the predicted NH_3-N concentrations for all the load scenarios are almost the same. The ammonia concentration rose to a value close to 0.5 mg/L during the period from late September to mid October primarily due to the low stream flowrate during that period. According to the water quality criteria of ammonia in fresh water in the tidal portion, 0.5 mg/L, the ammonia concentration is lower than the water quality criteria during the simulation period even when 10 times the original CSO load introduced.

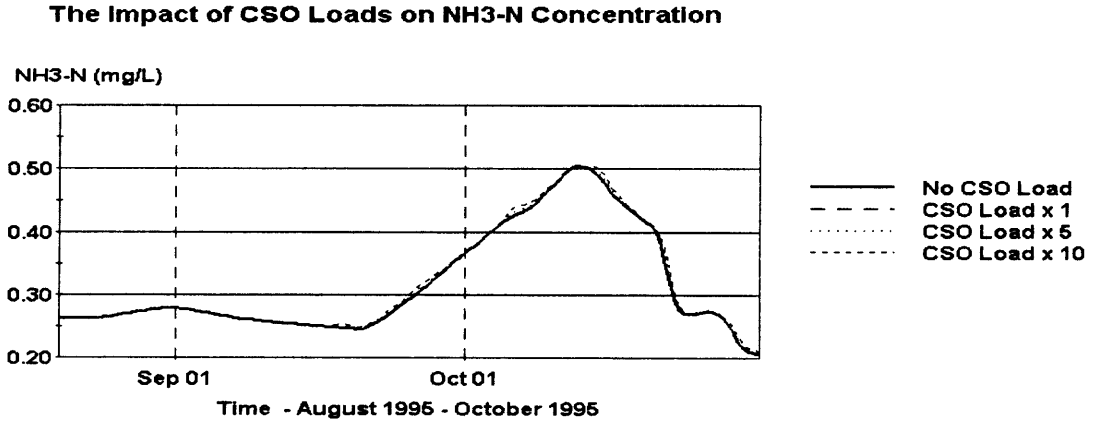

Figure 6.4 The Impact of CSO Loads on NH_3-N Concentration.

According to the simulation results, the CSO loads have little effect on the BOD/DO/NH_3-N system in the study area. In other words, CSO discharge is not a dominant source of the conventional pollutants in the Lower Hudson River. This finding is in agreement with another Hudson River water quality investigation report (Brosnan and O'Shea, 1996a). Table 6.4 presents the sources of the pollutants in the Hudson Estuary considered in that report. It illustrates that the relative significance of pollution sources is dependent on which pollutant is considered. The dominant load source of BOD

and nitrogen is municipal effluents, which contribute 58 and 63 percent of the total load of these two pollutants, respectively. The DO and BOD levels have improved considerably after the wastewater treatment processes were upgraded during the period from 1979 to 1994. Since CSO only discharges 19 % of the BOD load and 2 % of the nitrogen load, after interception and treatment, it does not change the DO and NH_3-N level enough to be of concern.

Table 6.4 Pollutant Loadings to the Hudson Estuary (in Percent) [a]

Parameter	Tributary	Municipal Effluents	CSO	Storm water	Other [b]	Total Load
Flow	81	15	1	4	< 0.5	765 m^3s^{-1}
Fecal coliform	2	< 0.1	89	9	< 0.1	$2.1x10^{16}$ d^{-1}
BOD	16	58	19	5	2	$5.7x10^5$ kg d^{-1}
TSS	80	11	5	3	1	$2.4x10^6$ kg d^{-1}
Nitrogen	29	63	2	2	4	$2.8x10^5$ kg d^{-1}
Phosphorus	16	75	4	4	< 0.5	$2.3x10^5$ kg d^{-1}

Source: T. M. Brosnan and M. L. O'Shea. "Sewage abatement and coliform bacteria trends in the Lower Hudson-Raritan Estuary since passage of the Clean Water Act", Water Environment Research. 68(1): 25-35.

a. Modified from HydroQual (1991) based on data from the late 1980s. Values across may not equal 100% due to rounding.

b. Other = industrial discharges, landfill leachate, and direct atmospheric deposition combined.

To further study the DO/BOD concentration in the study area with emphasis on loading sources, additional simulations, using the calibrated EUTRO model with various pollutant loads, were performed. The first condition, called the no load condition, is defined as a state where no pollutant is released during the simulation period. Under this condition, no loads from CSO and WWTP are discharged if sufficient control technology and advanced treatments were used. The second condition, called the CSO controlled condition, assumes that the municipal WWTP effluent is the only pollution source. No CSO is discharged if a good CSO control program were implemented. The original condition is set as the third condition, in which both CSO and WWTP contribute

pollution in the calibrated model. The last one is the no treatment condition, which assumes that WWTPs are out of order under unexpected conditions, such as power failure, and all the sanitary wastewater and CSO discharge into the receiving water without any treatment. These four different pollution load conditions were run and the results are compared in Figures 6.5 and 6.6.

The purpose of this simulation scenario is to find the impacts of the sources of the load. Figure 6.5 shows that the curve under the no load condition has the lowest BOD concentration since there is no pollution discharge in the study area, as expected. The difference of the simulation results between the first two conditions represents the impact of the municipal WWTP. A gap, with an average value of 0.4 mg/L BOD, is found between the curves under the no load condition and the CSO controlled condition. This gap shows how much the municipal WWTP would affect the BOD level in receiving water.

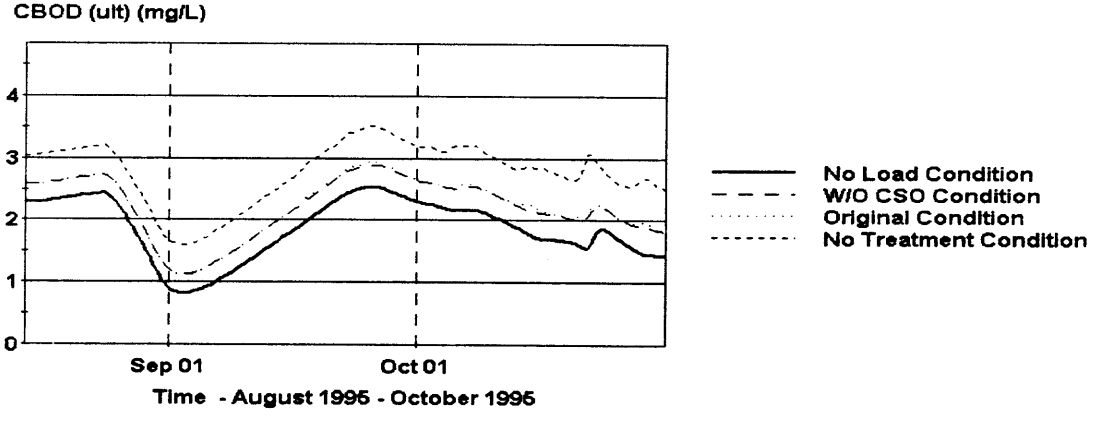

Figure 6.5 Effect of the Sources of BOD on Water Quality.

The original condition has the same input data as the CSO controlled condition except that there are additional CSO loads during the simulation period. Figure 6.5 shows that the curves with the original CSO load and no CSO conditions are almost identical,

which indicates that the CSO discharge has very small impact. The simulation result shows that the highest BOD concentration occurs under the 4th condition. When the WWTP is out of order, an average BOD concentration value of 0.6 mg/L and 1.0 mg/L is higher than the original and no load condition, respectively. Meanwhile, the difference between the no treatment and the original condition shows the improvement in water quality as far as municipal wastewater treatment is concerned.

Figure 6.6 shows the DO variation with various load conditions. DO concentration decreases with an average value of 0.2 mg/L when municipal effluent is introduced. This figure also shows that a small difference is observed when CSO loads are present. This confirms the previous finding that the WWTP load has more influence on water quality than the CSO load in the study area.

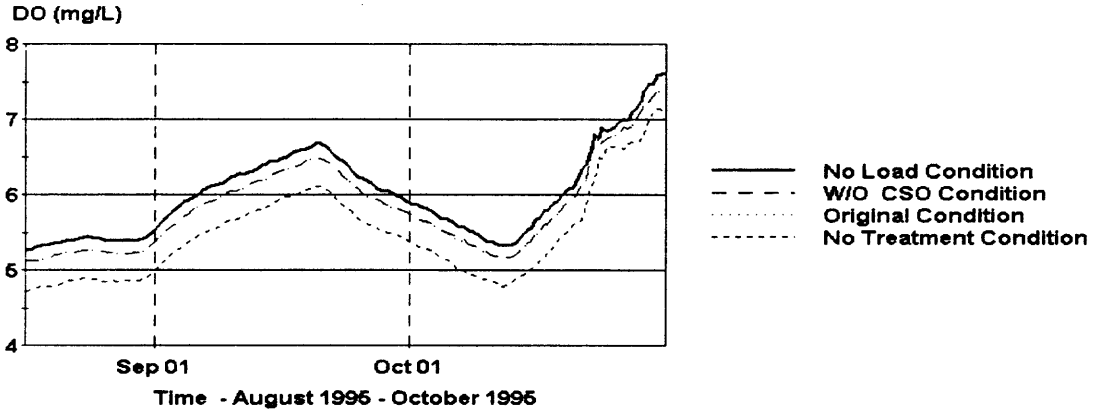

Figure 6.6 Effect of Pollution Sources on DO in River.

The worst water quality condition occurs when there is no wastewater treatment. Because of the presence of large amounts of untreated wastewater, the DO concentration drops an average value of 0.3 mg/L below the original condition. Furthermore, it is observed that DO level was less than 5 mg/L during late August and a short period of time in October under the no treatment condition. The low DO concentration is primarily

caused by these unexpected pollutant loads which exceed the repletion capacity from the reaeration of the Hudson River. According to EPA's DO criteria, 5 mg/L of DO is the minimum concentration that should be maintained at any given time to protect the diversity of aquatic life. This indicates a threat to the ecosystem and should be a concern if this situation occurs often. There are several engineering technologies that can be utilized to improve the DO. These control measures can be grouped as follows (Thomann and Mueller, 1987):

1) Point and non-point source reduction of BOD through reduction of effluent concentration and/or effluent flow.
2) Aeration of the effluent of a point source to improve the initial value of DO.
3) Increase in river flow through low flow augmentation to increase dilution.
4) Instream reaeration by turbines and aerators.
5) Control of SOD through dredging or other means of inactivation.
6) Control of nutrients to reduce aquatic plants and resulting DO variations.

Unlike BOD and nitrogen loading, the pathogen in CSO discharges is the primary pollutant source. Table 6.4 indicates that combined sewer overflows account for only 1 percent of the total freshwater flowrate but they contribute 89 percent of the total loading of fecal coliform bacteria. In other words, fecal coliform in the Lower Hudson River mainly comes from CSOs and the amount of CSO discharges would affect the FC level considerably. The simulation result from the water quality model, shown in Figure 6.7, also reflects this condition. Even though there was only one storm event, occurring on September 19, during the simulation period, a peak showing a drastic increase of FC concentration is seen in the plot.

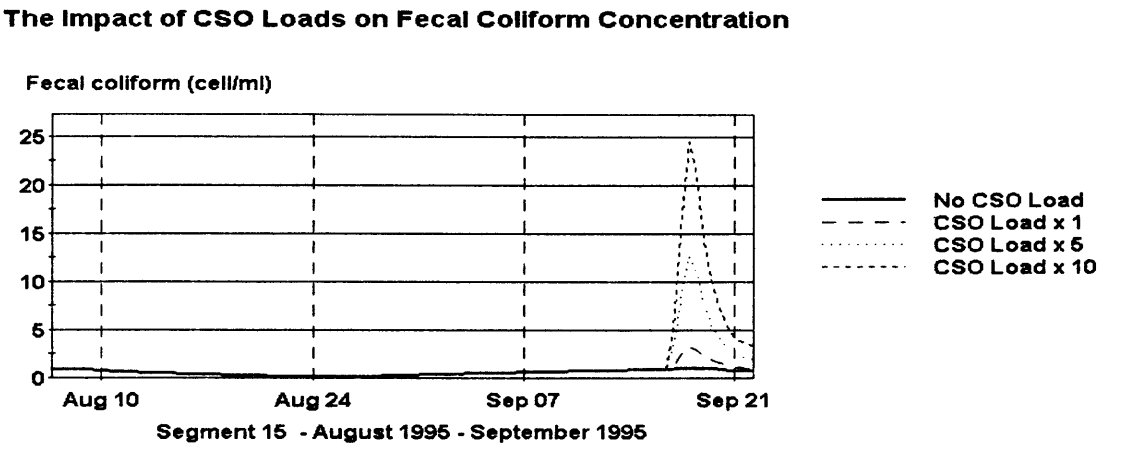

Figure 6.7 The Impact of CSO Loads on FC Concentration.

This figure also shows that since there was no other point and non-point source pollution in the river, the FC concentration kept a constant value of less than 100 cell/100ml until the CSO discharges into the river. Similar to the BOD plot, the concentration of fecal coliform increases during the time when the CSO discharges and it increases proportionally with the quantity of the CSO load. With the original CSO load, the FC concentration increases to a value close to 250 cell/100ml. When the CSO load rises to 5 times the original, the FC concentration increases from 250 to 1,250 cell/100ml. If 10 times the original CSO load were let in, the FC level increases to a concentration close to 2,500 cell/100ml. Compared with the BOD simulation result, which has only 33 percent concentration increase when 10 times the original CSO load was admitted, the FC response is more severe. It is found that 10 times the original FC concentration can be achieved if 10 times the original CSO load were added.

Bacterial pollution of water has been a factor in relation to aquatic life, not because of its effects on the organisms themselves but rather because of the danger to human beings from eating raw shellfish or by contaminating the food or drink through

careless actions. Different levels of FC show various degrees of impairment on water quality. The stringent condition in the allowable concentration for shell fishing (FC < 14 cell/100ml) is aimed at protecting the consumer of clams and oysters from communicable diseases such as hepatitis and gastrointestinal disorders. Since shellfish filter the overlying water and concentrate bacteria as part of the feeding process, the low concentration of bacteria in the water column is intended to result in an acceptable level in the organism itself. The simulation result shows that the FC concentration in the base flow condition (without CSO), which is between 20 to 100 cell/ml, is much higher than this criterion, and shell fishing should be limited in this area. On the other hand, this concentration is allowable for primary contact recreation such as bathing and water skiing, since it is lower than the criteria 200 cell/100ml. However, the FC concentration rises to 250 cell/100ml under the original CSO load condition and only secondary contact recreation such as boating and fishing is permitted. According to the water quality criteria with respect to fecal coliform, the FC concentration should not exceed 770 cell/100ml (7.7 cell/ml) in freshwater in the tidal portion of the water for all the contact reactions. This did not happen during the original CSO load condition. However, based upon the simulating result, the FC concentration is expected to be higher than the FC criteria when 3 times of the original CSO load discharges in the water system if all the other environmental parameters remain the same.

In the case where bacteria reaches to an actionable level, caused by CSO discharge, disinfection will become a necessary component in a CSO control system. Disinfection, which inactivates or destroys microorganisms in overflows, can be accomplished most commonly through contact with chlorine, although a variety of other

disinfection technologies are available without chlorine. For disinfection of CSOs, liquid sodium hypochlorite is the most common technology. Other alternative technologies include gaseous chlorine, liquid sodium hypochlorite, chlorine dioxide, ultraviolet radiation, and ozone. A comprehensive CSO control program is likely to incorporate one or more technologies. In reality, disinfection of CSOs often requires some level of solids reduction by one of the other technologies, such as coarse screening and swirl/vortex, for maximum effectiveness and reliability.

Figures 6.8 and 6.9 show the simulation results for the study of the impact of mercury in CSO in both water layers and sediment layers. It should be noticed that, except for the CSO loading data presenting the real condition in Hudson River, the mercury model in this study was created based on the pseudo initial and boundary concentrations, which were taken from historic water quality data of the Hudson River and a similar mercury simulation model (Ambrose and Wool, 2002). The initial Hg concentration was set at 0.3 μg/L (0.3 ppb) in the water column and 6.0 ng/g (6.0 ppb) in the sediment. The model predicted value should only be used as a reference because of the lack of calibration.

Similar to the FC simulation result, the Hg concentration responses to the CSO loads in both the water and sediment layers with respect to the time of discharge and the magnitude of the load. There are seven peaks shown in the plots. Each peak corresponds to a storm event during CSO discharges. Since CSO is the only mercury-loading source in this study, the Hg concentration in the water layer maintains a value of less than 500 ng/L (0.5 ppb) without much variation before CSO discharges. When the original CSO load is applied to the system, mercury concentration increases, depending on the quantity

of CSOs discharged in the storm event, to a value in a range of 1,000 to 2,500 ng/L (1.0 to 2.5 ppb), which is a 0.5 to 2.0 ppb increase in concentration compared with the no CSO load condition. It was found that the Hg concentration increment is proportional to the magnitude of the CSO loads. When 5 times the original CSO loads discharges into the river, the Hg concentration increment will rise to approximately 5 times, too, with mercury concentration between 4,000 to 10,000 ng/L (4.0 to 10.0 ppb) in the water layer. If CSO loads increase to 10 times the original load, the mercury concentration increment would also increase 10 times, and the Hg concentration in the water layer could be higher than 20,000 ng/L (20 ppb) in the largest storm event during the simulation period.

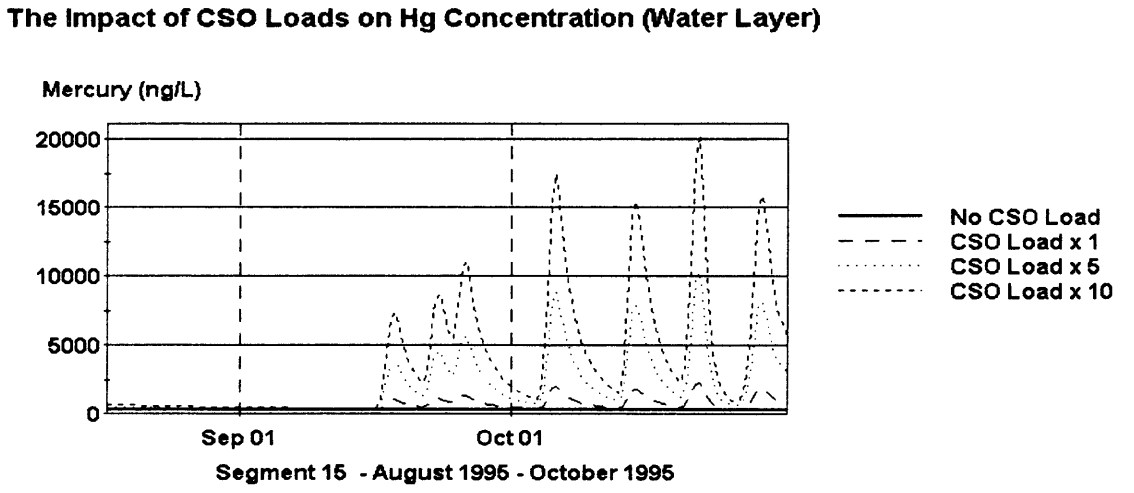

Figure 6.8 The Impact of CSO Loads on Mercury Concentration (Water Layer).

After pollutants enter the water body, part of the contaminants may settle in the sediments. Although many of the organic contaminants do degrade with time, the rates of degradation are generally slow and these toxicants tend to remain in the sediments for long periods of time, thus increasing their impact on the environment. Metals, as elements, do not degrade (US EPA, 1991). By comparing simulation plots of water layers

and sediment layers (Figures 6.8 and 6.9), flatter peaks over longer periods of time are observed in the sediment layer, but not in the water layer. This observation reveals that metals such as Hg and other toxic substances are easier to dilute or transport in the water phase than in the sediments. Furthermore, unlike the fluctuation of Hg concentration in several peaks in the water layer plot where the Hg concentration goes back to the original level once the CSO is removed, the Hg concentration in the sediment layer plot increases gradually and consistently from 20 to 45 ng/g (20 ppb to 45 ppb) after a series of CSO discharges. This indicates that mercury would stay in the sediment layer with accumulated concentration. This reveals that water quality is affected by Hg in a short term, but the sediments will be contaminated for much longer periods of time. Since some pollutants, including organic chemicals (pesticides, volatile and semi-volatile compounds) and toxic metals, are conservative in the sediments, they have been used to link with pollution load data to investigate the primary pollutant source by spatial distribution analysis recently (Iannuzzi et al., 1997). This application will be discussed further in the spatial distribution analysis later.

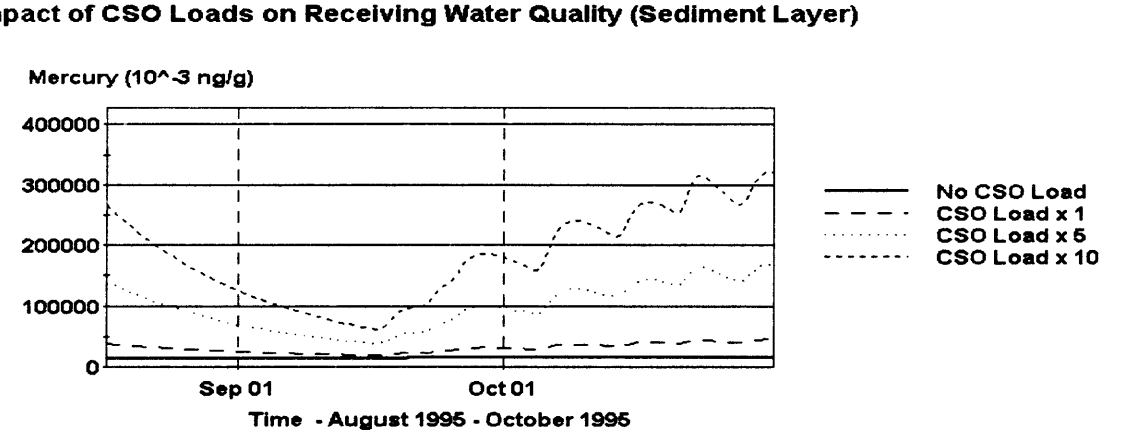

Figure 6.9 The Impact of CSO Loads on Mercury Concentration (Sediment Layer).

The toxic substance water quality problem can therefore be stated as the discharge of chemicals or metals into the aquatic environment with concentrations in the water or aquatic food chain at levels that are determined to be toxic, in a public health sense or to the aquatic ecosystem itself, and thus may interfere with the use of the water body for water supply or fishing or contribute to ecosystem instability (Thomann and Mueller, 1987). The water quality level of concern for mercury, resulting mainly from industrial activities such as electroplating, battery manufacturing, mining, smelting, and refining, is 2.0 ppb for the fresh water in New Jersey. The simulation result shows that the Hg concentration exceeds the level of concern when CSO discharges during the storm events. Since the Hudson River has been contaminated by toxic chemicals and metals, New York and New Jersey have issued fish and crustacean eating advisories and prohibited the sale, consumption, and/or harvesting of other fish, crustacean, and shellfish (NY/NJ HEP CCMP, 1996).

According to the simulation result, the Hg concentration in the Hudson River violates the water quality criteria only when CSO discharges during the storm events. The most efficient way to remedy the high Hg concentration contaminating the Hudson River is to reduce the magnitude of CSO discharges. For example, under the original CSO load condition, the Hg concentration will not violate the Hg criteria if only 85% of the original CSO is discharged into the river. To minimize the quantity of CSOs discharging to the receiving water, a variety of control technologies, such as in-system controls/in-line storage, near-surface off-line storage/sedimentation, deep tunnel storage, and swirl/vortex technologies, can be utilized to achieve the purpose. However, there is no standard for selection and design control programs for all the CSO conditions. CSO control

technologies are site specific due the various factors that will affect the selection of these technologies. These factors include system characteristics, performance goals, and CSO quality and treatability.

However, since the initial Hg concentrations in both water and sediment layer in this model are estimated values obtained from other reports, they may not represent the real Hg concentration in the Hudson River. To improve the applicability of the mercury model, two more scenarios with various initial Hg concentrations are simulated. Other than changing the initial Hg (II) concentration in the receiving water, which was 0.3 ppb in the water column and 6.0 ppb in sediments, to 2 times and one-half of the original concentration, all the other input data remain the same. Figures 6.10 and 6.11 show the effects of the initial Hg concentration in the receiving water on water quality.

It is seen in Figure 6.10 that concentration gaps exist between predicted curves and that these gaps are proportional to the initial Hg concentrations. For example, a concentration difference exists with an average value of 0.3 ppb and 0.15 ppb, between the original initial concentration condition and 2 times and one-half of the original condition, respectively. However, the predicted Hg concentrations all have the same variation patterns under all three conditions in both the water and the sediment layer. This means that the model still reflects the water quality conditions in response to the pollution loads, though it lacks calibration.

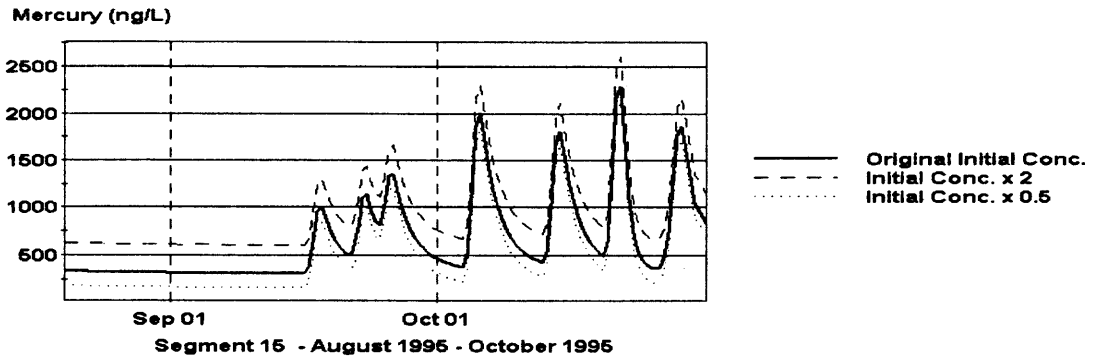

Figure 6.10 Effect of the Initial Hg Concentration on Water Quality (Water Layer).

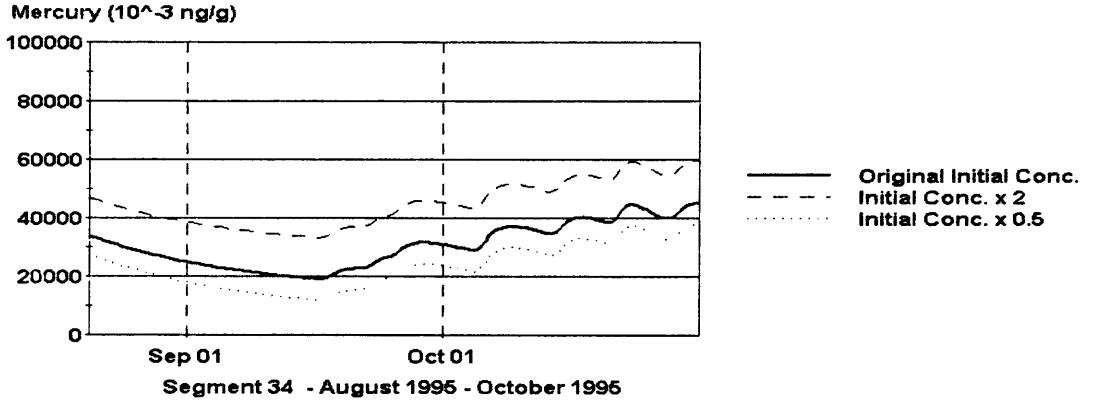

Figure 6.11 Effect of the Initial Hg Concentration on Water Quality (Sediment Layer).

Sediments are a very important part of aquatic ecosystems and they can become problematic under conditions where contaminants can accumulate in sediments to the point where they endanger human and/or ecosystem health. Contaminated sediments threaten human health when humans drink water contaminated with sediments, eat organisms contaminated through bioaccumulation in the food chain, or come into direct dermal contact with contaminated sediments. Contaminants impact ecosystems by increasing the mortality rates and/or by decreasing the growth or reproductive rates of susceptible populations. These impacts can be transferred throughout the ecosystem via food chain links and other ecological mechanisms (US EPA, 1991).

Typical trace and toxic metal contaminants, which may be seen in CSO, include copper, zinc, cadmium, lead, chromium, nickel, arsenic, selenium, mercury, and sometimes others. According to the New York-New Jersey Harbor Estuary Program Final Comprehensive Conservation and Management Plan (NY/NJ HEP CCMP), the primary toxic metals loaded in the Hudson River are copper (1342 kg/day), nickel (526 kg/day), lead (1029 kg/day), and mercury (9.5 kg/day). The plan also states that CSO is one of the primary pollution sources of these contaminating metals. CSO contributes 14%, 4 %, 12%, and 11% in total copper, nickel, lead, and mercury load in the Hudson River, respectively. These elements are usually present in soils and sediments at low concentrations from natural sources. It is when one or more of these contaminants is present at an elevated concentration that they pose a potential problem. Real problems exist if these excess levels of metals are released to the water column or are present in forms readily available to plants and animals that come in contact with the sediment material.

Metals may be mobilized or immobilized if the environment of the sediment or dredged material changes. Therefore, understanding these changes and interactions between sediments and contaminants are important to the selection and management of remediation alternatives, which may include no action, treatment, containment, and disposal, to minimize contaminant release. Thus, when people try to solve the problem of excessive sedimentation disrupting shipping in the Hudson River by use of maintenance dredging, the potential problem of released contaminants from the sediment should be considered in weighing the pros and cons of remediation decisions.

In summary, the pollutant concentrations in water are affected by the quantity of the CSO load and they change proportionally. However, due to the relatively smaller load compared with other pollution sources and the large stream flow, the concentration of conventional pollutants, which include DO and $CBOD_U$, do not change much with increasing CSO load. On the other hand, CSO is the dominant source of FC contamination based on the simulation result. The FC concentration can increase to 10 times the original concentration if 10 times the baseline CSO loading is introduced. It is also calculated that water quality criteria for FC will be violated if 3 times the original CSO loads are placed in the river. In the Mercury model, the concentrations of mercury in both water and sediment layers are proportional to the CSO loads entering the system. The result also reveals that mercury, discharged along with the CSOs, will be diluted or transported in the water layer after a short time but it will accumulate in the sediment layer over a longer period of time.

6.4 The Impact of Receiving Water Flowrate

"Dilution factor", the ability to minimize the impacts on the receiving water system, is an important element when investigating water quality in a river or estuary system, where the water volume has relatively larger variations than other water systems, such as lakes or ponds. Based on the perspective of mass balance, the pollutant concentration in the receiving water is related to the corresponding water volume in the segments. A small river and a high-flowrate stream would not show the same effect when the same pollutant load is being discharged as seen with the Lower Hudson River model. By the same token, same discharge loads will have more severe pollution problems in drought than under

normal conditions. In this section, the effects of river flowrate were investigated by the following approach.

Four models with various flowrate conditions were modified from the calibrated models for each module. The mainstream flow function of the calibrated EUTRO model was set as the original condition. Four degrees of scale factors, which include 0.1, 0.5, 2, and 10, are used for fraction or multiplication of the original flow function to represent four degrees of flow conditions: very low, low, high, and very high flowrate, respectively. The segment geometric input data, which include depth, volume, cross-section area, and stream velocity, were modified in accordance with the various flowrates. The method to define the relationship among velocity, depth, and stream flow, WASP6.1, follows the same implementation in QUAL2E (Brown and Barnwell, 1987). The velocity (v) and depth (D) are related to stream flow (Q) through power functions, for instance, $v = aQ^b$ and $D = cQ^d$. Since the hydraulic radius is approximately equal to the depth for wide streams, the exponents (b and d) for rectangular cross sections can be approximated to be 0.4 for velocity and 0.6 for depth, and the discharge coefficients (a and c) can be calibrated by the original flow function. New segment volume was derived by multiplying the new depth with the original width and length. In the "Exchange" group, cross-section area was calculated by multiplying the new depth by the original width. Except for the mainstream flowrate and geometric data, all the other boundary conditions and environmental parameters were kept the same as the calibrated model.

Figure 6.12 shows how the flowrate will affect the DO level in the receiving water under five different stream flows. It has been discussed in a previous section that the effects of CSO loads on the receiving water are represented by the appearance of

peaks in predicted curves. From the plot, no isolated peak is observed in any flowrate conditions as shown in Figure 6.8. This validates the fact that CSO loads have only small effects on the DO levels in the Lower Hudson River. Comparing the five curves in Figure 6.12, four of five scenarios have similar values and variation patterns, except for the very low-flowrate condition (one-tenth of the original flowrate). Despite the similar variation pattern as other scenarios, DO under one-tenth of original flowrate condition drops 0.5 to 1.0 mg/L in concentration compared with the other flowrate conditions. In addition, during most of the simulation period, the concentration of dissolved oxygen is less than 5 mg/L under this very low flowrate condition. According to the US EPA's DO criteria, 5 mg/L is the threshold concentration, which normally might not be deleterious to fish life. Waters that do not exceed this value should be suitable habitats for mixed fauna and flora. This means that low DO concentration, which may occur during drought, will have the potential for harming fish. Figure 6.12 also shows that the DO concentration in the Hudson River remains approximately the same with a value above 5 mg/l, when the river flowrate varies from half to 10 times the present flow.

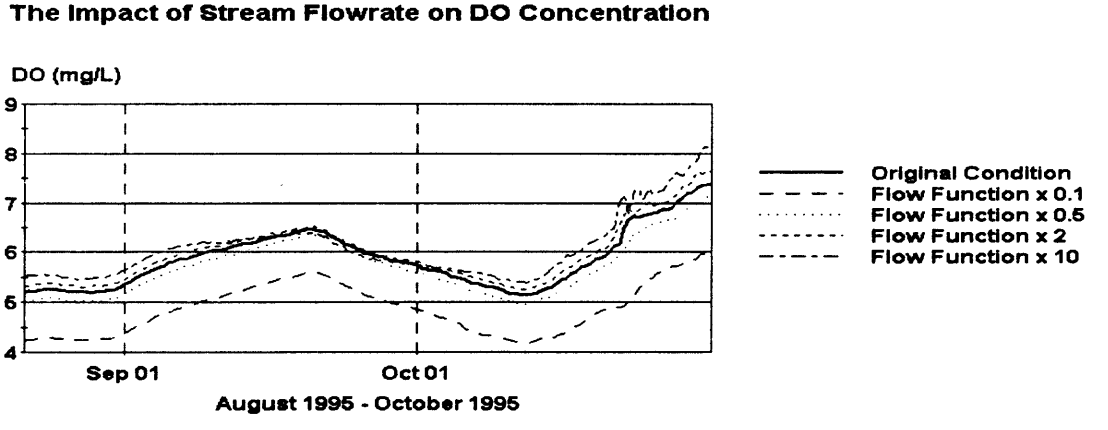

Figure 6.12 The Impact of Stream Flowrate on DO Concentration.

Figure 6.13 shows the impacts on BOD level due to change of the stream flowrates. In general, the BOD concentrations in the river are approximately the same for most of the flowrate conditions except for the very low flowrate scenario. The BOD concentration under the very low flowrate condition is much higher than those under the other conditions considered. This figure shows that even when the flowrate drops to half of its original, the BOD concentration will not change much. Only when the flowrate drops to one-tenth of the original, then the BOD level increases. The dilution of CSO loads by the river flowrate can be seen from Figure 6.13. The peaks, which occur due to the presence of the CSO loads, appear only under the very low flowrate condition. Since the stream has enough capacity to dilute the pollutant under other flowrate conditions, the peaks do not appear under other conditions.

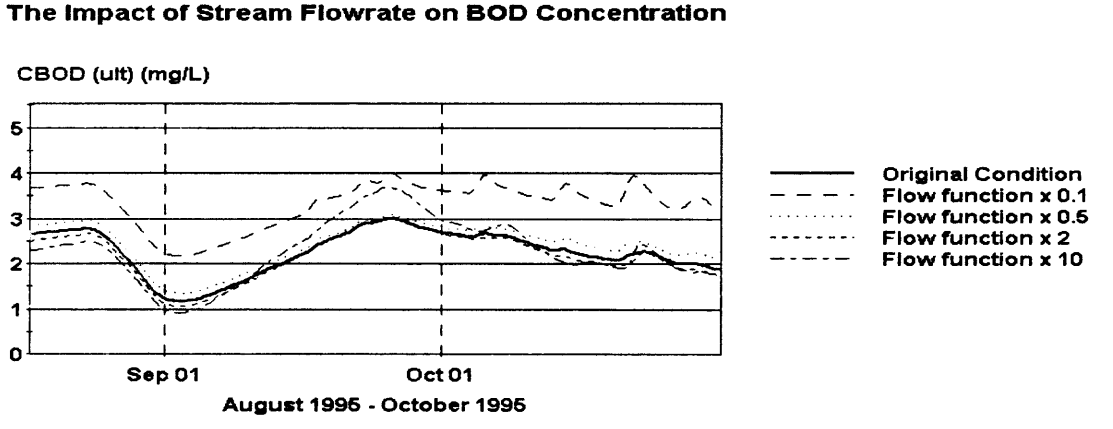

Figure 6.13 The Impact of Stream Flowrate on BOD Concentration.

According to the simulation results of DO and BOD, receiving water quality is affected by the stream flowrate only at very low flowrate condition. A similar finding has been reported in other studies. USGS and the Indianapolis Department of Public Works began a study to evaluate the effects of combined sewer overflows to Fall Creek on the White River in 1986. They describe the effects of CSO on the water quality of Fall Creek

during the summer of 1987 by comparing the water quality during base flow with that during storm events. Fall Creek, compared to the Hudson River, is a relatively small stream, with an average monthly flowrate of 1.13 m^3/s during the summer period. According to the investigation report (Martin, 1995), concentrations of dissolved oxygen in Fall Creek were less than the Indiana minimum ambient water quality criteria of 4.0 mg/L during all storm events, although only about 36.6 percent of the typical Lower Hudson River CSO loads were discharged.

Figure 6.14 shows how the flowrate will affect the NH_3-N concentration in the Lower Hudson River under various flowrate conditions. In general, the ammonia concentration is inversely proportional to the stream flowrate. The highest concentration occurs when the stream flowrate drops to one-tenth of the original. Under such a flowrate, the NH_3-N concentration rises to a value over 0.6 mg/l, and it violates the water quality for ammonia, 0.5 mg/l in early October. This means that the low flowrate will increase the probability for eutrophication. Since municipal effluent is the dominant pollution source of nutrients, WWTPs should provide a higher degree treatment for ammonia during the drought, if possible.

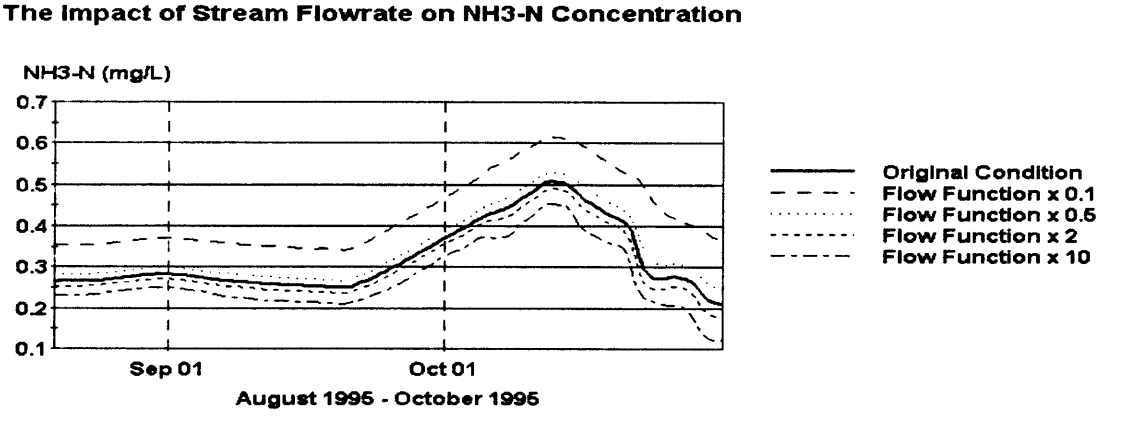

Figure 6.14 The Impact of Stream Flowrate on NH_3-N Concentration.

Another interesting point was found while simulating various flow conditions. As mentioned in an earlier part of this section, the segment geometric parameters were modified in accordance with the flowrate when different flow conditions were simulated. Since the quantity of the initial contaminants in the receiving water is related to the water volume in the segments, using the model without modifying the geometric data will cause fallacious predictions for pollutant concentrations. Figure 6.15 shows the simulation without modifying the geometric data. Comparing with Figure 6.13, the BOD concentration responses differently to the flowrate. When flowrate increases, the BOD concentration increases proportionally, which is contrary to common sense. This example shows the importance of modifying geometric data when conducting simulation with various flowrates.

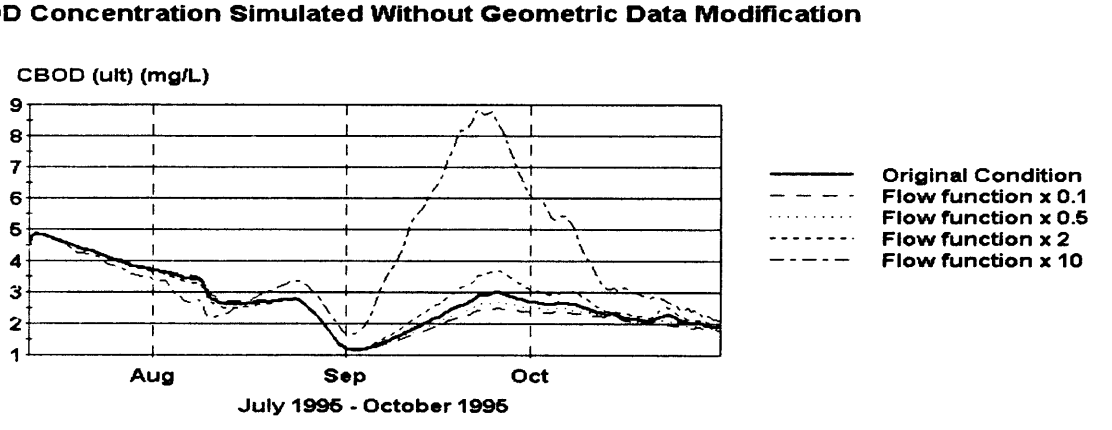

Figure 6.15 BOD Concentration Simulated Without Modifying Geometric Data.

Figure 6.16 illustrates the effect of stream flowrate on fecal coliform concentration. The peaks present on September 18 are the result of CSO discharge. This figure shows that FC concentration maintains a value of less than 100 cell/100ml before the appearance of the peak. The peak appears in all five simulated conditions and the height of the peak is related to the stream flowrate. For instance, FC concentration

increases from 100 cell/100ml to 330 cell/100ml under the original flow condition. When the flowrate is one half of its original, it rises to a concentration of close to 500 cell/100ml, which, though high, is still below the FC water quality criteria, 700 cell/100ml. If the flowrate drops to one-tenth of the original flow, the FC concentration is over 1000 cell/100ml and exceeds the criteria. On the other hand, high stream flowrate shows its ability to "dilute" the negative effect from CSO discharges. With the same amount of CSO load, the concentration of FC decreases from 330 cell/100ml to 230 cell/100ml and 130 cell/100ml when the flowrate is twice and ten times the original flowrate, respectively.

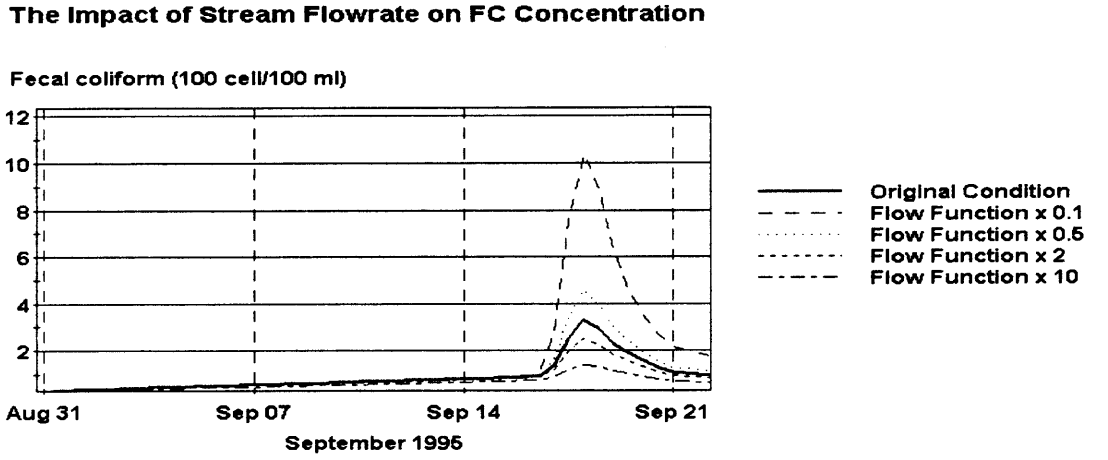

Figure 6.16 The Impact of Stream Flowrate on FC Concentration.

Figures 6.17 and 6.18 are the plots that show the stream flowrate affects the mercury concentrations in the water layer and the sediment layer, respectively. Figure 6.17 shows seven peaks, which represent seven individual storm events that occurred during the simulation period. Before CSO discharges, the mercury concentration maintained a value of less then 2,000 ng/L (2 ppb), which is the surface water quality criteria for Hg. A condition similar to the FC simulation is observed here in that the Hg

concentration increases with decreasing stream flowrate. In the original flow condition, the mercury concentration increases from a value of less than 500 ng/L (0.5 ppb) to 1,000 to 2,300 ng/L (1.0 to 2.3 ppb) depending on the quantity of CSO loads during storm events. When the flowrate is one half of the original, the concentration of mercury rises to values between 1,400 and 3,500 ng/L (1.4 and 3.5 ppb). If the flowrate drops to one-tenth of the original, the mercury concentration increases to values between 3,100 to 8,600 ng/L (3.1 to 8.6 ppb). Unlike the response to the CSO loads, the Hg concentration increment is inversely proportional to the stream flowrate. Under each condition, the mercury concentration is higher than the water quality criteria for mercury. The flow conditions that keep the Hg concentration under 2 ppb are when the stream flowrate is 5 and 10 times the original flow. This shows that the loaded mercury from CSO can be diluted by high stream flow.

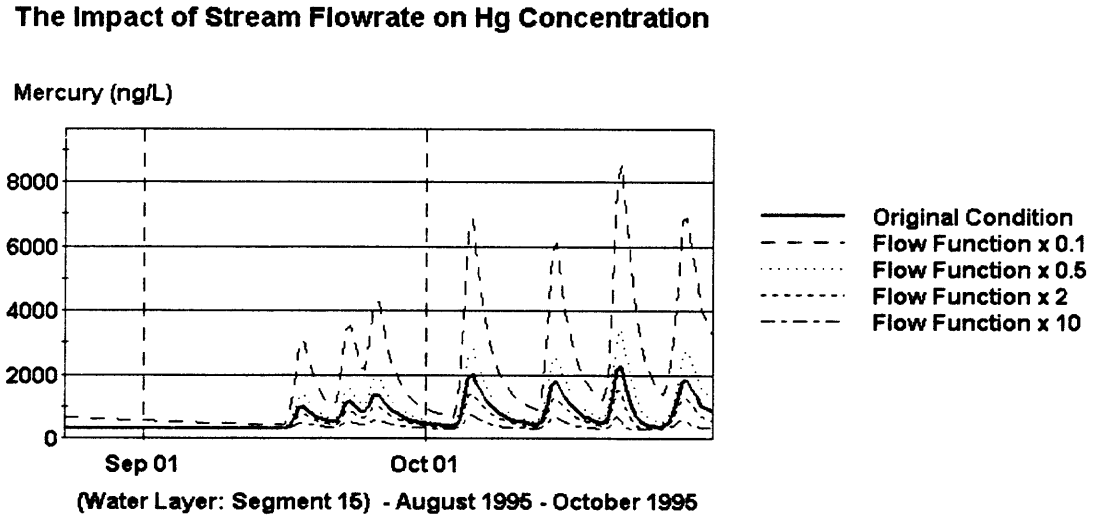

Figure 6.17 The Impact of Stream Flowrate on Mercury Concentration (Water Layer).

Figure 6.18 shows that the Hg concentration in sediment increases gradually after CSO is introduced and most Hg is accumulated in sediment. Comparing the mercury

concentration in sediment and water layers, the variation of stream flow has a similar impact on Hg concentration in sediment as in water. By reducing the stream flow to one-tenth of the original flow, the Hg concentration in sediment increases to a value between 45,000 ng/L to 150,000 ng/L (45 ppb to 150 ppb), which is the same rate of Hg concentration increment predicted for water layers.

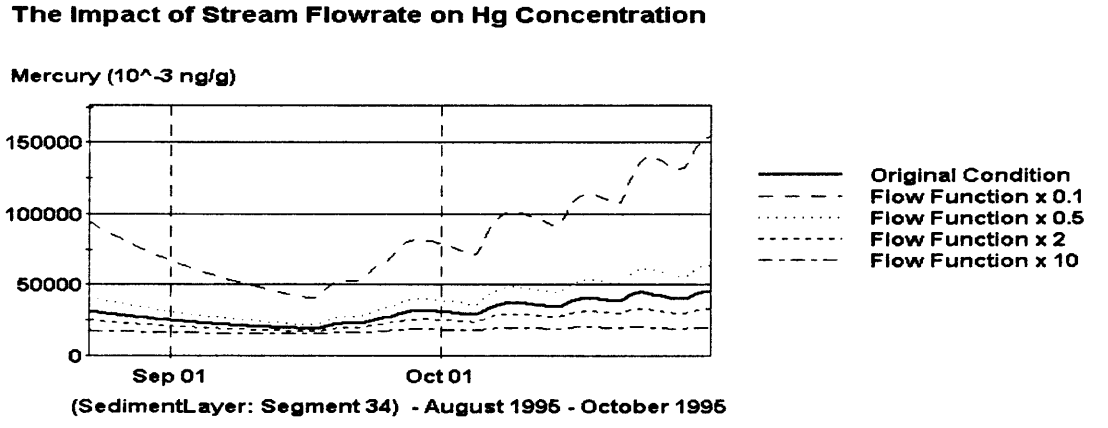

Figure 6.18 The Impact of Stream Flowrate on Mercury Concentration (Sediment Layer).

The simulations show that stream flowrate plays a much more important role for unconventional pollutants such as Hg, than it does for DO and BOD. According to the model results, the concentrations of FC and DO would exceed the water quality criteria only under the very low flowrate condition. The average flowrate during the simulation period was 246 m^3/s, thus, the average one-tenth of the original flowrate condition is 24.6 m^3/s. Based on the USGS flowrate record of the Hudson River, the lowest monthly flowrate during the summer (July to October) was 24.3 m^3/s, which is even lower than the very-low flowrate condition run in this study. Such a low flowrate condition has occurred occasionally in the past, however, it may happen more frequently in the future due to greater water demand and drought. Water demand and consumption in industry

and agriculture usage has increased steadily in the past 20 years. Drought has also become a common phenomenon in the last few years, perhaps because of the greenhouse effect. The low stream flow may well become more common in the future. The discharge of CSO to a low flow stream may be a serious concern in the near future.

The simulation results show that the stream flowrate does have an effect on the receiving water quality. In general, water quality is deteriorated under the low flowrate condition, while the high flowrate stream provides some degree of dilution. The DO level is under 5 mg/L for some of the time when the flowrate is reduced to one-tenth of the original flowrate. In the meantime, the BOD concentration increases approximately 1.5 mg/L only under the very low flowrate condition. The stream flowrate affects the FC concentration more than it does DO and BOD. The concentration of FC under the very low flowrate concentration is 1000 cell/100ml, which exceeds the water quality criteria (700 cell/100ml). Mercury concentration in water is over the surface water quality criteria for Hg, 2 ppb, when a CSO discharges. Water quality will get even worse when the stream flowrate gets smaller. Hg concentration is below the water quality criteria when the flowrate increases to five and ten times of the original. It was found for mercury that the variation of stream flowrate has similar impacts on both water and sediment. Under the same load condition, Hg concentration can increase to 500 percent of the level under the original flow condition in both layers when the flowrate drops to one-tenth of the original flowrate.

6.5 Spatial Distribution Analysis

The purpose of the spatial distribution analysis is to investigate the distribution or transport pattern of the pollutants in the receiving water after CSO discharge. Furthermore, the mathematical model can also reveal any correlation between the pollutant concentration and the distance to the location of the CSO outfall, and the result can be used to support other related CSO research, such as identification of primary sources of contamination.

Fecal coliform and mercury were selected as the indicator pollutants for the spatial distribution analysis, since DO / BOD does not response to CSO discharge as much as FC and Hg in the study area. To investigate the pollutant distribution after CSO discharge from a specific location, Segment 15 was selected as the sole discharge point in the created models, which has been modified from the previous calibrated models. All the hydraulic and water quality data were the same as those used in the calibrated models except for the loading data. For the convenience of comparing the impacts of CSO load, two individual cases, 10 times of the original CSO load and no CSO load conditions, were simulated. After running the model, the difference of concentration between the two curves will be the pollutants discharged from CSOs. In the spatial distribution analysis, the predicted curves are plotted with pollutant concentration versus segments for a specific date. In this study, September 18 and October 6 were selected as the output dates for the FC and Mercury models, respectively. The reason for selecting these dates is because the highest pollutant concentration was obtained on these two dates and they are the dates right after the largest storm events that occurred during the simulation period.

The result of spatial distribution analysis of fecal coliform is shown in Figure 6.19. The largest difference of FC concentrations between the two curves is close to 250 cell/100ml. This simulation shows that the FC concentration decreases gradually and symmetrically from the discharging point (Segment 15) to both the upstream and downstream of the river. In Segments 14 and 16, the concentration difference between the two curves is 230 cell/100ml, which is 20 cell/100ml less than that predicted in Segment 15. In Segments 13 and 17, the concentration difference drops to 200 cell/100ml, which is 50 cell/100ml less than the concentration at the discharging point. The large amount of pollutant moving upstream suggests that transport by tidal dispersion affects the spatial distribution of pollutants significantly in this estuary system.

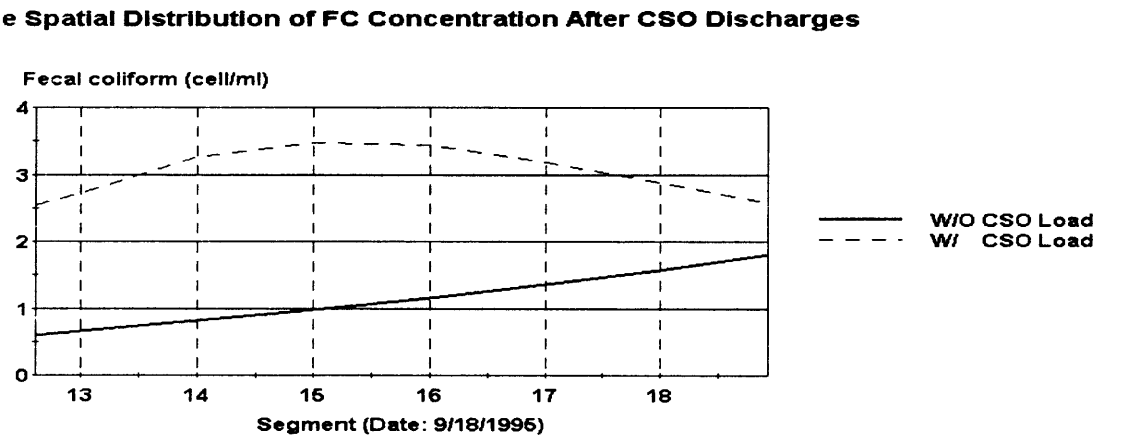

Figure 6.19 The Spatial Distribution of FC Concentration After CSO Discharges.

To investigate this perspective further, a scenario without dispersion was simulated. To study tidal effect in WASP models, as mentioned in Chapter 4, a tidally averaged model was used in this study. This aspect of the model assumes that the inflow of the tide equals the outflow of the tide within the control volume and that the mixing caused by the tide can be described by using a dispersion coefficient. To achieve a model

without dispersion, all the input data were kept the same as in the previous scenario except that the dispersion function in the "Exchange" group was not used. The simulation result is shown in Figure 6.20, Comparing Figure 6.20 with Figure 6.19, reveals two interesting discoveries from the plot. First, unlike the simulation with tidal dispersion, in which the spread of fecal coliform in both upstream and downstream directions are the same, the FC concentration drops back to its original level quickly in Segment 14 (upstream) if transport by dispersion is disabled. This is because transportation of the pollutant upstream primarily comes from the tidal effect. Without tidal dispersion, the amount of pollutant transported upstream would decrease considerably. Second, the FC concentration increases from 3.5 cell/ml in the case with dispersion to 20 cell/ml in the case without dispersion at the discharging point. This shows the dilution effect exerted by the tide in the estuary system. This reveals that the estuary system can accept a much higher pollution loading without affecting aquatic lives when compared with other types of system without much dispersion. This is the reason why the water quality criteria in an estuary system usually can be less strict than for other water systems.

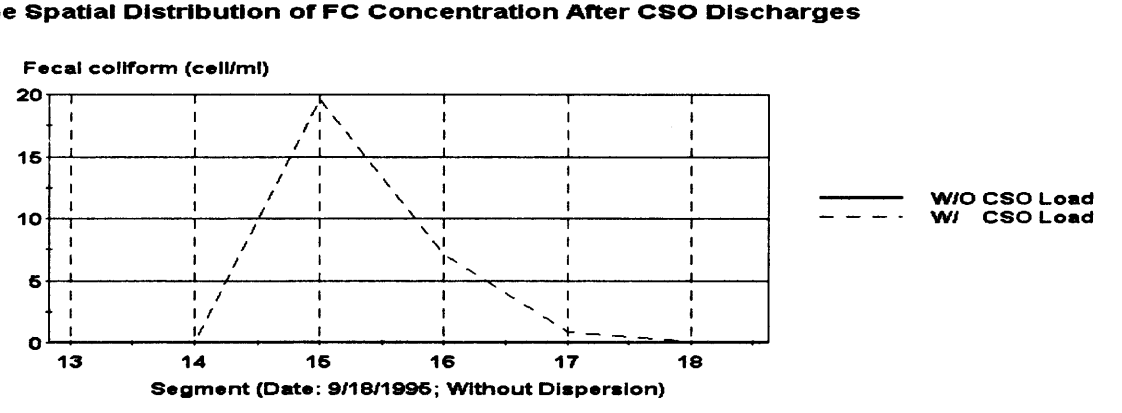

Figure 6.20 The Spatial Distribution of FC Concentration After CSO Discharges. (Without Dispersion)

Similar to what is found in the spatial distribution of fecal coliform, mercury also shows symmetry in concentration distribution in both the water layer (Figure 6.21) and the sediment layer (Figure 6.22). The mercury concentration increases from 300 ng/L to 2,350 ng/L (0.3 ppb to 2.35 ppb) in the water layer when CSO discharges, and the Hg concentration decreases gradually in both the upstream and downstream directions. It is observed from the figure that the Hg concentration decreased in a segment is related to the respective of distance to the location of the CSO outfall (Segment 15 in this study). In the downstream direction, the Hg concentration decreases were 0.16, 0.35, and 0.4 ppb per segment between adjacent segments from the discharging point (Segment 15) to Segment 18. The same phenomenon can be also found in the upstream direction. The Hg concentration decreases were 0.1 and 0.35 ppb per segment in Segments 14 and 13.

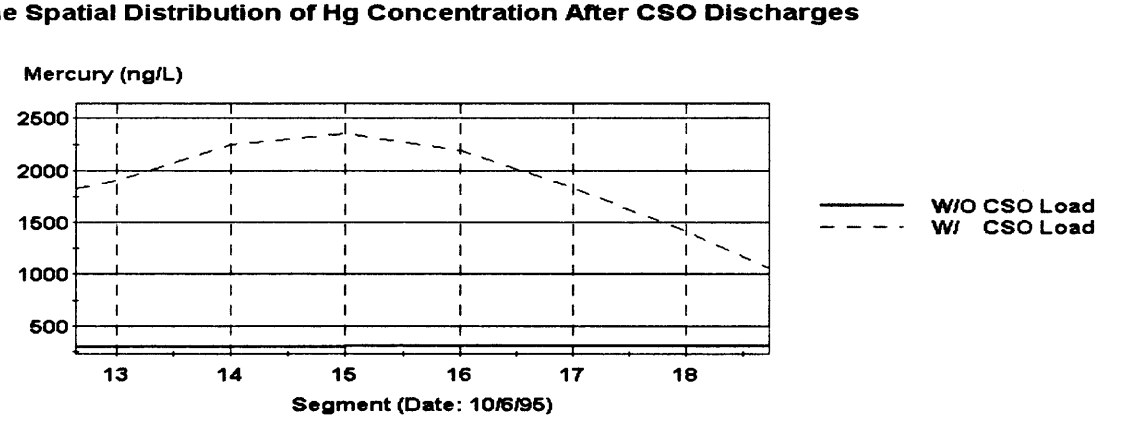

Figure 6.21 The Spatial Distribution of Mercury Concentration After CSO Discharges. (Water Layer)

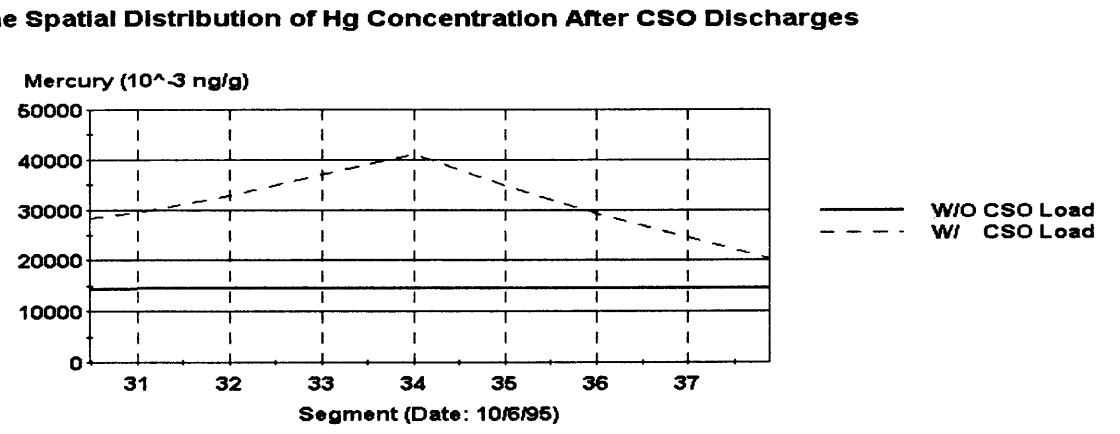

Figure 6.22 The Spatial Distribution of Mercury Concentration After CSO Discharges (Sediment Layer).

Figure 6.22 shows that the Hg concentration in the sediment is much higher. The Hg level rises from 15,000 ng/L to 41,000 ng/L (15 ppb to 41) ppb in Segment 34, which is the sediment layer beneath Segment 15, and it decreases 4 ppb and 6 ppb per segment upstream and downstream, respectively.

Comparing the decreasing Hg concentration in water and sediment layers, the decreasing of Hg level in adjacent segment is much higher for the sediment layer than for the water layer. This observation suggests that most mercury from the CSO is concentrated in the areas adjacent to the discharging locations and mostly stays in sediment due to the lack of dilution or transportation ability. This phenomenon has been reported in some recent research. Iannuzzi and co-workers (1997) collected sediment samples along the lower Passaic River in New Jersey and analyzed the priority organic and inorganic chemicals, which include toxic metals, polycyclic aromatic hydrocarbons (PAHs), polychlorinated biphenyls (PCBs), pesticides, and other organic chemicals. They evaluated various chemicals permitted to be discharged to the CSOs and have demonstrated that many chemicals present in sediments adjacent to these CSOs could be

directly linked to sources that discharge to the combined sewers. This link provides direct evidence that the CSOs are the primary source of contamination in sediments near these outfalls. They also stated that any attempts to remediate surface sediment for the purpose of improving sediment and water quality cannot be effective until CSOs and other point and non-point sources of chemicals are adequately controlled. This is an issue of increasing importance because of the regulatory impetus to "clean-up" contaminated sediments in many of the industrialized waterways of the U.S. like the Hudson River.

In summary, the results show that tides, which produce large dispersion, have significant impacts on pollutant distribution in their estuary system as evidenced from the spatial distribution analysis performed. Comparing the spatial distribution of contaminants in the water system without dispersion, the pollutant concentration decreases and spreads symmetrically in both upstream and downstream directions. The results show that total maximum daily loads (TMDLs) for an estuary system can be higher than other water systems that do not have such dispersion. It is also concluded that the linkage between the spatial distribution of contaminants in sediments and the pollution load data can be used to investigate the primary sources of pollutants.

6.6 Temporal Variation Analysis

It is mentioned in the previous discussion that the impacts of CSO loads on receiving water quality in water layers are temporal. The increased pollutant concentration will eventually return to the original condition after a short period of time once the CSOs stop discharging. The next questions will be: How long will take it to go back to the original concentration? How does the pollutant concentration vary with time? And, does the

magnitude of the CSO loads affect the temporal variation pattern? All of these questions can be answered by the use of temporal variation analysis.

The calibrated Mercury model was selected to be used in this analysis due to the large response of Hg concentration in the receiving water for CSO discharges. Several modifications were made to facilitate the analysis. Only one storm event that of September 17 was used in load data, all the other storm events were disabled. In addition, only the CSO loads discharged from Segment 15 in this very storm event were used. All the discharges from other segments are also made inactive. To investigate the impact of the magnitude of CSO loads on temporal variation of pollutant levels, four levels of CSO loads were simulated: no CSO load, original CSO load, and 5 times and 10 times the original CSO load.

Figure 6.23 presents the simulation results of temporal variation of mercury concentration in the water layer. Several phenomena are found from the plot. First, no matter what the magnitude of the CSO load is, the mercury concentration reaches a peak concentration within approximately the same period of time, 24 hours after the CSO discharge. This period of time cannot be explained as the occurrence of the "first flush". Usually, the first flush does not occur at the same period after the storm. Instead, it depends on the quantity of CSOs, the properties of CSSs, and the number of dry days preceding the storm event. CSO in this model is being put into the model as total loads per day in a specific segment, which is the multiplication of event mean concentrations (EMCs) and the CSO flowrate. Furthermore, the input CSO loads are calculated without concern about the properties of the conveyance system, such as slope of the sewers, and sewer material, etc., and therefore the simulation result from the WASP model cannot

describe the variation of pollutant concentration in combined sewers. However, the properties of combined sewer system can be simulated by other modeling tools, such as SWMM.

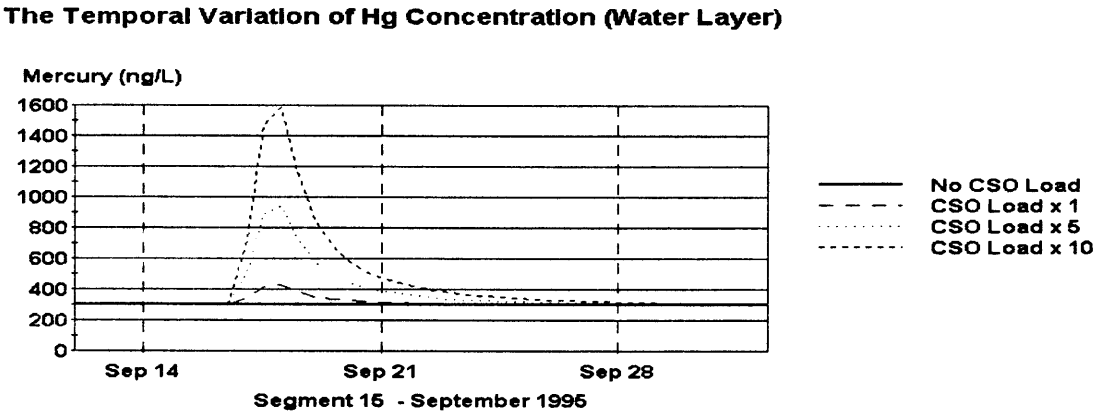

Figure 6.23 The Temporal Variation of Mercury Concentration (Water Layer).

Second, after reaching the peak concentration, the mercury concentration decreases rapidly. Although it takes at least 10 days for the Hg concentration (simulating with the original CSO load) to go back to its original condition, the figure shows that the pollutant concentration would reduce its concentration low enough in a relative short period of time. By taking the 10 times of the original CSO load case as an example, the Hg concentration increases from 300 ng/L (0.3 ppb) to the maximum concentration, close to 1,600 ng/L (1.6 ppb), on September 18, one day after CSO discharge. Then from September 18 to September 21, the mercury concentration decreases to 440 ng/L (0.44 ppb) in 3 days. This means 89.2 percent of the Hg was diluted in 4 days right after the CSO discharge and the remaining Hg will need a longer time to be diluted. The same trend can also be seen under other load scenarios.

The temporal variation of mercury concentration affected by the CSO load in sediment layers is shown in Figure 6.24. Similar to the simulation result in water layers,

the mercury concentration increases to the maximal concentration in approximately the same period of time after the CSO discharge. However, compared to the time of the appearance of the peak in both water and the sediment layer, the peaks in the sediment layers, shown in Figure 6.24, reach maximum 3 days after the water layer reaches its peak concentration. The longer time for Hg to reach its maximum concentration in sediment is primarily due to the time required for pollutant transportation from the water layer to the sediment layer.

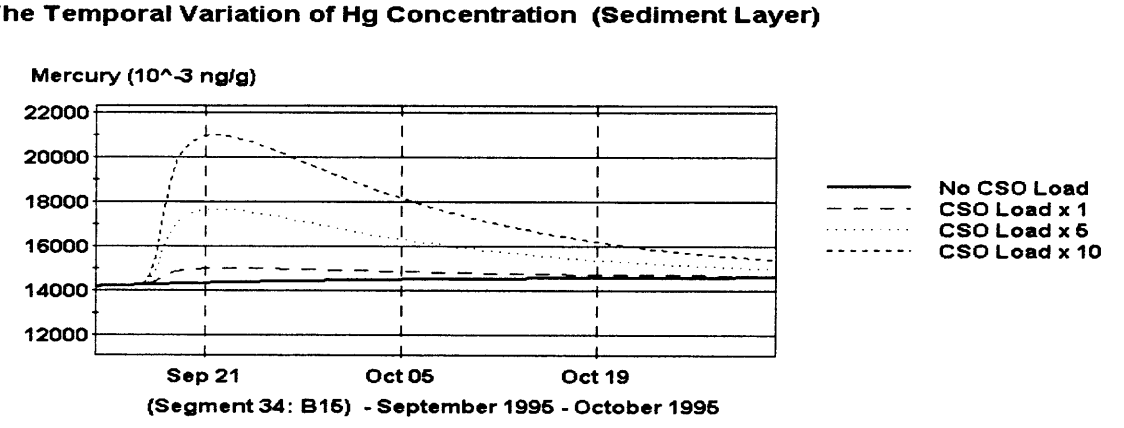

Figure 6.24 The Temporal Variation of Mercury Concentration (Sediment Layer).

Unlike the rapid decreasing of the Hg concentration in the water layer, mercury concentration decreases gradually in sediment layers after it reaches its peak concentrations. For instance, mercury concentration drops from 21,000 ng/L to 18,000 ng/L (21.0 ppb to 18.0 ppb) from September 21 to October 5 for the case of 10 times the original CSO load. Figure 6.24 shows that 50 percent of the mercury from CSO discharge still remains in the sediment after 14 days. It also can be observed that over 20 percent of the loaded mercury still exists in the sediment after 28 days. Similar trends can also be found in the other CSO load scenarios.

Comparing the simulation results of temporal variation of the pollutant in water and the sediment layer validates the conclusion about impacts of CSO loads discussed earlier in Section 6.3 that immediately after the discharge of CSO, the receiving water quality will be deteriorated for a short term, but that the sediments will be contaminated for a much longer period of time.

The next question in temporal analysis would be "how the stream flowrate will affect the pollutant variation?" In this scenario, the previous models used in temporal analysis were used except that the flowrate was changed to one-tenth of the original, and the geometric data were also modified simultaneously according to the flowrate. The simulation result was performed and the results are shown in Figure 6.25. Comparing the mercury concentration in Figure 6.23, the mercury concentration was increased proportionally to the low flowrate. However, the mercury concentration in Figure 6.25 drops to its original concentration in approximately the same time as in Figure 6.23.

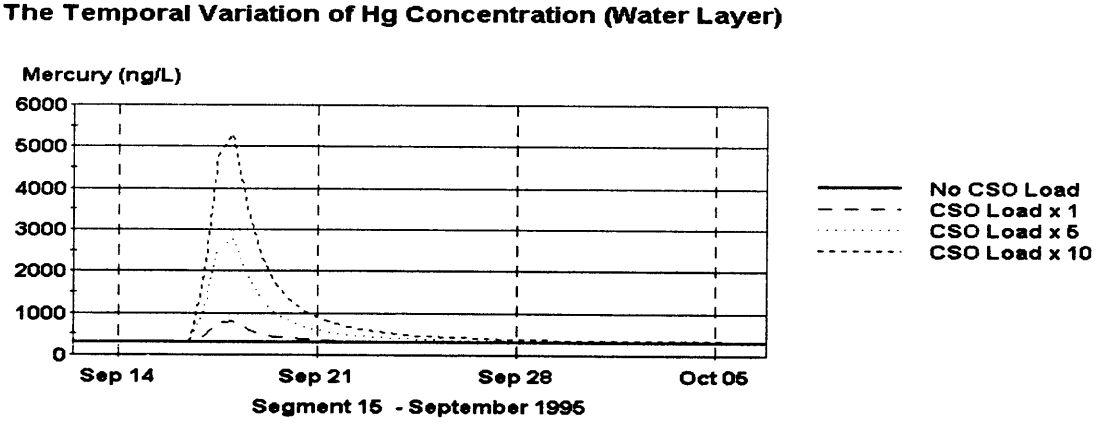

Figure 6.25 The Temporal Variation of Hg Concentration under One-Tenth of the Original Flowrate Condition.

The mercury concentration increases from 300 ng/L to 5,300 ng/L (0.30 ppb to 5.30 ppb) on September 18, one day after CSO discharge, in the 10 times the original

CSO load condition simulation. After 3 days, the Hg concentration decreases to 890 ng/L (0.89 ppb) on September 21. This means the mercury was diluted in a approximately the same rate at both simulated discharge levels, with the low flowrate, 88.2 percent mercury was diluted in 3 days, compared with the original flowrate (89.2 percent Hg diluted in 3 days). On the other hand, the higher Hg concentration introduced by the very low stream flowrate needs a longer time to reduce the concentration to acceptable levels, although it has the same dilution rate. By taking the 10 times the original CSO load case as an example, the mercury, after reaching its maximum concentration, needs more than 3 days to decrease its concentration to less than 1 ppb, but it takes only 1 day under the original flowrate to allow the Hg concentration to drop to that level. In addition, the remaining Hg will need a longer time to be diluted to its original concentration in both flowrate conditions.

CHAPTER 7

CONCLUSION AND RECOMMENDATIONS

7.1 Conclusion

To investigate the impacts of CSO on receiving water quality by mathematical water quality models, a case study for the Hudson River was developed. The Water Quality Analysis Simulation Program - WASP - 6.1 was used in this study due to its great flexibility under various simulation conditions. The water quality model was developed through data collection, model creation, model calibration and validation, and finally model application in water quality control programs. Three sets of data were used in this study, namely, water transport data, water quality data, and pollutant load data. Most of the data sets were obtained from existing sources, such as USGS, US EPA, and local water quality investigation reports. The remainder were estimated from technical reports or previous studies, such as CSO loads data. Three sub-models were developed to investigate various pollution concerns. They are EUTRO for DO/BOD/nitrogen simulation, Heat for fecal coliform simulation, and Mercury for Hg simulation.

The model was calibrated and validated with field data in the EUTRO model. However, due to limited field data, the calibration and validation phases were not performed with the Mercury model, and only calibration was performed in the Heat Model. The model results without completed calibration and validation were only used in sensitivity analysis to investigate the degree of impacts on water quality from various environmental factors. Generally, simulation results agree with observations for the DO/BOD/ammonia simulation and the FC model after calibration and validation. The

few poor statistical values of calibration and validation could result from the large-scale segmentation and inaccuracy of sampling and sample analysis. The statistics could be improved later by dividing segments into finer cells and employing an intensive sampling program to provide a more robust data set.

The calibrated water quality model was used to evaluate the impacts of CSO with a series of scenarios. According to the simulation results, the CSO loads have little effect on the EUTRO system in the study area. This observation was verified by a water quality investigation conducted in the Hudson River by other researchers, which also indicated CSOs are not the primary loading sources of BOD and nutrients in the river. Meanwhile, the simulation results from various loading scenarios also show that CSO can have great effect on the FC and Hg concentrations in the Hudson River, and how these pollutant concentrations respond to the CSO loads with respect to the time of discharge and the magnitude of the load. In the FC simulation, it is observed that water quality criteria for FC will be violated if 3 times of the original CSO loads are placed in the river. In the Mercury model, the predicted results reveal that mercury, discharged along with the CSOs, will be diluted or transported in the water layer after a short period of time but that the accumulation of mercury in the sediment layer lasts much longer.

The stream flowrate is another factor that will affect the water quality in the receiving water considerably. In general, water quality is deteriorated under the low flowrate condition, due to lack of enough dilution ability to minimize the negative impacts from loaded pollutants. The simulation results show that most of the pollutants will violate the surface water quality criteria under very low flowrate or drought

conditions. Higher degree of treatments in pollution control are required during the periods to avoid water quality problems.

The spatial distribution analysis indicates that the pollutants decrease gradually and symmetrically from the discharging point in both upstream and downstream direction. The analysis reveals the importance of dispersion by tide in pollutant transportation in estuaries. It is also found that the linkage between the spatial distribution of contaminants in sediments and the pollution load data can be used to investigate the primary sources of pollutants. The temporal variation analysis shows that the mercury concentration in the water layer would reduce its concentration low enough in a relative short period of time. The remained mercury in the water layer needs a longer time to be diluted to its original condition. Unlike the rapid decreasing of the Hg concentration in the water layer, mercury concentration decreases gradually in sediment layers. It validates that immediately after the discharge of CSO, the receiving water quality will be deteriorated for a short term, but that the sediments will be contaminated for a much longer period of time.

7.2 Recommendations

Because of the great range and variation of many factors, such as weather patterns, characteristics of combined sewer systems, and receiving water usage, all of which may affect the pollutant distribution in receiving waters after CSO discharges, it is unlikely that any receiving water quality model can be universally adopted for all water systems. It is necessary and desirable to calibrate the model to assure compatibility with the field data and apply it under a variety of conditions. Mathematical modeling of receiving water

greatly facilitates solutions to the need for simulation and prediction. The type of model employed can be adjusted with the various degrees of flow transportation patterns, the scope of study area, and other environmental conditions.

WASP is a powerful water quality-modeling tool. However, it needs a large amount of input information to produce useful results. Data availability was the major difficulty encountered during their simulation study. Incomplete data included physical characteristics of study area, constants of transformation processes, flow, and loading information. Furthermore, these data must be time-related. The difficulties in the modeling processes discussed earlier are mostly from the lack of sufficient field data. A well-developed monitoring plan will greatly facilitate success in water quality modeling.

However, due to the limited field data, the models created in this study simplified or neglected some of the transport and transformation processes that will affect the pollutant distribution in receiving waters. To improve the model's predictive capability, the following considerations are important in further studies.

Appropriate segmentation is a foundation to a successful water quality model. Further dissecting of the segments into smaller pieces is necessary when a more complicated transport pattern is concerned. For instance, the dispersion introduced by tides in estuaries is greater in both lateral and vertical directions than in rivers. Thus, for the purpose of detailed studies of pollutant spatial distribution in estuaries, finer segmentation in these two directions should be created. In addition, small-scale segmentation can also prevent the occurrence of unstable predicted concentrations, which may cause poor statistical results in the model calibration and validation processes.

However, segmentation corresponds to the available field data. Without enough field data, more segments do not help.

In this study, except the Mercury model applied to sediment layers, other models are simulated in one-dimension with water columns only. However, the sediment type plays an important role in bed segmentation and certain transformation processes. WASP 6.1 can simulate not only benthic layers but also lower benthic layers. Since sediment monitoring did not address public health risks in the past, they can only be used as alternatives when bacterial contamination is not a CSO concern. Also, high cost limits the extent of sediment monitoring in water quality sampling. The limited sediment field data constrains the model prediction and application. For example, supplemental SOD (sediment oxygen demand) concentration information and additional sediment segmentation will increase the accuracy of predicting DO concentration in both water columns and sediment layers.

Enhancements in transport and transformation processes in the model will improve the confidence in predicting pollutant variations in receiving waters. For example, in the EUTRO model, zooplankton and solar effects on DO concentration are simplified or neglected due to the lack of sufficient field data. However, based on biological concepts, these factors could change DO concentration in the river significantly. Furthermore, in the Mercury model, most of the transport and transformation process of mercury are complicated and uncertain. Further experiments and research are required to improve understanding of these processes. Minimizing the number of these unknown factors will improve the accuracy seen in the simulation results.

Based on the successful application of the water quality model in revealing the impacts of CSO on receiving waters, more applications with various other pollutants from CSO or other pollution sources on receiving water quality can be studied in the future. For example, nutrients such as nitrite, nitrate, and phosphorus, and chlorophyll-a can be simulated in the EUTRO model to predict the possibility of eutrophication; the simulation results for various type of pathogens can be used in the Heat model to study the sources of bacteria; chemicals such as PCBs, and metals such as lead and copper can be simulated in the Mercury model since they are the primary contaminants in the Hudson River. Furthermore these calibrated models can be applied to investigate the long-term effect from pollutants and also to predict ecological impacts that implicated by the military actions.

In result generation, more spatial-graphical information data (digital maps) are becoming available, which allows a better spatial exhibit. WASP 6.1 has a function to display the simulation results in a spatial grid, in which the model network is color shaded based upon the predicted concentration. Creating linkages between GIS (geographic information system) technology with the water quality model can enhance model applications and result interpretation.

This study has provided an approach to understand the impacts of CSOs on receiving water quality. With the great flexibility of the model, the water quality of the receiving water can be predicted easily under various conditions if sufficient data are provided. These conditions include not only the ordinary pollutants discharges, but also those unexpected contaminations, which were introduced by the terrorist attack or a spills

incidence. With more and more robust water quality and quantity monitoring programs developed in recent years, it was a trend to create water quality models for various water bodies. Based on the same approach, more water quality issues can be realized by appropriate receiving water quality models.

APPENDIX A

LOAD INPUT DATA

Appendix A summarizes the CSO load input data that were derived from the Tri-City monitoring data.

Table A.1 DO Load Input Data

Storm Event		7/28/1995	9/17/1995	9/22/1995	9/25/1995	10/5/1995	10/14/1995	10/21/1995	10/27/95A	10/27/95B
Avg. Load per Outfall (kg)*		17.02	31.47	29.98	36.64	62.98	64.62	78.63	8.01	34.37
Segment	1	0	0	0	0	0	0	0	0	0
	2	0	0	0	0	0	0	0	0	0
	3	0	0	0	0	0	0	0	0	0
	4	0	0	0	0	0	0	0	0	0
	5	0	0	0	0	0	0	0	0	0
	6	34.04	62.94	59.96	73.28	125.96	129.24	157.26	16.02	68.74
	7	17.02	31.47	29.98	36.64	62.98	64.62	78.63	8.01	34.37
	8	34.04	62.94	59.96	73.28	125.96	129.24	157.26	16.02	68.74
	9	34.04	62.94	59.96	73.28	125.96	129.24	157.26	16.02	68.74
	10	17.02	31.47	29.98	36.64	62.98	64.62	78.63	8.01	34.37
	11	17.02	31.47	29.98	36.64	62.98	64.62	78.63	8.01	34.37
	12	51.06	94.41	89.94	109.92	188.94	193.86	235.89	24.03	103.11
	13	34.04	62.94	59.96	73.28	125.96	129.24	157.26	16.02	68.74
	14	34.04	62.94	59.96	73.28	125.96	129.24	157.26	16.02	68.74
	15	51.06	94.41	89.94	109.92	188.94	193.86	235.89	24.03	103.11
	16	102.12	188.82	179.88	219.84	377.88	387.72	471.78	48.06	206.22
	17	0	0	0	0	0	0	0	0	0
	18	119.14	220.29	209.86	256.48	440.86	452.34	550.41	56.07	240.59
	19	136.16	251.76	239.84	293.12	503.84	516.96	629.04	64.08	274.96

* Tri-City Data
Load Unit: kg
Load (kg)=Avg. Load (kg)*(# of outfalls)

Table A.2 $CBOD_U$ Load Input Data

Storm Event		7/28/1995	9/17/1995	9/22/1995	9/25/1995	10/5/1995	10/14/1995	10/21/1995	10/27/95A	10/27/95B
Avg. Load per Outfall (kg)*		362.09	669.66	637.94	779.53	1339.99	1374.84	1673.04	170.46	731.19
Segment	1	0	0	0	0	0	0	0	0	0
	2	0	0	0	0	0	0	0	0	0
	3	0	0	0	0	0	0	0	0	0
	4	0	0	0	0	0	0	0	0	0
	5	0	0	0	0	0	0	0	0	0
	6	724.18	1339.32	1275.88	1559.06	2679.98	2749.68	3346.08	340.92	1462.38
	7	362.09	669.66	637.94	779.53	1339.99	1374.84	1673.04	170.46	731.19
	8	724.18	1339.32	1275.88	1559.06	2679.98	2749.68	3346.08	340.92	1462.38
	9	724.18	1339.32	1275.88	1559.06	2679.98	2749.68	3346.08	340.92	1462.38
	10	362.09	669.66	637.94	779.53	1339.99	1374.84	1673.04	170.46	731.19
	11	362.09	669.66	637.94	779.53	1339.99	1374.84	1673.04	170.46	731.19
	12	1086.27	2008.98	1913.82	2338.59	4019.97	4124.52	5019.12	511.38	2193.57
	13	724.18	1339.32	1275.88	1559.06	2679.98	2749.68	3346.08	340.92	1462.38
	14	724.18	1339.32	1275.88	1559.06	2679.98	2749.68	3346.08	340.92	1462.38
	15	1086.27	2008.98	1913.82	2338.59	4019.97	4124.52	5019.12	511.38	2193.57
	16	2172.54	4017.96	3827.64	4677.18	8039.94	8249.04	10038.24	1022.76	4387.14
	17	0	0	0	0	0	0	0	0	0
	18	2534.63	4687.62	4465.58	5456.71	9379.93	9623.88	11711.28	1193.22	5118.33
	19	2896.72	5357.28	5103.52	6236.24	10719.92	10998.72	13384.32	1363.68	5849.52

Table A.3 NH_3-N Load Input Data

Storm Event		7/28/1995	9/17/1995	9/22/1995	9/25/1995	10/5/1995	10/14/1995	10/21/1995	10/27/95A	10/27/95B
Avg. Load per Outfall (kg)*		3.28	6.35	6.16	7.38	13.09	12.98	16.25	1.87	7.94
Segment	1	0	0	0	0	0	0	0	0	0
	2	0	0	0	0	0	0	0	0	0
	3	0	0	0	0	0	0	0	0	0
	4	0	0	0	0	0	0	0	0	0
	5	0	0	0	0	0	0	0	0	0
	6	6.56	12.70	12.32	14.76	26.18	25.96	32.50	3.74	15.88
	7	3.28	6.35	6.16	7.38	13.09	12.98	16.25	1.87	7.94
	8	6.56	12.70	12.32	14.76	26.18	25.96	32.50	3.74	15.88
	9	6.56	12.70	12.32	14.76	26.18	25.96	32.50	3.74	15.88
	10	3.28	6.35	6.16	7.38	13.09	12.98	16.25	1.87	7.94
	11	3.28	6.35	6.16	7.38	13.09	12.98	16.25	1.87	7.94
	12	9.84	19.05	18.48	22.14	39.27	38.94	48.75	5.61	23.82
	13	6.56	12.70	12.32	14.76	26.18	25.96	32.50	3.74	15.88
	14	6.56	12.70	12.32	14.76	26.18	25.96	32.50	3.74	15.88
	15	9.84	19.05	18.48	22.14	39.27	38.94	48.75	5.61	23.82
	16	19.68	38.10	36.96	44.28	78.54	77.88	97.50	11.22	47.64
	17	0	0	0	0	0	0	0	0	0
	18	22.96	44.45	43.12	51.66	91.63	90.86	113.75	13.09	55.58
	19	26.24	50.80	49.28	59.04	104.72	103.84	130.00	14.96	63.52

Table A.4 NO_2-N Load Input Data

Storm Event		7/28/1995	9/17/1995	9/22/1995	9/25/1995	10/5/1995	10/14/1995	10/21/1995	10/27/95A	10/27/95B
Avg. Load per Outfall (kg)*		0.82	2.25	2.23	2.62	4.8	4.6	5.92	0.76	3.2
Segment	1	0	0	0	0	0	0	0	0	0
	2	0	0	0	0	0	0	0	0	0
	3	0	0	0	0	0	0	0	0	0
	4	0	0	0	0	0	0	0	0	0
	5	0	0	0	0	0	0	0	0	0
	6	1.64	4.50	4.46	5.24	9.60	9.20	11.84	1.52	6.40
	7	0.82	2.25	2.23	2.62	4.80	4.60	5.92	0.76	3.20
	8	1.64	4.50	4.46	5.24	9.60	9.20	11.84	1.52	6.40
	9	1.64	4.50	4.46	5.24	9.60	9.20	11.84	1.52	6.40
	10	0.82	2.25	2.23	2.62	4.80	4.60	5.92	0.76	3.20
	11	0.82	2.25	2.23	2.62	4.80	4.60	5.92	0.76	3.20
	12	2.46	6.75	6.69	7.86	14.40	13.80	17.76	2.28	9.60
	13	1.64	4.50	4.46	5.24	9.60	9.20	11.84	1.52	6.40
	14	1.64	4.50	4.46	5.24	9.60	9.20	11.84	1.52	6.40
	15	2.46	6.75	6.69	7.86	14.40	13.80	17.76	2.28	9.60
	16	4.92	13.50	13.38	15.72	28.80	27.60	35.52	4.56	19.20
	17	0	0	0	0	0	0	0	0	0
	18	5.74	15.75	15.61	18.34	33.60	32.20	41.44	5.32	22.40
	19	6.56	18.00	17.84	20.96	38.40	36.80	47.36	6.08	25.60

Table A.5 Organic-N Load Input Data

Storm Event		7/28/1995	9/17/1995	9/22/1995	9/25/1995	10/5/1995	10/14/1995	10/21/1995	10/27/95A	10/27/95B
Avg. Load per Outfall (kg)*		15.28	27.92	26.65	32.47	56.09	57.28	69.98	7.26	31.13
Segment	1	0	0	0	0	0	0	0	0	0
	2	0	0	0	0	0	0	0	0	0
	3	0	0	0	0	0	0	0	0	0
	4	0	0	0	0	0	0	0	0	0
	5	0	0	0	0	0	0	0	0	0
	6	30.56	55.84	53.30	64.94	112.18	114.56	139.96	14.52	62.26
	7	15.28	27.92	26.65	32.47	56.09	57.28	69.98	7.26	31.13
	8	30.56	55.84	53.30	64.94	112.18	114.56	139.96	14.52	62.26
	9	30.56	55.84	53.30	64.94	112.18	114.56	139.96	14.52	62.26
	10	15.28	27.92	26.65	32.47	56.09	57.28	69.98	7.26	31.13
	11	15.28	27.92	26.65	32.47	56.09	57.28	69.98	7.26	31.13
	12	45.84	83.76	79.95	97.41	168.27	171.84	209.94	21.78	93.39
	13	30.56	55.84	53.30	64.94	112.18	114.56	139.96	14.52	62.26
	14	30.56	55.84	53.30	64.94	112.18	114.56	139.96	14.52	62.26
	15	45.84	83.76	79.95	97.41	168.27	171.84	209.94	21.78	93.39
	16	91.68	167.52	159.90	194.82	336.54	343.68	419.88	43.56	186.78
	17	0	0	0	0	0	0	0	0	0
	18	106.96	195.44	186.55	227.29	392.63	400.96	489.86	50.82	217.91
	19	122.24	223.36	213.20	259.76	448.72	458.24	559.84	58.08	249.04

Table A.6 Ortho-Phosphate Load Input Data

Storm Event		7/28/1995	9/17/1995	9/22/1995	9/25/1995	10/5/1995	10/14/1995	10/21/1995	10/27/95A	10/27/95B
Avg. Load per Outfall (kg)*		1.32	2.36	2.13	2.75	4.61	4.85	5.78	0.53	2.29
Segment	1	0	0	0	0	0	0	0	0	0
	2	0	0	0	0	0	0	0	0	0
	3	0	0	0	0	0	0	0	0	0
	4	0	0	0	0	0	0	0	0	0
	5	0	0	0	0	0	0	0	0	0
	6	2.64	4.72	4.26	5.50	9.22	9.70	11.56	1.06	4.58
	7	1.32	2.36	2.13	2.75	4.61	4.85	5.78	0.53	2.29
	8	2.64	4.72	4.26	5.50	9.22	9.70	11.56	1.06	4.58
	9	2.64	4.72	4.26	5.50	9.22	9.70	11.56	1.06	4.58
	10	1.32	2.36	2.13	2.75	4.61	4.85	5.78	0.53	2.29
	11	1.32	2.36	2.13	2.75	4.61	4.85	5.78	0.53	2.29
	12	3.96	7.08	6.39	8.25	13.83	14.55	17.34	1.59	6.87
	13	2.64	4.72	4.26	5.50	9.22	9.70	11.56	1.06	4.58
	14	2.64	4.72	4.26	5.50	9.22	9.70	11.56	1.06	4.58
	15	3.96	7.08	6.39	8.25	13.83	14.55	17.34	1.59	6.87
	16	7.92	14.16	12.78	16.50	27.66	29.10	34.68	3.18	13.74
	17	0	0	0	0	0	0	0	0	0
	18	9.24	16.52	14.91	19.25	32.27	33.95	40.46	3.71	16.03
	19	10.56	18.88	17.04	22.00	36.88	38.80	46.24	4.24	18.32

Table A.7 Organic-P Load Input Data

Storm Event		7/28/1995	9/17/1995	9/22/1995	9/25/1995	10/5/1995	10/14/1995	10/21/1995	10/27/95A	10/27/95B
Avg. Load per Outfall (kg)*		3.69	6.71	6.43	7.81	13.27	13.79	16.6	1.61	6.92
Segment	1	0	0	0	0	0	0	0	0	0
	2	0	0	0	0	0	0	0	0	0
	3	0	0	0	0	0	0	0	0	0
	4	0	0	0	0	0	0	0	0	0
	5	0	0	0	0	0	0	0	0	0
	6	7.38	13.42	12.86	15.62	26.54	27.58	33.20	3.22	13.84
	7	3.69	6.71	6.43	7.81	13.27	13.79	16.60	1.61	6.92
	8	7.38	13.42	12.86	15.62	26.54	27.58	33.20	3.22	13.84
	9	7.38	13.42	12.86	15.62	26.54	27.58	33.20	3.22	13.84
	10	3.69	6.71	6.43	7.81	13.27	13.79	16.60	1.61	6.92
	11	3.69	6.71	6.43	7.81	13.27	13.79	16.60	1.61	6.92
	12	11.07	20.13	19.29	23.43	39.81	41.37	49.80	4.83	20.76
	13	7.38	13.42	12.86	15.62	26.54	27.58	33.20	3.22	13.84
	14	7.38	13.42	12.86	15.62	26.54	27.58	33.20	3.22	13.84
	15	11.07	20.13	19.29	23.43	39.81	41.37	49.80	4.83	20.76
	16	22.14	40.26	38.58	46.86	79.62	82.74	99.60	9.66	41.52
	17	0	0	0	0	0	0	0	0	0
	18	25.83	46.97	45.01	54.67	92.89	96.53	116.20	11.27	48.44
	19	29.52	53.68	51.44	62.48	106.16	110.32	132.80	12.88	55.36

Table A.8 Fecal Coliform Load Input Data

Storm Event		7/28/1995	9/17/1995	9/22/1995	9/25/1995	10/5/1995	10/14/1995	10/21/1995	10/27/95A	10/27/95B
Avg. Load per Outfall (billion colonies)*		16282	30184	28783	35234	60468	62089	75229	7699	32927
Segment	1	0	0	0	0	0	0	0	0	0
	2	0	0	0	0	0	0	0	0	0
	3	0	0	0	0	0	0	0	0	0
	4	0	0	0	0	0	0	0	0	0
	5	0	0	0	0	0	0	0	0	0
	6	0	0	0	0	0	0	0	0	0
	7	0	0	0	0	0	0	0	0	0
	8	0	0	0	0	0	0	0	0	0
	9	0	0	0	0	0	0	0	0	0
	10	0	0	0	0	0	0	0	0	0
	11	0	0	0	0	0	0	0	0	0
	12	32564	60368	57566	70468	120936	124178	150458	15398	65854
	13	16282	30184	28783	35234	60468	62089	75229	7699	32927
	14	32564	60368	57566	70468	120936	124178	150458	15398	65854
	15	32564	60368	57566	70468	120936	124178	150458	15398	65854
	16	16282	30184	28783	35234	60468	62089	75229	7699	32927
	17	16282	30184	28783	35234	60468	62089	75229	7699	32927
	18	48846	90552	86349	105702	181404	186267	225687	23097	98781
	19	32564	60368	57566	70468	120936	124178	150458	15398	65854

* Tri-City Data
Load Unit: billion colonies
Load (billion colonies)=Avg. Load (billion colonies)*(# of outfalls)

Table A.9 Hg Load Input Data

Storm Event		7/28/1995	9/17/1995	9/22/1995	9/25/1995	10/5/1995	10/14/1995	10/21/1995	10/27/95A	10/27/95B
Avg. Load per Outfall (10^{-3} kg)*		3382	8377	8788	9672	19654	16895	23752	3962	16485
Segment	1	0	0	0	0	0	0	0	0	0
	2	0	0	0	0	0	0	0	0	0
	3	0	0	0	0	0	0	0	0	0
	4	0	0	0	0	0	0	0	0	0
	5	0	0	0	0	0	0	0	0	0
	6	0	0	0	0	0	0	0	0	0
	7	0	0	0	0	0	0	0	0	0
	8	0	0	0	0	0	0	0	0	0
	9	0	0	0	0	0	0	0	0	0
	10	0	0	0	0	0	0	0	0	0
	11	0	0	0	0	0	0	0	0	0
	12	6764	16754	17576	19344	39308	33790	47504	7924	32970
	13	3382	8377	8788	9672	19654	16895	23752	3962	16485
	14	6764	16754	17576	19344	39308	33790	47504	7924	32970
	15	6764	16754	17576	19344	39308	33790	47504	7924	32970
	16	3382	8377	8788	9672	19654	16895	23752	3962	16485
	17	3382	8377	8788	9672	19654	16895	23752	3962	16485
	18	10146	25131	26364	29016	58962	50685	71256	11886	49455
	19	6764	16754	17576	19344	39308	33790	47504	7924	32970

* Tri-City Data
Load Unit: 10^{-3} kg
Load (10^{-3} kg)=Avg. Load (10^{-3} kg)*(# of outfalls)

APPENDIX B

REFERENCE VALUES AND SOURCES OF TRANSFORMATION CONSTANTS

Appendix B summarizes Reference Values and Sources of Transformation Constants for the EUTRO model.

Table B.1 Reference Values and Sources of Transformation Constants

Constant	Unit	Value	Source
Nitrification Rate @20°C	1/day	0.09~0.13	Roesch et al., 1979
Nitrification Temperature Coefficient	---	1.08	Roesch et al., 1979
Half-Saturation: Nitrification Oxygen Limit	mg O_2/L	2.0	Roesch et al., 1979
Denitrification Rate @20°C	1/day	0.09	Roesch et al., 1979
Denitrification Temperature Coefficient	---	1.045	Roesch et al., 1979
Half Saturation: Denitrification Oxygen Limit	mg O_2/L	0.1	Roesch et al., 1979
Dissolved Organic Nitrogen Mineralization Rate @20°C	1/day	0.075	Roesch et al., 1979
Dissolved Organic Nitrogen Mineralization Temperature Coefficient	---	1.08	Roesch et al., 1979
Organic Nitrogen Decay in Sediments @20°C	1/day	0.0004	Roesch et al., 1979
Organic Nitrogen Decay in Sediment Temperature Coefficient	---	1.08	Roesch et al., 1979
Fraction of Phytoplankton Death Recycled to Organic Nitrogen	---	0.5	Di Toro & Martystick ,1980
Mineralization Rate of Dissolved Organic Phosphorus @20°C	---	0.22	Roesch et al., 1979
Dissolved Organic Phosphorus Mineralization Temperature Coefficient	---	1.08	Roesch et al., 1979
Organic Phosphorus Decay Rate in Sediments	1/day	0.0004	Roesch et al., 1979
Organic Phosphorus Decay in Sediments Temperature Coefficient	---	1.08	Roesch et al., 1979
Fraction of Phytoplankton Death Recycled to Organic Phosphorus	---	0.5	Di Toro & Martystick ,1980
Oxygen::Carbon Stoichiometeric Ratio	---	32/12	Roesch et al., 1979
Reaeration Rate @20°C	1/day	2.0	Di Toro & Connolly ,1980
CBOD Decay Rate @20c	1/day	0.21,0.16	Roesch et al., 1979
CBOD Decay Rate Temperature Correction	---	1.047	Roesch et al., 1979
CBOD Decay Rate in Sediments @20°C	1/day	0.0004	WASP manual
CBOD Decay Rate in Sediments Temperature Correction	---	1.08	WASP manual
CBOD Half Saturation Oxygen Limit	mg O_2/L	0.5	Roesch et al., 1979

Table B.1 Reference Values and Sources of Transformation Constants (Continued)

Constant	Unit	Value	Source
Phytoplankton Maximum Growth Rate @20°C	1/day	2.0	Roesch et al., 1979
		1.3~2.5	O'Connor et al., 1975,1981
			Thomann & Fitzpatrick ,1982
			Di Toro & Connolly, 1980
			Di Toro & Martystick, 1980
			Salisbury et al., 1983
		1.8~2.53	Jorgensen, 1976
			Jorgensen et al., 1978
		0.2~8.0	Baca & Arnett, 1976
		0.58~3.0	Jorgensen, 1979
Saturation light intensity for phytoplankton	Ly/day	400~700 (latitude 30)	Weast & Astle, 1980
		300~350	Thomann et al., 1975,1979
			Salas & Thomann, 1978
			Di Toro et al., 1971
			O'Connor et al., 1975
		250~350	Scavia, 1980
		200~300	Youngberg, 1977
Phytoplankton Half-Saturation Constant for Nitrogen	mg-N/L	0.2	WASP manual
		0.2	Jorgensen, 1976,1983
			Jorgensen et al., 1978
		0.05	Desormeau, 1978
		0.0014~0.007	Jorgensen, 1979
Phytoplankton Half-Saturation Constant for Phosphorus	mg-P/L	0.001	WASP manual
		0.002~0.03	Jorgensen, 1976,1983
		0.02	Jorgensen et al., 1978
		0.07	Desormeau, 1978
		0.0028~0.053	Jorgensen, 1979

Table B.1 Reference Values and Sources of Transformation Constants (Continued)

Constant	Unit	Value	Source
P/C ratio in Phytoplankton	mg/mg	0.025	Di Toro et al., 1971
		0.024	Scavia et al., 1976
			Scavia, 1980
		0.024~0.24	Baca & Arnett, 1976
N/C ratio in Phytoplankton	mg/mg	0.17~0.25	Di Toro et al., 1971
		0.18	Scavia et al., 1976
			Scavia, 1980
		0.2	Canale et al., 1976
		0.05~0.17	Baca & Arnett, 1976
Phytoplankton Endogenous Respiration Rate @20°C	1/day	0.125	WASP manual
		0.05~0.20	Bowie et al., 1985
		0.05~0.15	O'Connor et al., 1975, 1981
			Thomann et al., 1974,1975,1979
			Di Toro &Connolly, 1980
			Di Toro & Matystick, 1980
			Salisbury et al., 1983
		0.088~0.6	Jorgensen, 1976
			Jorgensen et al., 1978
		0.005~0.12	Baca & Arnett, 1976
Phytoplankton Respiration Temperature Coefficient	---	1.045	Di Toro & Matystick, 1980
Phytoplankton Death Rate Non-Zooplankton Predation	1/day	0.02	Thomann & Fitzpatrick, 1982
		0.003~0.17	Baca & Arnett, 1976
		0.03	Scavia et al., 1976
		0.005~0.10	Salas & Thomann, 1978
		0.01~0.1	Jorgensen, 1976
			Jorgensen et al., 1978
Phytoplankton Zooplankton Grazing Rate	L/cell-day	0.1~1.5	Bowie et al., 1985

Table B.1 Reference Values and Sources of Transformation Constants (Continued)

Constant	Unit	Value	Source
Decomposition rate constant for phytoplankton in the sediment @20°C	1/day	0.02	Roesch et al., 1979
Decomposition Temperature Coefficient	---	1.08	Roesch et al., 1979
Phytoplankton Growth Temperature Coefficient	---	1.068	WASP manual
Phytoplankton Maximum Quantum Yield Constant	Mg-c/mole photons	720	Bannister, 1974
Phytoplankton Carbon:: Chlorophyll Ratio	---	20~50	US EPA, 1970,1977,1978
Chlorophyll Extinction Coefficient	Mg chla/m^3	0.01~0.02	WASP manual
		0.016	Bannister, 1974
Half-saturation constant for phytoplankton	mg Carbon/L	0.5~0.6	Jorgensen et al., 1978
		0.5	Jorgensen, 1976,1983

REFERENCES

1996 Clean water needs survey: Report to congress. (1996a). EPA 832-R-97-003. Washington, DC: Office of Water, US EPA.

2001 New York Harbor water quality report. (2001). NYC, NY: New York City Department of Environmental Protection (NYCDEP).

Ambrose, R. B., Jr. (Ed). (1992). Technical guidance manual for performing waste load allocations, Book III: Estuaries – Part 4: Critical review of coastal embayment and estuarine waste load allocation modeling (pp. 10-1 – 14-18). Washington, DC: Office of Water, US EPA.

Ambrose, R. B., Jr. (1987). Modeling volatile organics in the Delaware Estuary. J. Environmental Engineering, 113(4), pp. 703-721.

Ambrose, R. B., Jr., & Wool, T. (2002). Modeling tools used for mercury TMDLs in Georgia Rivers. In WASP course material. Athens, GA: US EPA.

Ambrose, R. B., Jr., Wool, T., & Martin, J. L. (1993a). The water quality analysis simulation program, WASP5: Part A – Model documentation. Athens, GA: Environmental Research Laboratory, US EPA.

Ambrose, R. B., Jr., Wool, T., & Martin, J. L. (1993b). The water quality analysis simulation program, WASP5: Part B – The WASP5 input data set. Athens, GA: Environmental Research Laboratory, US EPA.

Ambrose, R. B., Jr., Wool, T., Connolly, J. P., & Schanz, R. W. (1988). WASP4, a hydrodynamic and water quality model – Model theory. User's manual, and programmer's guide. EPA 600/3-87-039. Athens, GA: Environmental Research Laboratory, US EPA.

Ambrose, R. B., Jr., & Roesch, S. E. (1982). Dynamic estuary model performance. J. Environmental Engineering, 108(EE1), pp. 51-71.

Analysis of factors affecting historical dissolved oxygen trends in Western Long Island Sound. (1995). Job No. NENG0040. Prepared for the Management Committee of the Long Island Sound Study and New England Interstate Water Pollution Control Commission. Mahwah, NJ: HydroQual, Inc.

Atkinson, J. F., Gupta, S. K., DePinto, J. V., & Rumer, R. R. (1998). Linking hydrodynamic and water quality models with deferent scales. J. Environmental Engineering, 124(5), pp. 399-408.

Beck, M. B. (1985). Water quality management: A review of the development and application of mathematical models – Lecture notes in engineering 11. New York: Springer-Verlag.

Bierman, V. J., Jr., & Dolan, D. M. (1986). Modeling of phytoplankton in Saginaw Bay. I. Calibration phase. J. Environmental Engineering, 112(2), pp. 400-403.

Blumberg, A. F., Khan, L. A., & St. John, J. P. (1997). A three-dimensional hydrodynamic model of New York Harbor, Long Island Sound and New York Bight. Paper presented at 5th international conference on estuarine and costal modeling, October 22-24, 1997, Alexandria, VA.

Brosnan, T. M., & O'Shea, M. L. (1996). Long-term improvements in water quality due to sewage abatement in the Lower Hudson River. Estuaries, 19(4), pp. 890-900.

Brosnan, T. M., & O'Shea, M. L. (1996a). Sewage abatement and coliform bacteria trends in the Lower Hudson-Raritan Estuary since passage of the Clean Water Act. Water Environment Research, 68(1), pp. 25-35.

Brown, D. S., & Allison, J. D. (1987). MINTEQA1, an equilibrium metal speciation model: User's manual. EPA 600/3-87-012. Athens, GA: Environmental Research Laboratory, US EPA.

Brown, L. C., & Barnwell, T. O. (1987). The enhanced stream water quality model QUAL2E and QUAL2E-UNCAS: Documentation and user's manual. EPA 600/3-87-007. Athens, GA: Environmental Research Laboratory, US EPA.

Burns, B. J. (1982). Exposure analysis modeling system II, user's manual.

Canale, R. P., Owens, E. M., Auer, M. T., & Effler, S. W. (1995). Validation of water quality model for Seneca River, NY. J. Water Resources Planning and Management, 121(3), pp. 241-250.

Chatwin, P. C., & Allen, C. M. (1985). Mathematical models of dispersion in rivers and estuaries. Annu. Rev. Fluid Mech., 17, pp. 119-149.

Chebbo, G., Mouchel, J. M., Saget, A., & Gousailles, M. (1995). La pollution des rejets urbains per temps de pluie: Flux, nature et impacts. TSM, 90(11), pp. 796-806.

Cheng, H., & Lockerbie, D. (1994). Water quality modeling of the Upper Saint John River: A comparison study (p. 27). Scientific Series No. 196. Ottawa, Ontario: Environmental Conservation Service.

Clark, M. J. (1975). Screening/flotation treatment of combined sewer overflows, Volume II - Full-scale demonstration. US EPA Demonstration Grant No. 11023FWS. Washington, DC: US EPA.

Colston, N. V., Jr. (1974). Characterization and treatment of urban land runoff. EPA 670/2-74-096. Washington, DC: US EPA.

Combined sewer overflows and the multimetric evaluation of their biological effects: Case studies in Ohio and New York. (1996). EPA 832-R-96-002. Washington, DC: US EPA.

Combined sewer overflow control policy. (1994a). Washington, DC: US EPA.

Combined sewer overflow control manual. (1993). EPA 625-R-93-007. Washington, DC: US EPA.

Combined sewer overflows guidance for long-term control plan. (1995b). EPA 832-B-95-002. Washington, DC: US EPA.

Combined sewer overflows guidance for monitoring and modeling. (1999). EPA 832-B-99-002. Washington, DC: US EPA.

Combined sewer overflows guidance for nine minimum controls. (1995a). EPA 832-B-95-003. Washington, DC: US EPA.

Combined sewer overflow monitoring study – In fulfillment of the requirements of paragraph 16.e.v Hoboken-Union City-Weehawken (Tri-City) sewerage authority administrative consent order. (1996). Tri-City Sewerage Authority: CH2M HILL.

Comprehensive conservation and management plan, NY/NJ Harbor Estuary program. (1996). New York, NY: U.S. EPA, Region 2.

Connolly, J. P., & Winfield, R. (1984). A user's guide for WASTOX, a framework for modeling the fate of toxic chemicals in aquatic environments. Part 1: Exposure concentration. EPA 600/3-84-077. Gulf Breeze, FL: US EPA.

Crowder, B. M., Epp, D. J., & Pionike, H. B. (1984). The effect on farm income of constraining soil and plant nutrient losses: An application of CREAMS simulation model. Bulletin 850. PA: College of Agriculture, The Pennsylvania State University.

Davis, E. M. (1976). Maximum utilization of water resources in a planned community: Bacterial characteristics of stormwater in developing rural areas. US EPA Research Grant R-802433. Washington, DC: US EPA.

Davis, P. L., & Borchardt, F. (1974). Combined sewer overflow abatement plan, Des Moines, Iowa. EPA R2-73-170. Washington, DC: US EPA.

Development of heavy metal waste load allocations for the Deep River, North Carolina. Prepared for US EPA Office of Water Enforcement and Permits, Washington, DC. McLean, VA: JRB Associates.

Development of total maximum daily loads and wasteload allocations (TMDLs/WLAs) procedure for toxic metals in NY/NJ Harbor. (1995a). Job No. TETR0103. Prepared for the U. S. Environmental Protection Agency, Region 2. Mahwah, NJ: HydroQual, Inc.

DeVries, J. J., & Hromadka, T. V. (1992). Chapter 21: Computer models for surface water. In: Maidment, D. R., Handbook of Hydrology. Toronto: McGraw-Hill, Inc.

Diagnostic study of water quality conditions in Town Lake, Austin, Texas. (1992). City of Austin: Environmental and Conservative Service Department.

Dilks, D. W., Hinz, S. C., Ambrose, R. B., Jr., & Martin, J. L. (1990). Simplified illustrative examples. In: Martin, J.M., Ambrose, R.B., Jr., & McCutcheon, S.C., Technical guidance manual for performing waste load allocation, Book III: Estuaries, Part 2: Application of estuarine waste load allocation models (pp. 6-1 – 6-47).Washington, DC: US EPA.

Dillaha, T. A. (1998). Nonpoint source pollution. [Article posted on Web site College of Engineering at Virginia Tech]. Retrieved November 16, 2002 from the World Wide web: http://ate.cc.vt.edu/eng/bse/dillaha/bse4324/

Di Toro, D. M., Fitzpatrick, J. J., & Thomann, R. V. (1983). Water quality analysis simulation program (WASP) and model verification program (MVP) – Documentation. For US EPA, Duluth, MN, Contact No. 68-01-3872. Westwood, NY: Hydroscience, Inc.

Di Toro, D. M., & Connolly, J. P. (1980). Mathematical models of water quality in large lakes, Part 2: Lake Erie (pp.90-101). EPA 600/3-80-065. Athens, GA: Environmental Research Laboratory, US EPA.

Documentation report – FWQA dynamic estuary model. (1970). U.S. Department of the Interior, Federal Water Quality Administration: Feinger and Harris.

Doneker, R. L., & Jirka, G. H. (1990). Expert system for hydrodynamic mixing zone analysis of conventional and toxic submerged single port discharges (CORMIX). EPA 600/3-90-012. Athens, GA: Environmental Research Laboratory, US EPA.

Donigian, A. S., Jr., Bicknell, B. R., & Imhoff, J. C. (1995). Hydrological simulation program-FORTRAN (HSP-F). In: Singh, V.P. (Ed). Computer models of watershed hydrology (pp. 395-442). Colorado: Water Resource Publications.

Dynamic Toxics Waste Load Allocation Model (DYNTOX) [Computer software]. (1985). LimnoTech, Inc.

Faber, H. (1992, April 12). Striped bass running in the Hudson, but they're off limits to fishermen. The New York Times, p. 24.

Feasibility study for Lower Tha Chin River Basin wastewater management: Main report. (1995). Prepared for the Pollution Control Department, Ministry of Science, Technology and Environment, Bangkok. Bangkok, Thailand: Marco Consultants Co., Ltd.

Feuerstein, D. L., & Maddaus, W. O. (1976). Wastewater treatment program, Jamaica Bay, New York. Volume I: Summary report; Volume II: Supplemental data, New York City Spring Creek. EPA 600/2-76-222a. and EPA 600/2-76-222b. Washington, DC: US EPA.

Fischer, H. B., List, E. J., Koh, R. C., Imberger, Y. J., & Brooks, N. H. (1979). Mixing in inland and coastal waters. Orlando, FL: Academic Press.

Fisher, G. T., & Katz, B. G. (1988). Urban stormwater runoff – Selected background information and techniques for problem assessment, with a Baltimore, Maryland, case study (p.30). USGS Water-Supply Paper 2347.

Guidelines for the preparation of the 1996 state water quality assessments (305(b) Reports). (1995c). EPA 841-B-95-001. Washington, DC: US EPA.

Haan, C. T., & Zhang, J. (1996). Impact of uncertain knowledge of model parameters on estimated runoff and phosphorus loads in the Lake Okeechobee Basin. Transactions of the American Society of Agricultural Engineers, 39, pp. 511-516.

Handbook. Remediation of contaminated sediments. (1991). EPA 625/6-91/028. Washington, DC: Office of Research and Development, US EPA.

Heathcote, I. W. (1998). Integrated Watershed Management: Principles and Practice. Toronto: John Wiley & Sons, Inc.

Heathcote, I. W. (1987). Background review. In: James, W (Ed), Pollution control planning (pp. 23-41). Toronto: Ontario Ministry of the Environment.

Henderson-Sellers, B. (1991). Water quality modeling, Volume IV: Decision support techniques for lakes and reservoirs (p. 310). Boca Raton, Florida: CRC Press.

Heng, H. H., & Nikolaidis, N. P. (1998). Modeling of nonpoint source pollution of nitrogen at the watershed scale. J. American Water Research Association, 34(2), pp. 359-374.

Higgins, J. J., Muller, J. A., & St. John, J. P. (1978). Baseline and alternatives: Modeling. NYC 208 Task Report 512/522. Prepared for Hazen and Sawyer, Engineers. March: Hydroscience, Inc.

Huber, W. C. (1995). EPA stormwater management model - SWMM. In: Singh, V. P. (Ed), Computer models of watershed hydrology (pp. 783-808). Colorado: Water Resources Publications.

Huntley, S. L., Iannuzzi, T. J., Avantaggio, J. D., Carlson-Lynch, H., Schmidt, C. W., & Finley, B. L. (1997). Combined sewer overflows (CSOs) as sources of sediment contamination in the Lower Passaic River, New Jersey. II. Polychlorinated dibenzo-P-dioxins, polychlorinated dibenzofurans, and polychlorinated biphenyls. Chemosphere, 34(2), pp.233-250.

Iannuzzi, T. J., Huntley, S. L., Schmidt, C. W., Finley, B. L., McNutt, R. P., & Burton, S. J. (1997). Combined sewer overflows (CSOs) as sources of sediment contamination in the Lower Passaic River, New Jersey. I. Priority pollutants and inorganic chemicals. Chemosphere, 34(2), pp. 213-231.

Iseri, K. T., & Langbein, W. B. (1974). Large rivers of the United States. Circular No. 686. U.S. Department of the Interior, U. S. Geological Survey.

Jamal, I. B. (1986). Optimal allocation of BOD loading in Tidal River (p. 128). M.Sc. Thesis. Vancouver: University of British Columbia.

James, T. R., Martin, J., Wool, T., & Wang, P. F. (1997). A sediment resuspension and water quality model of Lake Okeechobee. J. American Water Resources Association, 33(3), pp. 661-680.

James, T. R., Jin, K., Lung, W., Loucks, D. P., Parks, R. A., & Tisdale, T. S. (1998). Assessing Lake Okeechobee eutrophication with water-quality models. Journal of Water Resources Planning and Management/January/February 1998, pp. 20-30.

James, T. R., & Bierman, V. J., Jr. (1995). A preliminary modeling analysis of water quality in Lake Okeechobee, Florida: Diagnostic and sensitivity analyses. Wat. Res., 29(12), pp. 2767-2775.

James, T. R., & Bierman, V. J., Jr. (1995a). A preliminary modeling analysis of water quality in Lake Okeechobee, Florida: Calibration results. Wat. Res., 29(12), pp. 2755-2766.

James, W. (1992). Stormwater management modeling: Conceptual workbook (pp. 28-63). Guelph, Ontario: Computational Hydraulics International.

Johnson, R. C., Imhoff, J. C., Kittle, J. L., Jr., & Donigian, A. S. (1984). Hydrological simulation program – FORTRAN (HSPF), user's manual for release 8.0. EPA 600/3-84-066. Athens, GA: Environmental Research Laboratory, US EPA.

Klein, L. A. (1974). Sources of metals in New York City wastewater. J. Water Pollution Control Federation, 46, pp. 2653-2662.

Lager, J. A. (1976). Development and application of a simplified stormwater management model. EPA 600/2-76-218. Washington, DC: US EPA.

Leo, W. M., St. John, J. P., & O'Connor, D. J. (1978). Seasonal steady state model. NYC 208 Task Report 314. Prepared for Hazen and Sawyer, Engineers. March: Hydroscience, Inc.

Limburg, K. E., Moran, M. A., & McDowell, W. H. (Eds). (1986). The Hudson River ecosystem. NYC, NY: Springer-Verlag.

Lin, W., & Kao, J. (1994). Development of an internal phosphorus loading estimation procedure for a lake or reservoir. M.Sc.Thesis. Hsinchu, Taiwan: National Chiao Tung University.

Lin, W. L., Kao, J. J., & Tsai, C. H. (1998). Dynamic spatial modeling approach for estimation of internal phosphorus load. Wat. Res., 32(1), pp. 47-56.

Linked watershed/waterbody model: User's manual. (1994). Prepared for the Southwest Florida Water Management District. Dames & Moore Inc. and AscI.

Lung, W. S. (1993). Water quality modeling, Volume III: Application to estuaries (p. 194). Boca Raton, Florida: CRC Press, Inc.

Lung, W. S. (1986). Assessing phosphorus control in the James River Basin. J. Environmental Engineering, 112(1), pp. 44-60.

Lung, W. S., & Larson, C. E. (1995). Water quality modeling of Upper Mississippi River and Lake Pepin. J. Environmental Engineering, 121(10), pp. 691-699.

Lung, W. S., & Paerl, H. W. (1988). Modeling Blue-Green algal blooms in the Lower Neuse River. Water Research, 22(7), pp. 895-905.

McCutcheon, S. T. (1989). Water quality modeling Volume I: Transport and surface exchange in river. French, R.H.(Ed), (p. 334). Boca Raton, Florida: CRC Press, Inc.

Manning, M. J. (1977). Nationwide evaluation of combined sewer overflows and urban stormwater discharges, Volume III: Characterization of discharges. EPA 600/2-77-064. Washington, DC: US EPA.

Martin, J. L., Wang, P. F., Wool, T., & Morrison, G. (1996). A mechanistic management – oriented water quality model for Tampa Bay (p.118). Florida: Surface Water Improvement and Management Department, Southwest, Florida Water Management District.

Martin, J. L., Ambrose, R. B., Jr., & McCutcheon, S. C. (Eds). (1990). Technical guidance manual for performing waste load allocation, Book III: Estuaries, Part 2: Application of estuarine waste load allocation models. Washington, DC: US EPA.

Martin, J. D. (1995). Effects of combined sewer overflows and urban runoff on the water quality of Fall Creek, Indianapolis, Indiana. U.S. Geological Survey water-Resources Investigations Report 94-4066. Indianapolis, Indiana: USGS.

Mason, D. G. (1977). Screening/floatation treatment of combined sewer overflows. Volume I: Bench scale and pilot plant investigations. EPA 600/2-77-069a. Washington, DC: US EPA.

Measurement and computation of streamflow: Volume 1: Measurement of stage and discharge. (1982). U.S. Geological Survey (USGS).

Measurements and Evaluation of Pollution Loads from a Combined Sewer Overflow. (1974). General report and Annex 1 Through 4. Ministry of the Environment; Ministry of Public Works: Coyne & Bellier Consulting Engineer.

MIKE 11: Short description. (1994). Horsholm, Denmark: Danish Hydraulic Institute (DHI).

Modified from approaches to combined sewer overflow program development: A CSO assessment report. (1994). Washington, DC: Association of Metropolitan Sewerage Authorities (AMSA).

Moffa, P. E., Byron, J. C., Freedman, S. D., Karanik, J. M., & Ott, R. (1980). Methodology for evaluating the impact and abatement of combined sewer overflows: A case study of Onondaga Lake, New York (p.106). EPA 600/8-80-048. Cincinnati, OH: Municipal Environmental Research Laboratory, US EPA.

Mueller, J. A., & Di Toro, D. M. (1981). Combined sewer overflow characteristics from treatment plant data. EPA-600/2-83/049. Bronx, New York: Manhattan College Environmental Engineering and Science Program.

Methodology for evaluating the impact and abatement of combined sewer overflows - A case study of Onondaga Lake, New York. (1980). EPA 600/8-80-048. Cincinnati, OH: Municipal Environmental Research Laboratory, US EPA.

New Jersey combined sewer overflow control program. (1999). Trenton, NJ: Division of Water Quality, NJDEP.

Newton Creek water pollution control project: East River water quality plan. (1999). Prepared for New York City Department of Environmental Protection, New York, NY. Mahwah, NJ: HydroQual, Inc.

New York-New Jersey harbor estuary program final comprehensive conservation and management plan. (1996). NYC, NY: New York-New Jersey Harbor Estuary Program (NY-NJ HEP).

NPDES storm water sampling guidance document. (1992). EPA 833-B-92-001. Washington, DC: Office of Water, US EPA.

NYC 208, task report, special water quality studies (PCP Task 317), City of New York, 208 Report. (1977). Prepared for Hazen & Sawyer, Managing Consultants. NYC, NY: Hydroscience, Inc.

O'Connor, D. J., & Muller, J. A. (1984). Water quality analysis of the New York Harbor complex. ASCE, Jour. Environ. Eng. Div., 110(6), pp. 1027-1047.

Orivieri, V. P. (1977). Microorganisms in urban stormwater. EPA 600/2-77-07. Washington, DC: US EPA.

Orlob, G. T. (1992). Water-quality modeling for decision making. J. Water Resources Planning and management, 118(3), pp. 295-305.

O'Shea, M. L., & Brosnan, T. M. (1997). New York Harbor water quality survey. Main report and appendices 1995. Wards Island, NY: New York Department of Environmental Protection, Bureau of wastewater Pollution Control, Division of Scientific Service, Marine Sciences Section.

Parker, C. A., & O'Reilly, J. E. (1991). Oxygen depletion in Long Island Sound: A historical perspective. Estuaries, 14(3), pp. 248-264.

Pickett, P. J. (1997). Pollutant loading capacity for the Black River, Chehalis River system, Washington. J. American Water Resources Association, 33(2), pp. 465-480.

Prevention and control of sewer system overflows. (1999). Alexandria, VA: Water Environment Federation (WEF).

Progress in water quality – An evaluation of the national investment in municipal wastewater treatment. (2000a). EPA-832-R-00-008. Washington, DC: Office of Water, US EPA.

Proposed UHR filtration pilot plant test program on combined sewer overflows and raw dry weather sewage at New York City's Newtown Creek sewage treatment plant. (1975). US EPA Demonstration Grant No. S-803271. NYC, NY: US EPA.

Report to Congress: Implementation and enforcement of the combined sewer overflow control policy. (2001). EPA 833-R-01-003. Washington, DC: Office of Water, US EPA.

Roesch, S. E., Clark, L. J., & Bray, M. M. (1979). User's manual for the dynamic (Potomac) estuary model. EPA 903/9-79-001. Annapolis, MD: US EPA.

Revkin, A.C. (1997, September 17). High PCB level is found in a Hudson bald eagle. The New York Times, p. B-4.

Section 208 areawide waste treatment management planning program. (1978). Draft final report to City of New York. New York, NY: Hazen and Sawyer.

Seidl, M., Huang, V., & Mouchel, J. M. (1997). Toxicity of combined sewer overflows on river phytoplankton: The role of heavy metals. Environmental Pollution, 101, pp. 107-116.

Seidl, M., Servais, P., & Mouchel, J. M. (1998). Organic matter transport and degradation in the River Seine (France) after a combined sewer overflow. Wat. Res, 32(12), pp. 3569-3580.

Selection criteria for mathematical models used in exposure assessments: surface water models. (1987). EPA 600/8-87-042. Washington, DC: Office of Health and Environmental Assessment, US EPA.

Shelley, P. E., & Kirkpatrick, G. A. (1975). Sewer flow measurement, a state-of-the-art assessment. EPA-600/2-75-027. Cincinnati, Ohio: US EPA.

Simplified Mathematical Modeling of Water Quality. (1971). Prepared for the Mitre Corporation and the US Environmental Protection Agency, Water Programs. Washington, DC: Hydroscience, Inc.

Simplified method program – Variable complexity stream toxics model (SMPTOX3): Version 2.0 [Computer software]. (1992) LimnoTech, Inc.

Simpson, H. J., & Anderson, R. (2001). Hudson River & Estuary contaminant behavior: dissolved oxygen, nutrients, persistent chlorinated hydrocarbons. In The Chemistry of Continental Waters. Lecture Notes. NYC, NY: Department of Earth and Environmental Sciences, Columbia University.

Siqueira, E. Q. (2000). WASP EUTRO5-Submodel-Structure and optional sensitivity analysis. In Course Material of Urban Stormwater Management. Guelph, ON, Canada: School of Engineering, University of Guelph.

Stefan, H. G., Ambrose, R. B., Jr., & Dortch, M. S. (1990). Surface water quality models: Modeler's perspective. In Proceedings of the International Symposium on Water Quality Modeling of Agricultural Non-point Sources (pp. 329-374). Washington, DC: U.S. Department of Agriculture.

Surface water quality standards, N.J.A.C. 7:9-4.1 et seq. (1985). Trenton, NJ: Division of Water Quality, NJDEP.

Technical guidance manual for developing total maximum daily loads. Book II: Streams and rivers. Part1: Biochemical oxygen demand/dissolved oxygen and nutrients/eutrophication. (1995d). EPA 823-B-95-007. Washington, DC: Office of Water, US EPA.

Testing the waters XI: A guide to water quality at vacation beaches. (2001). Washington, DC: Natural Resources Defense Council (NRDC).

The quality of our nation's waters: A summary of the national water quality inventory: 1998 Report to congress. (2000). EPA 841-S-00-001. Washington, DC: Office of Water, US EPA.

Themelis, N. J., & Gregory, A. F. (2001). Sources and material balance of mercury in the New York-New Jersey Harbor. Report to the New York academy of science (NYAS). In Industrial Ecology for Pollution Prevention Study of the NYAS Harbor Consortium. NYC, NY: Earth Engineering Center, Columbia University.

Thomann, R. V. (1992). Modeling application critique. In Ambrose, R.B., Jr (Ed), Technical guidance manual for performing waste load allocations, Book III: Estuaries – Part 4: Critical review of coastal embayment and estuarine waste load allocation modeling. Washington, DC: Office of Water, US EPA.

Thomann, R. V. (1982). Verification of water quality models. J. Environmental Engineering Division, 108(EE5), pp. 923-940.

Thomann, R. V. (1975). Mathematical modeling of phytoplankton in Lake Ontario, I. Model development and verification. EPA 600/3-75-005. Corvallis, OR: US EPA.

Thomann, R. V. (1972). Systems analysis and water quality management (p. 286). New York: McGraw-Hill. Reprinted by Oklahoma City, OK: J. Williams Book Co.

Thomann, R. V., Muller, J. A., Winfield, R. P., & Huang, C. (1991). Model of fate and accumulation of PCB homologues in Hudson Estuary. Journal of Environment Engineering, 117(2), pp. 161-178.

Thomann, R. V., & Muller, J. A. (1987). Principles of surface water quality modeling and control (p. 644). New York: Harper Collins Publisher, Inc.

Thomann, R. V., & Fitzpatrick, J. J. (1982). Calibration and verification of a mathematical model of the eutrophication of the Potomac Estuary. Washington, DC: Department of Environmental services, Government of the District of Columbia.

Thomann, R. V., Winfield, R. P., & Segna, J. J. (1979). Verification analysis of Lake Ontario and Rochester Embayment three dimensional eutrophication models. EPA 600/3-79-094. Grosse Ile, MI: US EPA.

Thomann, R. V., Winfield, R. P., Di Toro, D. M., & O'Connor, D. J. (1976). Mathematical modeling of phytoplankton in Lake Ontario, 2: Simulations using LAKE 1 model. EPA 600/3-76-076. Grosse Ile, MI: USEPA.

Tim, U. S., & Jolly, R. (1994). Evaluation of agricultural non-point source pollution using integrated geographic information systems and hydrology/water quality model. J. Environmental Quality, 23, pp. 25-35.

Urban stormwater management and technology: Update and users' guide. (1977). EPA 600/8-77-014. Cincinnati, OH: Municipal Environmental Research Laboratory.

Vieux, B. E., & Needham, S. (1993). Non-point pollution model sensitivity to grid-cell size. J. Water Resources Planning and Management, 119(2), pp. 141-157.

Water Quality Criteria. (1979). In Federal Register, Part V (pp. 15926–15981). Washington, DC: US EPA.

Water quality modeling analysis of hypoxia in Long Island Sound using LIS3.0. (1996). Job No. NENG0035. Prepared for the Management Committee of the Long Island Sound Study and New England Interstate Water Pollution Control Commission. Mahwah, NJ: HydroQual, Inc.

Water quality standards handbook, second edition. (1994b). EPA 823-94-006. Washington, DC: US EPA.

Water resources data for California, Part 2, water quality records. (1972). U.S. Geological Survey (USGS).

Whitehead, P., Beck, B., & O'Connell, E. (1981). A system model of streamflow and water quality in the Bedford Ouse River system - II. Water quality modeling. Water Research, 15, pp. 1157-1171.

Wool, T. A., Ambrose, R. B., Jr., Martin, J. M., & Comer, E. A. (2000). Water analysis simulation program (WASP) version 6.0 Draft: User's manual. Atlanta, GA: US EPA-Region 4.

Wool, T. A. (2002). Water quality modeling and TMDL development: The WASP model. In Course Material of WASP Training Course in Philadelphia, 2002. Atlanta, GA: Water Quality Assessment Section, US EPA, Region IV.

Wolman, M. G. (1971). The Nation's rivers. Science, 174, pp.905-917.

Water Resources Database (WRDB) 4.2 [computer software]. (1993). St. Louis, Mo: Clayton Engineering.

Young, R. A., Onstad, C. A., Bosch, D. D., & Anderson, W. W. (1989). AGNPS, Nonpoint source pollution model for evaluating agriculture watershed. J. Soil and Water Conservation, 44, pp. 168-173.

Zander, B., & Love, J. (1990). STREAMDO IV and supplemental ammonia toxicity models. Denver, CO: EPA Region VIII, Water Management Division.